DEVELOPMENT OF A UNIFIED RESONANCE SELF-SHIELDING METHODOLOGY FOR LATTICE PHYSICS CALCULATION IN LIGHT WATER REACTOR CORE ANALYSIS

Hiroki KOIKE

Department of Material, Physics, and Energy Engineering,

Graduate School of Engineering, Nagoya University

2017

This work is a study how accurately and efficiently to generate effective reaction probability of neutron from complicated resonance data for light water reactor core analysis.

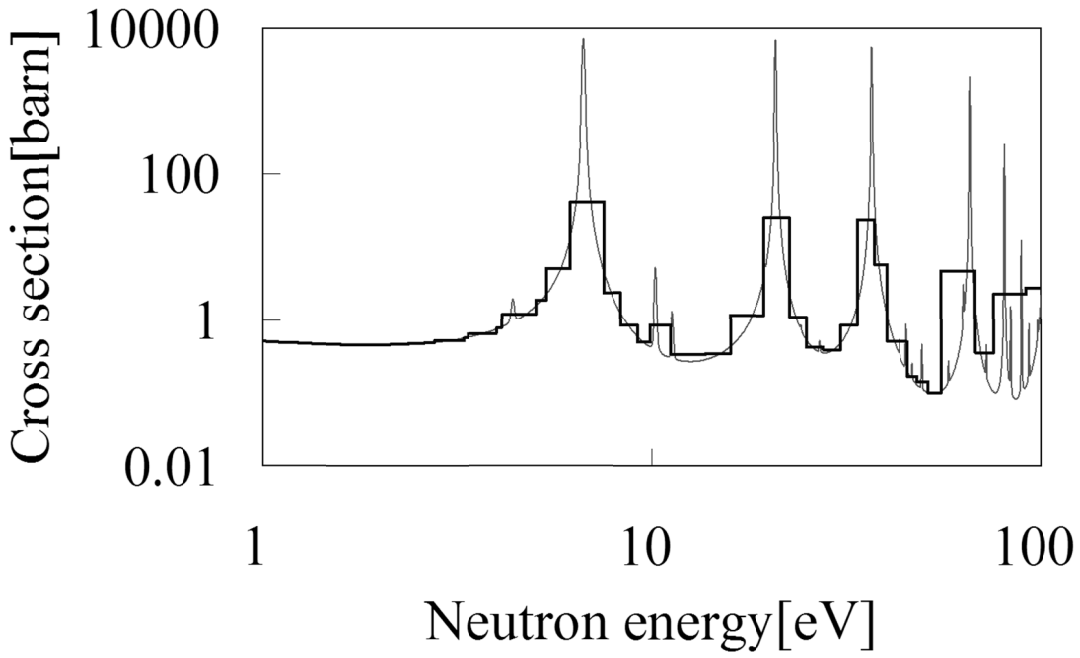

ABSTRACT

This dissertation is devoted to development of a unified resonance self-shielding methodology for generation of multi-group effective cross-sections in lattice physics calculation of light water reactor (LWR) core analysis. The new methodology can accurately and efficiently treat generalized multi-region geometry in a reactor core with extensive neutron spectrum conditions for LWRs.

The present methodology is established by theoretical enhancement and integration of conventional three resonance treatments, i.e., equivalence theory, ultra-fine-group slowing-down calculation and sub-group method. The integration works have been accomplished from the view point of maximizing the advantages and minimizing the disadvantages for each method. As a result, several important technical issues for conventional resonance treatments, i.e.,

(i) limitation for generalized lattice geometry,

(ii) black neutron absorber assumption,

(iii) scattering source approximation,

(iv) resonance interference treatment,

(v) radially/azimuthally dependent intra-pellet self-shielding treatment,

(vi) non-uniform fuel composition and temperature treatment within a pellet,

are simultaneously resolved in the framework of the unified theory. Solution for (i)(ii)(v) and (iii)(iv)(vi) enables treatment of generalized geometry and extensive spectrum conditions, respectively.

The present resonance self-shielding methodology can generate multi-group effective cross-sections used for the subsequent multi-group flux calculation, by considering complicated energy/space self-shielding effects driven by resonance absorption of heavy nuclides such as ^{238}U. By applying the effective cross-sections obtained from the present methodology to the lattice physics calculations, it is demonstrated that major neutronics parameters such as neutron multiplication factor and reactivities can be accurately predicted for generalized geometry under extensive spectrum conditions. The accuracy is comparable to the continuous energy Monte-Carlo results.

From the technical achievements in this dissertation, it is concluded that the present resonance treatment can accurately and efficiently generate effective cross-sections used in LWR core analysis. The present achievements will enable to perform the more accurate and efficient core nuclear design and safety analysis, which contributes to the activities for improvement of nuclear power safety.

TABLE OF CONTENTS

LIST OF TABLES

LIST OF FIGURES

NOMENCLATURES

A_k : relative atomic weight of nuclide k to the neutron

α_k : maximum energy loss ratio for nuclide k defined as $\alpha_k \equiv \left(\frac{A_k - 1}{A_k + 1} \right)^2$

α_n : n-th rational coefficient considering the heterogeneous and lattice effects

β_n : weight of n-th rational equation normalized as $\sum_{n=1}^{N} \beta_n = 1$

E : neutron energy

ε_n : n-th rational coefficient for mitigation of self-shielding effect in non-fuel region

f : fuel region

g : index for energy group (multi-group resolution)

k : index for nuclide

l_f : mean chord length of fuel lump

l_i : mean chord length of ring region i defined as $l_i \equiv 4V_i / S_f$ (S_f : pellet surface)

μ : self-shielding correction factor for non-fuel region

N : the number of rational equation terms

n : index for rational equation term

nf : non-fuel region

N_k^f : number density of nuclide k in fuel region

N_k^{nf} : number density of nuclide k in non-fuel region

ϕ_f : neutron flux in fuel region

ϕ_i : neutron flux in ring region i

φ_{nf} : non-asymptotic component of non-fuel flux

$P_{j\to i}$: collision probability from regions j to i

r : index for resonance nuclide

ρ_i : relative outer radius of ring i (normalized by pellet radius R)

ρ_{i-1} : relative inner radius of ring i (normalized by pellet radius R)

sg : index for energy group (sub-group resolution)

S_i : neutron source for region i

Σ_p^{nf} : macroscopic potential scattering cross-section in non-fuel region

Σ_{sd}^f : slowing-down cross-section in fuel region

Σ_t^f : macroscopic total cross-section in fuel region

Σ_t^i: macroscopic total cross-section in ring region $i \in f$

σ_s^k: microscopic elastic scattering cross-section for nuclide k

σ_x^r: microscopic cross-section for resonance nuclide r and reaction type x

θ: ratio of asymptotic spectrum in non-fuel region ($0 \le \theta \le 1$)

ufg: index for energy group (ultra-fine-group resolution)

V_i: volume for region i

x: index for reaction type

CHAPTER 1. INTRODUCTION

1.1 Background

1.1.1 Latest Requirements for Nuclear Core Analysis Methodologies

The Fukushima-Daiichi nuclear power plant accident in 2011 reconfirmed importance of nuclear safety, and improvement of nuclear power safety has strongly been promoting. The control of fission chain reaction in a reactor core is a key technology to assure nuclear power safety, and the safety is mainly confirmed through reactor core analysis. Therefore, the advancement of reactor core analysis methodology will directly contribute to the activities for further improvements of nuclear power safety, e.g., reflection of the latest knowledges, enhancement of analysis technologies.

Conventionally, the reactor core analysis for commercial LWR (light water reactor) nuclear power plants is composed of core nuclear design, thermal-hydraulic design, fuel mechanical design and safety design. In the framework of these design analyses, the core nuclear design is usually the uppermost stream both for the reactor analysis and total plant design.

The nuclear design can create the basic concept of a reactor core, and suggest the fundamental specifications of the core, e.g., core thermal power, core size, nuclear fuel specifications and reactivity control method for fission chain reaction. That is why the fundamental technologies associated with the nuclear design characterize many specifications of a nuclear power plant.

In addition, the various neutronics parameters obtained from nuclear design are

supplied as interface data for the subsequent stream of the design analyses. Therefore, the quality of nuclear design methodology influences on the analysis results of subsequent designs.

In order to improve the nuclear power safety, the advanced core analysis methodologies have been continuously investigated. From the view point of best-estimate evaluation for setting the more realistic safety margin in the nuclear reactor analysis, the core nuclear design methodology has been incorporated into the detailed safety analysis methodology based on a three-dimensional, nuclear/thermal-hydraulic coupling calculations [1-3].

In order to apply the nuclear design methodology as a part of the advanced safety analysis scheme, its applicable range must be extended to the irregular core conditions assumed in safety analysis. In the recent requirements for safety analysis, DEC (design extended conditions) and SA (severe accident) are assumed, in addition to the conventional application range, i.e., normal operating and DBE (design based event) conditions.

In order to preserve the appropriate prediction accuracy of nuclear design calculations against the extended application range for safety analysis, the advanced core nuclear design methodologies are now strongly required. The advancement will contribute not only to the enhancement of safety analysis methodology, but also to the further improvement of nuclear core design itself. Therefore, the advanced nuclear design methodology will contribute to the activities for enhancement of both the safety and economy in nuclear power.

1.1.2 Overview of Current Core Nuclear Design Methodology

From the extended requirements for core analysis methodology, this dissertation focuses on the core nuclear design methodology based on a reactor physics theory [4-8].

As shown in **Figure 1.1**, the current core nuclear design is generally based on a two-step calculation scheme [8], which is composed of lattice physics calculation followed by core calculation. Since a huge amount of core analysis is performed in the nuclear design for various fuel loading patterns, the lattice physics calculation (fuel assembly calculation) and the core calculation are separated for calculation efficiency.

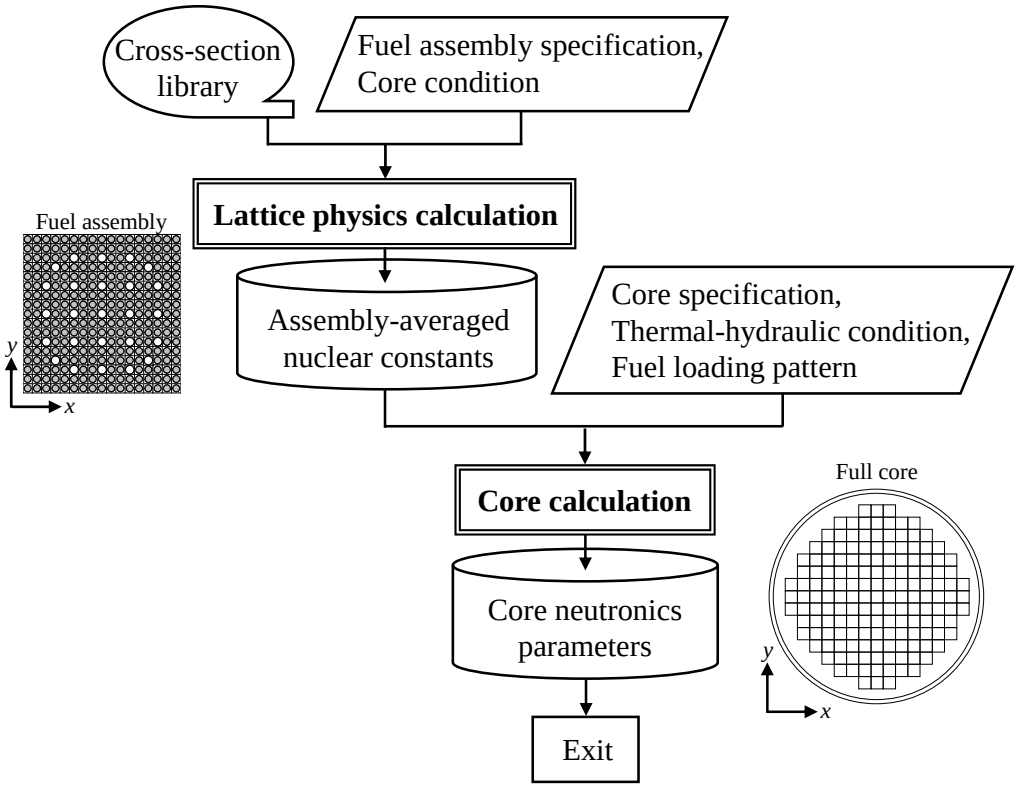

Figure 1.1 Current flow of core nuclear design based on a two-step calculation.

By tracing the flow of core nuclear design calculation stream, it can be seen that the final prediction accuracy of core neutronics parameters depends on the accuracy of assembly-averaged nuclear constants obtained from lattice physics calculations, which are the most important input data for the core calculations.

Here, the typical flow of lattice physics calculation is shown in **Figure 1.2**. The accuracy of lattice physics calculation itself is determined by the solutions of neutron transport calculation for fuel assembly geometry, i.e., space-dependent, multi-group neutron fluxes. If the appropriate multi-group effective cross-sections are generated from resonance calculation, and supplied as input of the rigorous neutron transport calculations, the neutron fluxes can accurately be obtained. The details for the resonance calculation are described in sub-sections 1.1.3 and 1.1.4.

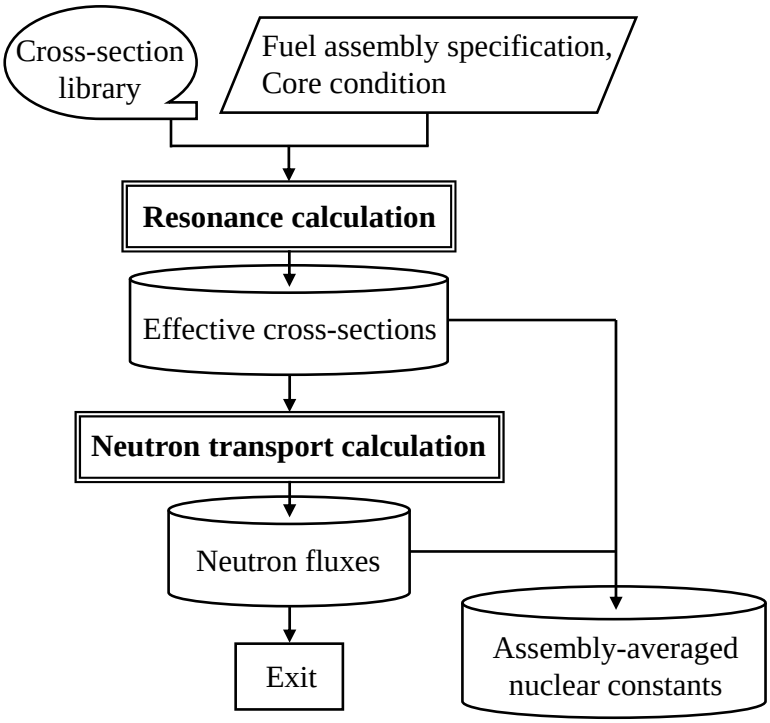

Figure 1.2 Typical flow of lattice physics calculation.

Recently, the method of characteristics (MOC) [9] is widely applied as a standard neutron transport calculation scheme in order to explicitly consider heterogeneous geometry such as pin-cell, fuel assembly and even full core. The MOC can be applied by utilizing the current high computational performance.

In contrast to the neutron transport calculation, the resonance calculation has several technical issues from the view point of sufficient accuracy with practical computation time. The accuracy of multi-group effective cross-sections obtained from the resonance calculation should be well-balanced with that of neutron fluxes.

The current core nuclear design calculation scheme suggests that the accuracy of multi-group effective cross-sections and its source (nuclear data) strongly influences on the final accuracy of core neutronics parameters. From this point of view, this dissertation is devoted to improvement of the accuracy for multi-group effective cross-sections.

As shown in **Figure 1.3**, the multi-group effective cross-sections are defined as the averaged cross-sections of original continuous energy cross-sections in a specific energy range. The multi-group energy structure is generally defined by dividing the whole neutron energy range in a reactor core (1.0×10^{-5}eV-20MeV) into approximately several dozen-a few hundreds energy groups. Since the group-averaged process for generating the effective cross-sections is especially important for resonance energy ranges, e.g., 6.0-8.0eV for ^{238}U, its processing is called as the resonance calculation [6]. In this dissertation, a new resonance calculation methodology is developed.

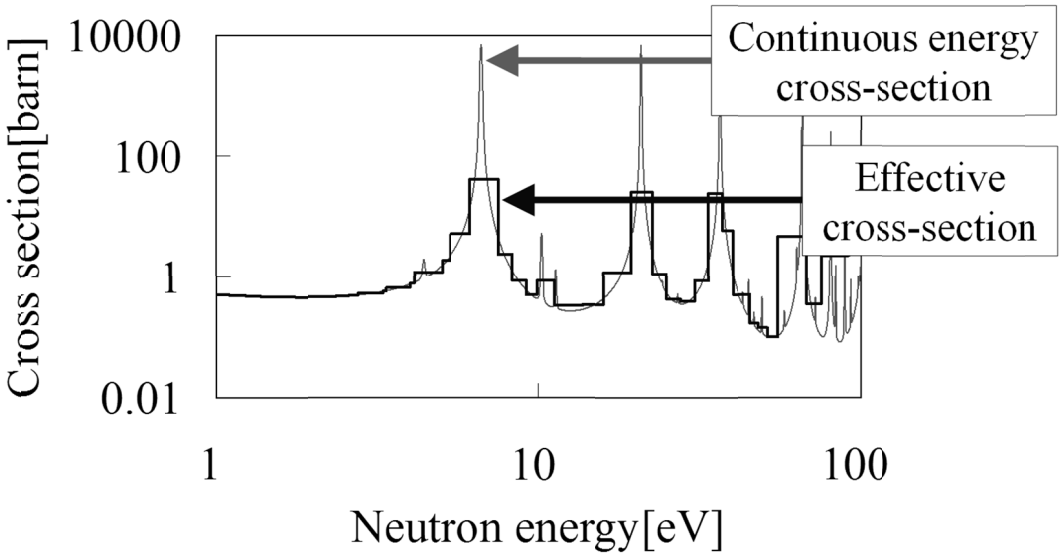

Figure 1.3 Relation between continuous energy cross-section and the corresponding multi-group effective cross-section.

1.1.3 Boltzmann's Neutron Transport Equation and Multi-Group Theory

The core nuclear design methodology is based on a reactor physics theory [4-8]. In the reactor physics theory, a fundamental equation to solve the neutron behavior in a reactor core is a Boltzmann's neutron transport equation written as:

$$\mathbf{\Omega} \cdot \nabla \psi(\mathbf{r}, E, \mathbf{\Omega}) + \Sigma_t(\mathbf{r}, E)\psi(\mathbf{r}, E, \mathbf{\Omega}) = Q(\mathbf{r}, E, \mathbf{\Omega}). \tag{1.1}$$

In the equation, the neutron population within a reactor core is modeled as if it were the gas transported in the media of reactor core. By providing the material-wise cross-sections Σ which correspond to the probability of neutron-nucleus reactions, the angular neutron flux ψ, i.e., the neutron density in a reactor core that depends on six phase spaces (spatial position $\mathbf{r} = (x, y, z)$, neutron energy E and neutron flight direction $\mathbf{\Omega} = (\theta, \varphi)$), is solved for a target reactor core.

As for the steady-state critical core, the neutron transport equation is numerically solved as an eigenvalue problem. For the eigenvalue problem, neutron source in Equation (1.1) is written as:

$$\begin{aligned} Q(\mathbf{r}, E, \mathbf{\Omega}) = &\int dE' \int d\mathbf{\Omega}' \Sigma_s(\mathbf{r}, E' \to E, \mathbf{\Omega}' \to \mathbf{\Omega}) \psi(\mathbf{r}, E', \mathbf{\Omega}') \\ &+ \frac{1}{k_{\text{eff}}} \frac{\chi(\mathbf{r}, E)}{4\pi} \int dE' \nu\Sigma_f(\mathbf{r}, E') \phi(\mathbf{r}, E'). \end{aligned} \tag{1.2}$$

The most fundamental solutions for Equations (1.1)-(1.2) are effective neutron multiplication factor k_{eff} (eigenvalue) and neutron flux $\psi(\mathbf{r}, E, \mathbf{\Omega})$ (eigenvector).

In the actual nuclear design calculations, the reactivity change $\Delta\rho$ and the reaction-rates $R(\mathbf{r})$ are often evaluated from k_{eff} and ψ (or scalar flux ϕ) as

follows:

$$\Delta\rho = \left(\frac{k'_{\text{eff}} - 1}{k'_{\text{eff}}}\right) - \left(\frac{k_{\text{eff}} - 1}{k_{\text{eff}}}\right) = \frac{1}{k_{\text{eff}}} - \frac{1}{k'_{\text{eff}}}, \tag{1.3}$$

$$R(\mathbf{r}) = \int dE \Sigma(\mathbf{r}, E)\phi(\mathbf{r}, E), \tag{1.4}$$

where the scalar flux is obtained by integrating the angular flux solution.

The typical examples of the neutronics parameters obtained from a LWR nuclear design are listed in **Table 1.1**. Though the various neutronics parameters are evaluated in the nuclear design, many of them are essentially the byproducts of k_{eff} and ϕ.

Table 1.1 Typical examples of neutronics parameters obtained from a LWR nuclear design.

Parameter type	Main category	Detailed category
Reactivity change	Doppler reactivity	Doppler temperature coefficient
		Doppler power defect
	Moderator reactivity	Moderator temperature coefficient
		Moderator density coefficient
		Boron worth
	Control rod worth	Differential worth
		Integral worth
	Others	Isothermal temperature coefficient
		Shut-down margin
Reaction-rate	Microscopic reaction-rate	Thimble reaction-rate for instrumented assembly (used for processing measured power distribution)
	Macroscopic reaction-rate	Radial assembly power distribution
		Axial power distribution
		Pin power distribution
		Nuclear enthalpy-rise hot channel factor (axially-integrated peak pin power)
		Thermal flux hot channel factor (3D local peak power)

As can be observed in Equations (1.1)-(1.2), the neutron transport equation can analytically be solved only for a very simple case, e.g., $\phi(E) = \frac{1}{E\Sigma_t(E)}$ in the case that the target system is an infinite homogeneous medium ($\mathbf{\Omega} \cdot \nabla \psi(\mathbf{r}, E, \mathbf{\Omega}) = 0$) and neutron source is asymptotic for neutron energy ($Q(E) = 1/E$). That is why the transport equation is numerically solved in the practical core nuclear design calculations. In the reactor physics theory, the fundamental equation has already been given as Equations (1.1)-(1.2). Therefore, the main interest for research and development is how to solve Equations (1.1)-(1.2) from the practical point of view.

The numerical approach to solve the transport equation is generally classified into two categories, i.e., stochastic method [10-11] and deterministic method [6]. In the stochastic method (or often referred as the Monte-Carlo method), there are no approximations for the treatment of each phase space. The space, energy and angular dependences of neutron flux are treated as continuous manner by directly tracing a series of neutron life with random number. As a result, the stochastic method enables accurate estimation of k_{eff} and ϕ, as long as many neutrons are traced and the corresponding statistical errors are negligible.

For the practical application of the stochastic method, the acceptable computation time is limited since the nuclear design calculations should be completed in the limited period for in-core fuel management. In such a realistic situation, the number of traced neutrons is limited, and the statistical error can be an issue for design calculation.

Especially for the evaluation of small reactivity changes such as the Doppler reactivity coefficient, and spatially local parameters such as pin-by-pin power

distribution, a huge amount of neutrons should be traced to reduce the statistical error in a practical level. In general, the number of traced neutrons is determined so that the statistical errors for the target neutronics parameters are sufficiently smaller than the neutronics uncertainties for the parameters used in the nuclear designs and their interface design applications.

In contrast, the deterministic method can evaluate neutronics parameters without statistical error. To perform computation within a practical computation time, the deterministic method introduces several modeling approximations associated with discretization and/or function expansion of each phase space (space, energy and angle).

In spite of the approximations, the deterministic method is widely applied to the current nuclear design calculations for LWRs owing to its high calculation efficiency. As for the approximate treatment on neutron energy, which is a main interest of this dissertation, the whole neutron energy range in a reactor core (1.0×10^{-5}eV-20MeV) is generally divided into the multi-group, as shown in **Figure 1.4**.

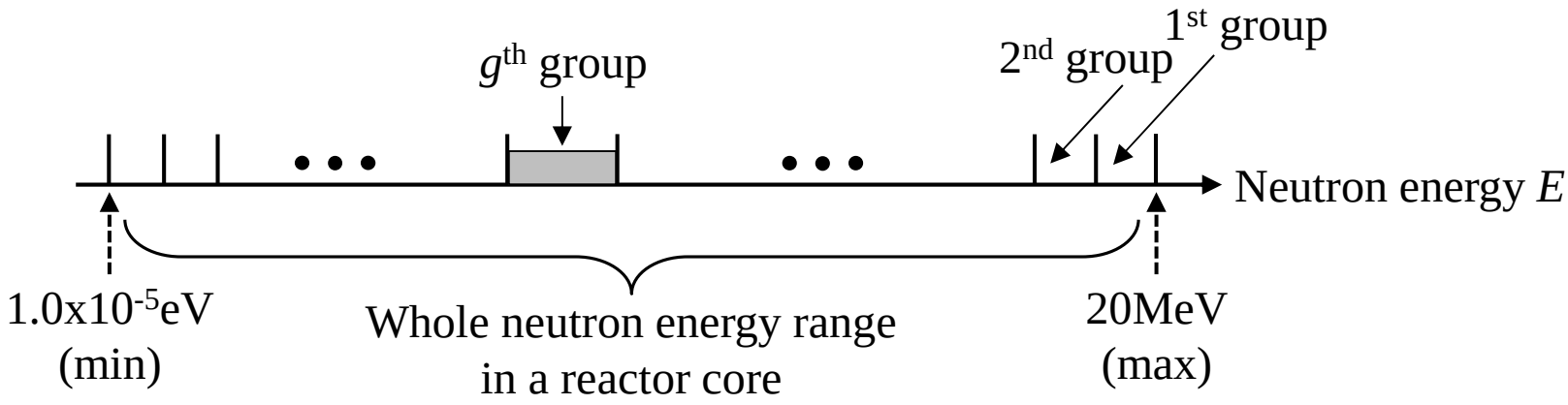

Figure 1.4 Concept of multi-group treatment.

In the multi-group treatment for neutron energy, the original transport equation for continuous energy form is transformed to the multi-group form. The multi-group transport equation for group g is derived by integrating Equation (1.1) for the corresponding energy range as follows:

$$\mathbf{\Omega} \cdot \nabla \psi_g(\mathbf{r}, \mathbf{\Omega}) + \Sigma_{t,g}(\mathbf{r}) \psi_g(\mathbf{r}, \mathbf{\Omega}) = Q_g(\mathbf{r}, \mathbf{\Omega}) . \tag{1.5}$$

In the derivation, the multi-group cross-sections, the neutron fluxes and the neutron sources are defined as:

$$\Sigma_{t,g}(\mathbf{r}) \equiv \frac{\int_g dE \Sigma_t(\mathbf{r}, E) \psi(\mathbf{r}, E, \mathbf{\Omega})}{\int_g dE \psi(\mathbf{r}, E, \mathbf{\Omega})} \cong \frac{\int_g dE \Sigma_t(\mathbf{r}, E) \phi(\mathbf{r}, E)}{\int_g dE \phi(\mathbf{r}, E)} , \tag{1.6}$$

$$\psi_g(\mathbf{r}, \mathbf{\Omega}) \equiv \int_g dE \psi(\mathbf{r}, E, \mathbf{\Omega}) , \tag{1.7}$$

$$Q_g(\mathbf{r}, \mathbf{\Omega}) \equiv \int_g dE Q(\mathbf{r}, E, \mathbf{\Omega}) . \tag{1.8}$$

where the angular dependence of neutron flux within a energy group g is approximately ignored in Equation (1.6). The multi-group cross-section Σ_g is defined so that the energy-integrated reaction-rate within the group g is preserved in the multi-group treatment, i.e., $\Sigma_g \psi_g(\mathbf{\Omega}) = \int_g dE \Sigma(E) \psi(E, \mathbf{\Omega})$.

Here, it should be noted that the multi-group angular flux ψ_g is accurately solved by Equation (1.5) only if the accurate multi-group cross-sections Σ_g are generated in advance. However, the multi-group cross-sections are defined as an averaged

cross-section for the specific energy range with the energy-dependent flux as a collapsing weight, as shown in Equation (1.6). This fact indicates that the energy-dependent neutron flux is necessary in advance, in spite that the neutron flux itself is a solution of the transport equation. This is “the chicken or the egg” situation, and an essential issue for multi-group treatment.

The example of continuous energy and corresponding multi-group cross-sections for ^{238}U is shown in **Figure 1.5** [12]. As for the smooth cross-section ranges, the above issue for flux weight is not essential as long as the continuous energy cross-section can be regarded as an almost constant within the specific energy group. In contrast, the continuous energy cross-sections for resonance ranges steeply vary for neutron energy. The corresponding energy-dependent neutron flux is strongly influenced by the resonance cross-sections. Therefore, the special care is necessary for generation of accurate multi-group cross-sections in which the original continuous energy cross-sections include resonances. The care corresponds to the reaction-rate preservation for each energy group mentioned above. It is sure that the reaction-rate preservation is performed by considering the temperature dependence of resonance cross-sections.

Continuous energy cross-section

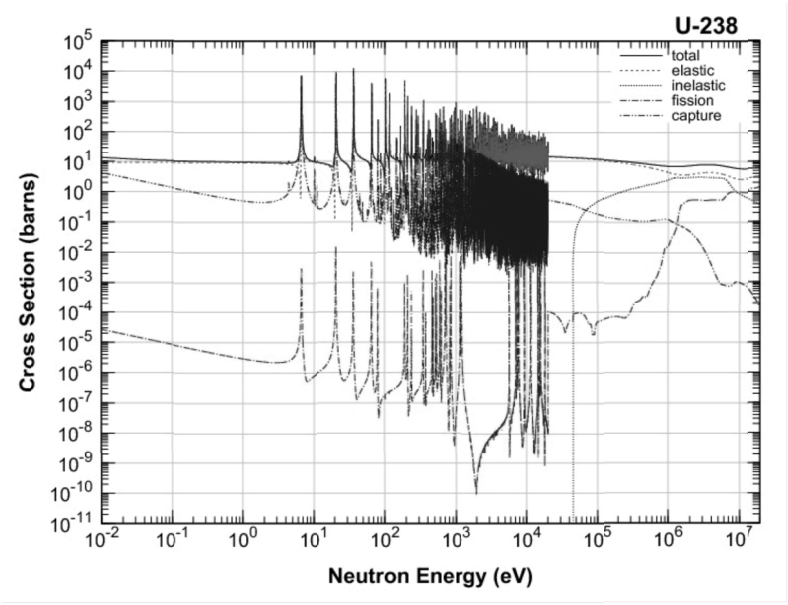

Multi-group cross-section

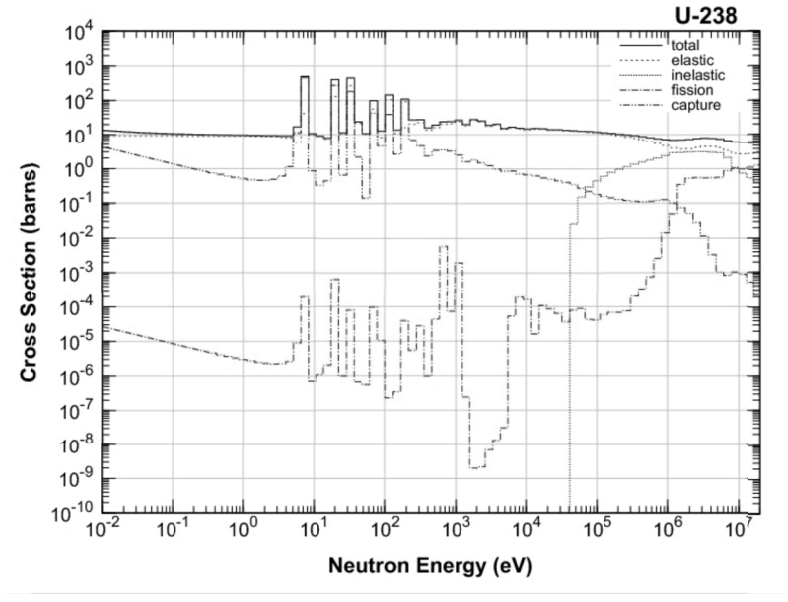

Figure 1.5 Continuous energy and corresponding multi-group cross-sections for ^{238}U [12].

The multi-group cross-sections obtained by considering the resonances are called as “effective cross-sections”, and their generation process is called as “resonance calculation” [6]. The resonance calculation is very important process for deterministic nuclear design calculations since the cross-sections of ^{238}U, which is a base nuclide of nuclear fuel material for LWRs, include several large resonances. This dissertation focuses on the resonance calculation methodology for LWR core analysis applications.

1.1.4 Resonance Self-Shielding Treatment

The resonance calculation is to generate multi-group effective cross-sections by considering the resonances in original continuous energy cross-sections. By reminding the example of very simple case for the solution of neutron transport equation in the previous sub-section, the neutron flux is written as:

$$\phi(E) = \frac{1}{E\Sigma_t(E)}, \tag{1.9}$$

where the target system is assumed as an infinite homogeneous medium, and the neutron source is regarded as an asymptotic function for neutron energy. As can be seen from Equation (1.9), the energy-dependent neutron flux is proportional to the inverse of macroscopic total cross-sections for the target medium. Therefore, the neutron flux corresponding to the resonance cross-sections for neutron energy is depressed, as shown in **Figure 1.6**.

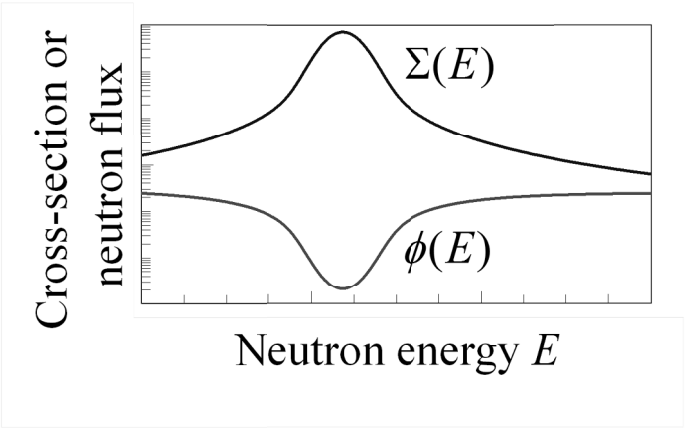

Figure 1.6 Relation between resonance cross-section and the corresponding neutron flux.

By considering the definition of multi-group cross-section, the effective cross-section is generated by the average of the continuous energy resonance cross-sections with corresponding fluxes as a collapsing weight:

$$\sigma_g = \frac{\int_g dE\sigma(E)\phi(E)}{\int_g dE\phi(E)}. \tag{1.10}$$

The neutron flux is strongly depressed for the resonance peak range. Thus the effective cross-section is smaller than the simple energy-averaged one. This mechanism is called as “resonance self-shielding effect” [6] since the large resonance cross-section itself reduces the corresponding effective cross-sections due to the flux depression.

The accurate and efficient treatment of self-shielding effect is a key issue for resonance calculation. The above self-shielding phenomenon is generally called as “energy self-shielding effect” since the effect is driven by the flux depression for neutron energy.

There is another self-shielding phenomenon called as “spatial self-shielding effect” [6] driven by the spatial flux depression within a fuel region. Since the fuel material for LWR is a strong neutron absorber, the incoming neutrons from the fuel surface is exponentially attenuated in the fuel region. Therefore the neutron flux has spatially distribution within a fuel region, as shown in **Figure 1.7**. The effective cross-sections show the spatial dependence, whose values are larger for the fuel surface than for the fuel center regions, due to spatial distribution of neutron flux.

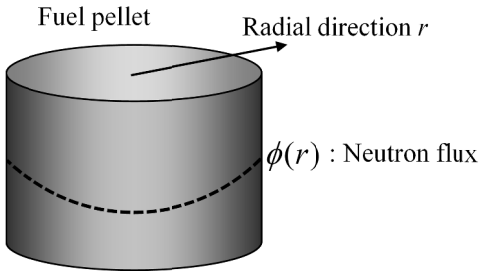

Figure 1.7 The spatial distribution of neutron flux within a neutron absorber.

In the resonance calculation, the energy and spatial self-shielding treatments are important for generation of appropriate effective cross-sections.

In the actual resonance self-shielding treatment, several numerical approaches are applied to the current nuclear design methodology. In the early days for nuclear technology, the reaction-rates associated with the resonance absorption of ^{238}U (so called "resonance integral" [5]) are directly measured, and the measured data are fitted with the function equation such as the Hellstrand's formula [5, 13]. The Hellstrand's formula is often applied to the resonance self-shielding treatment in the legacy methods [5] due to the limitation of computational resources in the era.

In contrast, several numerical approaches can be applied as a practical resonance self-shielding methodology in the current treatment owing to the rich computational resources. The current resonance self-shielding treatment is generally classified into three categories, i.e., the "equivalence theory", the "ultra-fine-group calculation" and the "sub-group method". Comparison of each methodology is summarized in **Table 1.2**. In the following, the outline for each methodology is described.

Table 1.2 Comparison of current resonance self-shielding treatment.

Methodology	Characteristics for theory	Treatment for geometry	Treatment for scattering source	Modeling resolution		Suitable application target
				Space	Neutron energy	
Ultra-fine-group calculation	Simple (First principle)	MOC[(1)]/CPM[(2)]	Slowing-down equation	Simplified	Fine	Accurate calculation for small geometry
Sub-group method	Simple	MOC/CPM	NR[(3)]/IR[(4)] approximation	Fine	Simplified	Efficient calculation for complicated geometry
Equivalence theory	Complicated	Rational approximation +Dancoff correction	NR/IR approximation	Fine /Simplified	Simplified	Efficient calculation for simplified geometry

(1) Method of characteristics
(2) Collision probability method
(3) Narrow resonance
(4) Intermediate resonance

(a) Ultra-fine-group calculation [14]

The ultra-fine-group calculation is to directly solve the energy-dependent neutron flux $\phi(E)$ for generation of effective cross-sections.

The example of energy-dependent neutron flux obtained from the ultra-fine-group calculation is shown in **Figure 1.8**. In the ultra-fine-group calculation, the obtained flux is directly used as a collapsing weight of resonance cross-sections in the ultra-fine energy group (or continuous energy) resolution.

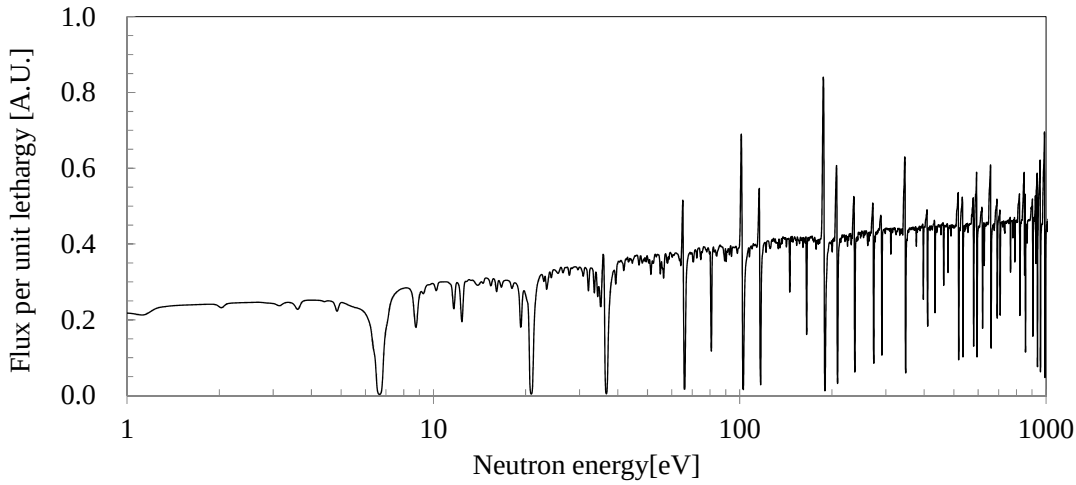

Figure 1.8 Energy-dependent neutron flux obtained from ultra-fine-group calculation.

The rigorous estimation of $\phi(E)$ does not make sense, since the flux is not a pre-determined input data but a primary solution of neutron transport equation.

Therefore, the approximated transport equation is solved for the treatment of energy dependence on neutron flux. The corresponding equation is referred as the "slowing-down equation", and is written as:

$$\Sigma_t(E)\phi(E) = \int_E^{\infty} dE' \Sigma_s(E' \to E)\phi(E') . \quad (1.11)$$

In the slowing-down equation, the fission source is usually ignored owing that the fission source is relatively smaller than the scattering source for the resonance energy ranges [15]. For the scattering source treatment, only the down scattering by elastic neutron-nucleus collision in the center-of-mass is taken into account since the other types of scattering reaction are commonly negligible for the target resonance energy ranges.

As shown in Equation (1.11), the neutron flux itself is included in the energy integration of scattering source, thus the slowing-down equation cannot analytically be solved in general. Fortunately, the scattering source includes only the down-scattering component in the slowing-down equation. Therefore, the neutron flux can numerically be solved from the upper to the lower energy ranges by using a recurrent relation. Any iterative calculations are not necessary, as different from general multi-group transport calculation for LWRs. That is why the energy-dependent neutron flux for the resonance energy ranges can efficiently be solved by the slowing-down equation.

Owing to the direct treatment of energy dependences for cross-section and neutron source, the ultra-fine-group calculation can accurately treat the energy-dependent scattering source and the resonance interference effect [8], which cannot be treated accurately in the sub-group method and the equivalence theory.

For the general heterogeneous geometry, the slowing-down equation is extended as:

$$\Sigma_{t,i}(E)\phi_i(E)V_i = \sum_j P_{j\to i}(E)V_j \int_E^\infty dE'\Sigma_{s,j}(E'\to E)\phi_j(E'), \qquad (1.12)$$

where the integral form of neutron transport equation based on the collision probability method [16] is applied as an example. While the slowing-down equation for the homogeneous system (Equation (1.11)) is efficiently solved, the slowing-down equation for the heterogeneous system requires a huge amount of computation burden due to the collision probability calculation for the ultra-fine-group resolution. Especially for the large and complicated geometry such as a fuel assembly or full core, the collision probability calculation for all the region-to-region combination is not practical for actual core nuclear design applications.

Therefore, the small geometry such as a pin-cell or multi-cell is a practical target for the current ultra-fine-group calculation.

(b) Sub-group method [17-18]

The sub-group method generates the effective cross-sections by dividing the specific energy range of multi-group resolution into several sub-groups according to the magnitude of resonance cross-section level, as shown in **Figure 1.9**.

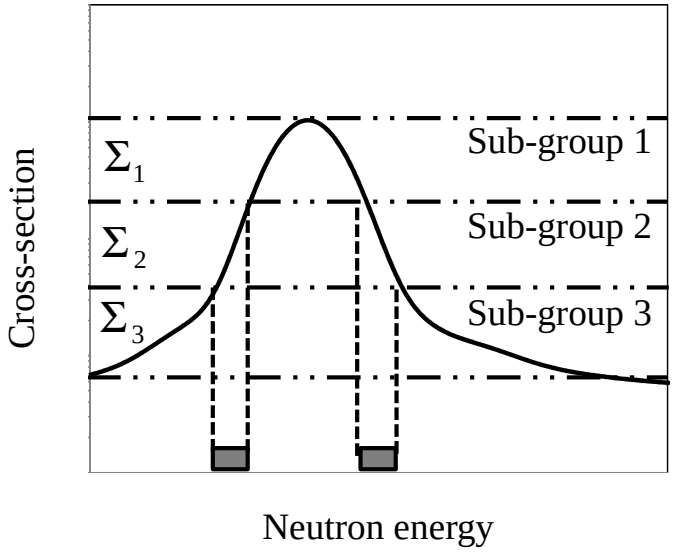

Figure 1.9 Concept of sub-group method (discrete energy range for sub-group 2 is shown as an example).

Since the energy dependence of neutron flux is almost proportional to the inverse of resonance cross-section (see Equation (1.9)), the sub-group definition according to the resonance cross-section level can efficiently consider the relation between the cross-section and the flux.

By solving the spatial neutron transport for each sub-group, the complicated geometry is efficiently treated for generation of effective cross-sections.

In the sub-group method, the following sub-group neutron transport equation is solved:

$$\mathbf{\Omega} \cdot \nabla \psi_{sg}(\mathbf{r}, \mathbf{\Omega}) + \Sigma_{t,sg}(\mathbf{r}) \psi_{sg}(\mathbf{r}, \mathbf{\Omega}) = Q_{sg}(\mathbf{r}, \mathbf{\Omega}) . \quad (1.13)$$

Here, the problem-independent sub-group cross-sections are usually generated in

advance based on a numerical scheme such as the fitting method [17] or the moment method [18].

By collapsing the sub-group cross-sections σ_{sg} with the obtained sub-group fluxes ϕ_{sg} multiplied by the band probabilities p_{sg}, the effective cross-section is generated as:

$$\sigma_g = \frac{\sum_{sg \in g} \sigma_{sg} \phi_{sg} p_{sg}}{\sum_{sg \in g} \phi_{sg} p_{sg}}. \tag{1.14}$$

Here, the band probability corresponds to the integration of energy width for the sub-group from the physical point of view. It should be noted that the concrete energy ranges are not explicitly specified in the fitting or the moment method.

The sub-group method can efficiently treat complicated geometry with the smaller number of sub-groups than the conventional multi-group energy discretization.

The sub-group method has an essential issue for prediction accuracy of effective cross-sections for several specific applications. Since the sub-group cross-sections are generated with the corresponding band probabilities, the corresponding energy ranges for each sub-group are not explicitly defined. In other words, the sub-group is implicitly defined through band probability. This fact leads to inconsistency of energy ranges among different temperature conditions because the resonance cross-sections strongly depend on temperature, and the pair of sub-group cross-sections and band probabilities are independently estimated for each temperature condition.

Therefore, the sub-group method includes the cause of error in the case of explicit

treatment for intra-pellet fuel temperature distribution. The error comes from the inconsistency of an implicit energy range for each spatial region with different temperatures in the sub-group transport calculation.

(c) Equivalence theory [6]

The equivalence theory generates the effective cross-sections for heterogeneous system by interpolating the pre-tabulated multi-group cross-sections for homogeneous system.

In the equivalence theory, the homogeneous multi-group cross-sections are tabulated in advance as a function of background cross-section, the definition of which is described later. Then the background cross-section for heterogeneous system is estimated by considering various heterogeneous effects for actual fuel assembly geometry. Finally, the effective cross-sections for the target heterogeneous system are generated by interpolating the homogeneous multi-group cross-sections with the background cross-section as an interpolation argument.

In this scheme, the homogeneous and the heterogeneous systems are assumed to be equivalent from the viewpoint of the resonance self-shielding effect, if the background cross-section for both systems is identical. That is why the method is called as equivalence theory. In the following, the theoretical background of the equivalence theory is qualitatively described.

First, the energy-dependent neutron flux is assumed to be proportional to the inverse of cross-sections, by reminding the very simple case for the solution of neutron

transport equation in sub-section 1.1.3. Then the neutron flux is expressed as:

$$\phi(E) = \frac{1}{E\Sigma_t(E)}. \tag{1.15}$$

Here, the target system is assumed as an infinite homogeneous medium which is composed of target resonance nuclide and hydrogen. The typical example of the resonance nuclide is ^{238}U, which is a main nuclide for nuclear fuel material. Hydrogen is a main contributor for neutron scattering source in LWRs.

In this assumption, the macroscopic total cross-section of the homogeneous system composed of a target resonance nuclide r and hydrogen is rewritten as:

$$\begin{aligned}\Sigma_t(E) &= N_r\sigma_t^r(E) + N_{\mathrm{H}}\sigma_t^{\mathrm{H}}(E) \cong N_r\sigma_t^r(E) + N_{\mathrm{H}}\sigma_p^{\mathrm{H}} \\ &= N_r \cdot \left[\sigma_t^r(E) + \frac{N_{\mathrm{H}}\sigma_p^{\mathrm{H}}}{N_r}\right] = N_r \cdot (\sigma_t^r(E) + \sigma_b),\end{aligned} \tag{1.16}$$

where σ_b denotes the background cross-section defined as:

$$\sigma_b \equiv \frac{N_{\mathrm{H}}\sigma_p^{\mathrm{H}}}{N_r}. \tag{1.17}$$

As shown in Equation (1.17), the background cross-section is defined as sum of cross-sections of other nuclide(s) per resonance nuclide.

Then the neutron flux is expressed as:

$$\phi(E) \propto \frac{1}{E}\frac{1}{\sigma_t^r(E) + \sigma_b}. \tag{1.18}$$

The relation between resonance cross-section of the target resonance nuclide and flux is shown in **Figure 1.10**. From Equation (1.18), the magnitude of flux depression depends on the background cross-section. This fact leads to make the background

cross-section as a quantitative index of the magnitude for the resonance self-shielding effect.

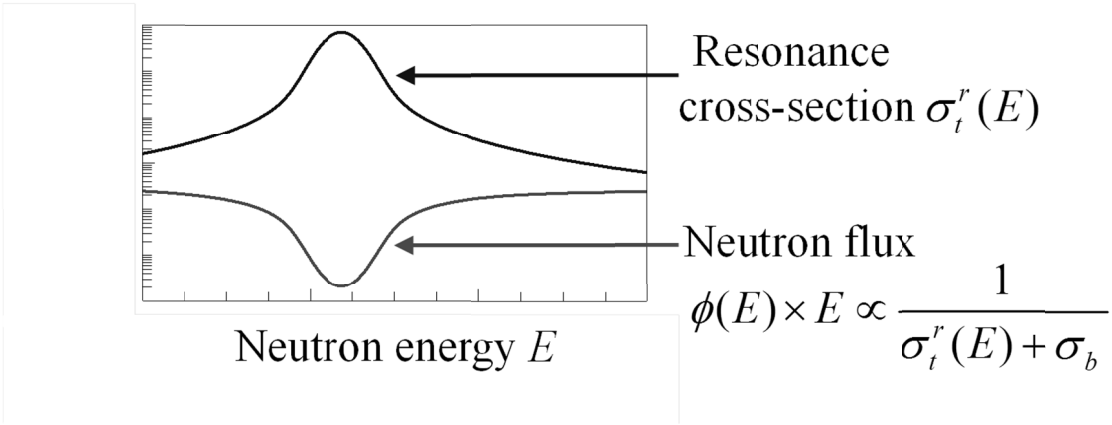

Figure 1.10 Relation between resonance cross-section and flux.

The fundamental mechanism for the dependence of effective cross-section on the background cross-section is shown in **Figure 1.11**. By considering both the Equation (1.18) and the definition of effective cross-section, the effective cross-section becomes smaller as the flux depression becomes larger due to the smaller background cross-section. The smaller background cross-section corresponds to the relatively large amount of the target resonance nuclide. Therefore, the effective cross-section becomes smaller as the amount of resonance nuclide becomes larger, which is a fundamental reason for calling “self-shielding” effect.

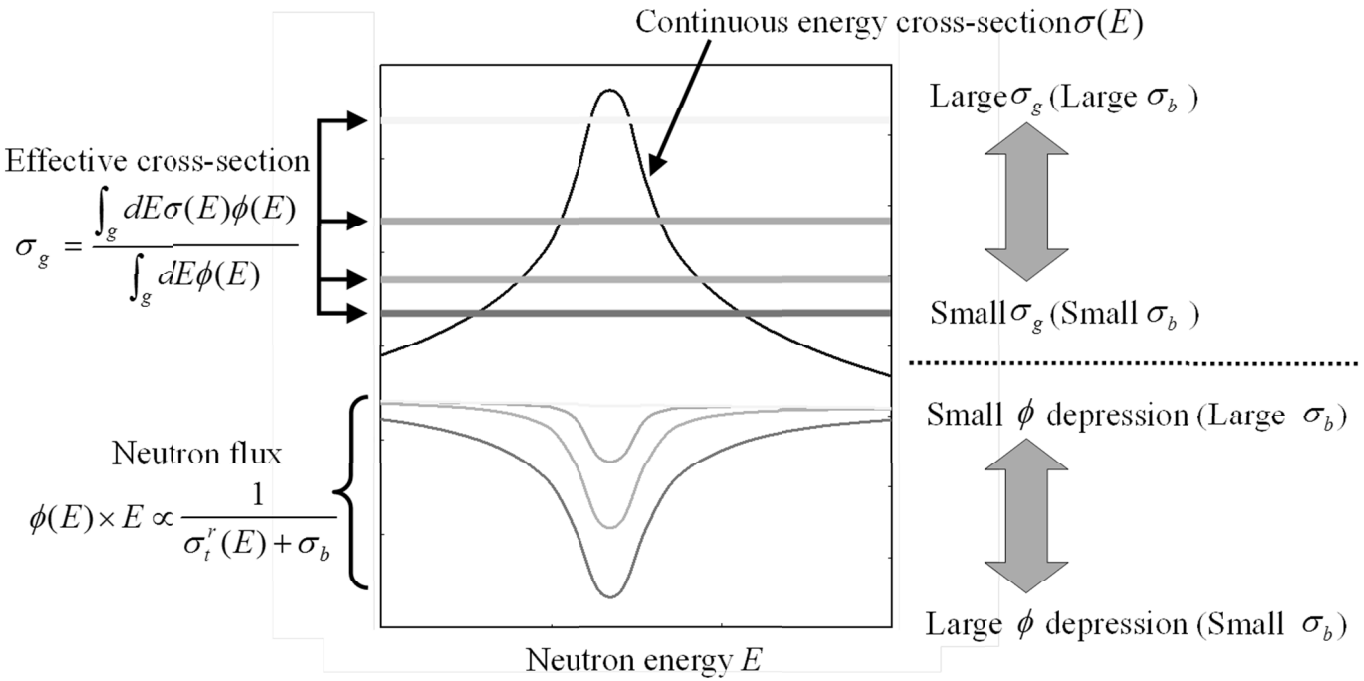

Figure 1.11 Mechanism for the dependence of effective cross-section on the background cross-section.

By considering the above discussion, the effective cross-section can be expressed as a function of background cross-section. The typical curve is shown in **Figure 1.12**. In the equivalence theory, the effective cross-section is pre-tabulated as a function of background cross-section for the homogeneous system.

It should be noted that the effective cross-section corresponding to the infinite background cross-section ($\sigma_b \to \infty$) is called as an infinite dilution cross-section since the condition corresponds to the infinitely-diluted situation of the target resonance nuclide in a hydrogen medium.

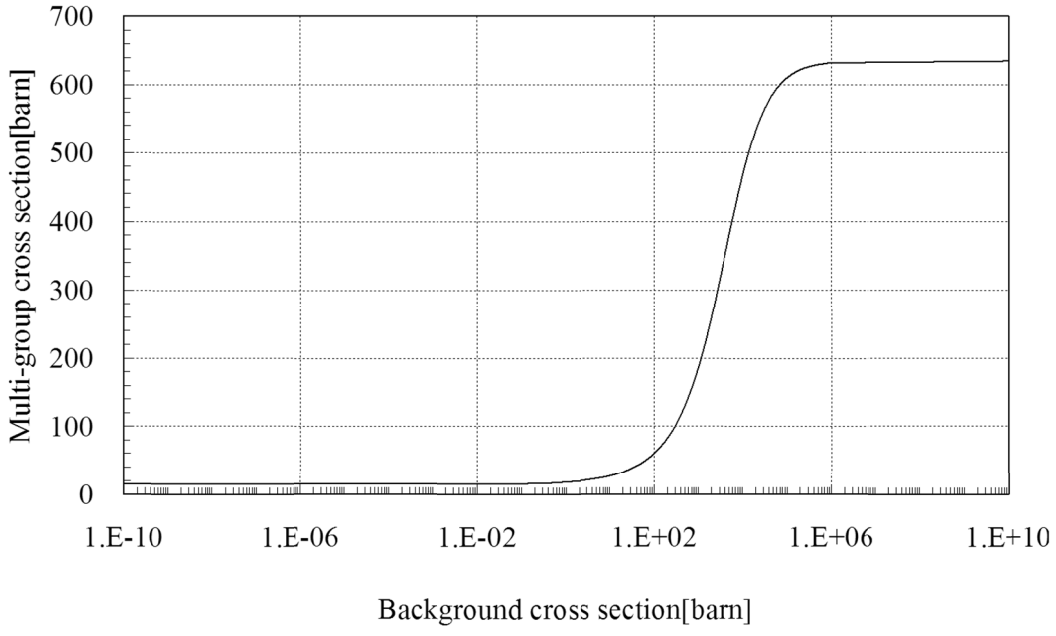

Figure 1.12 Effective cross-section as a function of background cross-section.

The homogeneous system discussed above is an ideal condition for simplified

calculation scheme. For an actual LWR fuel assembly, the fuel (^{238}U) and the moderator (hydrogen) regions are spatially distributed, i.e., the heterogeneous system. Therefore, the various heterogeneous effects should be considered to the effective cross-section. In the equivalence theory, the heterogeneous effect is simply considered by correcting the background cross-section used for the effective cross-section interpolation.

The example of homogeneous and heterogeneous systems is shown in **Figure 1.13**. In the homogeneous system, the fuel material (resonance nuclides such as ^{238}U) is homogeneously compounded in the medium, thus an escape probability of neutrons from the homogeneous medium is zero.

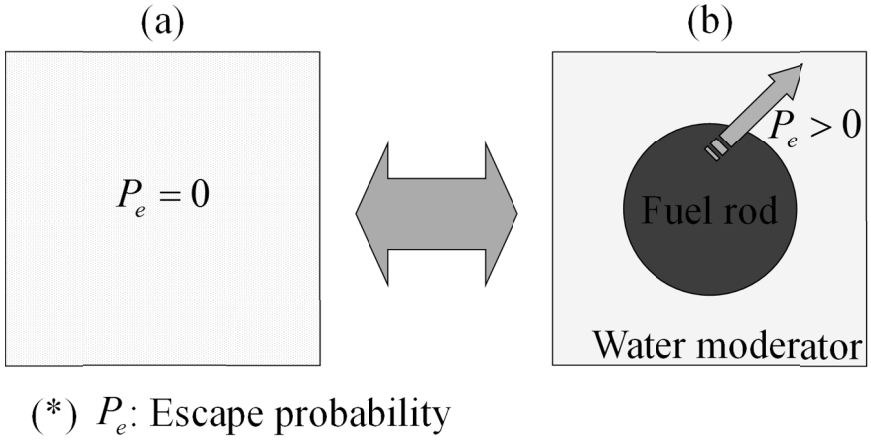

Figure 1.13 Homogeneous and heterogeneous systems ((a) Homogeneous system, (b) Heterogeneous system).

In contrast, the escape probability is always positive for general heterogeneous system owing to the finite spatial regions of fuel and moderator. The positive escape

probability promotes the mitigation of flux depression due to the resonance absorption, thus it leads to increase the effective cross-section. In the equivalence theory, the increase of effective cross-section is considered by adding the heterogeneous term against the background cross-section as follows:

$$\sigma_b \rightarrow \sigma_b + \frac{\Sigma_e}{N_r}. \tag{1.19}$$

The numerator of heterogeneous term Σ_e is called as escape cross-section, and it corresponds to the inverse of chord length for fuel lump. The chord length depends on fuel volume to surface ratio.

The above discussion for heterogeneous system considers an isolated fuel system, i.e., only one fuel lump is surrounded by infinite moderator. For the actual condition of LWR fuel assembly, the multiple cylindrical fuel rods are arranged with a lattice configuration, as shown in **Figure 1.14**.

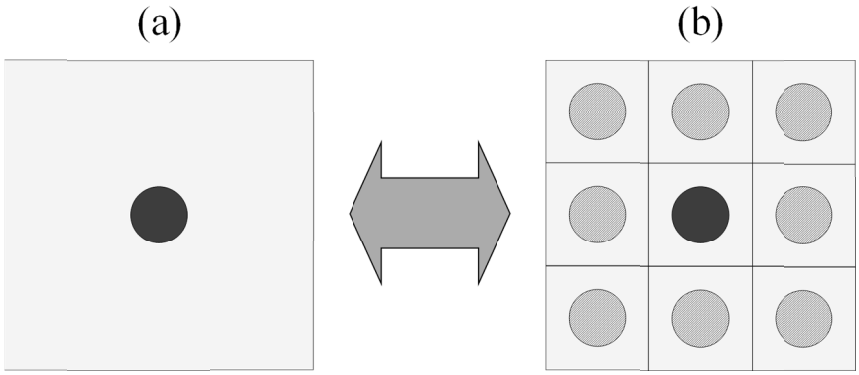

Figure 1.14 Isolated and lattice systems for heterogeneous geometry ((a) fuel isolated system, (b) fuel lattice system).

By taking into account of lattice configuration, the escape probability for the lattice system becomes smaller than that for the isolated system due to the resonance absorption of neighboring fuel rods. This effect is called as “shadowing effect” in the equivalence theory.

By incorporating the shadowing effect of neighboring fuel rods, the effective cross-sections become smaller than that for the isolated system. The decrease of effective cross-section is considered by correcting the heterogeneous term of the background cross-section as follows:

$$\sigma_b + \sigma_e \rightarrow \sigma_b + (1 - C)\frac{\Sigma_e}{N_r}. \tag{1.20}$$

The correction term C is called as a Dancoff correction factor [5-7], and it depends on the mean optical length of neutron for moderator in the lattice system.

As discussed above, the effective cross-section for the heterogeneous system is generated by interpolating the effective cross-section for the homogeneous system. The background cross-section is utilized as an interpolation argument for the magnitude of resonance self-shielding effect which includes various heterogeneous effects.

Though the above discussion is a little qualitative description, the equivalence theory is actually based on a complicated theoretical background. As a result of the many efforts in the theoretical derivation, it can achieve a very simple scheme for generation of effective cross-sections in the actual lattice physics calculation. This is an advantage of the equivalence theory, and at the same time, it is also a disadvantage for prediction accuracy of effective cross-sections due to many theoretical approximations.

1.1.5 Requirements for Advanced Resonance Self-Shielding Treatment

As shown in **Table 1.3**, the resonance self-shielding treatment influences on various neutronics parameters and related analyses.

Table 1.3 Neutronics parameters mainly related to resonance calculation.

Neutronics parameter mainly related to resonance calculation	Interface analysis
Criticality	Core nuclear design Criticality safety design (e.g., Spent nuclear fuel pool)
Doppler/moderator reactivities	Safety analysis
Intra-pellet power distribution	Fuel mechanical design (Evaluation of fuel centerline temperature)

In the conventional core design for LWRs, the equivalence theory has widely been applied as a standard resonance self-shielding treatment. It has an advantage for calculation efficiency in routine nuclear design works, while the several approximations are used. It should be reminded that the approximation sometimes assumes normal operating and shutdown condition. Thus care should be taken on the treatment of extended neutron spectrum conditions including lower moderator density ranges appeared in safety analysis.

Instead of the equivalence theory, the ultra-fine-group calculation has been applied as an alternative resonance treatment in recent years. The ultra-fine-group calculation can directly contribute to the accurate prediction of neutronics parameters such as reactivities and intra-pellet power distribution, while its huge amount of calculation

burden is an issue for practical use. In the current state, application of the ultra-fine-group calculation is generally limited to small geometries such as a pin-cell or multi-cell.

The sub-group method has the intermediate nature for calculation accuracy and efficiency, compared with the above two methods. As for the typical advantage of the sub-group method, it can efficiently predict the intra-pellet power distribution through generation of spatially-dependent effective cross-sections within a pellet. In spite of the advantage, it has also an issue for the prediction accuracy of Doppler reactivity considering non-uniform fuel temperature distribution.

From the above qualitative discussion among resonance treatments, it can be seen that the establishment of a unified resonance self-shielding methodology is an essential issue, in order to achieve both high accuracy and high efficiency for various application targets. Though the selection of the most appropriate method is one of the realistic approaches for each design application, the establishment of a unified resonance treatment will be a good alternative. The unified resonance treatment will have an advantage for the seamless treatment of extensive application ranges in the safety analysis.

1.1.6 Overall Direction for Development and Current Technical Issues

As discussed in the previous sub-section, the conventional three resonance treatments have its own advantages and disadvantages. Since all of the three resonance treatments have not been screened out on the basis of past huge amount of researches and development works, further improvement for each method is not very easy.

From this point of view, in the present study, a new resonance self-shielding methodology is developed by unifying the conventional three methods rather than the individual improvements for each method.

The target performance of the new methodology for the calculation accuracy and efficiency is illustrated in **Figure 1.15**.

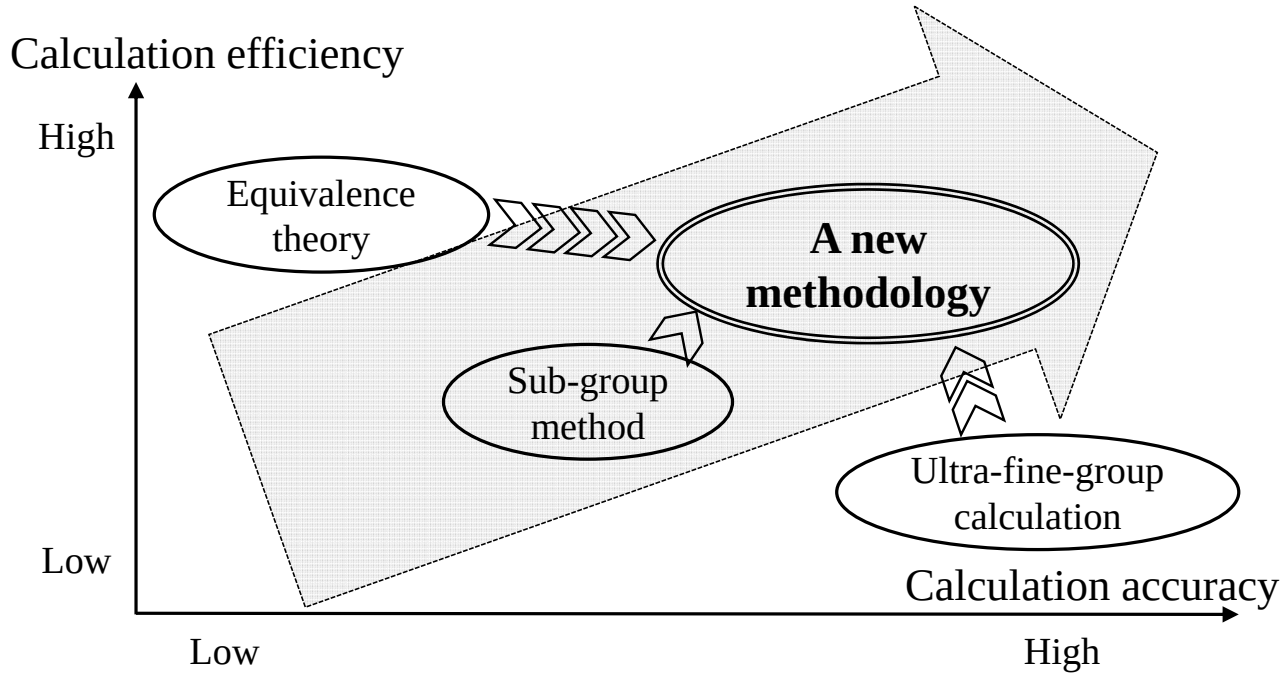

Figure 1.15 Target performance of the new methodology for the calculation accuracy and efficiency.

In the present study, the conventional equivalence theory is set as a starting point of the development. This is because the equivalence theory has an advantage for high calculation efficiency and its rich experiences for the application of lattice physics calculations. By analyzing the theoretical approximations in the conventional equivalence theory, the following technical issues can be extracted for the accuracy of equivalence theory:

(i) limitation for generalized lattice geometry

(ii) black neutron absorber assumption

(iii) scattering source approximation

(iv) resonance interference treatment

(v) radially/azimuthally dependent intra-pellet self-shielding treatment

(vi) non-uniform fuel composition and temperature treatment within a pellet

In the present study, the above issues are solved with step-by-step approach. In concrete, the essences of the ultra-fine-group calculation and the sub-group method are incorporated into the equivalence theory, while limiting additional computational burden.

By solving the above issues simultaneously, the accurate and efficient treatments of generalized geometry with extensive neutron spectrum conditions are achieved in the resonance calculation. The image for the extension of the applicable range is illustrated in **Figures 1.16-1.17**.

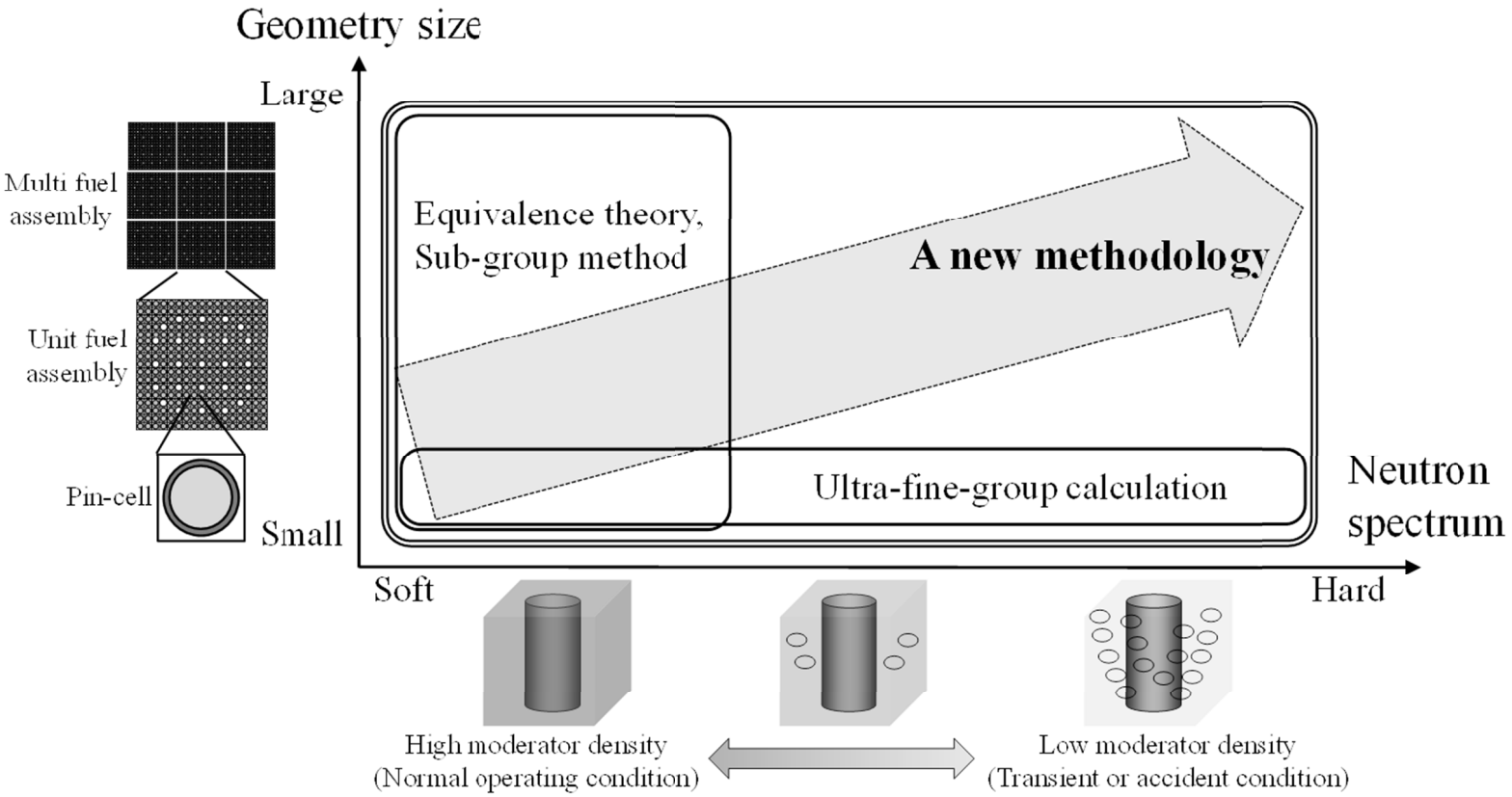

Figure 1.16 Image for the extension of global applicable range in the present resonance treatment.

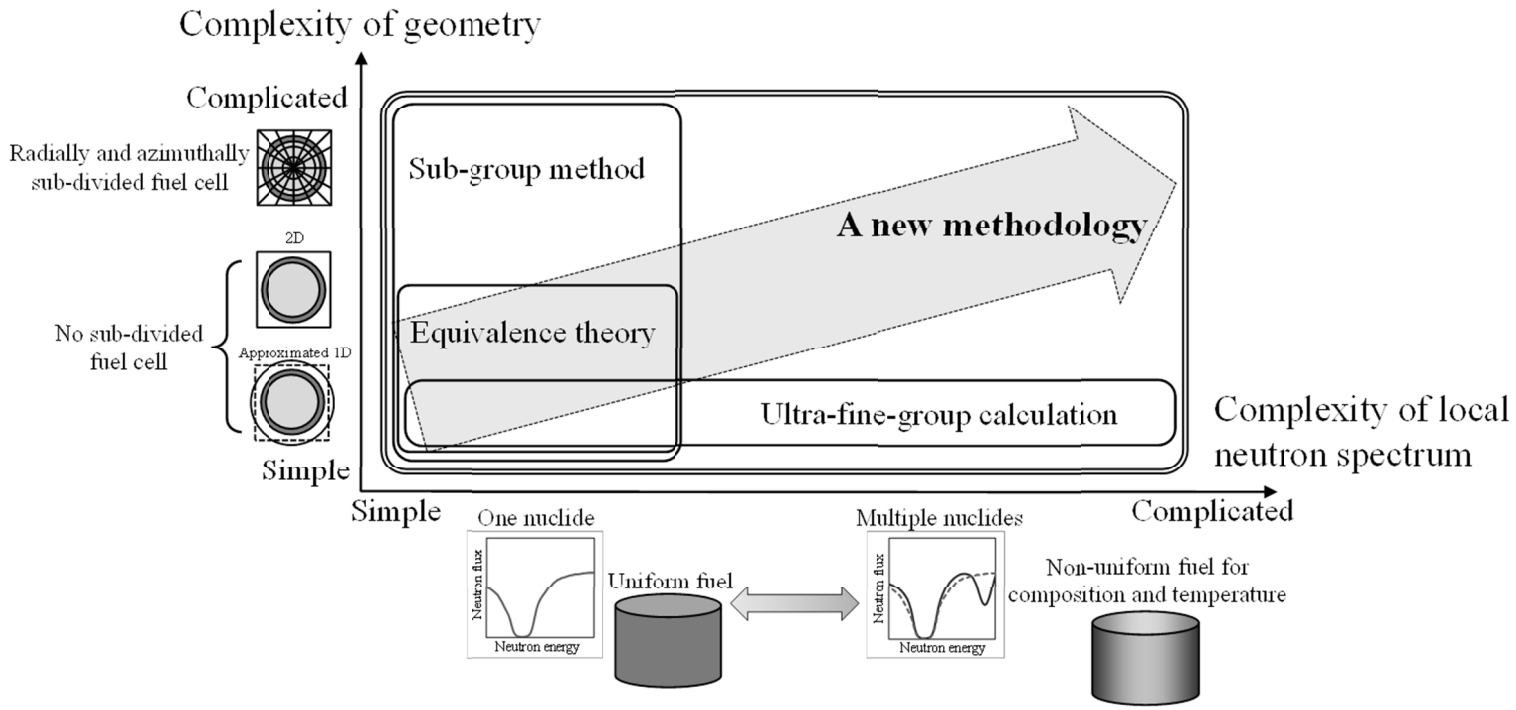

Figure 1.17 Image for the extension of local applicable range in the present resonance treatment.

1.2 Objective

From the background in the previous section, the objective of the present study is enhancement of the reactor analysis methodology through developing a unified resonance self-shielding treatment.

In this dissertation, the new resonance self-shielding methodology is established by simultaneously solving the several technical issues shown in the previous sub-section. As a result, the accurate and efficient treatments of generalized geometry with extensive neutron spectrum conditions are achieved in the resonance calculation.

Treatment of generalized geometry contributes to improvement of prediction accuracy for core nuclear design. It is also suitable for next generation core analysis methodology which can be applied to the uncertainty quantification and/or reduction of neutronics parameters.

Treatment of extensive neutron spectrum conditions contributes to the application of transient and severe accident conditions (lower moderator density ranges) appeared in safety analysis.

Through the enhancement of the methodology, the prediction accuracy of neutronics characteristics is improved, not only for the normal operation but also for the severe accident conditions of the reactors. These enhancements associated with the core analysis methodology contribute to the activities for improvement of nuclear power safety, which is an overall objective of this study.

1.3 Contents of This Dissertation

In this dissertation, the six technical issues for the resonance calculation (see sub-section 1.1.6) are solved with the step-by-step approach. By setting the conventional equivalence theory as a starting point of the development, each two issues are solved in Chapters 2-4, respectively. In a final methodology, the six issues are all solved simultaneously.

According to the above flow of the development, the contents for each chapter are briefly described as follows:

< Chapter 1 >

The background and the objective of the present study are described.

< Chapter 2 >

An advanced resonance self-shielding methodology based on the equivalence theory is developed. In the development, the two issues, i.e., (i) limitation for generalized lattice geometry and (ii) black neutron absorber assumption, are addressed by improving the conventional equivalence theory.

< Chapter 3 >

A hybrid resonance self-shielding methodology based on the equivalence theory and the ultra-fine-group calculation is developed. In the development, the two issues, i.e., (iii)

scattering source approximation and (iv) resonance interference treatment, are addressed by incorporating the essence of the ultra-fine-group calculation into the equivalence theory based method in Chapter 2.

< Chapter 4 >

A unified resonance self-shielding methodology based on the equivalence theory, the ultra-fine-group calculation and the sub-group method is developed. This is a final form of the new methodology. In the development, the two issues, i.e., (v) radially/azimuthally dependent intra-pellet self-shielding treatment and (vi) non-uniform fuel composition and temperature treatment within a pellet, are addressed by further incorporating the essence of the sub-group method into the hybrid method in Chapter 3. In the incorporating process, the sub-group method itself is improved for the non-uniform fuel composition and temperature treatment. Through the development in Chapters 2-4, all the six issues (i)-(vi) are solved simultaneously.

< Chapter 5 >

The summary and the future works of the present study are described.

1.4 References

[1] Fukuda R and Arita S. New MHI safety analysis code package for DBA (1) overview of new MHI DBA code package. Proc. of ICAPP2017 (ICAPP2017); 2017 April 24-28; Fukui and Kyoto, JPN [CD-ROM].

[2] Yamaji K, Koike H, Kirimura K and Kosaka S. New MHI safety analysis code package for DBA (2) core design code GalaxyCosmo-S. Proc. of ICAPP2017 (ICAPP2017); 2017 April 24-28; Fukui and Kyoto, JPN [CD-ROM].

[3] Sakamoto H, Maruyama M and Ogawa J. New MHI safety analysis code package for DBA (4) three-dimensional coupled code SPARKLE-2 for PWR Non-LOCA. Proc. of ICAPP2017 (ICAPP2017); 2017 April 24-28; Fukui and Kyoto, JPN [CD-ROM].

[4] Lamarsh JR. Introduction to nuclear reactor theory. Addison-Wesley, Reading, Mass; 1966.

[5] Duderstadt JJ and Hamilton LJ. Nuclear reactor analysis. John Wiley & Sons, Inc., New York; 1976.

[6] Stamm'ler RJJ, Abbate MJ. Methods of steady-state reactor physics in nuclear design. London: Academic Press; 1983.

[7] Kobayashi K. Reactor physics. Corona Publ., Tokyo, 1996 [in Japanese].

[8] Cacuci DG. Handbook of nuclear engineering, Springer, Berlin, 2010.

[9] Askew R. A characteristics formulation of the neutron transport equation in complicated geometries. Winfrith: Atomic Energy Authority; 1972 (AEEW-M1108).

[10] X-5 Monte Carlo Team. MCNP - A general N-particle transport code, version 5"

volume I: overview and theory. LA-UR-03-1987 (2003, updated 2005).

[11] Nagaya Y, Okumura K, Mori T and Nakagawa M. MVP/GMVP II: general purpose Monte Carlo codes for neutron and photon transport calculations based on continuous energy and multigroup methods. Ibaraki: Japanese Atomic Energy Research Institute (JAERI); 2005. (JAERI 1348).

[12] Homepage for Nuclear data center in Japanese Atomic Energy Agency (http://wwwndc.jaea.go.jp/index.html)

[13] Hellstrand E and Lundgren G. The resonance absorption of Uranium metal and oxide. Aktiebolaget Atomenergi, Sweden; 1962.

[14] Kier PH and Robba AA. A program for computation of resonance absorption in multiregion reactor cells. 1967. (ANL-7326).

[15] Sugimura N and Yamamoto A. Resonance treatment based on ultra-fine-group spectrum calculation in the AEGIS code. J. Nucl. Sci. Technol. 2007; **44**, 958.

[16] Okumura K, Kugo T, Kaneko K, and Tsuchihashi K. SRAC2006: A comprehensive neutronics calculation code system. Japanese Atomic Energy Agency (JAEA); 2007. JAEA 2007-004.

[17] Nikolaev MN, Ignatov AA, Isaev NV and Khokhlov VF. The method of subgroups for considering the resonance structure of the cross sections in neutron calculations. Sov. At. Energy, 1970; **29**, 689.

[18] Ribon P and Maillard J.M. Probability tables and gauss quadrature; Application to neutron cross-sections in the unresolved energy range. Topical meeting on advances in reactor physics and safety, 1986; Saratoga Springs.

CHAPTER 2. DEVELOPMENT OF ADVANCED RESONANCE SELF-SHIELDING METHODOLOGY FOR GENERALIZED LATTICE GEOMETRY AND GRAY NEUTRON ABSORBER BASED ON EQUIVALENCE THEORY

2.1 Introduction

In a recent trend of the neutron transport method, the method of characteristics (MOC) [1] is widely applied especially for the lattice calculation field. On this basis, numerical errors in multi-group neutron flux calculations become negligible. From this point of view, generation of an appropriate multi-group effective cross-section, which is used in the neutron flux calculations as an input, becomes crucial in lattice physics calculations. In the lattice physics code GALAXY [2], MOC has already been implemented as the basic method for the flux calculation. Therefore, this paper describes the detail of a new effective cross-section generation method for GALAXY.

Generation process of the effective cross-section is called the resonance calculation. In general, the resonance calculation method is classified into three categories [3], i.e., ultra-fine-group method [4], sub-group method [5] and Dancoff method [6] with equivalence theory [7]. The ultra-fine-group method gives an accurate effective cross-section, but has a limitation for the practical design applications of large and complicated geometries in the fuel assembly level because of the long computation time.

The sub-group method enables carrying out of the resonance calculation with more realistic calculation costs than the ultra-fine-group method, but it is still difficult to generate an appropriate sub-group cross-section with sufficient robustness. In contrast, the equivalence theory is the most suitable for design applications because of its short computation time and historically rich validation experiences, so it is adopted for many current lattice physics codes. However, the equivalence theory has not been improved for over 30 years, in spite of its many approximations which should be removed and are described later. From this point of view, in the present paper, the equivalence theory is selected for the improvement of its accuracy with keeping its short computation time.

The equivalence theory introduces background cross-section for considering the magnitude of resonance self-shielding effect. The multi-group cross-section is pre-tabulated as a function of the background cross-section in the homogeneous medium. Then the background cross-section for the heterogeneous system is generated considering lattice effect and multi-group effective cross-section for heterogeneous system is calculated by interpolating the above multi-group effective cross-section for homogeneous system. The equivalence theory leads to a reasonable calculation scheme because detailed information of an energy dependent cross-section is pre-computed in the cross-section library generation. However, the following approximations, which become drawbacks, are generally applied in the equivalence theory:

(1) Multi-group cross-section tabulation for discrete background cross-sections,

(2) Rational approximation for first-flight fuel escape probability,

(3) Black limit approximation for Dancoff correction,

(4) Two region approximation for heterogeneous system,

(5) Lump approximation for resonance material.

These approximations directly contribute to the reduction of calculation costs, but these are also drawbacks of the equivalence theory and cause several calculation errors.

In the present study, the above drawbacks (1)-(5) are resolved by introducing several unique and challenging techniques. The concept of the new resonance self-shielding method is described below.

Drawback (1) is resolved by developing a new cross-section library generation method based on polynomial hyperbolic tangent formulation. Drawback (2) causes inaccurate treatment of fuel escape probability for the isolated system, so it is improved by adopting multi-term rational equation for fuel escape probability with reaction-rate preservation scheme. Drawback (3) causes inaccurate treatment of fuel escape probability for the lattice system because actual resonance material is not a black material (perfect neutron absorber), so it is improved by determining coefficients in rational equation so that accuracy of the escape probability is preserved in gray resonance range. Drawback (4) is improved by executing two dimensional one-group fixed source MOC flux calculations and determining the rational coefficients using these MOC results. Drawback (5) is resolved by deriving a spatially dependent resonance self-shielding method for generation of spatially dependent effective cross-section within pellet.

In order to develop the new resonance self-shielding method, all the calculation processes based on the equivalent theory from cross-section library preparation to effective cross-section generation are reviewed and reframed by adopting the current enhanced methodologies for lattice calculations. On the basis of the above concepts, contents of each section in the present paper are summarized as follows.

Section 2.2 reviews the basic concept of the equivalence theory and derives a new cross-section library generation method. Section 2.3 clarifies the approximations of the conventional resonance self-shielding methods and derives a new resonance self-shielding method with multi-term rational approximation. Section 2.4 refers to the conventional intra-pellet power profile generation scheme and derives a new resonance self-shielding method for the treatment of spatially dependent resonance self-shielding within pellet. Section 2.5 mentions the conventional problem for the accuracy of multi-group reaction-rate and derives a formula for the reaction-rate preservation with multi-term rational equation. Section 2.6 verifies and validates the present resonance self-shielding method with lattice physics code GALAXY. Section 2.7 summarizes the conclusions of the present paper.

2.2 Cross-Section Library

2.2.1 Equivalence Theory

By applying isotropic and elastic down-scattering approximation in the center-of-mass system and ignoring fission source, the integral form of neutron transport equation is transformed to slowing down equation. The slowing down equation in the homogeneous medium is simplified by applying narrow resonance (NR) approximation for scattering source:

$$\Sigma_t(E)\phi(E) = \frac{\Sigma_p}{E}, \tag{2.1}$$

where $\Sigma_t(E)$, $\phi(E)$, and Σ_p denote macroscopic total cross-section and neutron flux for neutron incident energy E, and macroscopic potential scattering cross-section, respectively. From Equation (2.1), the neutron flux is rewritten as:

$$\phi(E) = \frac{1}{E}\frac{\Sigma_p}{\Sigma_t(E)} = \frac{1}{E}\frac{\sigma_p^r + \sigma_b^r}{\sigma_t^r(E) + \sigma_b^r}, \tag{2.2}$$

where $\sigma_t^r(E)$ and σ_p^r denote microscopic total and potential scattering cross-sections of the specific resonance nuclide r, respectively. Absorption and resonance scattering reactions for all the nuclides excluding nuclide r are ignored in the right hand side of Equation (2.2). In the following formulation, intermediate resonance (IR) parameter [8] proposed by Goldstein and Cohen will be multiplied to σ_p^r. σ_b^r corresponds to the background cross-section defined as:

$$\sigma_b^r \equiv \frac{\sum_{k \neq r} N_k \sigma_p^k}{N_r}, \tag{2.3}$$

where N_k denotes number density of the nuclide k. σ_b^r handles the magnitude of resonance self-shielding effect with competition of $\sigma_t^r(E)$ in the denominator of Equation (2.2).

Multi-group effective cross-section for multi-group transport calculation is derived with neutron flux weight for reaction-rate preservation within the energy group. Then the multi-group cross-section for group g is defined as follows:

$$\sigma_g \equiv \frac{\int_g dE \sigma(E) \phi(E)}{\int_g dE \phi(E)}. \tag{2.4}$$

As will be described in section 2.3.1, neutron flux in heterogeneous system is derived with the same form of the homogeneous one expressed in Equation (2.2). Then the same background cross-section value between heterogeneous (described in section 2.3.1) and homogeneous (Equation (2.3)) systems is regarded as an equivalent resonance self-shielding level. This assumption is called the “equivalence principle” between homogeneous and heterogeneous systems. The resonance self-shielding theory derived with the assumption of the equivalence principle is called “equivalence theory”.

On the basis of the above assumption, detailed information on the energy dependency of neutron flux for the resonance cross-section can be calculated in the homogeneous system. Specifically, the ultra-fine-group slowing down equation in homogeneous medium composed of a single resonant nuclide r (e.g., ^{238}U) and hydrogen (typical neutron moderator in LWR), is numerically solved at several σ_b

levels. Then energy dependency of $\phi(E)$ is calculated for each σ_b. By considering the definition of Equation (2.4), the multi-group cross-section in the homogeneous system is clearly expressed as a function of σ_b:

$$\sigma_g(\sigma_b) = \frac{\int_g dE\sigma(E)\phi(E,\sigma_b)}{\int_g dE\phi(E,\sigma_b)}. \tag{2.5}$$

In general resonance treatment, effective multi-group cross-section, which depends on the background cross-section, is pre-tabulated for each nuclide, reaction type, energy group and temperature, and edited as a cross-section library. Instead of the multi-group cross-section, self-shielding factor or resonance integral is often tabulated for the consistency of adopted resonance calculation methods. The self-shielding factor is defined as:

$$f_g(\sigma_b) \equiv \frac{\sigma_g(\sigma_b)}{\sigma_g(\infty)}, \tag{2.6}$$

and resonance integral is defined as:

$$I_g(\sigma_b) \equiv \frac{\int_g dE\sigma(E)\phi(E,\sigma_b)}{\Delta u_g}, \tag{2.7}$$

where Δu_g denotes lethargy width for group g.

2.2.2 New Derivation of Polynomial Hyperbolic Tangent Format Library

In many traditional lattice physics codes, the multi-group cross-section (or the resonance integral) table is prepared against less than 10 background cross-section points due to the NJOY [9] (cross-section processing code) execution constraints. This treatment is valid in the framework of conventional transport methods and energy group resolutions because the influence of cross-section interpolation accuracy is relatively small in the lattice calculations. However, the transport method adopted in GALAXY [2] is based on the more enhanced technology, i.e., the method of characteristics (MOC) [1], and the detailed XMAS 172 energy group structure [10] is directly handled in GALAXY. So the interpolation accuracy of the multi-group cross-section becomes "relatively" more obvious and the conventional expression of the cross-section library would be insufficient for cross-section interpolation. Furthermore, the multi-term rational approximation in section 2.4 handles the more wide range of background cross-section, so the cross-section interpolation accuracy should be preserved in the wide application range. From this point of view, a new robust representation method of the multi-group cross-section library is derived as follows.

The multi-group cross-section σ_g as a function of the background cross-section σ_b generally shows a logistic curve such as hyperbolic tangent function. **Figure 2.1** shows the example of logistic curve for σ_g versus σ_b. As shown in Figure 2.1, infinite dilution condition ($\sigma_b = \infty$) gives a maximum value of the multi-group cross-section, and perfect self-shielding condition ($\sigma_b = 0$) gives a minimum one. So

the following representation equation can be inductively derived:

$$\sigma_g(\sigma_b) = A\tanh\left\{a\ln\left(\frac{\sigma_b}{b}\right)\right\} + B, \tag{2.8}$$

where A, B, a and b denote arbitrary constants ($b > 0$). By taking a limit to $\sigma_b \to \infty$ or $\sigma_b \to 0$, A and B are analytically determined as:

$$\sigma_g(\infty) = A + B, \tag{2.9}$$

$$\sigma_g(0) = -A + B. \tag{2.10}$$

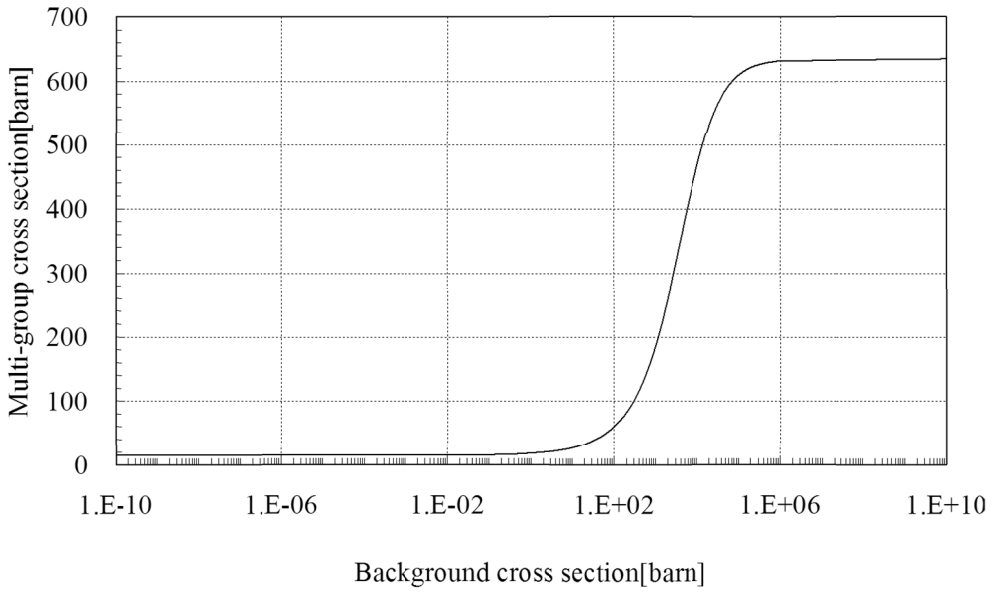

Figure 2.1 Logistic curve of multi-group cross-section versus background cross-section.

By substituting Equations (2.9) and (2.10) into Equation (2.8), σ_g is expressed as a hyperbolic tangent function of σ_b:

$$\sigma_g(\sigma_b) = \frac{\sigma_g(\infty) - \sigma_g(0)}{2} \tanh\left\{ a \ln\left(\frac{\sigma_b}{b} \right) \right\} + \frac{\sigma_g(\infty) + \sigma_g(0)}{2}. \qquad (2.11)$$

If the appropriate values of a and b are determined in all the σ_b range, the reproducibility of σ_g is improved. This equation is originally proposed for sub-group parameter generation [11], but σ_b dependency for the usual multi-group cross-section is larger than that for the sub-group cross-section. In order to improve the interpolation accuracy of σ_g, the polynomial hyperbolic tangent formulation is derived in the present study as a natural extension of Equation (2.11):

$$\sigma_g(\sigma_b) = \frac{\sigma_g(\infty) - \sigma_g(0)}{2} \sum_{l=1}^{L} c_l \tanh\left\{ a_l \ln\left(\frac{\sigma_b}{b_l} \right) \right\} + \frac{\sigma_g(\infty) + \sigma_g(0)}{2}, \qquad (2.12)$$

$$\sum_{l=1}^{L} c_l = 1. \qquad (2.13)$$

Here, a_l, b_l and c_l denote l-th coefficients ($b_l > 0$), and L denotes the number of polynomial expansion, respectively. The summation of c_l is normalized as unity. The coefficients (a_l, b_l, c_l) are determined by fitting the accurate cross-section set $(\sigma_b, \sigma_g(\sigma_b))$ with the non-linear least square fitting method. The present polynomial hyperbolic tangent expansion method enables to reduce the library storage because only $\sigma_g(\infty)$, $\sigma_g(0)$ and (a_l, b_l, c_l) are preserved. The present library represents the multi-group cross-section in all the background cross-section range with high accuracy and enough robustness when L is set to 5, as described in section 2.6.1.

2.3 Resonance Calculation with Multi-Term Rational Equation

2.3.1 Conventional Dancoff Method

The integral form of neutron transport equation for two region heterogeneous system consisting of fuel and moderator is written as:

$$\Sigma_t^f(E)\phi_f(E)V_f = \frac{1}{E}\left[P_{f\to f}(E)\Sigma_p^f V_f + P_{m\to f}(E)\Sigma_p^m V_m\right], \tag{2.14}$$

where NR (or IR) approximation is applied for scattering source. Indices f and m denote fuel region and moderator region, respectively. Here, the fuel and moderator regions correspond to the typical resonance and non-resonance material regions, respectively. V denotes region volume. $P_{f\to f}(E)$ and $P_{m\to f}(E)$ denote collision probabilities, e.g., $P_{m\to f}(E)$ is the probability that neutrons having incident energy E born in the moderator region suffer their first collisions in the fuel region.

By substituting the following reciprocity theorem and probability constraint into Equation (2.14):

$$P_{m\to f}(E)\Sigma_p^m V_m = P_{f\to m}(E)\Sigma_t^f(E)V_f, \tag{2.15}$$

$$P_{f\to f}(E) = 1 - P_{f\to m}(E), \tag{2.16}$$

neutron flux in the fuel region is formulated with analytical expression as follows:

$$\phi_f(E) = \frac{1}{E}\left[\{1 - P_{e,f}(E)\}\frac{\Sigma_p^f}{\Sigma_t^f(E)} + P_{e,f}(E)\right], \tag{2.17}$$

where $P_{f\to m}$ is rewritten as $P_{e,f}$, which corresponds to first-flight escape probability

from the fuel region.

Expression of the fuel escape probability is the main feature for the resonance self-shielding theory in the heterogeneous system based on the equivalence theory [7]. The fundamental expression is one-term rational approximation proposed by Wigner:

$$P_{e,f}^{iso}(E) = \frac{1}{\Sigma_t^f(E) l_f + 1}, \tag{2.18}$$

where l_f denotes mean chord length of the fuel lump and chord length distribution is assumed to be the exponential function. Equation (2.18) denotes the escape probability in isolated system, i.e., a single isolated fuel lump in an infinite moderator medium.

In the actual fuel assembly, multiple fuel rods are bundled with lattice arrangement and the escape probability becomes effectively smaller than that for the isolated system due to the shadowing effect of neighboring fuel rods. Physical property of the above phenomenon is considered as lattice effect in general resonance self-shielding theory. By applying isotropic approximation for incident neutrons, the fuel escape probability in the lattice system is derived as [12]:

$$P_{e,f}^{lat}(E) = \frac{(1-C)P_{e,f}^{iso}(E)}{1-\{1-\Sigma_t^f(E) l_f P_{e,f}^{iso}(E)\}C}, \tag{2.19}$$

where C denotes Dancoff correction. By substituting Equation (2.18) into Equation (2.19), $P_{e,f}^{lat}$ is generated as:

$$P_{e,f}^{lat}(E) = \frac{D}{\Sigma_t^f(E) l_f + D}, \tag{2.20}$$

where D corresponds to Dancoff factor, which satisfies:

$$D \equiv 1 - C . \tag{2.21}$$

By substituting Equation (2.20) into Equation (2.17), the neutron flux is formulated as:

$$\phi_f(E) = \frac{1}{E} \frac{\Sigma_p^f l_f + D}{\Sigma_t^f(E) l_f + D} = \frac{1}{E} \frac{\sigma_p^r + \sigma_b^r}{\sigma_t^r(E) + \sigma_b^r}, \tag{2.22}$$

where background cross-section for the heterogeneous lattice system is defined as:

$$\sigma_b^r \equiv \frac{\sum_{k \neq r} N_k^f \sigma_p^k + D / l_f}{N_r^f}, \tag{2.23}$$

where N_k^f denotes number density of the nuclide k in the fuel region. Equation (2.22) shows that the neutron flux in a heterogeneous system has the same form as that in a homogeneous system shown in Equation (2.2). In many legacy codes, the Dancoff factor is generated with the black limit condition and the heterogeneous background cross-section is calculated by Equation (2.23). Then the multi-group effective cross-section for the heterogeneous system is interpolated from the homogeneous cross-section library regarding the background cross-section as an interpolation variable.

In order to improve the accuracy of fuel escape probability, the following multi-term rational approximation for the isolated system is often applied instead:

$$P_{e,f}^{iso}(E) = \sum_{n=1}^{N} b_n \frac{a_n}{\Sigma_t^f(E) l_f + a_n}, \tag{2.24}$$

$$\sum_{n=1}^{N} b_n = 1, \tag{2.25}$$

where N denotes the number of rational equation terms. a_n and b_n denote the n

-th rational coefficients. For the cylindrical fuel lump, two-term coefficients proposed by Carlvik [7] are often used:

$$(a_1, b_1, a_2, b_2) = (2,2,3,-1). \tag{2.26}$$

The values in Equation (2.26) are generated by the black and white limit conditions for the escape probability and the blackness. By substituting Equations (2.24) and (2.25) into Equation (2.19) and using Equation (2.26), the escape probability in the lattice system is analytically derived [7] as follows:

$$P_{e,f}^{lat}(E) = \sum_{n=1}^{2} \beta_n \frac{\alpha_n}{\Sigma_t^f(E) l_f + \alpha_n}, \tag{2.27}$$

$$\alpha_1 \equiv \frac{C + 5 - \sqrt{C^2 + 34C + 1}}{2}, \tag{2.28}$$

$$\alpha_2 \equiv \frac{C + 5 + \sqrt{C^2 + 34C + 1}}{2}, \tag{2.29}$$

$$\beta_1 \equiv \frac{\alpha_2 - (1 - C)}{\alpha_2 - \alpha_1}, \tag{2.30}$$

$$\beta_2 \equiv 1 - \beta_1. \tag{2.31}$$

These coefficients, which correspond to the correction of Carlvik's two-term coefficients for considering the lattice effect, were formulated by Stamm'ler. Though C in Equations (2.28), (2.29) and (2.30) is calculated by taking into account the fuel transparency in the Stamm'ler correction, the transmission probability from the fuel surface to the cell boundary included in C is generated in the black limit condition. So the Stamm'ler correction still utilizes the black approximation. The Carlvik's two-term rational approximation with the above Stamm'ler correction is widely adopted in many current lattice physics codes.

2.3.2 Enhanced Neutron Current Method and Generalized Stamm'ler Correction

In the recent studies, the improved treatments for the resonance self-shielding are suggested. One is for complicated geometry handling [13], and another is for gray resonance treatment [14]. The above two methods are the basic concept of the new method derived in the next sub-section, so they are simply reviewed in this sub-section.

The Dancoff factor in Equation (2.23) is generally calculated by the collision probability method. Yamamoto proposed the Dancoff factor generation scheme by incorporation of MOC [13]. This is called the "enhanced neutron current method". By applying the black limit approximation consistent with the conventional Dancoff method, macroscopic total reaction-rate is converged as:

$$\lim_{\Sigma_t^f \to \infty} \Sigma_t^f \bar{\phi}_f(\Sigma_t^f) = \lim_{\Sigma_t^f \to \infty} \Sigma_t^f \frac{\Sigma_p^f l_f + D}{\Sigma_t^f l_f + D} = \Sigma_p^f + D/l_f \,, \tag{2.32}$$

where $\bar{\phi}_f$ denotes lethargy averaged neutron flux derived by Equation (2.22) with one-group approximation. Dancoff factor is then formulated by Equation (2.32) as:

$$D = \left[\lim_{\Sigma_t^f \to \infty} \Sigma_t^f \bar{\phi}_f(\Sigma_t^f) - \Sigma_p^f \right] \cdot l_f \,. \tag{2.33}$$

$\bar{\phi}_f$ is numerically obtained by the transport calculation with MOC. So the complicated spatial dependency of Dancoff factor can be handled explicitly by including neutron flux within the formulation.

On the other hand, Carlvik's two-term rational approximation with Stamm'ler correction described in the previous sub-section is often applied in many current lattice physics codes. Hébert proposed the generalization of Stamm'ler correction with

three-term equation [14]. The fuel-to-fuel collision probability in the lattice system is given by:

$$P_{f\to f}^{lat}(E) = 1 - P_{e,f}^{lat}(E) = \sum_{n=1}^{3} \beta_n \frac{\Sigma_t^f(E) l_f}{\Sigma_t^f(E) l_f + \alpha_n}, \tag{2.34}$$

$$\sum_{n=1}^{3} \beta_n = 1, \tag{2.35}$$

where n -th rational coefficients α_n and β_n are semi-analytically generated as described later, which is different from the scheme of the Stamm'ler correction. Specifically, $P_{f\to f}^{lat}$ is calculated with the collision probability method at five points of macroscopic cross-section point p and a set of $(\Sigma_t^f(p), P_{f\to f}^{lat}(p))$ is generated. Then the escape function is defined as:

$$\tilde{\Sigma}_e(\Sigma_t^f) \equiv \frac{\Sigma_t^f}{P_{f\to f}^{lat}(\Sigma_t^f)} - \Sigma_t^f . \tag{2.36}$$

In the following, the escape function $\tilde{\Sigma}_e(\Sigma_t^f)$ is considered instead of $P_{f\to f}^{lat}$ for convenience because $\tilde{\Sigma}_e(\Sigma_t^f)$ does not strongly depend on Σ_t^f. From the above set of $(\Sigma_t^f(p), P_{f\to f}^{lat}(p))$ with Equation (2.36), a set of $(\Sigma_t^f(p), E(p))$ is easily obtained. $\tilde{\Sigma}_e(\Sigma_t^f)$ can be reproduced with the following quadratic rational equation as:

$$\tilde{\Sigma}_e(\Sigma_t^f) = \frac{a(\Sigma_t^f)^2 + b\Sigma_t^f + c}{(\Sigma_t^f)^2 + d\Sigma_t^f + e}, \tag{2.37}$$

where a, b, c, d and e denote constants determined so that the set of $(\Sigma_t^f(p), \tilde{\Sigma}_e(p))$ is satisfied. By substituting Equation (2.37) into Equation (2.36), $P_{f\to f}^{lat}$ is

rewritten as:

$$P_{f\to f}^{lat} = \frac{\Sigma_t^f \cdot \{(\Sigma_t^f)^2 + d\Sigma_t^f + e\}}{(\Sigma_t^f)^3 + (a+d)(\Sigma_t^f)^2 + (b+e)\Sigma_t^f + c}. \tag{2.38}$$

On the other hand, $P_{f\to f}^{lat}$ is expressed with α_n and β_n by reducing Equation (2.34) to a common denominator as:

$$P_{f\to f}^{lat} = \frac{\Sigma_t^f \sum_{n=1}^{3} \beta_n \prod_{m\neq n} (\Sigma_t^f + \alpha_m / l_f)}{\prod_{n=1}^{3} (\Sigma_t^f + \alpha_n / l_f)}. \tag{2.39}$$

By comparing the denominator of Equations (2.38) and (2.39), the cubic equation for Σ_t^f is solved and α_n are obtained. Furthermore, by comparing the numerator of Equations (2.38) and (2.39), and considering Equation (2.35), β_n are analytically generated with d, e and α_n.

Though the calculation process of the Hébert method is a little complicated because medium parameter $\tilde{\Sigma}_e(\Sigma_t^f)$ is introduced, the essence of the method is that α_n and β_n in Equation (2.34) are determined so that the accurate escape probability of lattice system is reproduced in the various macroscopic total cross-section Σ_t^f including gray resonance range. This corresponds to the calculation process of coefficients (a, b, c, d and e) in Equation (2.37). α_n are finally generated by the above five coefficients and β_n by α_n, d and e.

On the Hébert method, the black limit approximation is excluded in the formulation.

In concrete, the accuracy of the escape probability is adaptively improved with the one-group fixed source transport calculations for various Σ_t^f points. In contrast, Carlvik's two-term rational approximation with the Stamm'ler correction includes the black approximation for derivation of the coefficients in the isolated system and the transmission probability. So the Hébert method is considerably different from the Stamm'ler correction in which the one-group fixed source transport calculation is carried out only for the black limit point. Besides, the Hébert method enables to treat the complicated geometry for which the collision probability is obtained. In the conventional methods, only the Hébert method can exactly treat the gray resonances and the complicated geometry in the framework of the multi-term rational approximation.

2.3.3 New Derivation of Multi-Term Rational Equation for General Lattice Geometry with Gray Resonance Absorbers

The resonance calculation method implemented in GALAXY [15] is based on the equivalence theory with multi-term rational equation. Though the classical equivalence theory has some approximations such as black limit assumption, the method adopted in GALAXY resolves some of these approximations and treat the more realistic neutronics behaviors for the resonance self-shielding than the conventional methods.

The conventional resonance self-shielding method adopted in many lattice physics codes for design applications, e.g., CASMO-4 [16] PHOENIX-P [7] and PARAGON [17], is based on Carlvik's two-term rational approximation with Stamm'ler correction [7]. It assumes the resonance material as a blackbody, i.e., a perfect neutron absorber. Furthermore, the geometrical configurations are treated with one-dimensional cylindrical approximation. Hébert's enhanced method adopted in DRAGON [14] can treat gray resonance absorbers (the actual material in the reactor core is not black but gray neutron absorber in general). However, it cannot be extended to the large lattice geometry because it is based on the collision probability method.

On the other hand, the new resonance calculation method described as follows can treat the general lattice geometry of the fuel assembly with the gray resonance absorbers by combination of Yamamoto's Dancoff factor generation scheme [13] and Hébert's resonance self-shielding method [14], both of which are reviewed in the previous sub-section.

In the framework of the multi-term rational approximation, the first-flight fuel escape probability in the lattice system is expressed by [14]:

$$P_{e,f}(E) = \sum_{n=1}^{N} \beta_n \frac{\alpha_n}{\Sigma_t^f(E) l_f + \alpha_n}. \tag{2.40}$$

α_n corresponds to the parameter for considering the lattice effect, and β_n corresponds to the weight of rational equation normalized as:

$$\sum_{n=1}^{N} \beta_n = 1. \tag{2.41}$$

By substituting Equations (2.40) and (2.41) into Equation (2.17), the neutron flux is rewritten as:

$$\phi_f(E) = \frac{1}{E} \sum_{n=1}^{N} \beta_n \frac{\Sigma_p^f l_f + \alpha_n}{\Sigma_t^f(E) l_f + \alpha_n} = \frac{1}{E} \sum_{n=1}^{N} \beta_n \frac{\sigma_p^r + \sigma_b^{nr}}{\sigma_t^r(E) + \sigma_b^{nr}}. \tag{2.42}$$

Here, n -th background cross-section is defined as:

$$\sigma_b^{nr} \equiv \frac{\sum_{k \neq r} N_k^f \sigma_p^k + \alpha_n / l_f}{N_r^f}. \tag{2.43}$$

Then, the microscopic effective cross-section for resonance nuclide r, reaction x and energy group g in a fuel region is derived as:

$$
\begin{aligned}
\sigma_{x,g}^{r,f} &= \frac{\int_g dE \sigma_x^r(E)\phi_f(E)}{\int_g dE \phi_f(E)} \\
&= \frac{\sum_{n=1}^{N} \beta_n \int_g dE \sigma_x^r(E) \frac{1}{E} \frac{\sigma_p^r + \sigma_b^{nr}}{\sigma_t^r(E) + \sigma_b^{nr}}}{\sum_{n=1}^{N} \beta_n \int_g dE \frac{1}{E} \frac{\sigma_p^r + \sigma_b^{nr}}{\sigma_t^r(E) + \sigma_b^{nr}}} \\
&= \frac{\sum_{n=1}^{N} \beta_n I_{x,g}^r(\sigma_b^{nr}) \Delta u_g}{\sum_{n=1}^{N} \beta_n \int_g dE \frac{1}{E} \cdot \left(1 - \frac{\sigma_a^r(E)}{\sigma_t^r(E) + \sigma_b^{nr}}\right)} \\
&= \frac{\sum_{n=1}^{N} \beta_n I_{x,g}^r(\sigma_b^{nr}) \Delta u_g}{\left(\sum_{n=1}^{N} \beta_n\right) \cdot \Delta u_g - \sum_{n=1}^{N} \beta_n \frac{1}{\sigma_p^r + \sigma_b^{nr}} \int_g dE \sigma_a^r(E) \frac{1}{E} \frac{\sigma_p^r + \sigma_b^{nr}}{\sigma_t^r(E) + \sigma_b^{nr}}} \\
&= \frac{\sum_{n=1}^{N} \beta_n I_{x,g}^r(\sigma_b^{nr})}{1 - \sum_{n=1}^{N} \beta_n \frac{I_{a,g}^r(\sigma_b^{nr})}{\sigma_p^r + \sigma_b^{nr}}},
\end{aligned}
\tag{2.44}
$$

by substituting Equation (2.42) using the definition of Equation (2.7) and considering Equation (2.41). Here, σ_x^r denotes the continuous energy cross-section for the resonance nuclide r and reaction x. $I_{x,g}^r(\sigma_b^{nr})$ denotes the effective resonance integral per lethargy width of the group for the resonance nuclide r, reaction x ($x = a$ for absorption reaction) and energy group g in the homogeneous medium, interpolated from the cross-section library with σ_b^{nr} as an argument.

Especially for the one-term rational approximation, the relationship between resonance integral and effective cross-section is derived from Equation (2.44) for reaction x and absorption reaction. By substituting the relation into Equation (2.44), the final form of effective cross-section is formulated as [15]:

$$\sigma_{x,g}^{r,f} = \frac{\sum_{n=1}^{N} \beta_n \sigma_{x,g}^{r}(\sigma_b^{nr}) \varphi_g^{r}(\sigma_b^{nr})}{\sum_{n=1}^{N} \beta_n \varphi_g^{r}(\sigma_b^{nr})}, \tag{2.45}$$

where $\sigma_{x,g}^{r}(\sigma_b^{nr})$ denotes the effective cross-section for the resonance nuclide r, reaction x ($x = a$ for absorption reaction) and energy group g in the homogeneous medium, interpolated from the cross-section library with σ_b^{nr} as an argument. $\varphi_g^{r}(\sigma_b^{nr})$ corresponds to the neutron flux of the n-th term defined as:

$$\varphi_g^{r}(\sigma_b^{nr}) \equiv \frac{\sigma_p^{r} + \sigma_b^{nr}}{\sigma_{a,g}^{r}(\sigma_b^{nr}) + \sigma_p^{r} + \sigma_b^{nr}}. \tag{2.46}$$

The microscopic effective scattering cross-section is derived in the same manner as:

$$\begin{aligned} \sigma_{s,g\to g'}^{r,f} &= \frac{\int_g dE \int_{g'} dE' \sigma_s^{r}(E \to E') \phi_f(E)}{\int_g dE \phi_f(E)} \\ &= \frac{\sum_{n=1}^{N} \beta_n I_{s,g\to g'}^{r}(\sigma_b^{nr})}{1 - \sum_{n=1}^{N} \beta_n \frac{I_{a,g}^{r}(\sigma_b^{nr})}{\sigma_p^{r} + \sigma_b^{nr}}} = \frac{\sum_{n=1}^{N} \beta_n \sigma_{s,g\to g'}^{r}(\sigma_b^{nr}) \varphi_g^{r}(\sigma_b^{nr})}{\sum_{n=1}^{N} \beta_n \varphi_g^{r}(\sigma_b^{nr})}. \end{aligned} \tag{2.47}$$

The form of Equation (2.44) and the intermediate form of Equation (2.47), which are expressed by the resonance integral, are the conventional expression and are not used in GALAXY. Instead, the final form of Equations (2.45) and (2.47), which is derived by using the relation between the resonance integral and effective cross-section, is applied.

In the present method, α_n and β_n are numerically calculated in order to accurately treat general lattice geometry and gray resonances. By averaging Equation (2.42) for the arbitrary lethargy range and assuming total cross-section to be constant in

this specific range (one-group approximation), lethargy averaged neutron flux $\bar{\phi}_f$ is formulated as:

$$\bar{\phi}_f(\Sigma_t^f) = \sum_{n=1}^{N} \beta_n \frac{\Sigma_p^f l_f + \alpha_n}{\Sigma_t^f l_f + \alpha_n}, \tag{2.48}$$

in the same manner of Equation (2.32).

Neutron flux is calculated by MOC at several macroscopic cross-section points p and a set of $(\Sigma_t^f(p), \bar{\phi}_f(p))$ is generated. Then α_n and β_n are numerically optimized so as to minimize the following objective function based on the least square fitting method:

$$\Delta\phi_{obj}^2 = \sum_{p=1}^{P} \left[\bar{\phi}_f(p) - \left\{ \sum_{n=1}^{N-1} \beta_n \frac{\Sigma_p^f l_f + \alpha_n}{\Sigma_t^f(p) \cdot l_f + \alpha_n} + \left(1 - \sum_{n=1}^{N-1} \beta_n\right) \cdot \frac{\Sigma_p^f l_f + \alpha_N}{\Sigma_t^f(p) \cdot l_f + \alpha_N} \right\} \right]^2, \tag{2.49}$$

where P denote the number of $(\Sigma_t^f(p), P_{e,f}^{lat}(p))$ data. Normalizing condition of β_n in Equation (2.41) is explicitly considered in Equation (2.49). By minimizing $\Delta\phi_{obj}^2$, α_n and β_n in Equation (2.42) are determined so that the accurate neutron flux is reproduced in the various optical length $\Sigma_t^f l_f$ including gray resonance range. Essentially, minimization of $\Delta\phi_{obj}^2$ is equivalent to determination of α_n and β_n so that the reproducibility of fuel escape probability in Equation (2.40) is improved. In this procedure, the rational coefficients in the isolated system are not necessary for derivation of the coefficients in the lattice system, which is a different point from the

Stamm'ler correction. Therefore, the present method enables to handle general geometries which beyond the simple infinite cylinder or the slab. Furthermore, the present method can treat the arbitrary number of rational equation term in principle because generation of α_n and β_n is merely numerical fitting procedure in accordance with Equation (2.49). As different from the present method, the number of rational equation term in the Hébert method is limited to three because the analytical solution of N -th equation can be derived substantially by the 3rd equation.

In the actual numerical treatment, several points of Σ_t^f between black (e.g., 10^5[1/cm]) and white (e.g., 10^{-5}[1/cm]) limit including actual gray resonance range (e.g., 10.0, 1.0, 0.1[1/cm]) are set and one group fixed source problem is solved for each Σ_t^f value. The same Σ_t^f value is set to all the resonance region because the accurate region-wise Σ_t^f is not pre-known. MOC can be adopted in the transport calculations because Equation (2.48) is expressed not as a collision probability, but as a neutron flux. In the present method, general lattice geometry can be exactly treated because MOC is directly applied for the flux calculations. Furthermore, gray resonance absorbers can be accurately treated because not only the black limit but also the gray resonance range of macroscopic total cross-sections are explicitly considered for generation of pin-wise α_n and β_n values. The present gray resonance self-shielding method can consistently treat both black and gray resonance self-shielding, and as a result, it can generate effective cross-sections with high accuracy.

In the Carlvik method with Stamm'ler correction, physical constraints only for the black and white limits are satisfied from the theoretical point of view. So the effect of

gray resonance is not “theoretically” and explicitly taken into account. On the other hand, the present resonance self-shielding method “theoretically” and explicitly takes into account the constraint to increase the accuracy of escape probability in gray resonance range with the fitting equation.

The advantage of the present method, i.e., the exact gray resonance treatment, is similar to that of the Hébert method, but the calculation process of the coefficients α_n and β_n is different between the present method and the Hébert method. In the Hébert method, the analytical treatment is partially introduced to the coefficient evaluation with a constraint which is necessary for the three-term rational equation, but the present method simply adopts to the numerical fitting procedure without any additional constraints. So the implementation of the present method is simpler than that of the Hébert method.

2.4 Spatial Self-Shielding Calculation for Intra-Pellet Power Profile Generation

2.4.1 Conventional Explicit Methods

Radial power profile within fuel pellet is required as input data for fuel integrity evaluation. In the evaluation, fuel centerline temperatures for various types of pellets are calculated with the radial power profile data given by a neutronics design code for the pin or assembly level. In order to make intra-pellet power profile data, a spatially dependent effective cross-section within the pellet should be generated.

Equivalence theory assumes that the configuration of resonance material is a lump. So, the direct formulation of the spatially dependent effective cross-sections for each ring region within the cylindrical fuel lump is a difficult task. For generation of the detailed effective cross-section data within the pellet, the more accurate resonance self-shielding methods such as sub-group method [5] or ultra-fine-group calculation method [4] are applied in general. These methods consider the detailed information of the spatial and energetic resonance self-shielding effects within each energy group, so it can directly treat the neutron balance within the pellet. In spite of this advantage, however, these methods require large calculation costs. From this background, a more simple and efficient method is desirable which suits daily design applications.

2.4.2 Stoker-Weiss Method

A resonance self-shielding method for generation of spatially dependent effective cross-section, which is based on the equivalence theory, was proposed by Stoker and Weiss [18]. In the Stoker-Weiss method, fuel escape probability from a specific ring region within the fuel lump is formulated by combination of the escape probability from each lump component. This method enables simplifying the generation scheme of spatially dependent effective cross-section. But the above escape probability of the ring region is derived for the fuel isolated system and the escape probability of ring i for the lattice system is approximately given by:

$$P_{e,i}^{lat}(E) = DP_{e,i}^{iso}(E) . \tag{2.50}$$

This approximation is not consistent with the general treatment of lattice effect in the equivalence theory, i.e., Equation (2.19).

2.4.3 New Derivation of Spatially Dependent Gray Resonance Self-Shielding Method

Inconsistency of the fuel escape probability treatment for the lattice system in Stoker-Weiss method is completely resolved in SDDM (Spatially Dependent Dancoff Method) [19] proposed by Matsumoto. But SDDM is an extension of Stamm'ler correction, so the black limit approximation, which assumes the resonance material as a blackbody, is still left. From this point of view, a new resonance self-shielding method, SDGM (Spatially Dependent Gray-Resonance-Self-Shielding Method), is derived in the present study.

SDGM is an extension of a new gray resonance self-shielding method described in section 2.3.3. Furthermore, SDGM incorporates a basic concept of the escape probability formulation for the ring region in Stoker-Weiss method and SDDM. It should be noted that the final form of effective cross-section in SDGM is the same as that in SDDM, but the coefficients α_n, β_n included in the effective cross-section are different between SDGM and SDDM.

In the Carlvik method with Stamm'ler correction, which is the basis of SDDM, the accuracy of fuel escape probability in gray resonance range is improved comparing with Wigner method with Dancoff correction. However, physical constraints only for the black and white limits are satisfied in the Carlvik method from the theoretical point of view. So the effect of gray resonance is not "theoretically" and explicitly taken into account. On the other hand, the present resonance self-shielding method described in section 2.3.3, which is the basis of SDGM, "theoretically" and explicitly takes into account the constraint to increase the accuracy of escape probability in gray resonance

range with the fitting equation. As a result, SDGM is a different approach from SDDM for the theoretical consideration of gray resonance.

Figure 2.2 shows the concept of formulating spatially dependent fuel escape probability in SDGM. It is based on the ideas of Stoker-Weiss method and SDDM. From this geometrical approach, the fuel escape probability of the specific ring i in a fuel region for the lattice system is formulated by extending the original definition of the escape probability as follows:

$$
\begin{aligned}
P_{e,i}(E) &= \frac{\text{"Effective" blackness of ring } i}{\text{Optical length of ring } i} \\
&= \frac{\left[\begin{array}{l}\text{Combination of (Escape fraction} \times \text{Blackness)} \\ \text{for four lumps which compose of ring } i\end{array}\right]}{\text{Optical length of ring } i} \\
&= \frac{1}{\Sigma_t^f(E) l_i} \times \left[\begin{array}{l} \left\{ \begin{array}{l} \rho_i \cdot \Sigma_t^f(E) l_{i,1} \sum_{n=1}^{N} \beta_n \dfrac{\alpha_n}{\Sigma_t^f(E) l_{i,1} + \alpha_n} \\ -\rho_i \cdot \Sigma_t^f(E) l_{i,2} \sum_{n=1}^{N} \beta_n \dfrac{\alpha_n}{\Sigma_t^f(E) l_{i,2} + \alpha_n} \end{array} \right\} \\ - \left\{ \begin{array}{l} \rho_{i-1} \cdot \Sigma_t^f(E) l_{i,3} \sum_{n=1}^{N} \beta_n \dfrac{\alpha_n}{\Sigma_t^f(E) l_{i,3} + \alpha_n} \\ -\rho_{i-1} \cdot \Sigma_t^f(E) l_{i,4} \sum_{n=1}^{N} \beta_n \dfrac{\alpha_n}{\Sigma_t^f(E) l_{i,4} + \alpha_n} \end{array} \right\} \end{array} \right] \\
&= \sum_{m=1}^{4} \gamma_{i,m} \sum_{n=1}^{N} \beta_n \frac{\alpha_n}{\Sigma_t^f(E) l_{i,m} + \alpha_n},
\end{aligned}
\tag{2.51}
$$

where $\gamma_{i,m}$ denotes the coefficient which captures the geometrical information of the ring i and is defined as:

$$
(\gamma_{i,1}, \gamma_{i,2}, \gamma_{i,3}, \gamma_{i,4}) \equiv \left(\frac{\rho_i l_{i,1}}{l_i}, -\frac{\rho_i l_{i,2}}{l_i}, -\frac{\rho_{i-1} l_{i,3}}{l_i}, \frac{\rho_{i-1} l_{i,4}}{l_i} \right). \tag{2.52}
$$

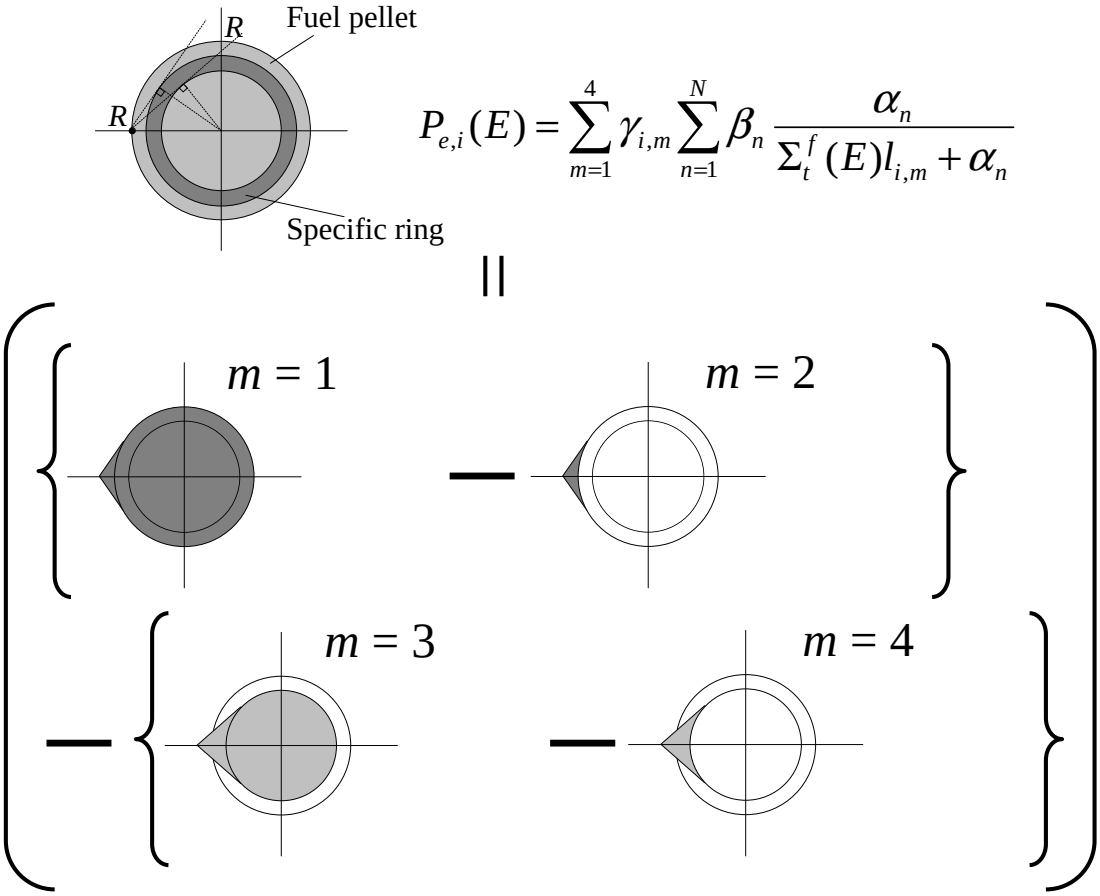

Figure 2.2 Geometrical treatment of spatially dependent fuel escape probability.

Here, l_i denotes the mean chord length derived as $l_i = 4V_i / S_f$ (V_i:volume of the ring i, S_f:pellet surface). ρ_i and ρ_{i-1} denote the relative outer and inner radii of the ring i, respectively (normalized by the pellet radius R). $l_{i,m}$ denotes the mean chord length of m-th lump (see Figure 2.2) derived by the following analytical form:

$$l_{i,m} = \frac{2R}{\pi} \cdot \left(\sqrt{1-\rho^2} + \frac{1}{\rho} \sin^{-1} \rho \pm \frac{\pi}{2} \rho \right), \quad \begin{cases} m = 1 : +\pi\rho/2, \rho = \rho_i \\ m = 2 : -\pi\rho/2, \rho = \rho_i \\ m = 3 : +\pi\rho/2, \rho = \rho_{i-1} \\ m = 4 : -\pi\rho/2, \rho = \rho_{i-1} \end{cases}. \qquad (2.53)$$

As shown in Equation (2.51), the escape probability of the fuel ring is expressed by adding and subtracting the contribution of the lumps 1, 2, 3, and 4. The relative radius ρ corresponds to the fraction of incoming neutrons which see the specific lump m from the pellet surface. So, ρ is multiplied to the first-flight blackness of each lump for considering effective escape fraction of neutrons. It should be noted that the blackness of a lump for optical length x is expressed by:

$$x \sum_{n=1}^{N} \beta_n \frac{\alpha_n}{x + \alpha_n}. \qquad (2.54)$$

Then, the neutron flux in the region i within a fuel region is described in the same manner of Equation (2.17) as:

$$\phi_i(E) = \frac{1}{E} \left[\{1 - P_{e,i}(E)\} \frac{\Sigma_p^f}{\Sigma_t^f(E)} + P_{e,i}(E) \right]. \qquad (2.55)$$

By substituting Equation (2.51) into Equation (2.55), the neutron flux is rewritten as:

$$\phi_i(E) = \frac{1}{E} \sum_{m=1}^{4} \gamma_{i,m} \sum_{n=1}^{N} \beta_n \frac{\Sigma_p^f l_{i,m} + \alpha_n}{\Sigma_t^f(E) l_{i,m} + \alpha_n}, \qquad (2.56)$$

by using the following normalizing condition for $\gamma_{i,m}$:

$$\sum_{m=1}^{4} \gamma_{i,m} = 1, \qquad (2.57)$$

which is easily obtained by substituting Equation (2.53) into Equation (2.52).

By dividing both of the numerator and the denominator in Equation (2.56) by the number density of nuclide r, Equation (2.56) is transformed to the nuclide dependent flux as:

$$\phi_i(E) = \frac{1}{E}\sum_{m=1}^{4}\gamma_{i,m}\sum_{n=1}^{N}\beta_n \frac{\sigma_p^r + \sigma_b^{nmr}}{\sigma_t^r(E) + \sigma_b^{nmr}}, \tag{2.58}$$

where n-th background cross-section for m-th lump is defined as:

$$\sigma_b^{nmr} \equiv \frac{\sum_{k\neq r} N_k^f \sigma_p^k + \alpha_n / l_{i,m}}{N_r^f}. \tag{2.59}$$

Finally, by using Equation (2.58), the microscopic effective cross-section for the resonance nuclide r, reaction x and energy group g in a region i within the fuel pellet is derived as:

$$\sigma_{x,g}^{r,i} = \frac{\int_g dE\,\sigma_x^r(E)\phi_i(E)}{\int_g dE\,\phi_i(E)} = \frac{\sum_{m=1}^{4}\gamma_{i,m}\sum_{n=1}^{N}\beta_n I_{x,g}^r(\sigma_b^{nmr})}{1-\sum_{m=1}^{4}\gamma_{i,m}\sum_{n=1}^{N}\beta_n \frac{I_{a,g}^r(\sigma_b^{nmr})}{\sigma_p^r + \sigma_b^{nmr}}} = \frac{\sum_{m=1}^{4}\gamma_{i,m}\sum_{n=1}^{N}\beta_n \sigma_{x,g}^r(\sigma_b^{nmr})\varphi_g^r(\sigma_b^{nmr})}{\sum_{m=1}^{4}\gamma_{i,m}\sum_{n=1}^{N}\beta_n \varphi_g^r(\sigma_b^{nmr})}. \tag{2.60}$$

The present resonance self-shielding method can generate spatially dependent effective cross-sections by Equation (2.60) with numerically generated coefficients α_n, β_n and analytically calculated coefficient $\gamma_{i,m}$ which capture the effect of exact gray resonances and detailed geometrical configurations. Though the fundamental derivation of the spatially dependent effective cross-section is based on SDDM, α_n and β_n of

SDDM correspond to those of Stamm'ler correction derived in section 2.3.1, which is based on the black assumption in Dancoff correction. In contrast for SDGM, α_n and β_n are generated considering the exact gray resonances as described in section 2.3.3. It means that SDGM can handle the more actual behavior of neutrons to resonance material than SDDM for generation of spatially dependent effective cross-section.

2.5 Reaction-Rate Preservation for Multi-Term Rational Equation

2.5.1 Conventional Methods

Many lattice physics codes adopt multi-term rational approximation such as Carlvik's two-term method with Stamm'ler correction. In spite of the remarkable improvement in the accuracy of escape probability, however, the multi-term method often shows less accuracy for multi-group reaction-rate than Wigner's one-term method with Dancoff correction. This problem has been solved by empirical correction of resonance integral table or partial implementation of the ultra-fine-group slowing down calculation in many current lattice physics codes.

2.5.2 Derivation of Constraint for Integrated Reaction-Rate Preservation

In the present study, a fundamental reason for the reaction-rate error based on the multi-term rational approximation is discussed and a constraint equation is derived from the view point of the reaction-rate preservation, which is completely consistent with the multi-term expression based on the equivalence theory.

This method is originally suggested in Ref. 20, and a detailed explanation of this method is described there, so supplementary verification is carried out in section 2.6.4 with the gray resonance self-shielding method (see section 2.3.3).

The integrated reaction-rate for the resonance nuclide r, reaction x and energy group g in fuel region (resonance material region) is rigorously written as:

$$RR_{x,g}^{r,f}(continuous) = \int_g dE \sigma_x^r(E)\phi_f(E). \tag{2.61}$$

It can be evaluated by the continuous energy Monte-Carlo or the ultra-fine-group slowing down calculations.

On the other hand, for the deterministic lattice code, multi-group effective cross-section $\sigma_{x,g}^{r,f}$ is generated by resonance calculation, and by using $\sigma_{x,g}^{r,f}$, multi-group neutron flux $\phi_{f,g}$ is obtained by transport calculation. On this basis, the integrated reaction-rate is derived as:

$$RR_{x,g}^{r,f}(multi\ group) = \sigma_{x,g}^{r,f}\phi_{f,g}. \tag{2.62}$$

Ratio of the reaction-rates based on multi-group (Equation (2.62)) and the continuous energy (Equation (2.61)) is transformed to the ratio of fluxes as follows:

$$\frac{\sigma_{x,g}^{r,f}\phi_{f,g}}{\int_g dE\sigma_x^r(E)\phi_f(E)} = \frac{\frac{\int_g dE\sigma_x^r(E)\phi_f(E)}{\int_g dE\phi_f(E)}\cdot\phi_{f,g}}{\int_g dE\sigma_x^r(E)\phi_f(E)} = \frac{\phi_{f,g}}{\int_g dE\phi_f(E)}. \tag{2.63}$$

In the multi-term rational approximation, neutron flux per lethargy is derived from Equation (2.42):

$$\begin{aligned}\frac{\phi_{f,g}}{\Delta u_g} &= \sum_{n=1}^{N}\beta_n\frac{\sigma_p^r+\sigma_b^{nr}}{\sigma_{t,g}^{r,f}+\sigma_b^{nr}} = \sum_{n=1}^{N}\beta_n\frac{\sigma_p^r+\sigma_b^{nr}}{\frac{\int_g dE\sigma_t^r(E)\phi_f(E)}{\int_g dE\phi_f(E)}+\sigma_b^{nr}} \\ &= \int_g dE\phi_f(E)\cdot\sum_{n=1}^{N}\beta_n\frac{\sigma_p^r+\sigma_b^{nr}}{\int_g dE[\sigma_t^r(E)+\sigma_b^{nr}]\cdot\phi_f(E)}.\end{aligned} \tag{2.64}$$

By substituting Equation (2.64) into Equation (2.63) and considering Equation (2.42), the reaction-rate ratio is expressed as:

$$\frac{\sigma_{x,g}^{r,f}\phi_{f,g}}{\int_g dE\sigma_x^r(E)\phi_f(E)} = \sum_{n=1}^{N}\beta_n\frac{[\sigma_p^r+\sigma_b^{nr}]\cdot\Delta u_g}{\int_g dE[\sigma_t^r(E)+\sigma_b^{nr}]\frac{1}{E}\sum_{l=1}^{N}\beta_l\frac{\sigma_p^r+\sigma_b^{lr}}{\sigma_t^r(E)+\sigma_b^{lr}}}. \tag{2.65}$$

The right hand side of Equation (2.65) is not unity except for the one-term rational approximation ($N=1$). This fact implies that the multi-group reaction-rate does not reproduce the continuous energy-based reaction-rate on the assumption of the multi-term rational approximation. This is why the multi-term rational approximation cannot obtain high accuracy of the multi-group reaction-rate without empirical corrections.

On the other hand, the present resonance self-shielding method described in section 2.3.3 reproduces the multi-group neutron flux or the reaction-rate based on the

multi-term rational approximation. Here, it should be noted that the non-preservation of the reaction-rate shown in Equation (2.65) is discussed within the framework of the multi-term rational approximation based on the equivalence theory, thus the present discussion cannot be expanded to other resonance treatments such as the ultra-fine-group method. The general discussion for the non-preservation of the reaction-rate in a resonance calculation is described in Ref. 21 using the SPH factor.

In order to improve the accuracy of resonance calculation, the effective cross-section should be generated so that the continuous energy-based reaction-rate is preserved. By considering Equation (2.42) and the effective cross-section derivation scheme in Equation (2.44), the continuous energy-based reaction-rate is transformed as:

$$\begin{aligned} RR_{x,g}^{r,f} &= \int_g dE\sigma_x^r(E)\phi_f(E) = \sum_{n=1}^{N}\beta_n\int_g dE\sigma_x^r(E)\phi_f(E,\sigma_b^{nr}) \\ &= \sum_{n=1}^{N}\beta_n I_{x,g}^r(\sigma_b^{nr})\Delta u_g = \sum_{n=1}^{N}\beta_n\sigma_{x,g}^r(\sigma_b^{nr})\varphi_g^r(\sigma_b^{nr})\Delta u_g \\ &= \sum_{n=1}^{N}\beta_n\sigma_{x,g}^r(\sigma_b^{nr})\frac{\sigma_p^r+\sigma_b^{nr}}{\sigma_{a,g}^r(\sigma_b^{nr})+\sigma_p^r+\sigma_b^{nr}}\Delta u_g . \end{aligned} \tag{2.66}$$

On the other hand, the multi-group-based reaction-rate is expressed as:

$$RR_{x,g}^{r,f} = \sigma_{x,g}^{r,f}\phi_{f,g} = \sigma_{x,g}^{r,f}\sum_{n=1}^{N}\beta_n\frac{\sigma_p^r+\sigma_b^{nr}}{\sigma_{t,g}^{r,f}+\sigma_b^{nr}}\Delta u_g = \sigma_{x,g}^{r,f}\sum_{n=1}^{N}\beta_n\frac{\sigma_p^r+\sigma_b^{nr}}{\sigma_{a,g}^{r,f}+\sigma_p^r+\sigma_b^{nr}}\Delta u_g . \tag{2.67}$$

As shown in the above discussion through Equation (2.65), Equations (2.66) and (2.67) are not consistent in multi-term rational approximation. From this point of view, the effective cross-section in Equation (2.67) should be modified so that the

reaction-rate given by Equation (2.67) reproduces that by Equation (2.66). By defining the modified effective cross-section and neutron flux as $\tilde{\sigma}_{x,g}^{r,f}$ and $\tilde{\phi}_{f,g}$, respectively, Equation (2.67) is rewritten as:

$$RR_{x,g}^{r,f} = \tilde{\sigma}_{x,g}^{r,f}\tilde{\phi}_{f,g} = \tilde{\sigma}_{x,g}^{r,f}\sum_{n=1}^{N}\beta_n \frac{\sigma_p^r + \sigma_b^{nr}}{\tilde{\sigma}_{t,g}^{r,f} + \sigma_b^{nr}}\Delta u_g = \tilde{\sigma}_{x,g}^{r,f}\sum_{n=1}^{N}\beta_n \frac{\sigma_p^r + \sigma_b^{nr}}{\tilde{\sigma}_{a,g}^{r,f} + \sigma_p^r + \sigma_b^{nr}}\Delta u_g ,$$

(2.68)

where $\tilde{\sigma}_{x,g}^{r,f}$ in Equation (2.68) is different from the result of Equation (2.45), and $\tilde{\phi}_{f,g}$ in Equation (2.68) is formulated by integrating Equation (2.42) for the energy group g and assuming total cross-section to be constant in this specific group (one-group approximation). Equation (2.68) consists with the formulation of the multi-term rational equation.

For generation of the appropriate $\tilde{\sigma}_{x,g}^{r,f}$, the right hand side of Equation (2.68) should preserve the right hand side of Equation (2.66). From this necessary condition, the following equation is derived:

$$\tilde{\sigma}_{x,g}^{r,f}\sum_{n=1}^{N}\beta_n \frac{\sigma_p^r + \sigma_b^{nr}}{\tilde{\sigma}_{a,g}^{r,f} + \sigma_p^r + \sigma_b^{nr}} = \sum_{n=1}^{N}\beta_n \sigma_{x,g}^r(\sigma_b^{nr}) \frac{\sigma_p^r + \sigma_b^{nr}}{\sigma_{a,g}^r(\sigma_b^{nr}) + \sigma_p^r + \sigma_b^{nr}} . \qquad (2.69)$$

Each physical quantity except for $\tilde{\sigma}_{x,g}^{r,f}$ is already generated in the conventional resonance calculation scheme described in section 2.3.3. For the actual generation of $\tilde{\sigma}_{x,g}^{r,f}$, the effective absorption cross-section is first modified by the following iteration scheme:

$$\tilde{\sigma}_{a,g}^{r,f}(\mathrm{n}+1)=\frac{\sum_{n=1}^{N}\beta_n\sigma_{a,g}^{r}(\sigma_b^{nr})\dfrac{\sigma_p^r+\sigma_b^{nr}}{\sigma_{a,g}^{r}(\sigma_b^{nr})+\sigma_p^r+\sigma_b^{nr}}}{\sum_{n=1}^{N}\beta_n\dfrac{\sigma_p^r+\sigma_b^{nr}}{\tilde{\sigma}_{a,g}^{r,f}(\mathrm{n})+\sigma_p^r+\sigma_b^{nr}}}, \tag{2.70}$$

where Equation (2.70) is derived from Equation (2.69). $\tilde{\sigma}_{a,g}^{r,f}(\mathrm{n})$ and $\tilde{\sigma}_{a,g}^{r,f}(\mathrm{n}+1)$ denote the modified effective absorption cross-sections in n-th and n+1-th iterations, respectively. $\tilde{\sigma}_{a,g}^{r,f}$ for n+1-th iteration is generated by using n-th iteration results and the iteration is repeated until $\tilde{\sigma}_{a,g}^{r,f}$ is converged. The modified effective cross-section except for absorption reaction is then generated by once through process as:

$$\tilde{\sigma}_{x,g}^{r,f}=\frac{\sum_{n=1}^{N}\beta_n\sigma_{x,g}^{r}(\sigma_b^{nr})\dfrac{\sigma_p^r+\sigma_b^{nr}}{\sigma_{a,g}^{r}(\sigma_b^{nr})+\sigma_p^r+\sigma_b^{nr}}}{\sum_{n=1}^{N}\beta_n\dfrac{\sigma_p^r+\sigma_b^{nr}}{\tilde{\sigma}_{a,g}^{r,f}+\sigma_p^r+\sigma_b^{nr}}}. \tag{2.71}$$

The method can easily generate the effective cross-section that preserves the multi-group reaction-rate, only by using the intermediate quantities generated in the resonance calculation.

2.6 Verification and Validation

In this section, verification and validation of the present resonance self-shielding method are carried out. Sub-sections 2.6.1-2.6.4 correspond to the verification of key component methods described in sections 2.2, 2.3, 2.4 and 2.5, respectively. Sub-sections 2.6.5-2.6.7 correspond to the validation of the present resonance self-shielding method with transport and depletion calculation methods adopted in the lattice physics code GALAXY. The actual contents of each sub-section are shown below.

<Sub-section 2.6.1>

Verification of cross-section interpolation accuracy for polynomial hyperbolic tangent format library described in section 2.2

<Sub-section 2.6.2>

Verification of one-group, multi-term reaction-rate accuracy for gray resonance optical range based on new and conventional methods described in section 2.3

<Sub-section 2.6.3>

Verification of reaction-rate accuracy for intra-pellet multi-region geometry based on a new spatially dependent resonance self-shielding method described in section 2.4

<Sub-section 2.6.4>

Verification of multi-group reaction-rate accuracy based on a reaction-rate preservation scheme described in section 2.5

<Sub-section 2.6.5>

Validation of effective multiplication factor and pin-by-pin fission rate accuracies of fuel assembly calculated by the present resonance self-shielding method with the method of characteristics, which is the transport method implemented to GALAXY

The validation is carried out by comparison with continuous energy Monte-Carlo calculation results.

<Sub-section 2.6.6>

Validation of spatially dependent burnup and nuclide composition accuracies calculated by the present resonance self-shielding method with the transport and depletion methods implemented to GALAXY

The validation is carried out by the post irradiation examination analysis.

<Sub-section 2.6.7>

Validation of fuel rod power accuracies calculated by the present resonance self-shielding method with the transport method implemented to GALAXY

The validation is carried out by the critical experiment analysis of VIP.

2.6.1 Interpolation Accuracy of Hyperbolic Tangent Library

First verification is to evaluate the interpolation accuracy of cross-section for hyperbolic tangent format library described in section 2.2.2. The accuracy of the multi-group capture cross-section of ^{238}U for 300.0K in 6.16-7.52eV (88th group in XMAS 172 group structure [10]) is verified because large resonance of ^{238}U in 6.7eV corresponds to the most typical resonance of fuel material and its calculation accuracy is important in LWR lattice calculations. 40 sets of the multi-group cross-section versus background cross-section data between infinite dilution and fully self-shielding conditions are prepared by execution of NJOY GROUPR module [9]. The order of polynomial L in Equation (2.12) is changed from 1 to 5 in order to confirm an appropriate L value. It should be noted that the larger L becomes, the better accuracy is expected, but at the same time, the more memory storage is necessary.

Figure 2.3 shows the result of the above verification with reference cross-section and indicates that accuracy of the cross-section for overall range of the background cross-section is merely less than 0.5% when L is set to 5. The influence of maximum error (0.5%) to the effective multiplication factor is very small.

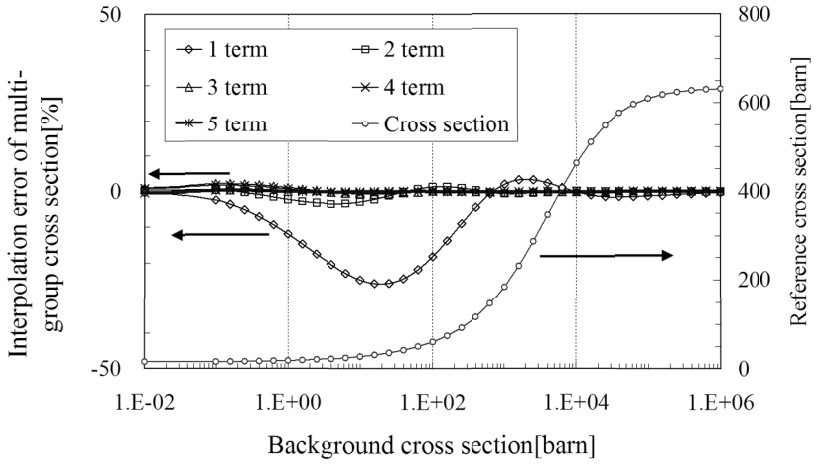

Figure 2.3 Interpolation accuracy of cross-section for polynomial hyperbolic tangent format library.

In this case, the number of original NJOY output is $40\times2=80$ and the number of the present library data is $5\times3+2=17$, respectively. It corresponds to almost 80% reduction of library data with preservation of the accuracy for the cross-section. Here, 40 points of the cross-section data is required especially for SDGM application. In SDGM, the order of background cross-section for ^{238}U is 10-1000 barn, so the more detailed and robust cross-section reconstruction is required comparing to the conventional resonance treatment which treats a resonance material as a lump.

From this result, the applicability and efficiency of the cross-section library with the present polynomial hyperbolic tangent format for lattice physics code are confirmed, and GALAXY library has been unified to hyperbolic tangent format in the actual development.

2.6.2 Reconstruction Accuracy of Reaction-Rate for Gray Resonance

Second verification is to evaluate the reconstruction accuracy of reaction-rate for gray resonance self-shielding method described in section 2.3.3. Rational coefficients (α_n, β_n) are numerically generated and the following multi-term rational equation based on macroscopic total reaction-rate is reconstructed:

$$RR_t^f(\Sigma_t^f) = \Sigma_t^f \bar{\phi}_f(\Sigma_t^f) = \Sigma_t^f \sum_{n=1}^{N} \beta_n \frac{\Sigma_p^f l_f + \alpha_n}{\Sigma_t^f l_f + \alpha_n}. \tag{2.72}$$

The coefficients (α_n, β_n) of the present gray resonance self-shielding method are generated by fitting procedure of Equation (2.49). For comparison, (α_n, β_n) of the conventional methods are also calculated. In Wigner's one-term rational approximation with Dancoff correction, (α_n, β_n) are given by:

$$(\alpha_1, \beta_1) = (D, 1), \tag{2.73}$$

which is easily obtained by comparison between Equation (2.20) and Equation (2.40).

On the other hand, in Carlvik's two-term rational approximation with Stamm'ler correction, (α_n, β_n) are given by Equations (2.28)-(2.31). Stoker-Weiss method with no-subdivision of pellet needs a little different treatment. By applying Equation (2.24) to Equation (2.50) and substituting the escape probability into Equation (2.17) with a little complicated formulation, the following macroscopic total reaction-rate is derived:

$$RR_t^f(\Sigma_t^f) = \Sigma_t^f \bar{\phi}_f(\Sigma_t^f) = \Sigma_t^f \cdot \left[(1-D)\frac{\Sigma_p^f}{\Sigma_t^f} + D\sum_{n=1}^{N} b_n \frac{\Sigma_p^f l_f + a_n}{\Sigma_t^f l_f + a_n} \right], \tag{2.74}$$

where coefficients (a_n, b_n) for isolated system are given by Equation (2.26) in the present verification. Dancoff factor D (or Dancoff correction C) used in the above conventional methods is calculated by Equation (2.33).

The benchmark problem for the present verification is a simplified single fuel pin cell model shown in **Figure 2.4**. Details of the model are shown in **Table 2.1**. These conditions represent a typical LWR situation. The uranium oxide fuel and the water moderator in the room temperature condition are assumed. The cladding is omitted for simplicity. The detailed calculation conditions are shown in **Table 2.2**.

Table 2.1 Specifications of the unit-cell model.

Physical quantity		Set up value
Number density in fuel region[1/barn/cm]	^{238}U	2.0×10^{-2}
	^{235}U	1.0×10^{-3}
	^{16}O	4.0×10^{-2}
Number density in moderator region[1/barn/cm]	^{1}H	6.0×10^{-2}
	^{16}O	3.0×10^{-2}
Temperature[K]		293
Fuel radius[cm]		0.4
Cell pitch[cm]		1.26

Table 2.2 Calculation conditions.

Item	Conditions
Calculated quantity	Microscopic effective capture cross section of ^{238}U
Energy group	88, 80, 75, 69 and 67th group in XMAS 172 group [10]
Energy range	88th: 6.16-7.52[eV]
	80th: 19.45-22.60[eV]
	75th: 33.72-37.27[eV]
	69th: 55.60-67.90[eV]
	67th: 75.67-91.66[eV]
Flux solver	GALAXY [2]
Cell boundary condition	Perfect reflection
Evaluated nuclear data file	ENDF/B-VII.0
Point wise cross section calculator	NJOY (Ver.99.259) [9]
Another methods for comparison	Wigner's single term rational approximation [6]
	Stamm'ler's two terms rational approximation [7]
Methods for evaluating background cross section and Dancoff correction factor	Enhanced neutron current method [13]

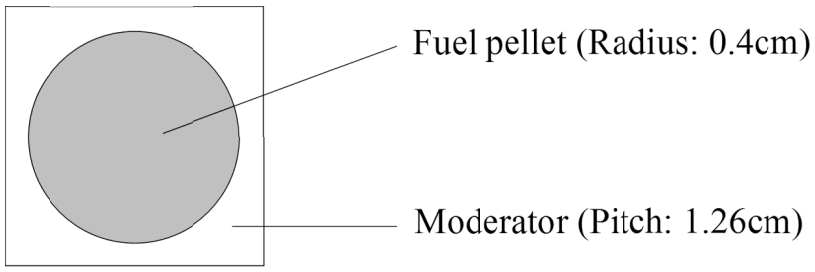

Figure 2.4 Simplified unit-cell model.

Table 2.3 shows the calculated results of coefficients for the multi-term rational equation. **Figure 2.5** shows the accuracy of reaction-rate reconstructed by Equations (2.72) and (2.74) versus various optical length $\Sigma_t^f l_f$ for each method. Accuracy of the

reaction-rate depends on the accuracy of flux in Equation (2.42). Fundamentally, it is equivalent to the accuracy of fuel escape probability in Equation (2.40). The reference reaction-rate is generated by the one-group fixed source MOC transport calculations for each Σ_t^f .

Table 2.3 Results of coefficients for multi-term rational equation.

Method		Wigner	Stamm'ler	Present		
The number of terms		1	2	1	2	3
Coefficients[-]	α_1	0.77915 [1)]	1.14774	0.81306	1.62393	1.16794
	β_1	1.00000	1.12600	1.00000	4.73022	23.98950
	α_2		4.07311		1.85156	1.34937
	β_2		-0.12600		-3.73022	-11.39820
	α_3					1.02325
	β_3					-11.59130
[1)] Dancoff factor						

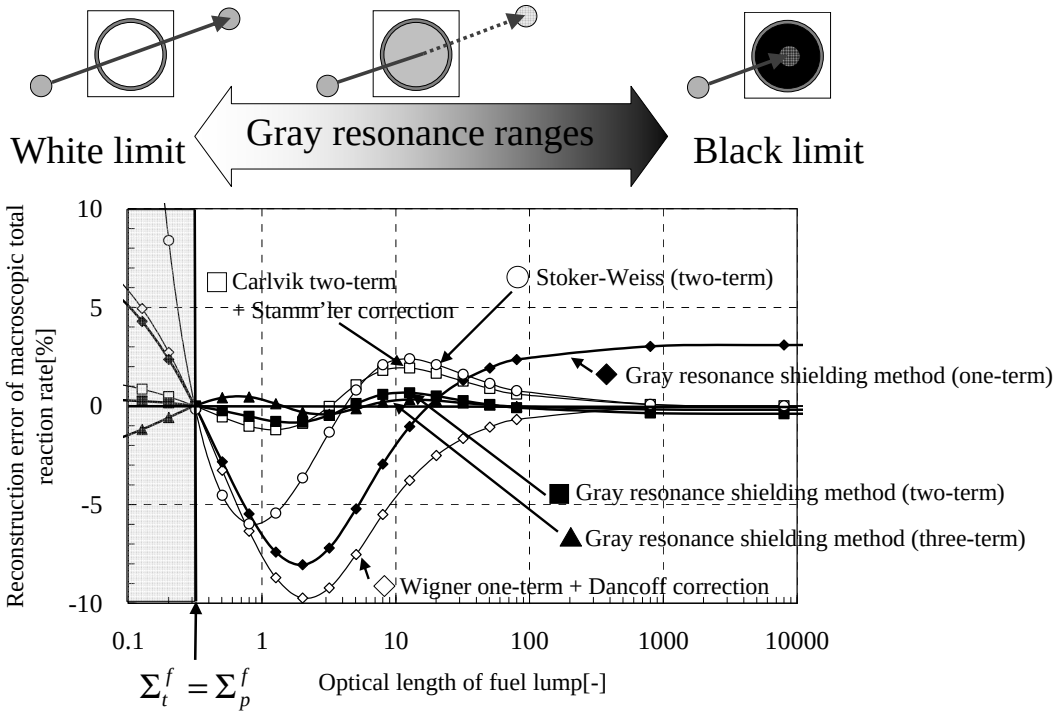

Figure 2.5 Reconstruction accuracy of macroscopic total reaction-rate for each method.

As shown in Figure 2.5, Wigner's one-term method with Dancoff correction preserves the reaction-rate in the black limit, but cannot reconstruct the reaction-rate in gray resonance range. Carlvik's two-term method with Stamm'ler correction improves the accuracy of Wigner's method. The accuracy of the Stoker-Weiss method with no-subdivision of pellet has an intermediate trend between Wigner and Carlvik methods. The present multi-term gray resonance self-shielding method further improves the accuracy of Carlvik method with Stamm'ler correction.

The relative difference of ^{238}U effective capture cross-sections from reference

solutions is shown in **Table 2.4**. The reference solutions are obtained from the direct ultra-fine-group calculation for heterogeneous geometry. In order to quantify the net improvement for the present method, the NR approximations are applied to the scattering source for the reference calculations.

From Table 2.4, it can be seen that the present method for $N = 3$ produces the more accurate results than the Stamm'ler's method for all the energy groups. It is also found that the present method can consistently generate the effective cross-sections including "gray resonances" with high accuracy. The present method for $N = 2$ produces slightly better results than that for $N = 3$ in most cases, but $N = 3$ gives better results for 67^{th} group, which is rather small resonance thus considered as gray compared to other resonances.

Table 2.4 Relative difference of ^{238}U effective capture cross-sections from reference solutions for unit-cell.

Method	The number of rational function terms	Relative diference[%]				
		88^{th} gr.	80^{th} gr.	75^{th} gr.	69^{th} gr.	67^{th} gr.
Wigner	1	-0.37	-1.38	-2.10	-3.69	-6.72
Stamm'ler	2	0.72	0.55	0.59	0.58	-0.21
Present	1	0.87	-0.01	-0.51	-1.94	-5.33
	2	0.14	0.05	0.04	0.06	-0.37
	3	-0.22	-0.17	-0.14	0.08	-0.13

This verification clarifies the effectiveness of considering gray resonances in Equation (2.49). While the conventional methods do not explicitly treat the gray

resonance range to the reaction-rate (or the fuel escape probability), the present gray resonance self-shielding method explicitly handles the gray resonance absorption. From the discussion, the applicability of the present method for the effective cross-section generation is confirmed. The present gray resonance self-shielding method shows high accuracy in gray resonance range, so the method improves the accuracy not only for the large and wide resonances in low energy range but also for the narrow resonances in the higher energy range (> 100eV).

Simplified multi-cell model is also prepared as shown in **Figure 2.6**. It consists of 4×4 square unit-cells and the part of them is water cells without any resonance nuclides. The composition of isotopes in the water cell is the same with the moderator composition for the above pin-cell model. The irregular lattice effect in this model can easily be considered by the present method without any analytical formulation efforts such as Stamm'ler's [7].

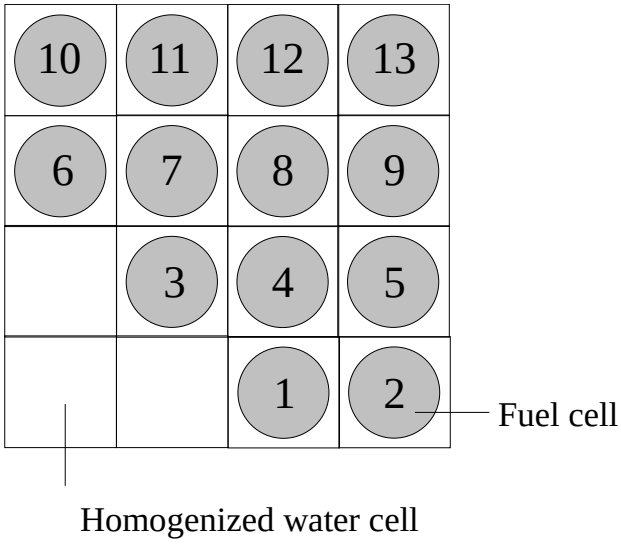

Figure 2.6 Simplified multi-cell model.

The relative difference of ^{238}U effective capture cross-sections from reference solutions is shown in **Table 2.5**. Effective cross-sections for 67th group are generated since 67th group includes the gray resonances of ^{238}U. Each region number in Table 2.5 corresponds to those in Figure 2.6. From Table 2.5, it is confirmed that the present method can generate effective cross-sections with high accuracy not only for the simplified single pin-cell model, but also for the irregular multi-cell model.

Table 2.5 Relative difference of ^{238}U effective capture cross-sections from reference solutions for multi-cell.

Method	The number of rational function terms	Relative difference [%]							
		Reg.1	Reg.2	Reg.3	Reg.4	Reg.5	Reg.8	Reg.9	Reg.13
Wigner	1	-7.24	-6.86	-7.64	-6.96	-6.79	-6.84	-6.77	-6.79
Stamm'ler	2	-0.20	-0.36	-0.22	-0.33	-0.28	-0.33	-0.27	-0.30
Present	1	-5.78	-5.45	-6.12	-5.53	-5.40	-5.43	-5.38	-5.38
	2	-0.48	-0.39	-0.57	-0.41	-0.39	-0.38	-0.38	-0.37
	3	-0.15	-0.13	-0.18	-0.13	-0.13	-0.15	-0.13	-0.13

2.6.3 Comparison with Monte-Carlo Results for Intra-Pellet Multi-Region Geometry

Third verification is to evaluate the accuracy of intra-pellet reaction-rate distribution generated by SDGM described in section 2.4.3. The gray resonance self-shielding method in section 2.3.3 and SDGM have been implemented to GALAXY. For the verification of SDGM, absorption reaction-rate distributions within a fuel pellet obtained by GALAXY are compared with those by continuous energy Monte Carlo code MVP [22]. The simple pin cell models for the typical UO_2 and MOX fuel at room temperature condition of PWR are prepared for the calculations. Reflective boundary condition is applied. The absorption reaction-rate distributions of the important actinide nuclides are calculated by subdividing the pellet into 10 equal volume rings for radial direction. The specifications of the calculation condition are shown in **Table 2.6**, and geometrical configuration is shown in **Figure 2.7**.

Table 2.6 Specifications of the unit-cell Monte-Carlo benchmark.

Physical quantity	Set up conditions
Material temperature[K]	300.0
Pellet radius[cm]	0.4095
Pellet division	10 regions with equal volume
Cladding outer radius[cm]	0.4750
Cladding thickness[cm]	0.0655 (gap is omitted for simplicity)
Cell pitch[cm]	1.260
Fuel type	UO_2(4.1wt%^{235}U)
	MOX (7.1wt%Pu fissile contents)
Cladding type	Zr4 (Few nuclides except for Zr are omitted for simplicity)
Moderator type	H_2O
Boron concentration[ppm]	500

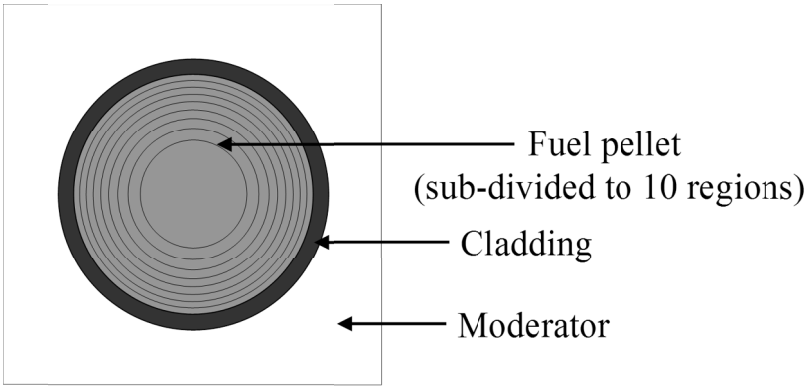

Figure 2.7 Geometrical configuration of unit cell model.

Figures 2.8 and **2.9** show the comparison of microscopic absorption reaction-rates for ^{238}U in UO_2 and MOX between GALAXY with SDGM (square points) and MVP (rectangular lines). The accuracy of reaction-rates for 88^{th} (6.16-7.52eV), 80^{th} (19.5-22.6eV) and 75^{th} (33.7-37.3eV) groups including wide resonances of ^{238}U in XMAS 172 energy group structure are confirmed. The relative differences are smaller than 16% for UO_2 and 9% for MOX fuels, respectively. On the other hand, **Figures 2.10** and **2.11** show the comparison of energy integrated macroscopic absorption reaction-rates for each nuclide between GALAXY with SDGM (square points) and MVP (rectangular lines). The relative differences are smaller than 1% for UO_2 and 2% for MOX fuels except for ^{242}Pu in center region. The results obtained by GALAXY with SDGM and MVP show some differences for the multi-group wise reaction-rate distribution in detailed XMAS 172 group structure. However, the energy integrated reaction-rate, which is a more important parameter to estimate the intra-pellet power profile, shows good agreement. Therefore, it can be concluded that SDGM can predict

nuclide dependent reaction-rate distributions with high accuracy for practical applications.

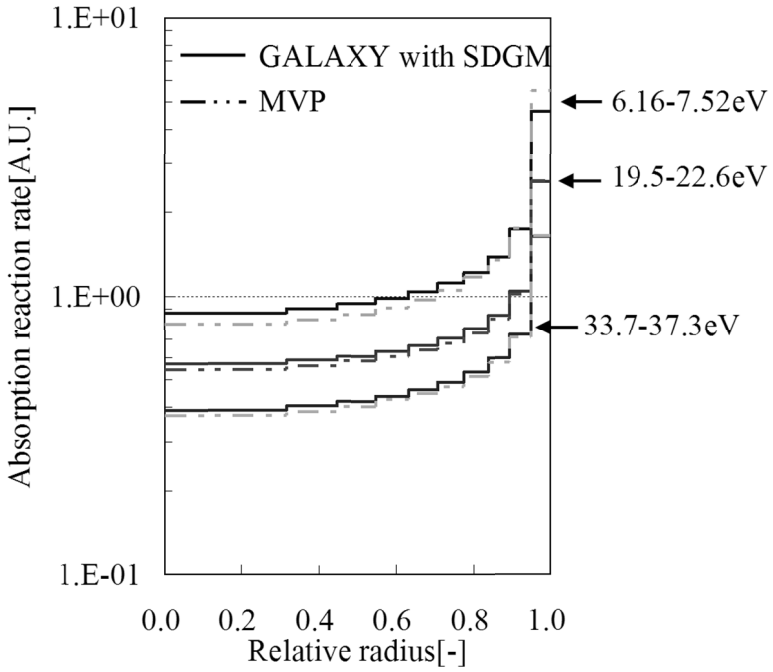

Figure 2.8 Comparison of intra-pellet microscopic absorption reaction-rate distribution for UO_2 between GALAXY with SDGM and MVP for important resonances of ^{238}U.

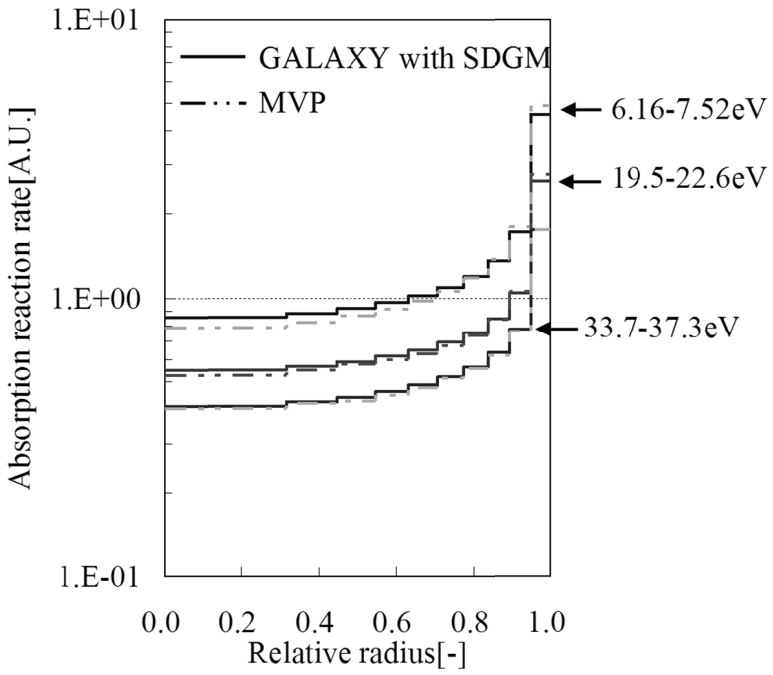

Figure 2.9 Comparison of intra-pellet microscopic absorption reaction-rate distribution for MOX between GALAXY with SDGM and MVP for important resonances of ^{238}U.

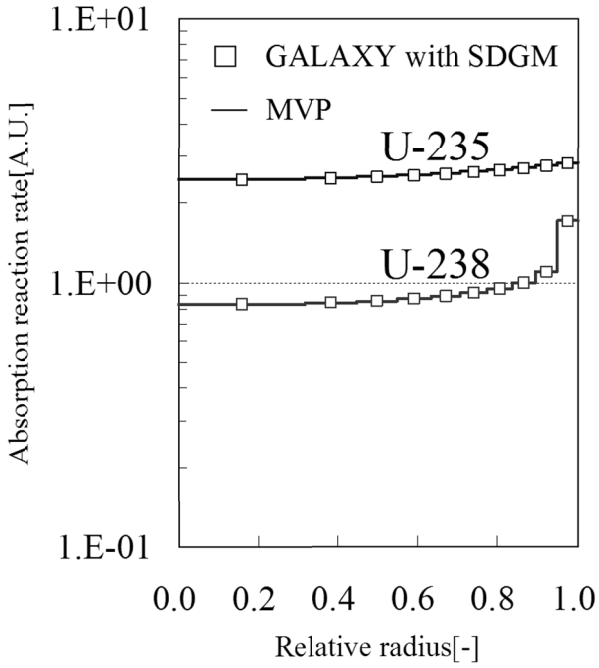

Figure 2.10 Comparison of intra-pellet macroscopic absorption reaction-rate distribution for UO_2 between GALAXY with SDGM and MVP for each nuclide.

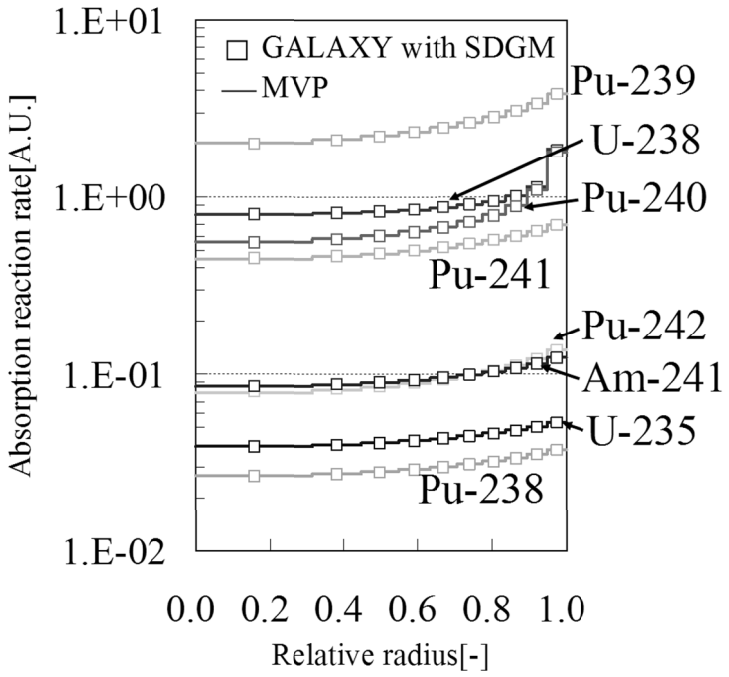

Figure 2.11 Comparison of intra-pellet macroscopic absorption reaction-rate distribution for MOX between GALAXY with SDGM and MVP for each nuclide.

The important advantage of GALAXY for the application of power profile generations is short computation time comparing with a continuous energy Monte Carlo code. Especially for the microscopic depletion calculation with radial subdivision of pellet, extremely large computational load is necessary in the Monte Carlo code in order to achieve small statistical error. Furthermore, the number of actinide and fission product nuclides directly affects computation time of Monte Carlo code. Deterministic code such as GALAXY does not have such a disadvantage at all. The calculation speed of GALAXY with depletion calculation is much faster than that of continuous energy Monte Carlo code.

The verification of SDGM for irregular multi-cell geometry is also carried out. The specifications of the calculation condition are shown in **Table 2.7**, and the geometrical configuration is shown in **Figure 2.12**. Each pellet is numbered (1 to 8) for convenience.

Table 2.7 Specifications of the multi-cell Monte-Carlo benchmark.

Physical quantity	Set up conditions
Material temperature[K]	300.0
Pellet radius[cm]	0.4095
Pellet division	10 regions with equal volume
Cladding outer radius[cm]	0.4750
Cladding thickness[cm]	0.0655 (gap is omitted for simplicity)
Guide tube outer radius[cm]	0.612
Guide tube thickness[cm]	0.041
Cell pitch[cm]	1.260
Fuel type	UO_2(4.1wt%^{235}U)
	MOX (7.1wt%Pu fissile contents)
	UO_2(2.6wt%^{235}U) with 6.0wt%Gd_2O_3
Cladding and guide tubes type	Zr4 (Few nuclides except for Zr are omitted for simplicity)
Moderator type	H_2O
Boron concentration[ppm]	500

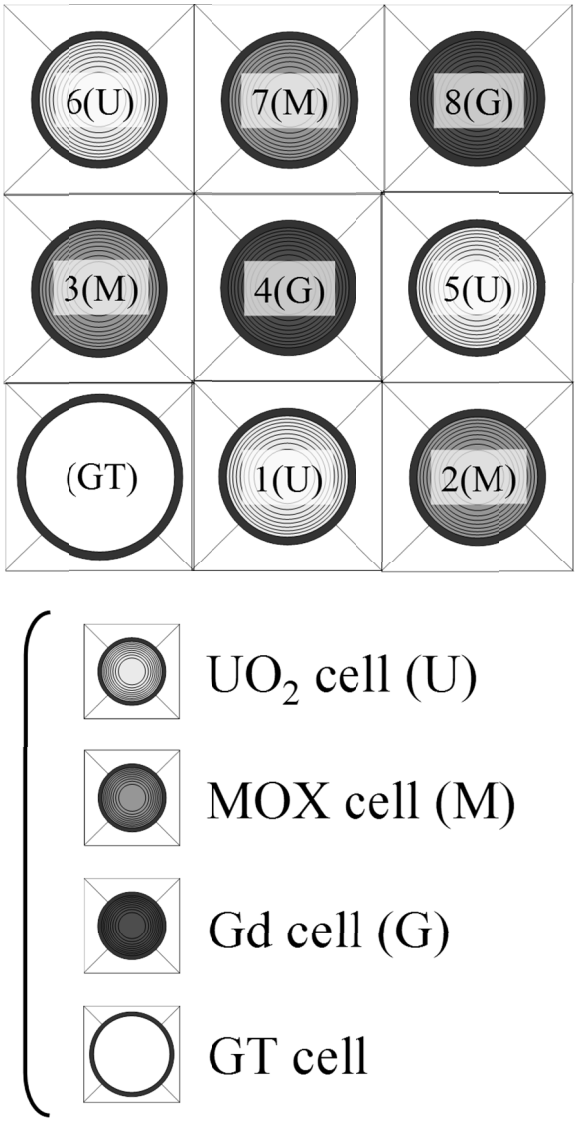

Figure 2.12 Geometrical configuration of multi-cell model.

A 3×3 multi-cell model, including three UO_2 fuel cells, three MOX fuel cells, two UO_2 + Gd_2O_3 fuel cells and one guide tube cell, is prepared for the calculation. The room temperature condition is assumed. The specification of this 3×3 multi-cell model is a pseudo one only used for the overall verification. The geometrical configuration of this benchmark is complicated because of irregularity including the non-fuel cell located

in the asymmetrical position. Boundary condition of this problem is perfect reflection, so the guide tube region simply simulates a large water hole located in the center of BWR fuel assembly. On this basis, each pellet region is divided into 10 equal volume rings for radial direction. Four types of color cells in the range between black and white resonance absorption are irregularly arranged, i.e., MOX fuels and UO_2 + Gd_2O_3 fuels are almost black, UO_2 fuels are gray and guide tube region is almost white from the viewpoint of resonance calculation. If the calculation accuracy for the present four-color problem is good, the robustness of SDGM can be confirmed.

Figure 2.13 shows the comparison of the energy-integrated macroscopic absorption reaction-rate distributions for each pellet between GALAXY with SDGM (points) and MVP (rectangular lines). The relative differences are smaller than 2% for all rings in each pellet. From this result, the good agreement is confirmed. Because MOX and UO_2 + Gd_2O_3 fuels are the strong neutron absorbers, the steep gradient of reaction-rate distribution is observed within pellet. As widely known in the field of "microscopic reactor physics", the gradient for UO_2 + Gd_2O_3 pellet is especially remarkable from the neutronics point of view.

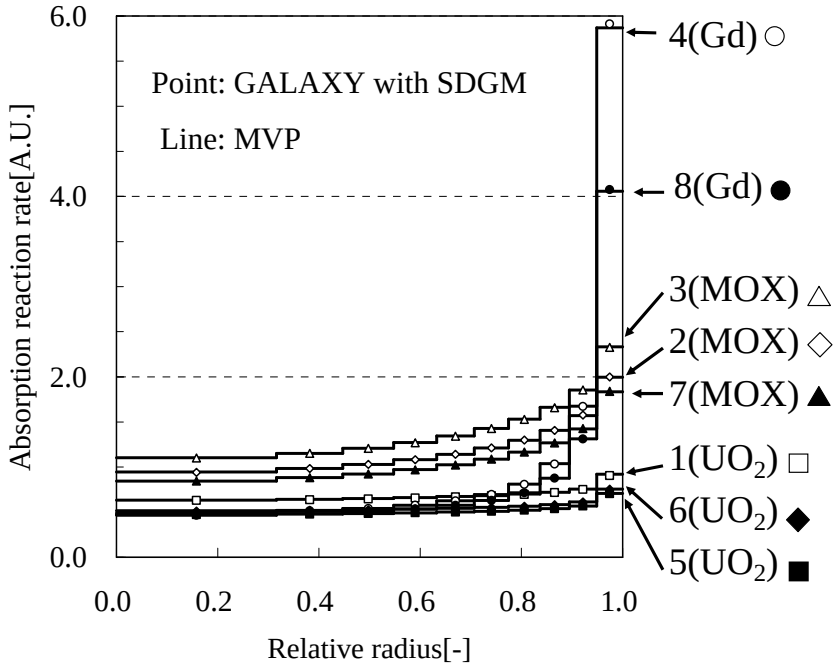

Figure 2.13 Comparison of intra-pellet macroscopic absorption reaction-rate distribution between GALAXY with SDGM and MVP for each fuel rod.

Both SDGM and SDDM (conventional method) obtain effective cross-sections of an annularly sub-divided pellet (multi-region system) based on the resonance calculation result of a pellet (one-region system) using the geometrical information of intra-pellet sub-division. So the improvement from SDDM (implemented to the current nuclear design code) to SDGM (implemented to GALAXY) is shown in the difference of pellet one-region result between the current nuclear design code and GALAXY.

From the view point of applicability to PWR core analysis, the accuracy of reactivity is excellent in both codes, but the accuracy of fuel rod power is improved in GALAXY within the uncertainty of nuclear hot channel factor. Not only the pin-cell but also the 3× 3 multi-cell results shown above already clarify the effect of gray resonance and

two-dimensional lattice treatment in GALAXY. The effect of overall improvement from the current nuclear design code to GALAXY would be more clearly shown through comparison with the reference value, i.e., measurement. From this point of view, calculation accuracy of fuel rod power is confirmed through critical experiment analysis in sub-section 2.6.7.

It can be concluded that SDGM can accurately predict the reaction-rate distribution of highly heterogeneous system with the complicated geometry. It means that GALAXY can execute both transport and resonance calculations consistently with the exact two-dimensional geometry from the pellet to assembly level.

2.6.4 Comparison with Monte-Carlo Results for Multi-Group Reaction-Rate

Fourth verification is to evaluate the accuracy of multi-group reaction-rate with reaction-rate preservation method described in section 2.5.2. The method has been implemented to GALAXY. The simple pin cell models for the typical UO_2 fuel at room temperature condition of PWR are prepared for the calculations. The multi-group transport calculation is carried out and both the effective multiplication factor and the multi-group absorption reaction-rate of ^{238}U are obtained. The specification of the calculation condition is the same as that of the UO_2 pin cell problem in the section 2.6.3, but pellet region is not sub-divided. The gray resonance self-shielding method with reaction-rate preservation is applied in GALAXY calculation. Furthermore, the gray resonance self-shielding method without reaction-rate preservation and Wigner's one-term method with Dancoff correction are also carried out for comparison. The reference result is obtained by MVP.

Table 2.8 shows the comparison of the effective multiplication factor between GALAXY and MVP. **Figure 2.14** shows the absolute difference of the multi-group absorption reaction-rate between GALAXY and MVP. In the case of the gray resonance self-shielding method without reaction-rate preservation, the overestimation for multi-group absorption reaction-rate of ^{238}U influences the underestimation of the multiplication factor. On the other hand, the gray resonance self-shielding method with reaction-rate preservation improves the accuracy of multi-group reaction-rate, and as a result, the multiplication factor is accurately calculated. Wigner's one-term method with Dancoff correction generates the accurate effective multiplication factor, but it is a result of group-to-group cancel-out, as shown in Figure 2.14. From this result, the

applicability of the present method for the reaction-rate preservation is confirmed.

Table 2.8 Comparisons of effective multiplication factor between GALAXY and MVP.

Code	Methodology	Effective multiplication factor[-]	Difference from MVP results[pcm]
GALAXY	Gray resonance method with reaction rate preservation	1.38313	-17
	Gray resonance method without reaction rate preservation	1.37956	-275
	Wigner one term method with Dancoff correction	1.38369	23
MVP	Continuous energy Monte-Carlo method	1.38337	10 (Statistical error)
			Note: (GALAXY-MVP)/MVPx10^5

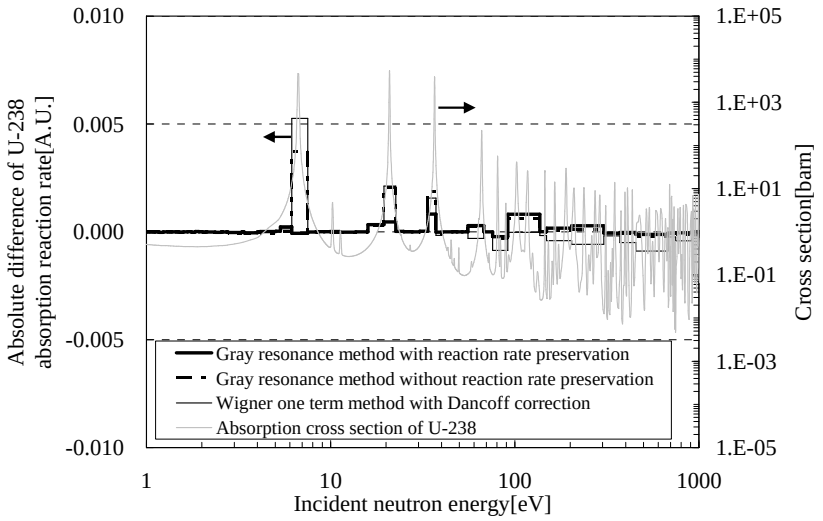

Figure 2.14 Comparison of multi-group reaction-rate between GALAXY and MVP.

2.6.5 Extensive Monte-Carlo Benchmark for Commercial PWR Fuel Assembly

For the total validation of new resonance self-shielding methods with multi-group MOC transport calculation, the effective multiplication factor and the pin-by-pin fission rate distribution in commercial PWR fuel assembly obtained by GALAXY are compared with those by MVP. The verification of each key method described in sections 2.2, 2.3, 2.4 and 2.5 has been carried out in the previous sub-sections. The objective of this validation is to confirm the overall accuracy of the present resonance self-shielding method with the transport calculation method for the PWR fuel assembly calculations, which are the main use of the lattice physics code GALAXY.

The specifications of the calculation condition are shown in **Table 2.9**. As shown in Table 2.9, fuel type, lattice arrangement, fuel composition, thermal-hydraulic condition, boron concentration and type of inserted rod are widely changed for overall validation. The present extensive benchmark problem is generated by orthogonal table [23], which is widely applied in quality engineering field. The number of parameter combinations based on Table 2.9 is about several tens of thousands, so the reduction of the benchmark set is required for efficient validation. By introducing the orthogonal table, the number of calculations in the benchmark is effectively reduced to less than one thousand.

Table 2.9 Specifications of the extensive Monte-Carlo benchmark.

Parameter	Condition
Fuel type	UO_2, UO_2 with Gd_2O_3, MOX, UO_2 with Er_2O_3
Lattice arrangement	14x14, 15x15, 17x17
Fuel composition	0.75-9.0wt% ^{235}U in UO_2
	6.0, 10.0wt% Gd_2O_3 in UO_2 + Gd_2O_3
	3.1-13.0wt% Pu contents in MOX
	5.0wt% Er_2O_3 in UO_2 + Er_2O_3
Thermo-hydraulic condition	300-1800K for fuel temperature
Boron concentration	0-3500ppm
Inserted rod	Non insertion, RCC, BP (Pyrex, B_4C)

Figure 2.15 shows the difference of effective multiplication factor between GALAXY and MVP. The differences are almost smaller than 200pcm (0.2% Δk) in all cases. The accuracy of effective cross-section has a large influence for predicting the appropriate effective multiplication factor, so the present resonance self-shielding methods drastically contribute to the robust accuracy of lattice physics calculations.

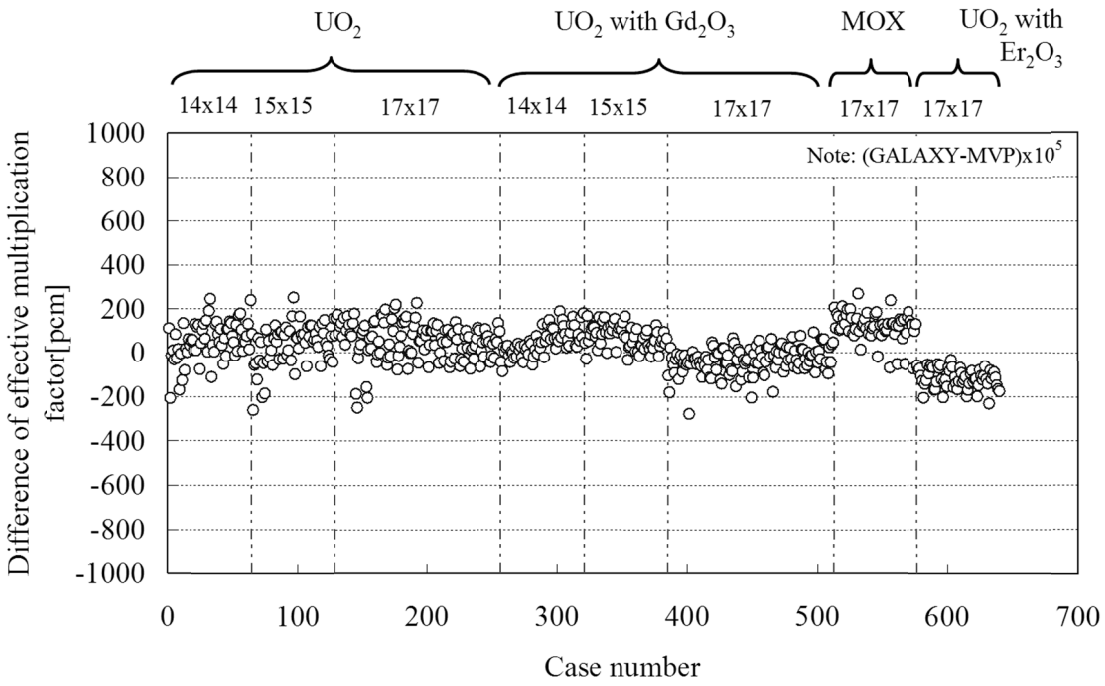

Figure 2.15 Comparison of effective multiplication factor between GALAXY and MVP.

On the other hand, **Figure 2.16** shows the standard deviation for the difference of pin-by-pin fission rate spatial distribution between GALAXY and MVP. The standard deviations are almost smaller than 0.5% in all cases. The accuracy of reaction-rate spatial distribution is roughly determined by the selected transport method. So, the present resonance self-shielding methods and MOC are the good combination for generating both the effective multiplication factor and the fission rate distribution with high accuracy.

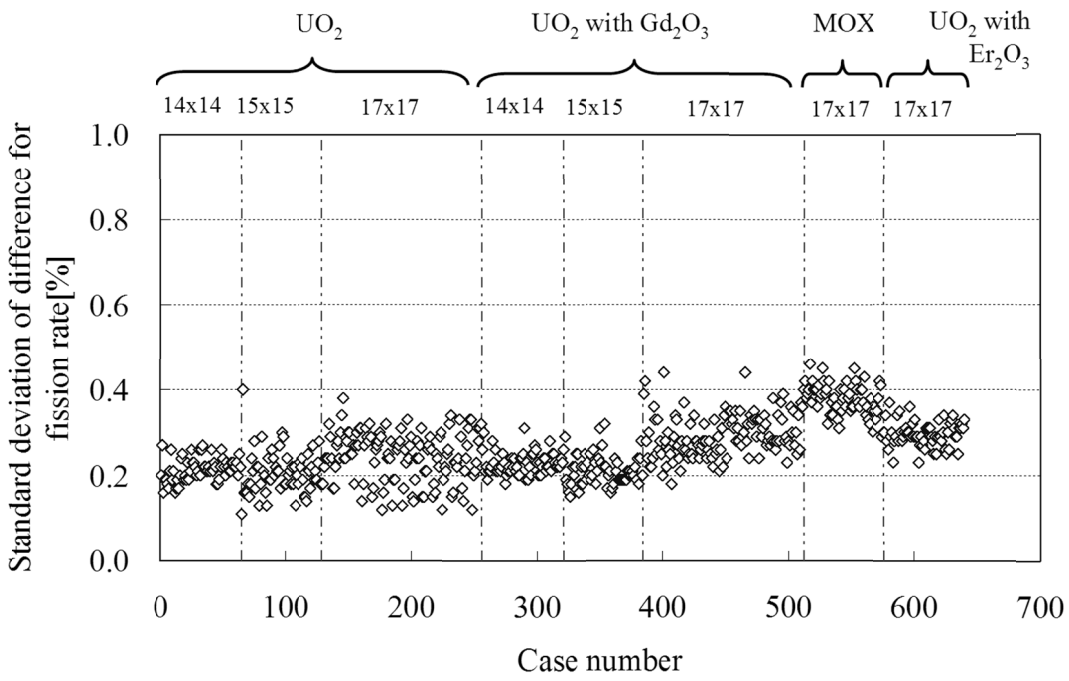

Figure 2.16 Standard deviation of difference for pin-by-pin fission rate between GALAXY and MVP.

2.6.6 Post Irradiation Examination Analysis

For the total validation of new resonance self-shielding methods including SDGM with multi-group MOC transport and microscopic depletion calculations, the post irradiation examination (PIE) analysis is carried out. The spatial burnup and nuclide composition distributions within a fuel pellet obtained by GALAXY are compared with those by measurements reported by Central Research Institute of Electric Power Industry (CRIEPI) [24]. The verification of each component method described in sections 2.2, 2.3, 2.4 and 2.5 has been carried out in the previous sub-sections. The objective of this validation is to confirm the overall accuracy of the present resonance self-shielding method with the transport and depletion calculation methods of GALAXY.

In the microscopic depletion calculation of GALAXY, Krylov sub-space method is adopted for direct loop chain treatment in exponential depletion matrix [25]. UO_2 (3.8wt% ^{235}U) pellet is irradiated and the maximum averaged burnup is 74.5GWd/t in this PIE. For the calculation of GALAXY, the pellet is first divided into 10 equal volume rings and then the outer 3 rings are re-divided into 13 equal volume rings. So, the pellet is totally divided into 20 rings for radial direction. Pellet temperature is assumed to be constant for radial direction and 900K is used.

Figures 2.17, **2.18** and **2.19** show the comparison of the spatial burnup and nuclide composition distributions within a fuel pellet between calculations by GALAXY (rectangular lines) and measurements (circle points). For the evaluation of nuclide composition, ^{235}U, ^{236}U and ^{238}U are taken into account for the uranium isotopes (U), and ^{238}Pu, ^{239}Pu, ^{240}Pu, ^{241}Pu and ^{242}Pu are for the plutonium isotopes (Pu), respectively.

Spatially dependent weight ratio of U and Pu nuclides is normalized so that the total ratio becomes unity (100%) for each ring. From these results, the good agreement is confirmed between calculation and measurement values. Therefore, it can be concluded that GALAXY can appropriately carry out the microscopic depletion calculations with the present resonance self-shielding treatment.

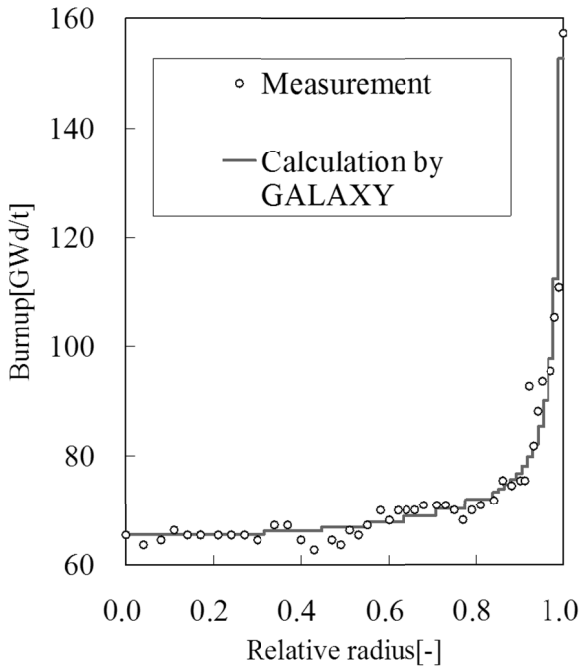

Figure 2.17 Comparison of burnup distribution between calculation by GALAXY and measurement.

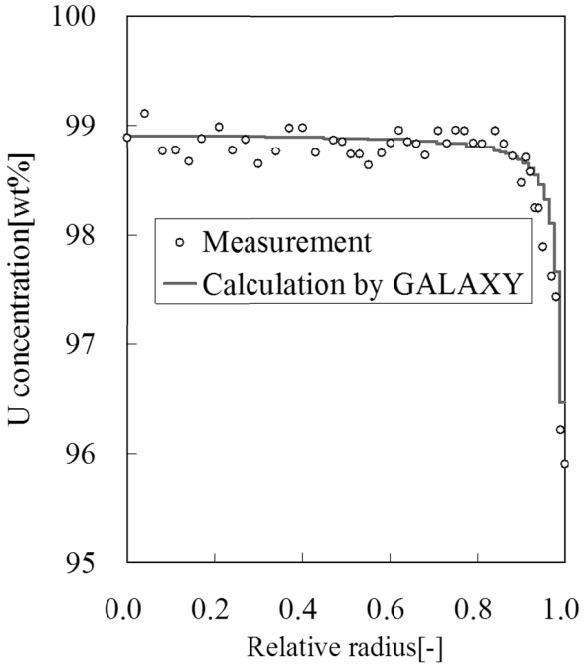

Figure 2.18 Comparison of U composition distribution between calculation by GALAXY and measurement.

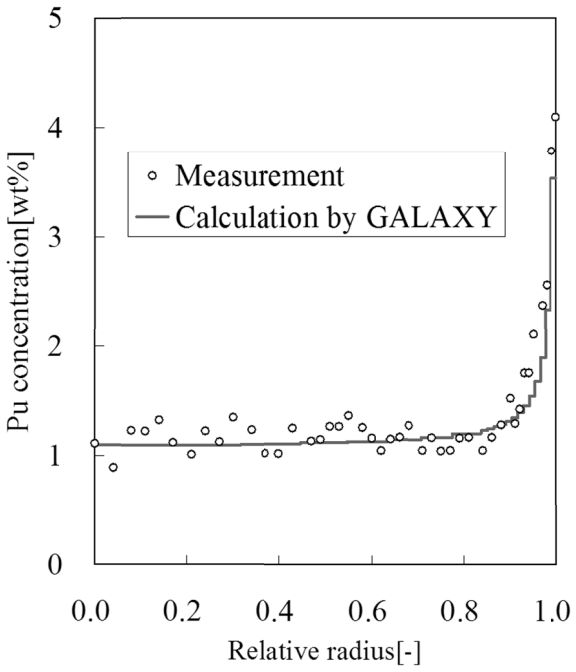

Figure 2.19 Comparison of Pu composition distribution between calculation by GALAXY and measurement.

2.6.7 Critical Experiment Analysis

For the overall validation of new resonance self-shielding methods with multi-group MOC transport calculation, the critical experiment analysis is carried out. The VENUS International Program (VIP) critical experiment is chosen for analysis. The fuel rod powers obtained by the current nuclear design code and GALAXY are compared with those by the measurements reported in Ref. 26. Pellet region is not sub-divided in the calculations. The objective of this validation is to confirm the difference of overall accuracy between the current nuclear design code and GALAXY.

The VIP critical experiments were mainly conducted by Belgonucléaire (B/N) and the Belgian Nuclear Research Center (SCK/CEN). The power distribution was measured for the PWR 17×17 lattice configuration shown in **Figure 2.20**. The layout of the experiment consists of a MOX fuel assembly surrounded by 4 UO_2 fuel assemblies. The uranium enrichment of UO_2 assembly is 3.0 wt%. The MOX fuel assembly has three different plutonium total contents. The total plutonium contents ($(Pu+^{241}Am)/(U+Pu+^{241}Am+^{16}O)$) are 12.6 wt%, 8.6 wt% and 4.8 wt% for the high-, medium- and low-content MOX rods, respectively. These fuel assemblies are surrounded by a driver fuel region with 3.0 wt% and 4.0 wt% UO_2 fuel rods.

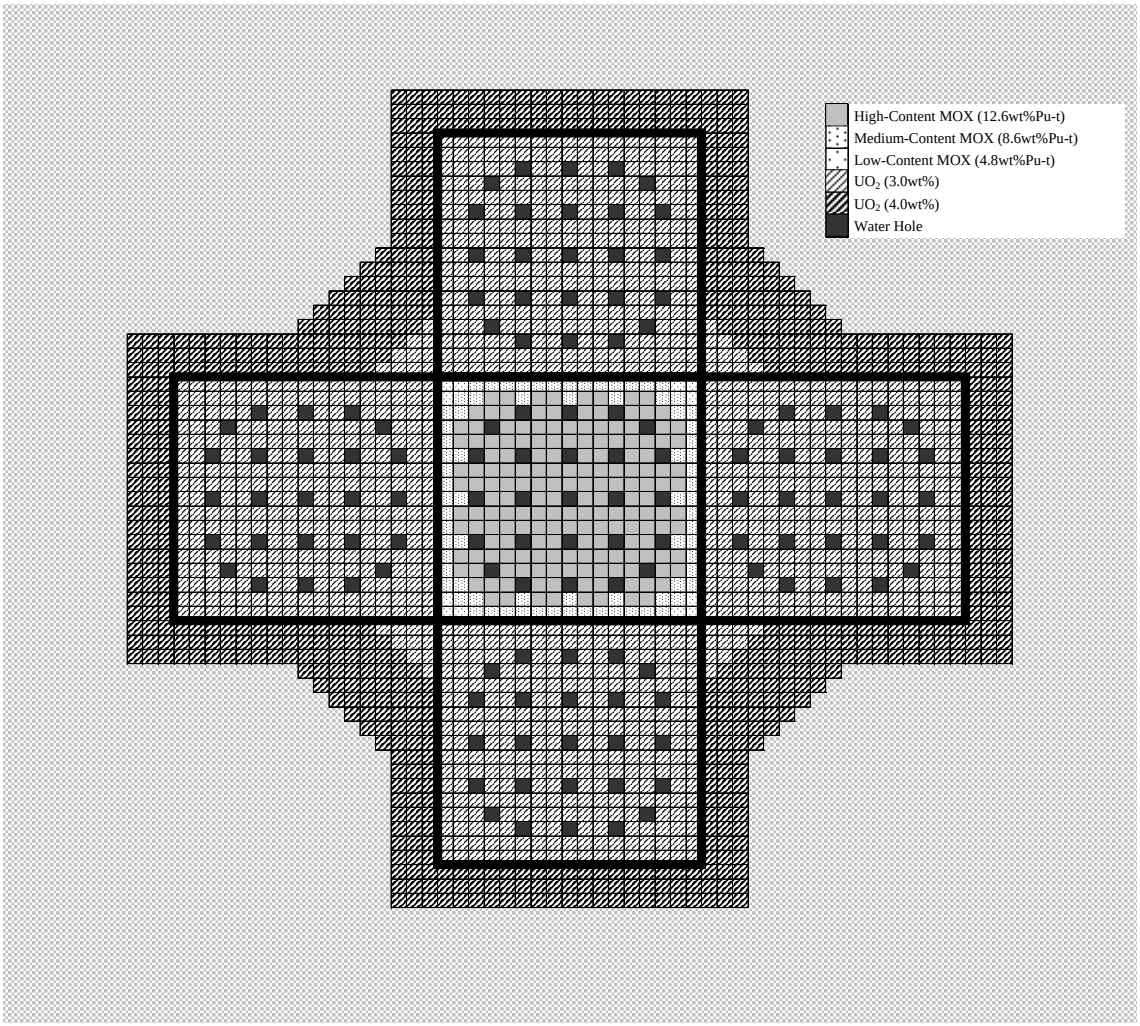

Figure 2.20 Core configuration of VIP critical experiment.

The fuel rod power distributions obtained by the current nuclear design code and GALAXY are compared with the measurements obtained by the gamma scan method. The differences of power distribution for “current nuclear design code calculation versus measurement” and “GALAXY calculation versus measurement” are depicted in **Figures 2.21** and **2.22** for MOX and UO_2 fuel assemblies, respectively. The maximum differences of rod power in the current nuclear design code and GALAXY calculations

are 5.7% and -3.6%, respectively. For the current nuclear design code, the standard deviations of the difference are 2.2% and 1.5% for MOX and UO_2, respectively. In contrast, in GALAXY, the standard deviations are 0.8% and 1.2% for MOX and UO_2, respectively.

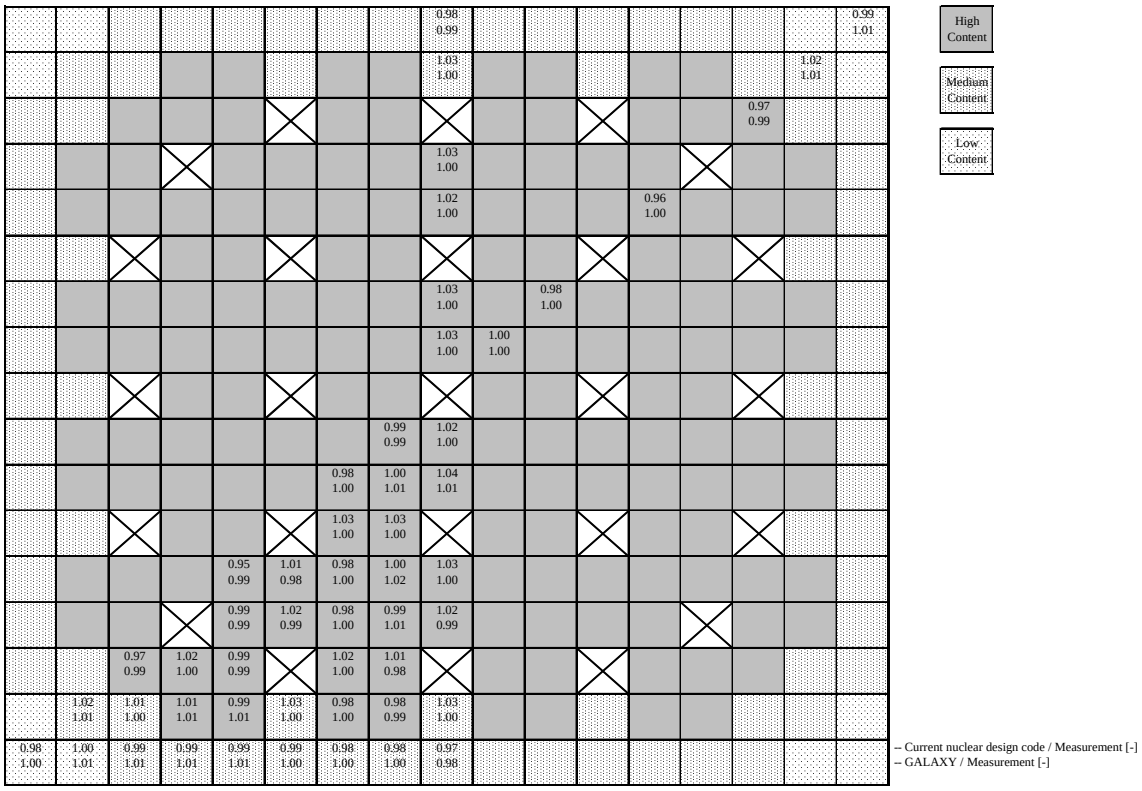

Figure 2.21 Calculation to measurement ratio of power distribution for MOX fuel assembly in VIP critical experiment.

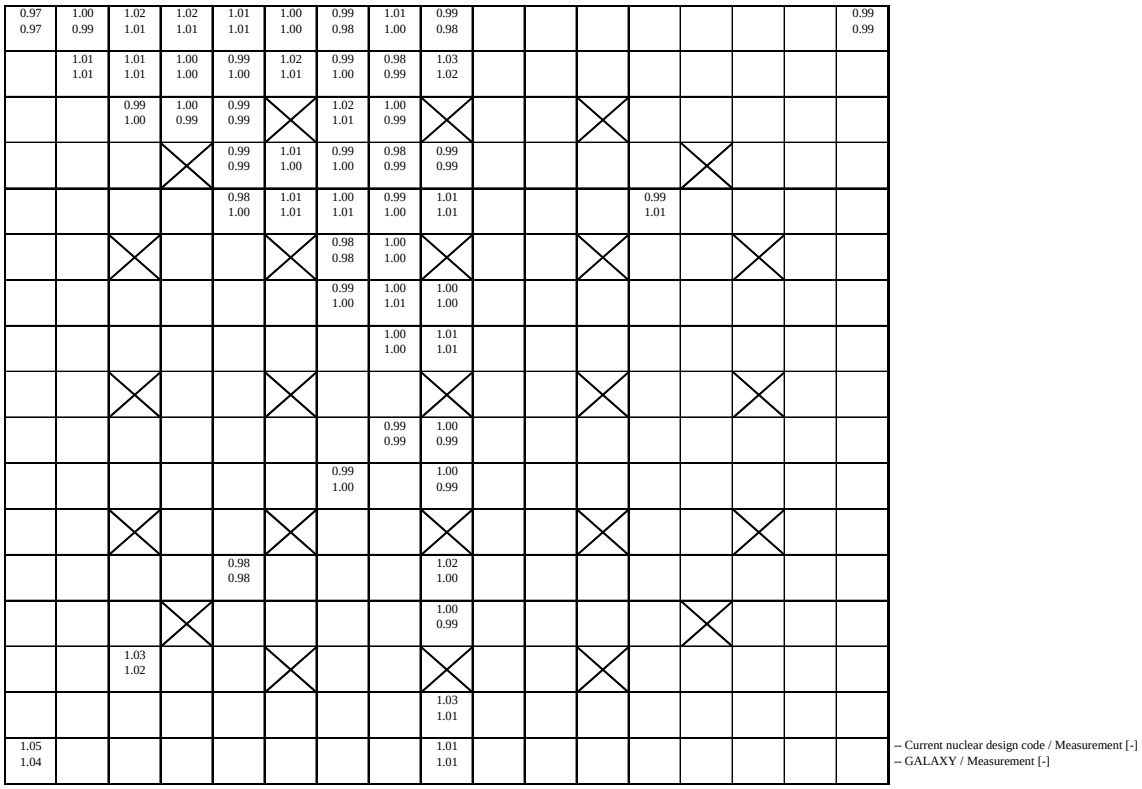

Figure 2.22 Calculation to measurement ratio of power distribution for UO_2 fuel assembly in VIP critical experiment.

From these results, the improvement of overall calculation accuracy from the current nuclear design code to GALAXY is confirmed.

2.7 Conclusion

A new resonance self-shielding method based on the equivalence theory is developed for general application to the lattice physics calculations. The present scope includes commercial light water reactor design applications which require both calculation accuracy and calculation speed. In order to develop the new resonance self-shielding method, all the calculation processes from cross-section library preparation to effective cross-section generation are reviewed and reframed by adopting the current enhanced methodologies for lattice calculations. The new method is composed of the following four key methods: (1) cross-section library generation method with a polynomial hyperbolic tangent formulation, (2) resonance self-shielding method based on the multi-term rational approximation for general lattice geometry and gray resonance absorbers, (3) spatially dependent gray resonance self-shielding method for generation of intra-pellet power profile and (4) integrated reaction-rate preservation method between the multi-group and the ultra-fine-group calculations. From the various verifications and validations, applicability of the present resonance treatment is totally confirmed. As a result, the new resonance self-shielding method is established, not only by extension of a past concentrated effort in the reactor physics research field, but also by unification of newly developed unique and challenging techniques for practical application of the lattice physics calculations.

In addition to the topics of the present study, treatment of the thermal motion of heavy nuclides for resonance scattering kernel [27], [28] is important for the exact modeling of the actual physical phenomenon. Furthermore, consideration of the resonance interference effect is also important theme of resonance treatment from the

view point of improvement of the reactor physics theory and reduction of the calculation error. These are still open problems.

Conventionally, the validity of resonance self-shielding method has not sufficiently been analyzed so far when the method was implemented to lattice physics codes, in spite of the many approximations in the resonance self-shielding theory. However, the resonance treatment is a key part of reactor physics theory and would dominate the final accuracy of lattice physics calculations. From this point of view, a series of products in the present study will be useful, not only for the development of GALAXY, but for the deeper insight and improvement of reactor physics theory.

2.8 References

[1]Askew R. A characteristics formulation of the neutron transport equation in complicated geometries. Winfrith: Atomic Energy Authority; 1972 (AEEW-M1108).

[2]Yamaji K, Matsumoto H, Kirimura K, Takeda T and Yamamoto A. Development of a new lattice physics code GALAXY for flexible geometry representation in next generation core analysis system. Trans. Am. Nucl. Soc. 2007; **97**: 573 [CD-ROM].

[3]Cacuci DG. Handbook of Nuclear Engineering, Springer, Berlin, 2010.

[4]Kier PH and Robba AA. A program for computation of resonance absorption in multiregion reactor cells. 1967. (ANL-7326).

[5]Nikolaev MN, Ignatov AA, Isaev NV and Khokhlov VF. The method of subgroups for considering the resonance structure of the cross sections in neutron calculations. Sov. At. Energy, 1970; **29**, 689.

[6]Carlvik I. The Dancoff correction in Square and Hexagonal Lattice. Nucl. Sci. Eng. 1967; **29**, 325.

[7]Stamm'ler RJJ, Abbate MJ. Methods of steady-state reactor physics in nuclear design. London: Academic Press; 1983. IX, Group constants in the resonance region; 286.

[8]Goldstein R and Cohen ER. Theory of resonance absorption of neutrons. Nucl. Sci. Eng. 1962; **13**, 132.

[9]MacFarlane RE and Miur DW. The NJOY nuclear data processing system version 91. Los Alamos National Laboratory; 1994. LA-17740-M.

[10] Sartori E. Standard energy group structures of cross section libraries for reactor

shielding, reactor cell and fusion neutronics applications: VITAMIN-J, ECCO-33, ECCO-2000 and XMAS, JEF/DOC-315, Revision 3. 1990; NEA Data Bank.

[11] Yamamoto T. Background-cross-section-dependent subgroup parameters. J. Nucl. Sci. Technol., 2003; **40**, 370.

[12] Kobayashi K. Reactor physics. Corona Publ., Tokyo, 1996 [in Japanese].

[13] Yamamoto A. Evaluation of background cross section for heterogeneous and complicated geometry by the enhanced neutron current method. J. Nucl. Sci. Technol., 2008; **45**, 1287.

[14] Hébert A and Marleau G. Generalization of the Stamm'ler method for the self-shielding of resonant isotopes in arbitrary geometries. Nucl. Sci. Eng., 1991; **108**, 230.

[15] Koike H, Yamaji K, Sato D, Tsubota S, Matsumoto H and Yamamoto A. A resonance calculation method based on the multi-terms rational approximation for general geometry with gray resonance absorbers. Proc. Int. Conf. on Physics of Reactors (PHYSOR2010); 2010 May 9-14; Pennsylvania, USA [CD-ROM].

[16] Rhodes J, et al. CASMO-4 user's manual rev. 4. SSP-01/400 Rev. 4, Studsvik Scandpower, 2004.

[17] Ouisloumen M. et al. PARAGON: The new Westinghouse lattice code. Proc. ANS Int. Meeting on Mathematical Methods for Nuclear Applications, Salt Lake City, Utah, USA, Sept., 2001.

[18] Stoker CC and Weiss ZJ. Spatially dependent resonance cross sections in a fuel rod. Ann. Nucl. Energy, 1996; **23**, 765.

[19] Matsumoto H, Ouisloumen M and Takeda T. Development of spatially

dependent resonance shielding method. J. Nucl. Sci. Technol. 2005; **42**, 688.

[20] Yamamoto A, Endo T, and Koike H. Improved derivation of multigroup effective cross section for heterogeneous system by equivalence theory. Nucl. Sci. Eng. 2011; **168**, 75.

[21] Sugimura N, Yamamoto A. Resonance treatment based on ultra-fine-group spectrum calculation in the AEGIS code. J. Nucl. Sci. Technol. 2007; **44**, 958.

[22] Nagaya Y, Okumura K, Mori T, and Nakagawa M. MVP/GMVP II: general purpose Monte Carlo codes for neutron and photon transport calculations based on continuous energy and multigroup methods. Japanese Atomic Energy Agency (JAEA); 2005. JAERI 1348.

[23] Hedayat A. S., et al., Orthogonal arrays: Theory and Applications. Springer, 1999.

[24] Sasahara A., et al., Post irradiation examination and the validity of computational analysis for high burnup UO_2 and MOX spent fuels. CRIEPI, Rep. T95012, Komae Research Laboratory, 1996.

[25] Yamamoto A, Tatsumi M, Sugimura N. Numerical Solution of Stiff Burnup Equation with Short Half Lived Nuclides by the Krylov Subspace Method. J. Nucl. Sci. Technol. 2007; **44**, 147.

[26] Charlier A., Basselier J., Leenders L. VENUS International Program (VIP) A Nuclear Data Package for LWR Pu Recycle. Proc. Int. Conf. on Physics of Reactors (PHYSOR90); 1990 September; Marseille, France.

[27] Lee D, Smith K, and Rhodes J. The Impact of ^{238}U resonance elastic scattering approximations on thermal reactor Doppler reactivity. Nucl. Sci. Eng., 2009; **36**,

274.

[28] Mori T, Nagaya Y. Comparison of resonance elastic scattering models newly implemented in MVP continuous-energy Monte Carlo code. J. Nucl. Sci. Technol. 2009; **46**, 793.

CHAPTER 3. DEVELOPMENT OF HYBRID RESONANCE SELF-SHIELDING METHODOLOGY FOR ENERGY DEPENDENT SCATTERING SOURCE AND RESONANCE INTERFERENCE EFFECT BASED ON INTEGRATION OF EQUIVALENCE THEORY AND ULTRA-FINE-GROUP SLOWING-DOWN CALCULATION

3.1 Introduction

Resonance treatment is one of the important elements for the lattice physics calculation in the reactor physics field. In the current lattice physics codes, the microscopic reaction-rates and the neutron multiplication factor are usually evaluated through the resonance calculation and the (single or multi stage) flux calculation. The resonance calculation is to generate multi-group effective cross-sections considering the resonance self-shielding effect. The choice of the method for resonance self-shielding treatment is very important because the effective cross-section directly influences on the result of subsequent multi-group flux calculation in a heterogeneous geometry.

In conventional lattice physics codes, the equivalence theory [1] has been widely applied as a fundamental method for resonance self-shielding treatment. The equivalence theory can easily treat the resonance self-shielding effect by assuming the

equivalence between homogeneous and heterogeneous systems using the background cross-section. The resonance self-shielding treatment based on the equivalence theory has been successfully applied by its simple and fast calculation features, which are the most advantages of this method.

In the recent trend of core analysis, extension of the applicable range tends to be required for the lattice physics code while keeping its prediction accuracy. For the resonance self-shielding treatment based on the equivalence theory, the following three features are especially the important items to be addressed to extend the applicable range with keeping sufficient accuracy, i.e., (1) flexible geometry treatment, (2) consideration for the variety of fuel compositions and (3) wider application range for the water moderator density. Items (1) and (2) are important for the innovative fuel designs, and (3) is important for the safety analysis applications of LWRs (Light Water Reactors). In the conventional equivalence theory, the above three items are approximately treated as follows:

(1) Geometry: One-dimensional cylindrical approximation [2] with Dancoff method [1],

(2) Fuel composition: No resonance interference effect [1] among multiple resonance nuclides in the fuel material,

(3) Moderator density: Optimized for the normal operation condition assuming the 1/E asymptotic spectrum for the scattering source approximation.

In order to reduce the influence of the above approximations, the ultra-fine-group treatment has been investigated for the resonance calculation in the recent studies [3, 4, 5]. In this treatment, the resonance cross-sections steeply varying to the neutron energy is directly taken into account on the ultra-fine energy group resolution. The direct ultra-fine-group slowing-down calculation is an approach to generate effective cross-sections with high accuracy, but its application is usually limited to the pin-cell geometry. Extension to the fuel assembly geometry considering the variety of pin-wise fuel compositions and the irregular lattice effect due to the non-fuel cells is not very easy.

To remove the limitation in the ultra-fine-group treatment, the more direct approach has also been investigated by reflecting the current high computational performance, *i.e.*, increasing the number of energy groups for the multi-group flux calculation step in the fuel assembly geometry [6, 7]. The influence of the resonance calculation can be reduced by increasing the number of energy groups, and the detailed energy dependence of the resonance cross-section and the neutron flux is directly taken into account in flux calculation step. This treatment is surely straightforward approach, but it cannot be applied easily for the design applications which require many branch calculations in the nuclear constants generation.

By investigating the past beneficial studies for the resonance treatment mentioned above, the advanced method for resonance self-shielding treatment is newly developed in the present study. The target of the new method is to achieve high accuracy without increasing the number of energy groups in the flux calculation step. Especially, the main

features to address the above three approximated treatments are summarized as follows:

(1) Geometry

In the past study, the gray resonance self-shielding treatment method [8] based on the equivalence theory was established for MHI (Mitsubishi Heavy Industries, Ltd.) lattice physics code GALAXY [9]. This method can generate the coefficients of the multi-term rational equation (α_n and β_n shown in section 2) to consider the heterogeneity between fuel and non-fuel regions, and the irregular lattice effect in the fuel assembly geometry. The coefficients are generated so as to obtain the accurate flux response by the rational equation against all the optical length ranges of the fuel regions. The optical length includes the intermediate range between the black (perfect neutron absorber) and the white (pure neutron scatter) limit conditions, and this intermediate range is called as the “gray resonance range” [8] in contrast to the “black” or “white” limits. In the method, the effect of gray resonance and the two-dimensional exact geometry can be directly handled by using the one-group MOC (method of characteristics) [10] fixed source calculations.

In the resonance self-shielding treatment newly established in the present study, the coefficients of the multi-term rational equation for the neutron flux in the heterogeneous system capture the various spatial effects for the exact geometry mentioned above. To achieve the efficient spatial treatment, a new form of energy dependent neutron flux is proposed based on the flux derivation scheme in the equivalence theory consistent with the multi-term rational equation of the gray resonance treatment method. The coefficients can be generated for pin-by-pin resolution, thus the new method can

efficiently handle a two-dimensional exact assembly geometry.

(2) Fuel composition

The spatial effect is accurately treated by the concept described in (1). Another important element is the accurate treatment of energy dependence for the neutron flux. In the equivalence theory, the resonance cross-sections except for the target resonance nuclide are usually not considered to achieve the simple and fast calculations. The approximated treatment of the cross-sections neglects the resonance interference effect among the multiple resonance nuclides in the fuel region. Though the resonance interference effect itself can be considered easily by the RIF (resonance interference factor) method [11, 12], another important approximation in the equivalence theory, i.e., the scattering source approximation, also needs to be reviewed for the more accurate treatment [13]. To remove the above two approximations, all the resonance cross-sections for the important resonance nuclides in the fuel region, and the accurate scattering source in the fuel region which appears on the slowing-down equation, are taken into account for the flux derivation scheme in the present study.

(3) Moderator density

The scattering source of the non-fuel region is also important element. The simple 1/E spectrum is assumed as a flux for the non-fuel regions in the conventional equivalence theory [1]. The approximation may be valid for the normal operation condition of LWR, in which plenty hydrogen exists in the moderator region and many neutrons are slowed down to the epi-thermal energy ranges. The 1/E flux approximation

is not sufficient for the low moderator density condition, and the flux in the moderator region is directly influenced by the flux in the fuel region. It should be noted that the prediction accuracy of the moderator flux also affects the accuracy of the fuel flux through the scattering source provided from the moderator region, hence the accurate moderator flux treatment is important. In order to treat the scattering source of the non-fuel region more accurately, the resonance self-shielding effect in the fuel region is theoretically taken into account to the flux in the non-fuel region in the present study.

By the above three treatments, a new form of energy dependent neutron flux is derived. The fundamental form is the multi-term rational equation, and at the same time, it is the slowing-down equation. The former aspect corresponds to consideration of the spatial dependence of the flux (pin-by-pin resolution), and the latter corresponds to consideration of the energy dependence of the flux (ultra-fine-group resolution), respectively. As a result of the new derivation scheme, a new method for resonance self-shielding treatment is established as a hybrid model of the equivalence theory and the ultra-fine-group slowing-down calculation.

On the basis of the above concepts, contents of each section in the present paper are summarized as follows.

<Section 3.2>

A new slowing-down equation is proposed with a multi-term rational form. The equivalence theory and the ultra-fine-group treatment are theoretically integrated in the

derivation scheme.

<Section 3.3>

A correction factor equation is derived to preserve the reaction-rate between multi-group and ultra-fine-group treatments.

<Section 3.4>

Numerical treatments with discretized equations are shown for actual implementation of the new method.

<Section 3.5>

A new method for resonance self-shielding treatment established in sections 3.2-3.4 is verified for unit pin-cell problem with lattice physics code GALAXY.

<Section 3.6>

A new method for resonance self-shielding treatment is verified for UO_2/MOX multi-assembly problem with lattice physics code GALAXY.

<Section 3.7>

Extensive Monte-Carlo pin-cell benchmark is carried out for infinite multiplication

factor (k-infinity) and reactivity coefficients in wide application range by comparison between GALAXY and continuous energy Monte-Carlo code MVP.

<Section 3.8>

The conclusions of the present study are summarized.

3.2 Derivation of Slowing-Down Equation with Multi-Term Rational Form

3.2.1 Slowing-Down Equation for Two-Region Heterogeneous System

The integral form of neutron transport equation for two region heterogeneous system consisting of fuel and non-fuel regions is written as:

$$\Sigma_t^f(E)\phi_f(E)V_f = S_f(E)V_f P_{f\to f}(E) + S_{nf}(E)V_{nf}P_{nf\to f}(E). \tag{3.1}$$

In the following derivation, the non-fuel region is defined as multiple regions except for fuel. For the typical LWR (light water reactor) unit cell, non-fuel region is composed of cladding and moderator regions.

In the resolved resonance energy ranges, the fission source can be omitted. The (n, 2n) reaction is also negligible in this energy range. Therefore the neutron source term for fuel region can be written as scattering source:

$$S_f(E) = \sum_k \int_0^\infty dE' N_k^f \sigma_s^k(E'\to E)\phi_f(E'), \tag{3.2}$$

The neutron source for non-fuel region can be written as the same manner.

By applying the isotropic and elastic-down scattering in the center-of-mass system, the scattering cross-section matrix is derived as:

$$\sigma_s^k(E'\to E) = \begin{cases} \dfrac{\sigma_s^k(E')}{(1-\alpha_k)E'} & (E \le E' \le E/\alpha_k) \\ 0 & (E' < E \text{ or } E' > E/\alpha_k). \end{cases} \tag{3.3}$$

By substituting Equation (3.3) into Equation (3.2), the scattering source for the fuel region is written as:

$$S_f(E) = \sum_k \int_E^{E/\alpha_k} dE' N_k^f \frac{\sigma_s^k(E')}{(1-\alpha_k)E'} \phi_f(E') = \sum_k \frac{N_k^f}{(1-\alpha_k)} \int_E^{E/\alpha_k} \frac{dE' \sigma_s^k(E') \phi_f(E')}{E'}. \quad (3.4)$$

The scattering source for the non-fuel region is also written as:

$$S_{nf}(E) = \sum_k \frac{N_k^{nf}}{(1-\alpha_k)} \int_E^{E/\alpha_k} \frac{dE' \sigma_s^k(E') \phi_{nf}(E')}{E'}. \quad (3.5)$$

By substituting Equations (3.4) and (3.5) into Equation (3.1), neutron slowing-down equation for the fuel region can be obtained as:

$$\phi_f(E) = \frac{P_{f\to f}(E)}{\Sigma_t^f(E)} \sum_k \frac{N_k^f}{(1-\alpha_k)} \int_E^{E/\alpha_k} \frac{dE' \sigma_s^k(E') \phi_f(E')}{E'} + \frac{V_{nf}}{V_f} \frac{P_{nf\to f}(E)}{\Sigma_t^f(E)} \sum_k \frac{N_k^{nf}}{(1-\alpha_k)} \int_E^{E/\alpha_k} \frac{dE' \sigma_s^k(E') \phi_{nf}(E')}{E'}. \quad (3.6)$$

The equation for the non-fuel region is obtained as the same manner. The more general equation for the multiple region system (more than two regions) can be easily derived in similar way. In the resonance self-shielding treatment based on the conventional ultra-fine-group calculation, the slowing-down equation for a heterogeneous system is directly solved with several tens of thousands of energy groups. As can be seen from Equation (3.6), the slowing-down equation cannot be solved analytically except for the very simple case because the flux itself is included in the scattering source term. In the actual numerical treatment of Equation (3.6), the ultra-fine-group flux is solved from the fast to the lower energy ranges as a fixed source problem without fission source updates (outer iterations) and scattering source updates (inner iterations).

3.2.2 Flux and Scattering Source for Non-Fuel Region

In the present study, the ultra-fine-group slowing-down equation in the heterogeneous system, i.e., Equation (3.6) or the more general one, is not directly solved for fast calculation. Besides, the NR or IR approximation [1, 14] of the scattering source conventionally used in the equivalence theory is not also applied to improve the prediction accuracy of energy dependent neutron flux. To achieve this concept, further theoretical approximations are not applied for the scattering source of the fuel region.

The efficient treatment of non-fuel region is more important for fast and accurate resonance calculation. The effect of resonance scattering for the non-fuel region is usually small relative to that for the fuel region. By using this assumption, the scattering source for the non-fuel region (Equation (5)) is approximated as:

$$S_{nf}(E) \cong \sum_k \frac{N_k^{nf}\sigma_p^k}{(1-\alpha_k)} \int_E^{E/\alpha_k} \frac{dE'\phi_{nf}(E')}{E'}, \tag{3.7}$$

where σ_p^k denotes the microscopic potential scattering cross-section of nuclide k.

The neutron flux in the non-fuel region ($\phi_{nf}(E)$) is usually influenced by the flux in the fuel region. $\phi_{nf}(E)$ is not a simple $1/E$ asymptotic spectrum, and includes the self-shielding effect induced by the resonances in the fuel region. The treatment of non-asymptotic effect is especially important for the low moderator density conditions assumed in safety analysis. To incorporate the effect, $\phi_{nf}(E)$ is expressed as a following equation in the present study:

$$\phi_{nf}(E) = \theta \frac{1}{E} + (1-\theta)\varphi_{nf}(E), \tag{3.8}$$

where $\varphi_{nf}(E)$ denotes the non-asymptotic component of the flux in the non-fuel region. θ denotes the ratio of asymptotic spectrum ($0 \le \theta \le 1$). $\varphi_{nf}(E)$ can be derived from corrected neutron flux in the fuel region ($\phi_f(E)$). $\phi_f(E)$ is not derived in this intermediate process, hence the concrete form of $\varphi_{nf}(E)$ is discussed in the following sub-section (section 3.2.4).

In the extreme condition for $\theta \to 0$, $\phi_{nf}(E)$ approaches to $\varphi_{nf}(E)$ (or $\phi_f(E)$). This special case corresponds to the situation in which the neutrons would not collide in the non-fuel region. This means that the non-fuel region is in the vacuum condition. For the typical example in the reactor core or the spent nuclear fuel pool for the LWR, most of the water surrounding the fuel rods evaporates and becomes low density mist condition.

By substituting Equation (3.8) into Equation (3.7), $S_{nf}(E)$ can be transformed as:

$$\begin{aligned} S_{nf}(E) &= \sum_k \frac{N_k^{nf}\sigma_p^k}{(1-\alpha_k)} \int_E^{E/\alpha_k} \frac{dE'}{E'} \cdot \left[\theta \frac{1}{E'} + (1-\theta)\varphi_{nf}(E') \right] \\ &= \theta \frac{\Sigma_p^{nf}}{E} + (1-\theta) \sum_k \frac{N_k^{nf}\sigma_p^k}{(1-\alpha_k)} \int_E^{E/\alpha_k} \frac{dE'\varphi_{nf}(E')}{E'} \\ &= \left[\theta + (1-\theta) \frac{E}{\Sigma_p^{nf}} \sum_k \frac{N_k^{nf}\sigma_p^k}{(1-\alpha_k)} \int_E^{E/\alpha_k} \frac{dE'\varphi_{nf}(E')}{E'} \right] \cdot \frac{\Sigma_p^{nf}}{E}, \end{aligned} \tag{3.9}$$

where Σ_p^{nf} denotes the macroscopic potential scattering cross-section in the non-fuel region.

By defining the part of the intermediate product in Equation (3.9) by:

$$\mu(E) \equiv \theta + (1-\theta)\frac{E}{\Sigma_p^{nf}} \sum_k \frac{N_k^{nf}\sigma_p^k}{(1-\alpha_k)} \int_E^{E/\alpha_k} \frac{dE'\varphi_{nf}(E')}{E'} \quad , \tag{3.10}$$

$S_{nf}(E)$ is rewritten as:

$$S_{nf}(E) = \mu(E)\frac{\Sigma_p^{nf}}{E} \equiv \mu(E)\Sigma_p^{nf}\varphi_{as}(E), \tag{3.11}$$

where the asymptotic spectrum $1/E$ is rewritten as $\varphi_{as}(E)$.

The conventional form of $S_{nf}(E)$ is Σ_p^{nf}/E in the equivalence theory, therefore $\mu(E)$ corresponds to the correction factor to consider the self-shielding effect by the resonances in a fuel region.

3.2.3 Incorporation of Multi-Term Rational Equation for Fuel Escape Probability

By substituting Equation (3.11) into Equation (3.1), the transport equation for the two region heterogeneous system is rewritten as:

$$\Sigma_t^f(E)\phi_f(E)V_f = S_f(E)V_f P_{f\to f}(E) + \mu(E)\Sigma_p^{nf}\varphi_{as}(E)V_{nf}P_{nf\to f}(E). \qquad (3.12)$$

The following formulation is based on the flux derivation scheme for the multi-term rational approximation [8] in the equivalence theory. The fuel to fuel collision probability satisfies the following probability relation:

$$P_{f\to f}(E) = 1 - P_{f\to nf}(E) = 1 - P_e(E), \qquad (3.13)$$

where $P_{f\to nf}(E)$ denotes the fuel to non-fuel collision probability, which corresponds to the first-flight fuel escape probability in the lattice system, $P_e(E)$ [1]. $P_e(E)$ includes the lattice effect due to the neutron current induced by the neighboring fuel rods or the non-fuel regions.

The reciprocity theorem between the fuel and the non-fuel regions is also written as:

$$\Sigma_t^f(E)V_f P_{f\to nf}(E) = \Sigma_p^{nf}V_{nf}P_{nf\to f}(E), \qquad (3.14)$$

where the total cross-section for the non-fuel region is approximated as the potential scattering cross-section, i.e., $\Sigma_t^{nf}(E) \cong \Sigma_s^{nf}(E) \cong \Sigma_p^{nf}$, in the right hand side of the equation. In this approximation, the non-fuel material is assumed as a pure scatterer to the neutron for the target resonance energy ranges, which do not include the thermal energy ranges. The effect of resonance scattering for the non-fuel region is also regarded as small relative to that for the fuel region, which is consistent with the assumption in

Equation (3.7).

By substituting Equations (3.13) and (3.14) into the right hand side of Equation (3.12), Equation (3.12) is rewritten as:

$$\Sigma_t^f(E)\phi_f(E)V_f = S_f(E)V_f\{1-P_{f\to nf}(E)\} + \varphi_{as}(E)\mu(E)\Sigma_t^f(E)V_f P_{f\to nf}(E)\,. \tag{3.15}$$

Further transformation of Equation (3.15) can yield:

$$\begin{aligned}\phi_f(E) &= \{1-P_{f\to nf}(E)\}\cdot\frac{S_f(E)}{\Sigma_t^f(E)} + \varphi_{as}(E)\mu(E)P_{f\to nf}(E)\\ &= \varphi_{as}(E)\cdot\left[\{1-P_{f\to nf}(E)\}\cdot\left\{\left(\frac{S_f(E)}{\varphi_{as}(E)}\right)\Big/\Sigma_t^f(E)\right\} + \mu(E)P_{f\to nf}(E)\right]\\ &= \varphi_{as}(E)\cdot\left[\{1-P_e(E)\}\cdot\frac{\Sigma_{sd}^f(E)}{\Sigma_t^f(E)} + \mu(E)P_e(E)\right],\end{aligned} \tag{3.16}$$

where

$$\Sigma_{sd}^f(E) \equiv \frac{S_f(E)}{\varphi_{as}(E)}\,. \tag{3.17}$$

$\Sigma_{sd}^f(E)$ denotes the "slowing-down cross-section" newly named and defined in the present study. It should be noted that the dimension for $\varphi_{as}(E)$ in Equation (3.17) corresponds to that for the neutron flux. Considering that the dimension for $S_f(E)$ corresponds to that for the macroscopic reaction-rate (i.e., product of the macroscopic cross-section and the flux), the dimension for $\Sigma_{sd}^f(E)$ is, after all, equal to that for the macroscopic cross-section. It is sure that $\Sigma_{sd}^f(E)$ is not a pure cross-section in the

physical point of view, but it can be converted to the macroscopic potential cross-section in case of the NR approximation (details are discussed in section 3.2.6). Thus $\Sigma_{sd}^{f}(E)$ is formally written as a cross-section.

In the multi-term rational approximation of the fuel escape probability, $P_e(E)$ is expressed as [1, 8]:

$$P_e(E) = \sum_{n=1}^{N} \beta_n \frac{\alpha_n}{\Sigma_t^f(E) l_f + \alpha_n}, \tag{3.18}$$

where l_f denotes the mean chord length of the fuel lump. N denotes the number of rational equation terms. α_n corresponds to the n-th coefficient considering the heterogeneous and lattice effects. β_n corresponds to the weight of rational equation normalized as:

$$\sum_{n=1}^{N} \beta_n = 1. \tag{3.19}$$

By substituting Equations (3.18) and (3.19) into Equation (3.16), the energy dependent neutron flux in the fuel region is derived as:

$$
\begin{aligned}
\phi_f(E) &= \varphi_{as}(E)\cdot\left[\{1-P_e(E)\}\cdot\frac{\Sigma_{sd}^f(E)}{\Sigma_t^f(E)}+\mu(E)P_e(E)\right] \\
&= \frac{1}{E}\left[\{1-P_e(E)\}\cdot\frac{\Sigma_{sd}^f(E)}{\Sigma_t^f(E)}+\mu(E)P_e(E)\right] \\
&= \frac{1}{E}\left[\begin{aligned}&\left\{\sum_{n=1}^{N}\beta_n-\sum_{n=1}^{N}\beta_n\frac{\alpha_n}{\Sigma_t^f(E)l_f+\alpha_n}\right\}\cdot\frac{\Sigma_{sd}^f(E)}{\Sigma_t^f(E)} \\ &+\mu(E)\sum_{n=1}^{N}\beta_n\frac{\alpha_n}{\Sigma_t^f(E)l_f+\alpha_n}\end{aligned}\right] \\
&= \frac{1}{E}\left[\sum_{n=1}^{N}\beta_n\frac{\Sigma_{sd}^f(E)l_f}{\Sigma_t^f(E)l_f+\alpha_n}+\sum_{n=1}^{N}\beta_n\frac{\mu(E)\alpha_n}{\Sigma_t^f(E)l_f+\alpha_n}\right] \\
&= \frac{1}{E}\sum_{n=1}^{N}\beta_n\frac{\Sigma_{sd}^f(E)l_f+\mu(E)\alpha_n}{\Sigma_t^f(E)l_f+\alpha_n}.
\end{aligned}
\tag{3.20}
$$

3.2.4 A New Set of Slowing-Down Equation

From Equations (3.4), (3.10), (3.17) and (3.20), the neutron flux in the fuel region is formulated as:

$$\phi_f(E) = \frac{1}{E}\sum_{n=1}^{N}\beta_n \frac{\Sigma_{sd}^f(E)l_f + \mu(E)\alpha_n}{\Sigma_t^f(E)l_f + \alpha_n}, \tag{3.21}$$

where

$$\Sigma_{sd}^f(E) = \frac{S_f(E)}{\varphi_{as}(E)} = E\sum_k \frac{N_k^f}{(1-\alpha_k)}\int_E^{E/\alpha_k} \frac{dE'\sigma_s^k(E')\phi_f(E')}{E'}, \tag{3.22}$$

$$\mu(E) = \theta + (1-\theta)\frac{E}{\Sigma_p^{nf}}\sum_k \frac{N_k^{nf}\sigma_p^k}{(1-\alpha_k)}\int_E^{E/\alpha_k} \frac{dE'\varphi_{nf}(E')}{E'}. \tag{3.23}$$

As referred in section 3.2.2, $\varphi_{nf}(E)$ in Equation (3.23) denotes the non-asymptotic component of the flux in the non-fuel region. For the neutron flux in the non-fuel region, the self-shielding effect propagated by the resonances of the fuel region is somewhat mitigated. Therefore $\varphi_{nf}(E)$ can be approximated by correcting the heterogeneous term α_n of Equation (3.21) as:

$$\varphi_{nf}(E) = \frac{1}{E}\sum_{n=1}^{N}\beta_n \frac{\Sigma_{sd}^f(E)l_f + \mu(E)\varepsilon_n\alpha_n}{\Sigma_t^f(E)l_f + \varepsilon_n\alpha_n}, \tag{3.24}$$

where ε_n denotes the n-th coefficient considering the mitigation of resonance self-shielding effect in the non-fuel region.

Equations (3.21)-(3.24) are the new set of slowing-down equation for a two-region

heterogeneous system. In the actual numerical treatment, $\phi_f(E)$, $\Sigma_{sd}^f(E)$, $\mu(E)$ and $\varphi_{nf}(E)$ are solved successively from the fast to the lower energy ranges as a fixed source problem without fission source updates (outer iterations) and scattering source updates (inner iterations). The detail of the numerical treatment is described in section 3.4.1.

With the byproducts of the solution for Equations (3.21)-(3.24), the neutron flux in a non-fuel region can be reconstructed using Equations (3.8) and (3.24) as:

$$\phi_{nf}(E) = \frac{1}{E}\left[\theta + (1-\theta)\sum_{n=1}^{N}\beta_n \frac{\Sigma_{sd}^f(E)l_f + \mu(E)\varepsilon_n\alpha_n}{\Sigma_t^f(E)l_f + \varepsilon_n\alpha_n}\right]. \quad (3.25)$$

3.2.5 Essential Roles of θ and ε_n

The coefficients θ and ε_n are the essential elements to represent the flux in a non-fuel region by the following reasons.

(1) Essential role and the number of H atom dependence of θ

Figure 3.1 shows the typical example of fluxes in a fuel and a non-fuel region for the wide range of fuel optical length obtained from the MOC one-group fixed source calculation. In this figure, fluxes are calculated on 4.8wt%UO_2 pin-cell geometry analyzed in section 3.5. In the black limit, the macroscopic total cross-section reaches to $\Sigma_t^f \to \infty$, as a result of $\Sigma_a^f \to \infty$. In this extreme case, the flux in a fuel region is converged as zero ($\lim_{\Sigma_t^f \to \infty} \phi_f = 0$, see Equation (3.21)), but the flux in a non-fuel region must be always positive ($\phi_{nf} > 0$) due to the scattering source in the non-fuel region, as long as some materials exist in the non-fuel region. The value of θ plays a role in the asymptotic component of ϕ_{nf} which is independent to variation of Σ_t^f, whereas $(1-\theta)\varphi_{nf}$ depends on Σ_t^f. These properties can be followed by Figure 3.1. Mathematical meaning of θ is clarified in section 3.2.7 (Equation (3.38)).

Note that θ strongly depends on the moderator density. **Figure 3.2** shows the example for moderator density dependence of θ. In this figure, θ is plotted for various moderator density conditions of 4.8wt%UO_2 pin-cell geometry analyzed in section 3.5. The moderator density dependence is shown both for the normal cell pitch

condition of PWR (Pressurized Water Reactor) and the pseudo wide pitch condition. The moderator to fuel volume ratios (V_m/V_f) are 1.67 and 10.71, respectively. As shown in Figure 3.2, θ is larger for the water enriched conditions than for the lower moderator density conditions. By rearranging the behavior of θ shown in Figure 3.2, θ depends on the number of ^{1}H atom in a fuel cell, as shown in Figure 3.3 (the number of ^{1}H atom is normalized by that of ^{238}U atom). As shown in Figure 3.3, θ is large for the high $^{1}H/^{238}U$ conditions than for the lower $^{1}H/^{238}U$, respectively.

(2) Essential role of ε_n

As described in section 3.2.2, $\phi_{nf}(E)$ approaches to $\varphi_{nf}(E)$ in case of the limited condition, i.e., $\theta \to 0$. In this extreme case, the non-fuel region is on the vacuum condition, hence the corresponding two region system is, after all, equivalent to the homogeneous medium composed of the fuel material only. Therefore, $\phi_{nf}(E) = \varphi_{nf}(E) = \phi_f(E)$ in case of $\theta \to 0$. In this extreme case, $\varepsilon_n = 1$.

Application of ε_n is more important for the heterogeneous geometry $(0 < \theta \leq 1)$ than for the homogeneous medium $(\theta = 0)$. In the general heterogeneous case, the non-asymptotic component of the flux in the non-fuel region, i.e., $\varphi_{nf}(E)$, is not completely equal to $\phi_f(E)$. Therefore, ε_n is newly introduced as a correction factor in order to well approximate $\varphi_{nf}(E)$ by means of correcting $\phi_f(E)$.

As shown in Figure 3.1, the gradient (or sensitivity) of ϕ_{nf} or $(1-\theta)\varphi_{nf}$

associated with Σ_t^f change is generally different from that of ϕ_f. The above sensitivity is essentially determined by the relation of magnitude between $\Sigma_t^f l_f$ and α_n in the denominator of Equation (3.21). The different sensitivity effect of a non-fuel region comparing with a fuel region can be controlled by correcting α_n in the rational equation. Therefore ε_n plays a role in the sensitivity correction factor in a non-fuel region against Σ_t^f change. The sensitivity of φ_{nf} (Equation (3.24)) induced by Σ_t^f change can be mitigated by ε_n.

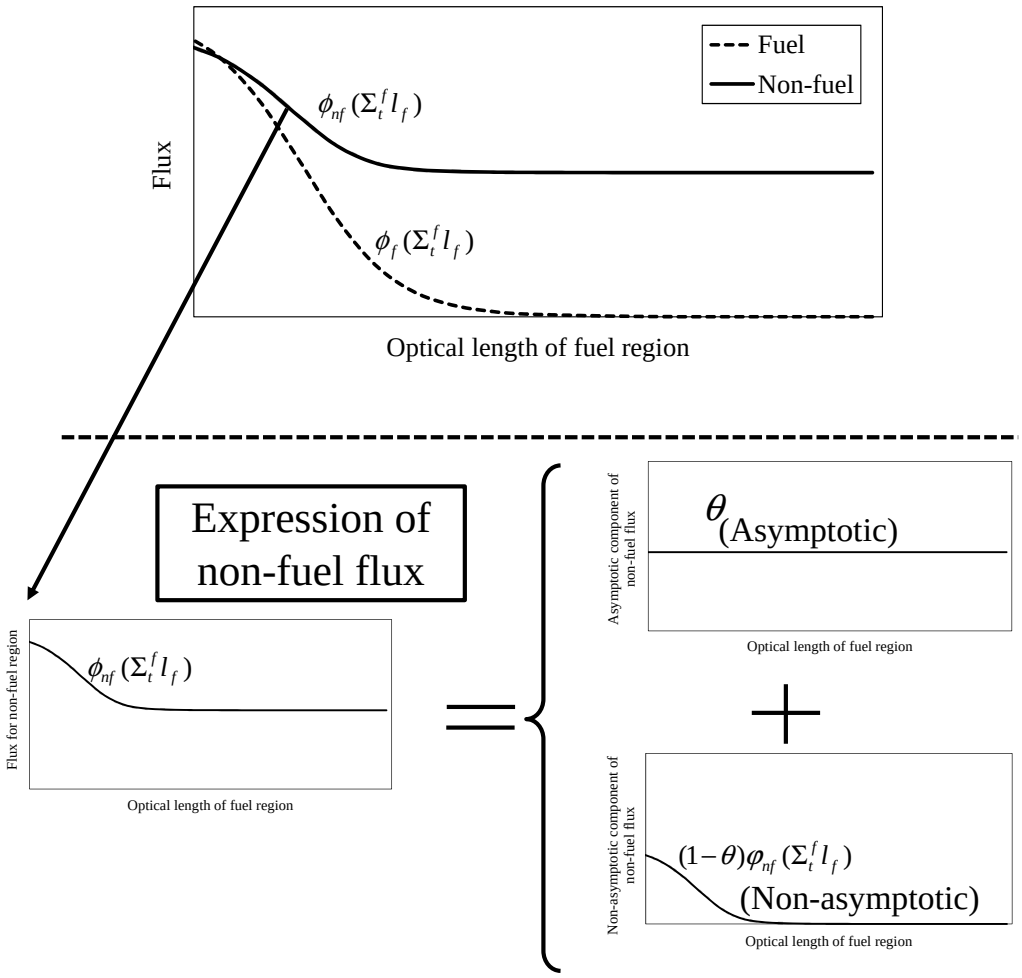

Figure 3.1 Fluxes by the MOC one-group fixed source calculations for wide range of optical length and expression of non-fuel flux.

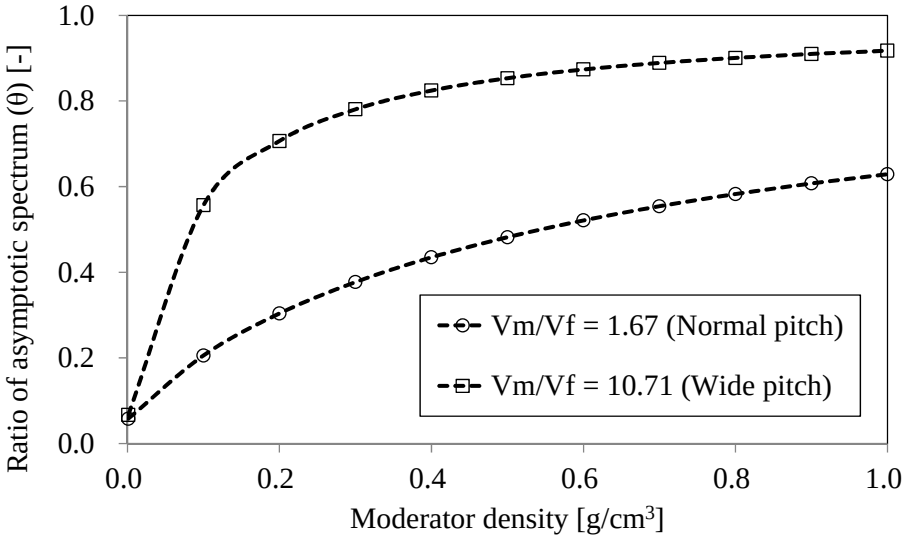

Figure 3.2 Moderator density dependence of θ.

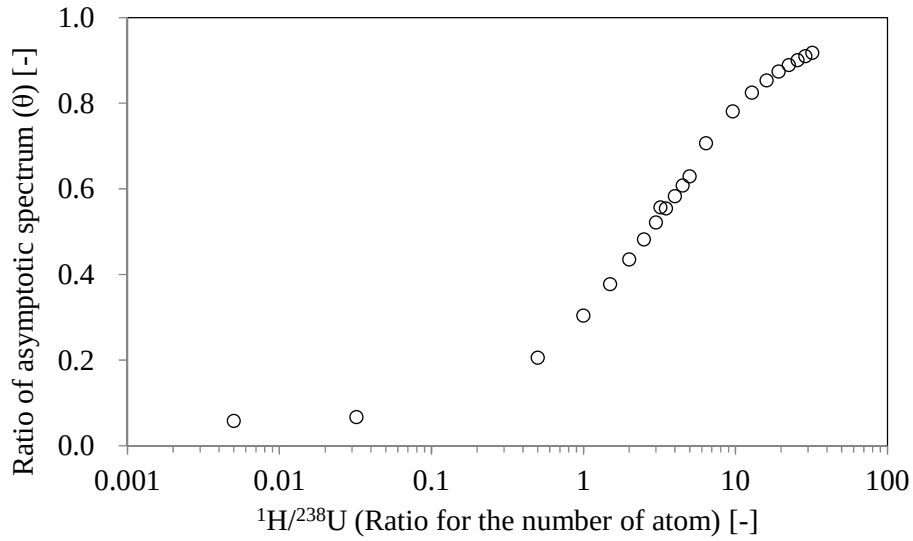

Figure 3.3 $^{1}H/^{238}U$ (ratio for the number of atom) dependence of θ.

3.2.6 Comparison with Conventional Equivalence Theory

A new set of the slowing-down equation shows a theoretical hybrid form of the equivalence theory and the ultra-fine-group treatment. In this sub-section, it is confirmed that Equations (3.21)-(3.25) can be transformed to the equations generally used in the equivalence theory by the conventional scattering source approximation.

By the NR approximation, Equation (3.22) is approximated as:

$$\Sigma_{sd}^{f}(E) \approx E\sum_{k}\frac{N_k^f}{(1-\alpha_k)}\int_{E}^{E/\alpha_k}\frac{dE'\sigma_p^k}{E'}\frac{1}{E'} = E\cdot\frac{\Sigma_p^f}{E} = \Sigma_p^f, \tag{3.26}$$

where Σ_p^f denotes the macroscopic potential scattering cross-section in the fuel region.

The NR approximation is also applied for the non-fuel region. The flux in the non-fuel region is approximated as a simple $1/E$ form, thus $\theta \approx 1$. As a result, the following simple relation is derived from Equation (3.23):

$$\mu(E) \approx 1. \tag{3.27}$$

By substituting Equations (3.26) and (3.27) into Equations (3.21), and by considering $\theta \approx 1$, the flux in the fuel and the non-fuel regions are approximated as:

$$\phi_f(E) \approx \frac{1}{E}\sum_{n=1}^{N}\beta_n\frac{\Sigma_p^f l_f + \alpha_n}{\Sigma_t^f(E) l_f + \alpha_n}, \tag{3.28}$$

$$\phi_{nf}(E) \approx \frac{1}{E}. \tag{3.29}$$

Equations (3.28) and (3.29) are the general form of the neutron flux in the equivalence theory using the NR approximation. As can be confirmed by comparisons

of Equations (3.21) and (3.25) with Equations (3.28) and (3.29), a new form of the slowing-down equations is completely equivalent to the conventional equations based on the equivalence theory by applying the following conversion.

<Numerator in Equation (3.21)>

$$\Sigma_{sd}^{f}(E) \rightarrow \Sigma_{p}^{f}$$

<Numerator in Equation (3.21)>

$$\mu(E) \rightarrow 1$$

<Equation (3.25)>

$$\theta \rightarrow 1$$

3.2.7 Numerical Generation of Rational Coefficients for Gray Resonance Ranges

In the present method, the coefficients α_n, β_n, ε_n and θ in the rational equation are required in advance to solve Equations (3.21)-(3.24). The coefficients are generated so as to reproduce the neutron fluxes by one-group fixed source MOC (method of characteristics) calculations against the several optical lengths including gray resonance ranges. The fundamental concept is the same as that for the gray resonance self-shielding treatment method [8].

In the fixed source MOC calculations, the neutron transport equation is written as:

$$\frac{d\psi(s,E)}{ds}+\Sigma_t(E)\psi(s,E)=\frac{Q(E)}{4\pi}, \tag{3.30}$$

where $\psi(s,E)$ denotes the angular flux for neutron energy E at spatial position s along with the specific characteristics line. The neutron source is assumed to be isotropic and written as $Q(E)/4\pi$. In the NR approximation consistent with Equation (3.26), the neutron source of Equations (3.4) and (3.5) can be expressed as $Q(E)=\Sigma_p/E$ by approximating the scattering cross-sections as the potential scattering cross-sections, and the fluxes within the energy integration as the $1/E$ asymptotic form. Then Equation (3.30) is rewritten as:

$$\frac{d\psi(s,E)}{ds}+\Sigma_t(E)\psi(s,E)=\frac{1}{E}\frac{\Sigma_p}{4\pi}. \tag{3.31}$$

By multiplying E for both sides of Equation (3.31), the following equation is derived:

$$\frac{d\psi(s,u)}{ds}+\Sigma_t(u)\psi(s,u)=\frac{\Sigma_p}{4\pi}, \tag{3.32}$$

where $E\psi(s,E)$ is rewritten as $\psi(s,u)$ denoting the angular flux for lethargy unit.

By assuming one-group fixed source problem, Equation (3.32) is simplified as:

$$\frac{d\psi(s)}{ds}+\Sigma_t\psi(s)=\frac{\Sigma_p}{4\pi}. \tag{3.33}$$

The scalar fluxes for each heterogeneous region are obtained by integrating the angular flux solutions of Equation (3.33) against each characteristics line, polar and azimuthal angles. As shown in Equation (3.33), the one-group equation is completely independent to the energy groups. In the MOC calculations for the present method, the final target is to generate the energy independent coefficients α_n, β_n, ε_n and θ for the rational equation, i.e., the flux response to the macroscopic total cross-section change. The energy dependence of the flux is implicitly taken into account on the fluctuation of the macroscopic cross-section instead of energy, which covers the range between the black and the white limits including the real gray resonance optical length.

The flux in the fuel region is expressed as Equation (3.28) in the equivalence theory. By averaging Equation (3.28) to the specific energy ranges assuming constant cross-section, the lethargy averaged flux in the fuel region becomes independent to energy and is written as a function of the optical length $\Sigma_t^f l_f$:

$$\phi_f(\Sigma_t^f l_f)=\sum_{n=1}^{N}\beta_n\frac{\Sigma_p^f l_f+\alpha_n}{\Sigma_t^f l_f+\alpha_n}. \tag{3.34}$$

In the present method, the coefficients α_n, β_n are first generated so as to well reproduce the one-group MOC result by Equation (3.34). In concrete, the following objective function is minimized:

$$\left(\frac{\Delta\phi_f}{\phi_f}\right)^2 = \sum_{l=1}^{L}\left[\frac{1}{\phi_{f,l}}\cdot\left\{\left(\sum_{n=1}^{N}\beta_n\frac{\Sigma_p^f l_f+\alpha_n}{\Sigma_{t,l}^f l_f+\alpha_n}\right)-\phi_{f,l}\right\}\right]^2, \tag{3.35}$$

where ($\Sigma_{t,l}^f$, $\phi_{f,l}$) denote the set of macroscopic total cross-section and the flux in the fuel region by the MOC calculations for several macroscopic cross-section points (L: the number of macroscopic cross-section points). Value of $\Sigma_{t,l}^f$ covers the range between the black and the white limits including the gray resonance ranges. Value of $\phi_{f,l}$ is obtained from the one-group fixed source calculation in the exact geometry by MOC. Thus the effect of geometry is directly incorporated into the fitted coefficients α_n, β_n for the pin-by-pin resolution in a fuel assembly.

In the present method, the coefficients ε_n and θ for the flux in the non-fuel region are also required. By substituting only Equations (3.26) and (3.27) into Equation (3.25), the flux in the non-fuel region is expressed as:

$$\phi_{nf}(E) = \frac{1}{E}\left[\theta+(1-\theta)\sum_{n=1}^{N}\beta_n\frac{\Sigma_p^f l_f+\varepsilon_n\alpha_n}{\Sigma_t^f(E) l_f+\varepsilon_n\alpha_n}\right]. \tag{3.36}$$

By averaging Equation (3.36) to the specific energy ranges assuming constant cross-section, the lethargy averaged flux in the non-fuel region becomes independent to energy and is also written as a function of the optical length $\Sigma_t^f l_f$:

$$\phi_{nf}(\Sigma_t^f l_f) = \theta+(1-\theta)\sum_{n=1}^{N}\beta_n\frac{\Sigma_p^f l_f+\varepsilon_n\alpha_n}{\Sigma_t^f l_f+\varepsilon_n\alpha_n}. \tag{3.37}$$

From Equation (3.37), the coefficient θ is easily obtained as the non-fuel flux in

the black limit condition:

$$\theta = \lim_{\Sigma_t^f \to \infty} \phi_{nf}(\Sigma_t^f l_f). \tag{3.38}$$

In the α_n, β_n and θ fixed condition, ε_n is then generated so as to well reproduce the one group MOC result by Equation (3.37). In concrete, the following objective function is minimized:

$$\left(\frac{\Delta\phi_{nf}}{\phi_{nf}}\right)^2 = \sum_{l=1}^{L}\left[\frac{1}{\phi_{nf,l}}\cdot\left\{\left(\theta+(1-\theta)\sum_{n=1}^{N}\beta_n\frac{\Sigma_p^f l_f+\varepsilon_n\alpha_n}{\Sigma_{t,l}^f l_f+\varepsilon_n\alpha_n}\right)-\phi_{nf,l}\right\}\right]^2, \tag{3.39}$$

where ($\Sigma_{t,l}^f$, $\phi_{nf,l}$) denote the set of macroscopic total cross-section in the fuel region and the flux in the non-fuel region by the MOC calculations for several points. $\phi_{nf,l}$ is obtained from the above one-group fixed source calculation by the MOC. The effects of geometry and moderator density are also directly incorporated into the coefficients ε_n, θ for the pin-by-pin resolution in a fuel assembly.

3.3 Derivation of Correction Factor Equation for Reaction-Rate Preservation

3.3.1 Conventional SPH Method for Reduction of Multi-group Condensation Error

In the multi-group (100~200 energy groups) transport calculation, the effective cross-section is used as the input data. The effective cross-section for g –th energy group is defined as:

$$\sigma_{x,g}^{r,f} = \frac{\int_g dE \sigma_x^r(E)\phi_f(E)}{\int_g dE \phi_f(E)}, \tag{3.40}$$

where $\sigma_x^r(E)$ denotes the continuous energy cross-section for the resonance nuclide r and the reaction type x. In the multi-group treatment, the multi-group reaction-rate for the resonance nuclide r, the reaction type x and the energy group g in the fuel region, which is expressed by $rr_{x,g}^{r,f}$, is written as:

$$rr_{x,g}^{r,f}(\text{multi\_group}) = \sigma_{x,g}^{r,f}\phi_{f,g}, \tag{3.41}$$

where $\phi_{f,g}$ denotes the multi-group neutron flux obtained from the transport calculation using $\sigma_{x,g}^{r,f}$.

In contrast to the above multi-group calculation, the multi-group reaction-rate obtained from the continuous energy or the ultra-fine-group (several tens of thousands of energy groups) treatment is written as:

$$rr_{x,g}^{r,f}(\text{continuous\_energy}) = \int_g dE \sigma_x^r(E)\phi_f(E). \tag{3.42}$$

In usual, Equations (3.41) and (3.42) are not equal, that is:

$$\int_g dE\,\sigma_x^r(E)\phi_f(E) \neq \sigma_{x,g}^{r,f}\phi_{f,g}\,. \tag{3.43}$$

The above inconsistency comes from the error due to cross-section condensation on energy. Flux obtained by multi-group transport solution does not reproduce that obtained by ultra-fine-group calculation even if the exact multi-group effective cross-sections, i.e., those directly obtained by ultra-fine-group calculation, are used. As a result, $rr_{x,g}^{r,f}(\text{multi\_group})$ cannot preserve $rr_{x,g}^{r,f}(\text{continuous\_energy})$ without correction.

The inconsistency on the multi-group reaction-rates obtained by the continuous energy and by the multi-group treatments directly causes the difference of the neutron multiplication factor between two treatments. In order to reduce the difference in the multi-group treatment, the following approach ((1) or (2)) is usually applied:

(1) Increasing the number of energy groups in the multi-group transport calculation [6, 7],

(2) Applying the cross-section correction methods such as SPH (Super homogenization) method [3].

Approach (2) is the more efficient one in order to avoid the additional computation time in the transport calculation. The SPH method is usually applied for the reduction of spatial homogenization error [15], but it can also be applied for the reduction of multi-group condensation error. In the SPH method, the effective cross-section is

corrected by the group dependent correction factor f_g as follows:

$$\tilde{\sigma}_{x,g}^{r,f} = f_g \sigma_{x,g}^{r,f} . \tag{3.44}$$

The role of f_g is to preserve the multi-group reaction-rate obtained from the continuous energy treatment, therefore the following relation is derived:

$$\int_g dE \sigma_x^r(E)\phi_f(E) = (f_g \sigma_{x,g}^{r,f}) \cdot \phi_{f,g} . \tag{3.45}$$

By using the definition of the effective cross-section (Equation (3.40)), f_g is rewritten as:

$$\begin{aligned} f_g &= \frac{\int_g dE \sigma_x^r(E)\phi_f(E)}{\sigma_{x,g}^{r,f}\phi_{f,g}} = \left[\frac{\int_g dE \sigma_x^r(E)\phi_f(E)}{\phi_{f,g}}\right] \Bigg/ \left[\frac{\int_g dE \sigma_x^r(E)\phi_f(E)}{\int_g dE \phi_f(E)}\right] \\ &= \frac{\int_g dE \phi_f(E)}{\phi_{f,g}}. \end{aligned} \tag{3.46}$$

f_g can be generated using the results of resonance calculation based on the ultra-fine-group treatment. The numerator of Equation (3.46) is directly calculated by integrating the neutron flux from the ultra-fine-group slowing-down calculation. The denominator of Equation (3.46) is calculated by the additional one-group fixed source calculation for each group g. As for the well-known SPH method, the iterative transport calculation is required so that the left and right hand sides of Equation (3.45) become equal. The correction factor f_g is converged as the iteration proceeds.

For the additional fixed source MOC calculations, the following one-group neutron transport equation is solved independently for each energy group g :

$$\frac{d\psi_g(s)}{ds} + f_g \Sigma_{t,g} \psi_g(s) = \frac{S_g}{4\pi}, \tag{3.47}$$

where $\psi_g(s)$ denotes the angular flux for group g at spatial position s along with the specific characteristics line. The scalar fluxes for each heterogeneous region are obtained by integrating the angular flux solutions of Equation (3.47) against each characteristics line, polar and azimuthal angles.

The neutron source is assumed to be isotropic and written as $S_g / 4\pi$. The macroscopic effective total cross-section $\Sigma_{t,g}$ is given from the ultra-fine-group flux weight scheme based on Equation (3.40). The neutron source S_g is generated from $S_g = \int_g dE S(E)$ by integrating the energy dependent scattering source $S(E)$ within group g, which is the byproduct of the ultra-fine-group slowing-down calculation. The SPH factor f_g is multiplied to $\Sigma_{t,g}$ for solving Equation (3.47) and it is updated in the iterative scheme until f_g is converged.

3.3.2 A Correction Factor Equation for Reaction-Rate Preservation

The new method for resonance self-shielding treatment derived in section 3.2 is based on the ultra-fine-group calculation, thus the SPH method described in section 3.3.1 can be applied in principle. The SPH method requires the additional flux calculations with iterative scheme, which requires longer computation time.

Fortunately, the present resonance self-shielding treatment includes the essence of the equivalence theory. The energy dependent neutron flux can be reconstructed by the analytical form of the multi-term rational equation. This feature becomes advantage comparing with the conventional SPH method, which is based on a pure numerical approach. In the following part, an equation to solve the correction factor f_g, which corresponds to the SPH factor in Equation(3.46), is derived based on the fundamental concept of the reaction-rate preservation scheme in the equivalence theory [16].

By using Equations (3.40) and (3.42), the multi-group reaction-rate obtained from the ultra-fine-group treatment is rewritten as:

$$\begin{aligned} rr_{x,g}^{r,f}(\text{continuous\_energy}) &= \int_g dE\sigma_x^r(E)\phi_f(E) \\ &= \left[\frac{\int_g dE\sigma_x^r(E)\phi_f(E)}{\int_g dE\phi_f(E)}\right]\cdot\int_g dE\phi_f(E) \\ &= \sigma_{x,g}^{r,f}\int_g dE\phi_f(E). \end{aligned} \tag{3.48}$$

In the multi-group treatment, the multi-group reaction-rate in Equation (3.41) is corrected as:

$$rr_{x,g}^{r,f}(\text{multi\_group}) = \tilde{\sigma}_{x,g}^{r,f}\phi_{f,g} = f_g\sigma_{x,g}^{r,f}\phi_{f,g}, \tag{3.49}$$

where Equation (3.44) is applied for Equation (3.41).

By assuming the constant cross-section within the energy group g for Equation (3.21), which is consistent with the multi-group treatment, the neutron flux in Equation (3.49) is derived as:

$$\begin{aligned}\phi_{f,g} &= \int_g dE \frac{1}{E} \sum_{n=1}^{N} \beta_n \frac{\Sigma_{sd}^f(E) l_f + \mu(E)\alpha_n}{f_g \Sigma_{t,g}^f l_f + \alpha_n} \\ &= \sum_{n=1}^{N} \beta_n \frac{\int_g dE \frac{1}{E} \Sigma_{sd}^f(E) l_f + \int_g dE \frac{1}{E} \mu(E)\alpha_n}{f_g \Sigma_{t,g}^f l_f + \alpha_n} \\ &= \sum_{n=1}^{N} \beta_n \frac{\Sigma_{sd,g}^f l_f + \mu_g \alpha_n}{f_g \Sigma_{t,g}^f l_f + \alpha_n},\end{aligned} \tag{3.50}$$

where the scattering source term for the fuel region, and the self-shielding correction term for the non-fuel region, are each defined as:

$$\Sigma_{sd,g}^f \equiv \int_g dE \frac{1}{E} \Sigma_{sd}^f(E) = \int_g dE \frac{1}{E} \cdot ES_f(E) = \int_g dE S_f(E), \tag{3.51}$$

$$\mu_g \equiv \int_g dE \frac{1}{E} \mu(E). \tag{3.52}$$

By substituting Equation (3.50) into Equation (3.49), the following equation is derived:

$$rr_{x,g}^{r,f}(\text{multi\_group}) = f_g \sigma_{x,g}^{r,f} \sum_{n=1}^{N} \beta_n \frac{\Sigma_{sd,g}^f l_f + \mu_g \alpha_n}{f_g \Sigma_{t,g}^f l_f + \alpha_n}. \tag{3.53}$$

Finally, by assuming that Equation (3.53) is equal to Equation (3.48), and dividing both sides by $\sigma_{x,g}^{r,f}$, the following equation to solve f_g is formulated as:

$$f_g \sum_{n=1}^{N} \beta_n \frac{\Sigma_{sd,g}^f l_f + \mu_g \alpha_n}{f_g \Sigma_{t,g}^f l_f + \alpha_n} = \int_g dE \phi_f(E). \tag{3.54}$$

Equation (3.54) is a correction factor equation for reaction-rate preservation, which suits with the hybrid method for resonance self-shielding treatment in section 3.2. All the terms except for f_g are byproducts of the solution of the new set of slowing-down equation in section 3.2.4. f_g is easily obtained from iterative calculation until f_g is converged. From Equation (3.54), f_g for (i+1)-th iteration is generated using i-th result as follows:

$$f_g(\mathrm{i}+1) = \frac{\int_g dE \phi_f(E)}{\sum_{n=1}^{N} \beta_n \frac{\Sigma_{sd,g}^f l_f + \mu_g \alpha_n}{f_g(\mathrm{i}) \Sigma_{t,g}^f l_f + \alpha_n}}. \tag{3.55}$$

The method includes the iteration scheme, but any additional iterative flux calculations are no longer required. The calculation time of f_g is negligible comparing with the conventional SPH method. Besides, Equation (3.54) can be rewritten as N-th order linear equation. Therefore the analytical solution of f_g is easily obtained in case of the one-term or the two-terms rational equation, in which the iteration of Equation (3.55) is not necessary at all.

3.4 Numerical Procedure and Calculation Flow

3.4.1 Numerical Discretization and Calculation Scheme for Slowing-Down Equation

A new set of the slowing-down equation is solved numerically by energy discretization. The discretized form of the equation and its fundamental calculation scheme are described in this section.

$\phi_f(E)$, $\varphi_{nf}(E)$, $\Sigma_{sd}^f(E)$ and $\mu(E)$ in section 3.2.4 are discretized for energy and written as:

$$\phi_{f,fg} = \frac{1}{\overline{E}_{fg}} \sum_{n=1}^{N} \beta_n \frac{\Sigma_{sd,fg}^f l_f + \mu_{fg}\alpha_n}{\Sigma_{t,fg}^f l_f + \alpha_n}, \tag{3.56}$$

$$\varphi_{nf,fg} = \frac{1}{\overline{E}_{fg}} \sum_{n=1}^{N} \beta_n \frac{\Sigma_{sd,fg}^f l_f + \mu_{fg}\varepsilon_n\alpha_n}{\Sigma_{t,fg}^f l_f + \varepsilon_n\alpha_n}, \tag{3.57}$$

$$\Sigma_{sd,fg}^f = \begin{cases} 0 \ (fg=1) \\ \overline{E}_{fg} \sum_k \frac{N_k^f}{(1-\alpha_k)} \sum_{fg'_k} \frac{\Delta E_{fg'_k} \sigma_{s,fg'_k}^k \phi_{f,fg'_k}}{\overline{E}_{fg'_k}} \ (fg=2,3,\cdots,FG) \end{cases}, \tag{3.58}$$

$$\mu_{fg} = \begin{cases} \theta \ (fg=1) \\ \theta + (1-\theta)\frac{\overline{E}_{fg}}{\Sigma_p^{nf}} \sum_k \frac{N_k^{nf}\sigma_p^k}{(1-\alpha_k)} \sum_{fg'_k} \frac{\Delta E_{fg'_k} \varphi_{nf,fg'_k}}{\overline{E}_{fg'_k}} \ (fg=2,3,\cdots,FG) \end{cases}, \tag{3.59}$$

where

FG: The number of ultra-fine energy group,

fg: An ultra-fine energy group for the range $E_{fg} \le E < E_{fg-1}$,

E_{fg-1}, E_{fg}: Upper and lower energy boundaries for group fg,

$\overline{E}_{fg}$: Lethargy averaged energy for group fg ($\overline{E}_{fg} = \sqrt{E_{fg-1}E_{fg}}$),

ΔE_{fg}: Energy width for group fg ($\Delta E_{fg} = E_{fg-1} - E_{fg}$),

$fg'_k = \{E_{fg'} \mid E_{fg} < E_{fg'} \le E_{fg}/\alpha_k\}$: Incoming neutron energy group for scattering source integration of the nuclide k.

In the energy discretization, the ultra-fine-group structure is assumed to be fine enough so that the resonance cross-sections are constant within each group fg and the self-scattering can be ignored. Besides, the energy width ΔE_{fg} for each ultra-fine-group is assumed to be small enough relative to the scattering length for energy, i.e., $E_{fg}/\alpha_k - E_{fg}$. In the actual implementation, the ultra-fine-group structure is designed so as to satisfy the above assumptions.

For the slowing-down calculation, the ultra-fine-group neutron flux is solved successively from the fast to the lower energy ranges without iteration. This feature is specific for the slowing-down equation.

First, the 1st group fluxes are solved based on Equations (3.56)-(3.59) as:

$$\phi_{f,1} = \frac{1}{\overline{E}_1}\sum_{n=1}^{N}\beta_n \frac{\Sigma^f_{sd,1} l_f + \mu_1 \alpha_n}{\Sigma^f_{t,1} l_f + \alpha_n} = \frac{1}{\overline{E}_1}\sum_{n=1}^{N}\beta_n \frac{0\cdot l_f + \theta\cdot\alpha_n}{\Sigma^f_{t,1} l_f + \alpha_n} = \frac{1}{\overline{E}_1}\sum_{n=1}^{N}\beta_n \frac{\theta\alpha_n}{\Sigma^f_{t,1} l_f + \alpha_n}, \quad (3.60)$$

$$\varphi_{nf,1} = \frac{1}{\overline{E}_1}\sum_{n=1}^{N}\beta_n \frac{\Sigma^f_{sd,1} l_f + \mu_1 \varepsilon_n \alpha_n}{\Sigma^f_{t,1} l_f + \varepsilon_n \alpha_n} = \frac{1}{\overline{E}_1}\sum_{n=1}^{N}\beta_n \frac{\theta\varepsilon_n \alpha_n}{\Sigma^f_{t,1} l_f + \varepsilon_n \alpha_n}. \quad (3.61)$$

Second, the 2nd group slowing-down cross-section and self-shielding correction

factor are obtained based on Equations (3.58)-(3.59) using the above numerical solutions for $\phi_{f,1}$, $\varphi_{nf,1}$ as:

$$\Sigma_{sd,2}^{f} = \overline{E}_2 \sum_k \frac{N_k^f}{(1-\alpha_k)} \frac{\Delta E_1 \sigma_{s,1}^k \phi_{f,1}}{\overline{E}_1}, \tag{3.62}$$

$$\mu_2 = \theta + (1-\theta) \frac{\overline{E}_2}{\Sigma_p^{nf}} \sum_k \frac{N_k^{nf} \sigma_p^k}{(1-\alpha_k)} \frac{\Delta E_1 \varphi_{nf,1}}{\overline{E}_1}. \tag{3.63}$$

Then the 2nd group fluxes are solved based on Equations (3.56)-(3.57) using the above numerical solutions for $\Sigma_{sd,2}^{f}$, μ_2. From the 3rd group calculations, ($\Sigma_{sd,fg}^{f}, \mu_{fg}$) and ($\phi_{f,fg}, \varphi_{nf,fg}$) are solved simultaneously. The above procedure is repeated for successive energy groups.

3.4.2 Fast Calculation Scheme for Scattering Source Integration

The energy integration of the scattering source, i.e., $(\Sigma^f_{sd,fg}, \mu_{fg})$ calculation in this paper, needs long computation time. In order to reduce the computation time, the energy group boundary $fg_{k,\min}$ corresponding to the maximum energy E_{fg}/α_k for the fg-th group scattering source integration, is pre-evaluated and tabulated in cross-section library. This treatment enables to avoid the conditional branch processing for the scattering source integration in the actual implementation.

For the additional fast calculation, the scattering source for fg-th group is calculated using $(fg-1)$-th group result based on the efficient numerical scheme developed by Kier [17]. The fg-th group scattering source for the fuel region, which is a part of $\Sigma^f_{sd,fg}$, is written as:

$$S^f_{fg} = \sum_k \frac{N^f_k}{(1-\alpha_k)} \sum_{fg'_k} \frac{\Delta E_{fg'_k} \sigma^k_{s,fg'_k} \phi_{f,fg'_k}}{\overline{E}_{fg'_k}}. \tag{3.64}$$

The relation of scattering source integration range between fg-th and $(fg-1)$-th groups is shown in Figure 3.4. As shown in Figure 3.4, the majority of the scattering integration range is common. Therefore, fg-th scattering source S^f_{fg} is easily obtained from $(fg-1)$-th source S^f_{fg-1} by adding $(fg-1)$-th integration part and subtracting the part which is out of the fg-th integration range. The corresponding equation is derived as:

$$S^f_{fg} = S^f_{fg-1} + \sum_k \frac{N^f_k}{(1-\alpha_k)} \left\{ \frac{\Delta E_{fg-1} \sigma^k_{s,fg-1} \phi_{f,fg-1}}{\overline{E}_{fg-1}} - \sum_{fg'_k} \frac{\Delta E_{fg'_k} \sigma^k_{s,fg'_k} \phi_{f,fg'_k}}{\overline{E}_{fg'_k}} \right\}, \tag{3.65}$$

where the energy integration range for the subtracting part is only $(fg-1)'_{k,\min} \le fg'_k \le fg'_{k,\min} - 1$ ($fg'_{k,\min}$: Minimum incoming neutron energy group for scattering source integration of nuclide k to the outgoing neutron energy group fg). This treatment is very effective comparing with the direct integration for all the energy ranges in Equation (3.64).

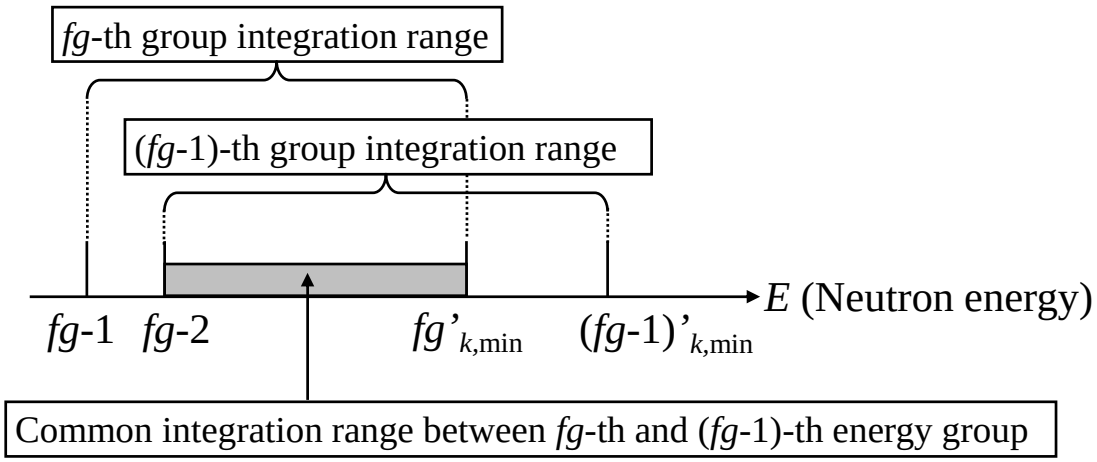

Figure 3.4 Relation of scattering source integration range between fg -th and $(fg-1)$ -th groups.

Finally, the slowing-down cross-section can be obtained as $\Sigma^f_{sd,fg} = \overline{E}_{fg} S^f_{fg}$. μ_{fg} can also be obtained with the same manner.

3.4.3 Calculation Flow of New Resonance Self-Shielding Treatment

Calculation flow of the method established in sections 3.2-3.4 is shown in **Figure 3.5**. The calculation procedure is described as follows:

(1) Read the microscopic ultra-fine-group cross-section data σ_{fg} (fg : ultra-fine-group number) from the library.

(2) Read the relative atomic weight to the neutron, A, and the microscopic potential scattering cross-section σ_p.

(3) Read the heterogeneous region volume V and the number density N.

(4) Perform the one-group MOC fixed source calculations using Equation (3.33) and obtain the fluxes for each region. In this step, each non-fuel region such as the cladding and moderator is treated as the individual regions. Each non-fuel region data are homogenized in steps (6) and (7).

(5) Generate α_n and β_n by fitting the MOC flux data for fuel region using Equation (3.35).

(6) Calculate N_k^{nf} and Σ_p^{nf} from the non-fuel heterogeneous regions data for the cladding and moderator. Here, N_k^{nf} is a volume averaged number density in the non-fuel region and is obtained as $N_k^{nf} = \sum_{i \in nf} N_k^i V_i \Big/ \sum_{i \in nf} V_i$ (i: each heterogeneous region included in the non-fuel region). Σ_p^{nf} is then

obtained as $\Sigma_p^{nf} = \sum_k N_k^{nf} \sigma_p^k$.

(7) Calculate $\phi_{nf}(\Sigma_t^f)$ using the one-group MOC results for the non-fuel heterogeneous regions. $\phi_{nf}(\Sigma_t^f)$ is a volume averaged flux in the non-fuel region and is obtained as $\phi_{nf}(\Sigma_t^f) = \sum_{i \in nf} \phi_i(\Sigma_t^f) V_i \Big/ \sum_{i \in nf} V_i$.

(8) Generate the rational coefficient θ by substituting value of $\lim_{\Sigma_t^f \to \infty} \phi_{nf}(\Sigma_t^f)$ based on Equation (3.38).

(9) Generate ε_n by fitting the MOC flux data for non-fuel region using Equation (3.39).

(10) Calculate the first group flux data ($\phi_{f,1}, \varphi_{nf,1}$) in the ultra-fine-group resolution using Equations (3.60) and (3.61).

(11) Calculate the fg -th ultra-fine-group $\Sigma_{sd,fg}^f$ and μ_{fg} based on Equations (3.58) and (3.59). In the actual numerical scheme, the scattering source term is solved by Equation (3.65) using $(fg-1)$ -th group results (The part of μ_{fg} can also be obtained with the same manner).

(12) Calculate the fg -th ultra-fine-group flux data ($\phi_{f,fg}, \varphi_{nf,fg}$) using $\Sigma_{sd,fg}^f$, μ_{fg} and Equations (3.56) and (3.57).

(13) Carry out the steps (11) and (12) for $2 \le fg \le FG$ (FG: the number of ultra-fine-group) successively without iterations.

(14) Generate the effective cross-section $\sigma_{x,g}^{r,f}$ using $\phi_{f,fg}$ and Equation (3.40).

(15) Calculate the correction factor f_g using Equation (3.54) and multiply it to $\sigma_{x,g}^{r,f}$.

(16) Apply the evaluated effective cross-sections for the multi-group flux calculation.

In case of the fuel assembly calculations, step (4) (one-group MOC fixed source calculations) is performed for the exact two-dimensional assembly geometry, not for the unit pin-cell. The flux data is obtained for pin-by-pin resolution by the MOC calculations, thus the following steps (5)-(15) can be performed individually for each fuel cell in the target geometry.

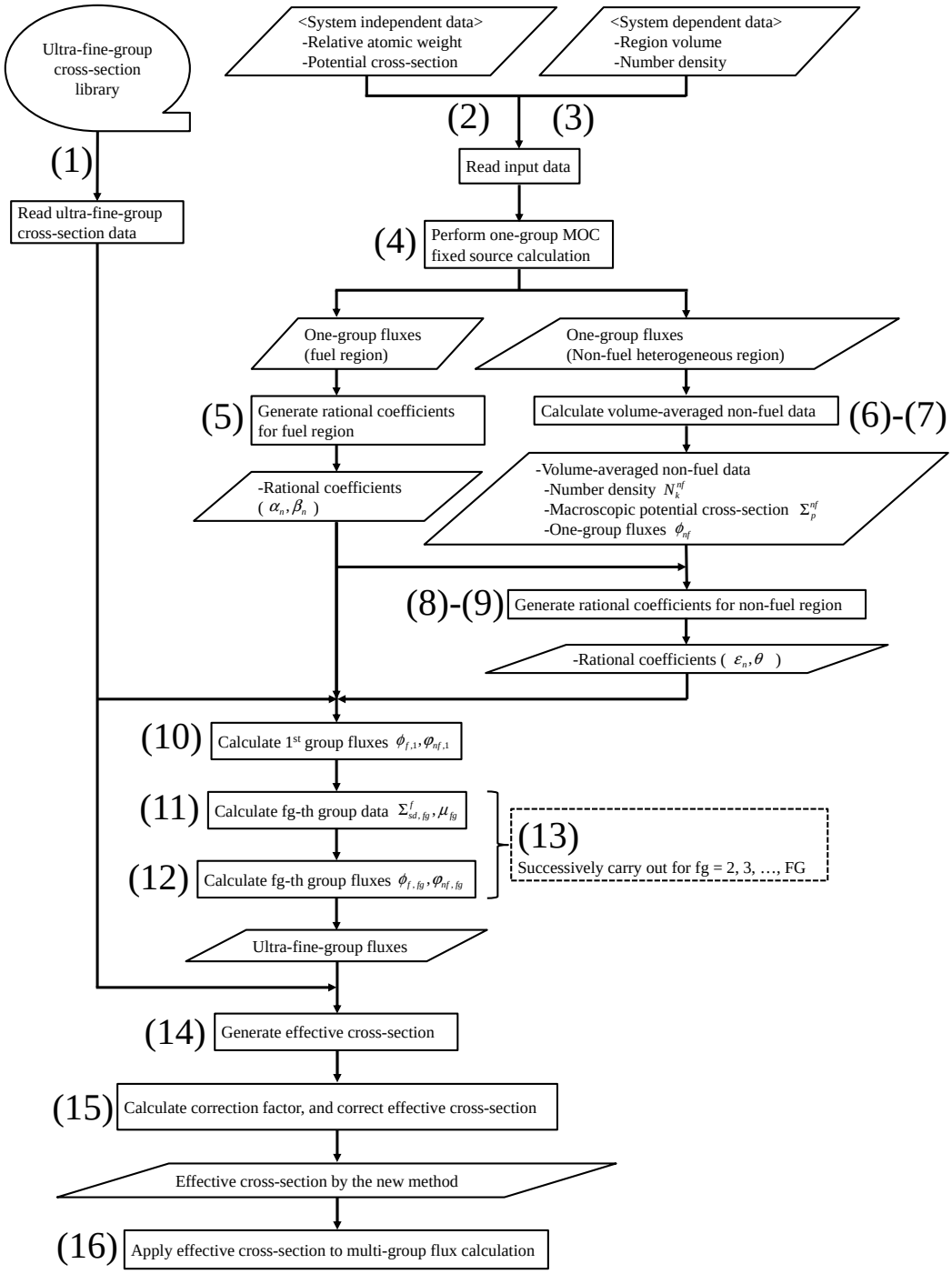

Figure 3.5 Calculation flow of a new resonance self-shielding treatment.

3.5 Verification for Unit Pin-Cell Problem

3.5.1 Analysis Condition

In this section, verifications of the new method for resonance self-shielding treatment are carried out using unit pin-cell problem. The present method is implemented in the MHI (Mitsubishi Heavy Industries, Ltd.) lattice physics code GALAXY [8, 9], and the GALAXY is used for all the verifications.

The one hundred and twenty thousands (120,000) of ultra-fine energy group cross-section library is generated by editing the output of NJOY BROADR module [18] using the ENDF/B-VII.0 nuclear data files [19]. The obtained ultra-fine-group library is incorporated as a part of the GALAXY cross-section library based on the ENDF/B-VII.0. The list of nuclides considering the ultra-fine-group resonance cross-section and the scattering source in this verification are shown in **Table 3.1**. The energy group structure of the 120,000 groups is shown in **Table 3.2**, which is based on the structure of SLAROM-UF code [5] except for the fast and thermal energy ranges. It should be noted that the multi-group flux calculation is carried out with XMAS 172 energy group structure [20] in GALAXY. The above ultra-fine-group library is used only for the ultra-fine-group flux calculations to generate the multi-group effective cross-sections.

Table 3.1 List of nuclides considered in the verification of ultra-fine-group calculation.

Condition	Target heterogeneous region	Nuclides
Consideration of both ultra-fine-group resonance XS[1)] and scattering source	Fuel	^{235}U, ^{238}U, ^{238}Pu, ^{239}Pu, ^{240}Pu, ^{241}Pu, ^{242}Pu, ^{241}Am, ^{16}O (in fuel region)
Consideration of only ultra-fine-group scattering source with potential scattering XS	Non-fuel	^{1}H, ^{16}O (in moderator region), ^{10}B, ^{90}Zr, ^{91}Zr, ^{92}Zr, ^{94}Zr, ^{96}Zr
1) XS: cross-section		

Table 3.2 Ultra-fine-group energy structure.

Energy boundary [eV]		Mesh division
Upper	Lower	(Equal division for lethargy)
20000000	52475	10000
52475	9118.8	56000
9118.8	4307.4	12000
4307.4	961.12	12000
961.12	130.07	8000
130.07	0.32242	12000
0.32242	0.00001	10000

The number of rational equation term is $N = 2$. The ultra-fine-group flux calculation by the new method is carried out from the fast to the epithermal energy ranges (20MeV-0.625eV). The effective cross-sections in the range between 0.82MeV-0.625eV are generated by the present method. The effective cross-sections except for the above energy ranges are generated by the gray resonance self-shielding method [8] based on the equivalence theory. The effective cross-sections for Zr nuclides in the cladding region are generated by the enhanced neutron current method [21].

These conditions are applied for all the analyses in this article.

UO_2 (4.8wt% ^{235}U) and MOX (7.2wt% Pu fissile contents) pin-cells with Hot Full Power (HFP) operating conditions are set as the typical LWR (Light Water Reactor) neutron spectrum conditions. The specifications of the pin-cell problem are shown in **Table 3.3**, and the geometrical configuration is shown in **Figure 3.6**.

Table 3.3 Specifications of the pin-cell model.

Item		Specification
Material	Fuel	UO_2 case: 4.8wt% ^{235}U UO_2
		MOX case: 7.2wt%Pu-f MOX
	Cladding	Zr
	Moderator	Borated water
Temperature	Fuel	976K
	Cladding	600K
	Moderator	580K
Boron concentration		1000ppm
Geometry	Cell pitch	1.26cm
	Pellet radius	0.4095cm
	Cladding outer radius	0.475cm
	Cladding thickness (Gap is omitted)	0.0655cm

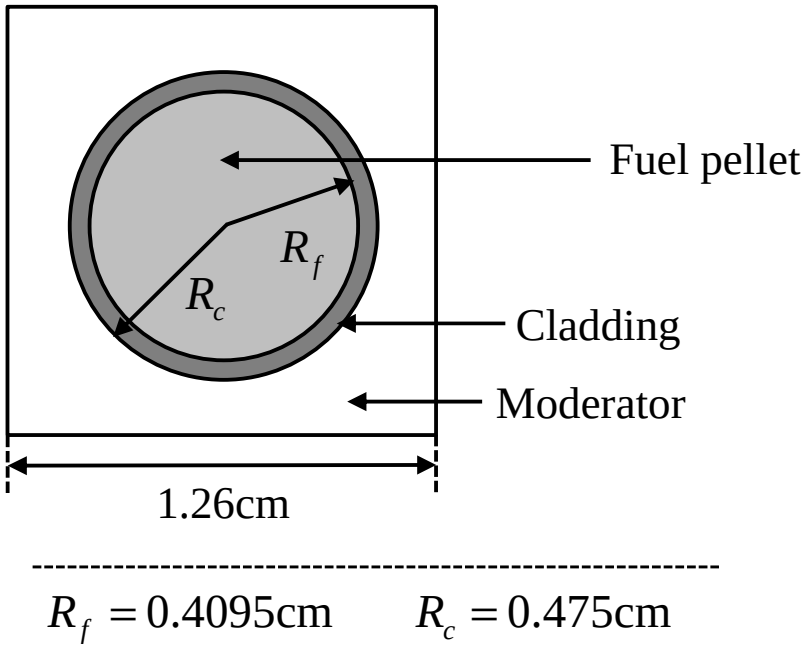

Figure 3.6 Geometry of pin-cell model.

Especially for sub-sections 3.5.3, 3.5.4 and 3.5.6, the calculation results by GALAXY are compared with those by continuous-energy Monte-Carlo code MVP [22]. ENDF/B-VII.0 [19] nuclear data library is used in all the MVP calculations to be consistent with GALAXY calculations. The total number of neutron sampling for MVP calculations is set to 100 million histories, in which the one sided statistical uncertainty of *k-infinity* is about 5pcm ($5\times10^{-5}\,\Delta k/k$).

3.5.2 Reproducibility of Flux for Gray Resonance Ranges

The reproducibility of the flux by the rational equation is confirmed in this sub-section for the calculation conditions shown in section 3.5.1

As described in section 3.2.7, the coefficients α_n, β_n, ε_n and θ in the multi-term rational equation are generated so as to reproduce the flux by the MOC one-group fixed source calculations. The above set of the coefficients have an important role in the fundamental accuracy of the present method.

For the UO_2 pin-cell case, the reproducibility of the fluxes by the rational equation of Equations (3.34) and (3.37) is shown in **Figure 3.7**. In Figure 3.7, the MOC results are set as a reference. As shown in Figure 3.7, the multi-term rational equation of Equations (3.34) and (3.37) can well reproduce the MOC results for overall optical length ranges between black and white limits including gray resonance ranges. The reproducibility can be confirmed both for the fuel and the non-fuel regions.

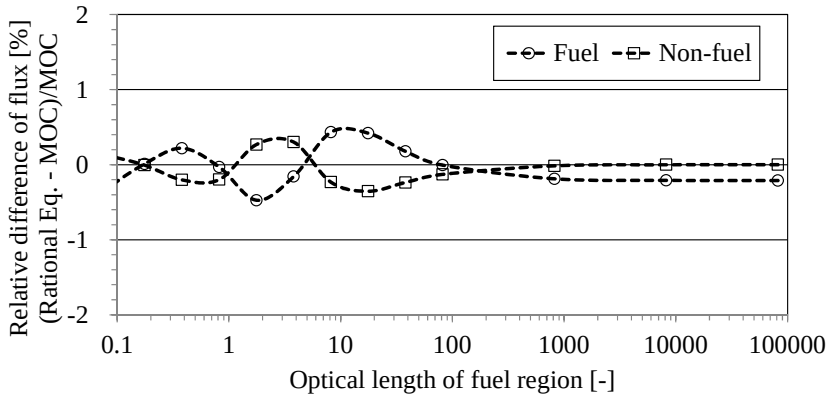

Figure 3.7 Reproducibility of fluxes by the rational equation for wide range of optical length.

3.5.3 Ultra-Fine-Group Neutron Flux

The ultra-fine-group neutron flux by the present resonance self-shielding treatment is compared with the continuous-energy Monte-Carlo result in this sub-section.

As described in section 3.2.4, a new set of the slowing-down equations (Equations (3.21)-(3.24)) are solved to calculate the ultra-fine-group neutron flux. The prediction accuracy of the flux directly influences on the accuracy of the multi-group effective cross-section.

The ultra-fine-group fluxes in a fuel region by GALAXY with the present method and those by MVP are shown in **Figures 3.8-3.9** for UO_2 and MOX cases against the important resonance energy ranges of ^{238}U. The fluxes based on the equivalence theory with NR approximation are also shown for comparisons. The equivalence theory based fluxes are analytically obtained from the multi-term rational equation assuming that the target resonance nuclide is ^{238}U.

As shown in these Figures, the present method can accurately predict the ultra-fine-group neutron flux, which is almost equivalent to the continuous-energy Monte-Carlo results. The present method can directly consider the resonance interference effect (local flux depression) induced by the multiple resonance nuclides except for ^{238}U. The equivalence theory cannot incorporate the effect without some additional cares [11-13].

It should be noted that both GALAXY and MVP codes uses the scattering kernel based on the asymptotic model shown in Equation (3.3), thus the treatment of scattering source term is consistent between GALAXY and MVP in this verification.

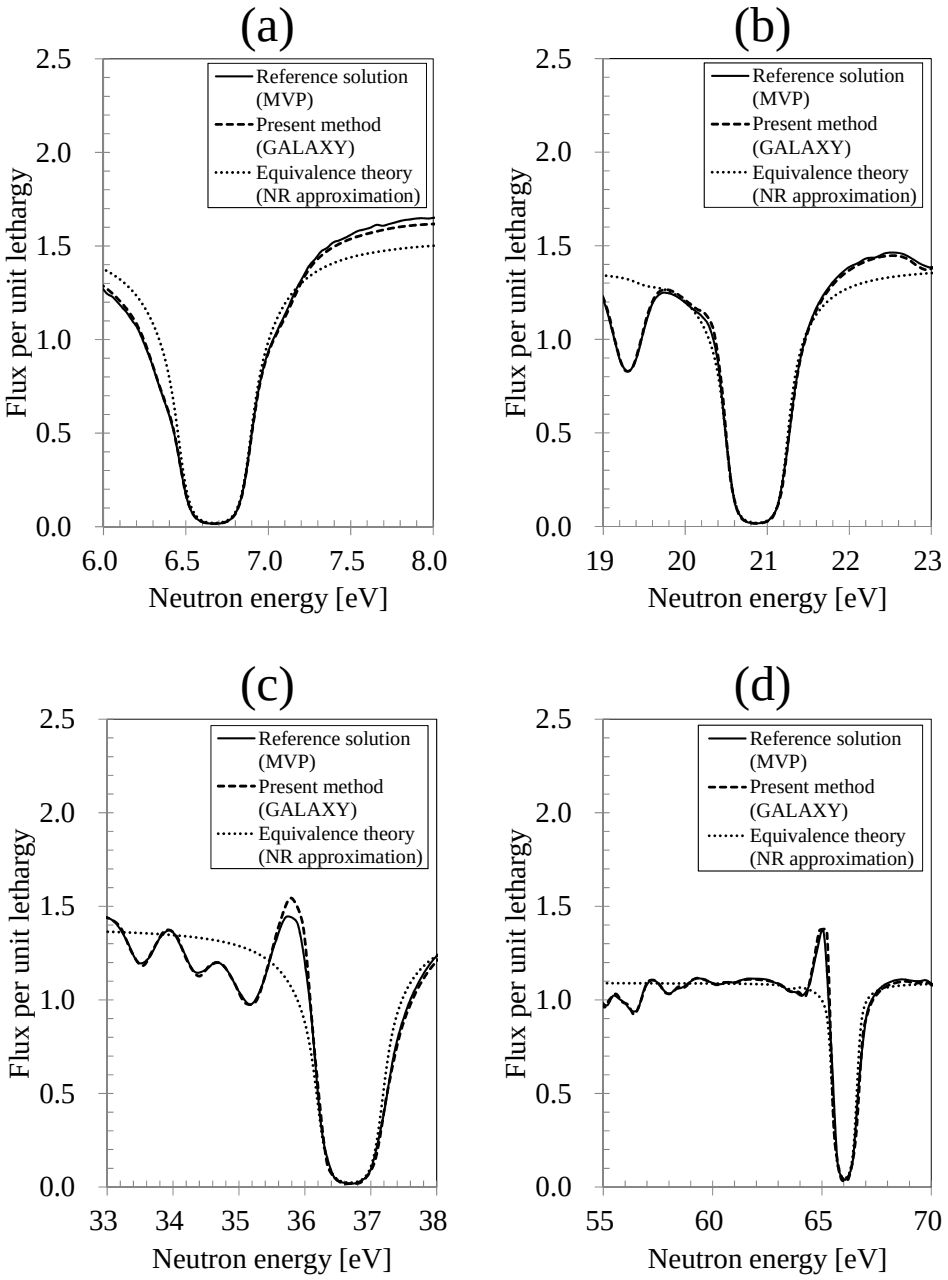

Figure 3.8 Comparison of ultra-fine-group fluxes between GALAXY and MVP for UO_2 fuel ((a) 6-8eV, (b) 19-23eV, (c) 33-38eV, (d) 55-70eV).

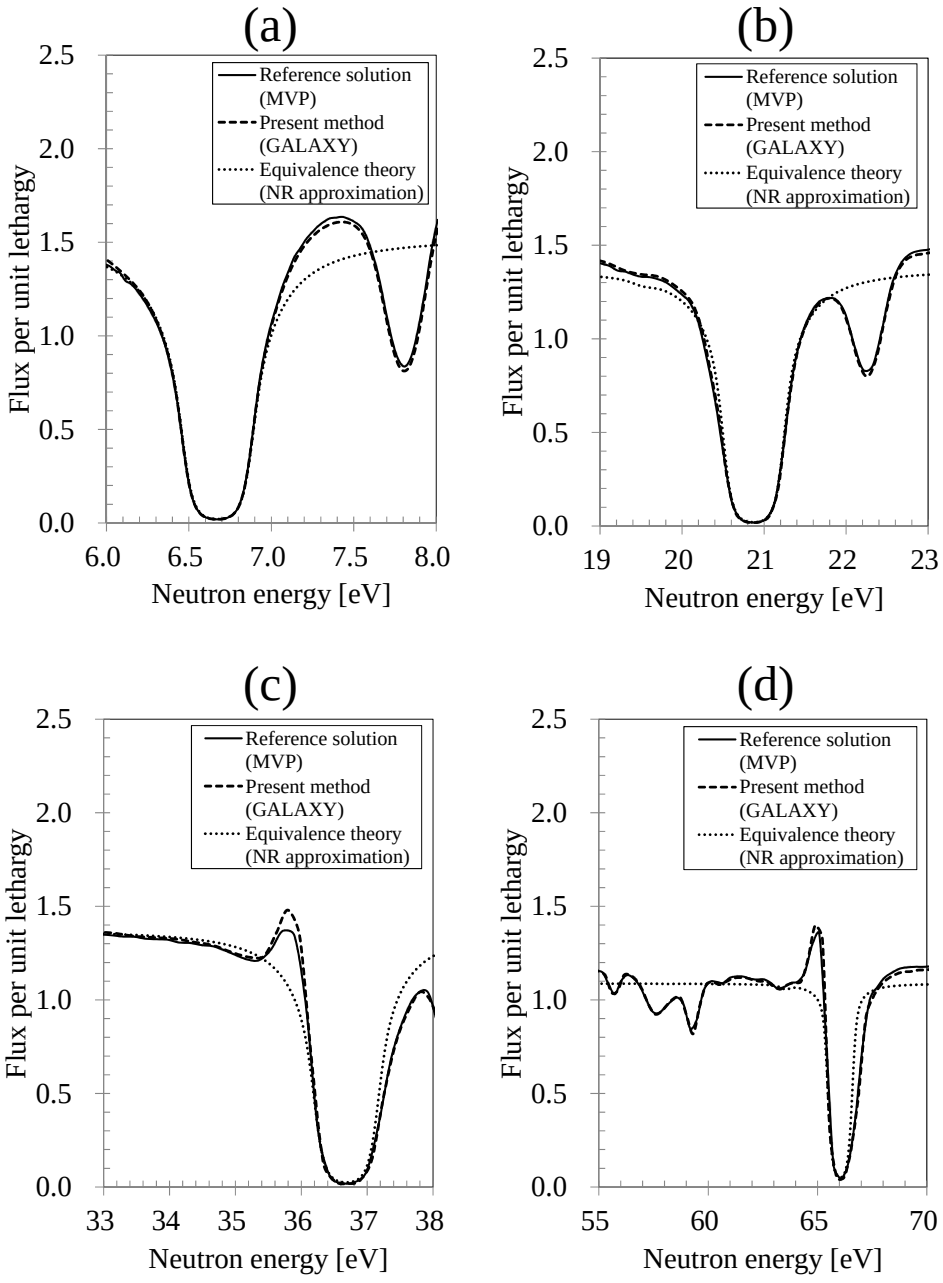

Figure 3.9 Comparison of ultra-fine-group fluxes between GALAXY and MVP for MOX fuel ((a) 6-8eV, (b) 19-23eV, (c) 33-38eV, (d) 55-70eV).

The important byproducts of the ultra-fine-group flux calculations in the present method, i.e., $\Sigma_{sd}^{f}(E)$ (Equation (3.22)) and $\mu(E)$ (Equation (3.23)), are also shown in **Figures 3.10-3.11** for UO_2 case. As discussed in section 3.2.6, the conventional equivalence theory corresponds to $\Sigma_{sd}^{f}(E) \approx \Sigma_{p}^{f}$ and $\mu(E) \approx 1$. From these figures, the differences of $\Sigma_{sd}^{f}(E)$ from Σ_{p}^{f} and $\mu(E)$ from unity are clearly observed.

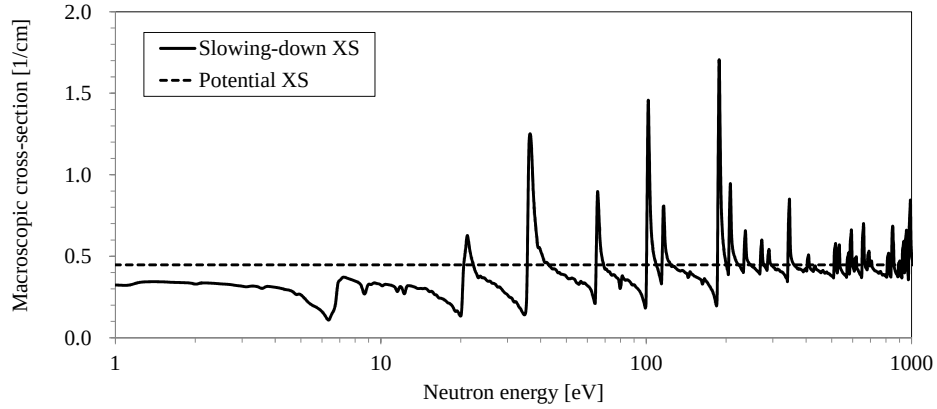

Figure 3.10 Energy dependence of $\Sigma_{sd}^{f}(E)$.

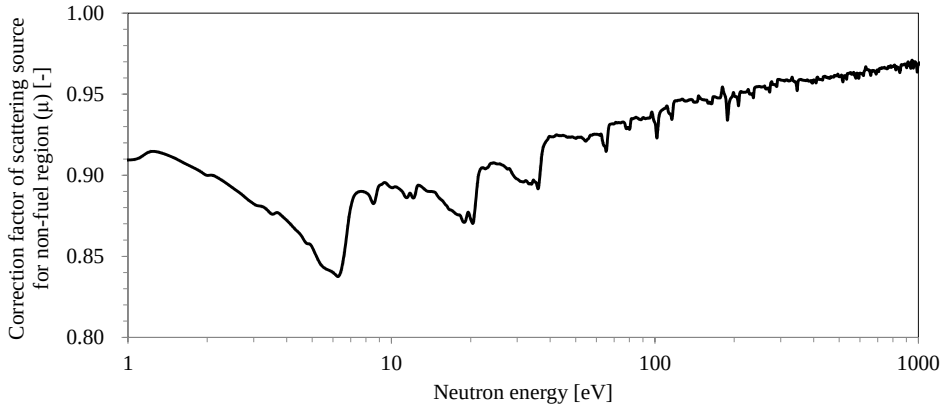

Figure 3.11 Energy dependence of $\mu(E)$.

The difference of $\Sigma_{sd}^{f}(E)$ from Σ_{p}^{f} corresponds to the effect of accurate intermediate resonance treatment for resonance cross-sections because Σ_{p}^{f} is obtained from the NR approximation. In the conventional equivalence theory, the effect of intermediate resonances is considered by the IR parameter and it is handled in multi-group resolution. The present method, in contrast, the intermediate resonances are directly considered in the ultra-fine-group resolution by the slowing-down calculation.

The difference of $\mu(E)$ from unity corresponds to the correction factor for the accurate scattering source treatment in a non-fuel region (see Equation (3.11)). In the conventional equivalence theory, the scattering source for a non-fuel region is approximated as Σ_{p}^{nf}/E, as mentioned in section 3.2.2. The actual scattering source has a locally more complicated energy dependence, and $\mu(E)$ can directly consider the effect. From the view point of numerical calculations, $\mu(E)$ essentially handles the slowing-down source in a non-fuel region, and it enables to carry out the ultra-fine-group flux calculation for the heterogeneous system as if it were the slowing-down calculation for the infinite homogeneous medium. This feature leads to the smaller computational burdens comparing with the pure numerical method for the heterogeneous slowing-down calculation.

The accurate treatment of $\Sigma_{sd}^{f}(E)$ and $\mu(E)$ directly contributes to improve the accuracy of the ultra-fine-group flux against the equivalence theory without significant increase of computational burdens.

3.5.4 Multi-Group Effective Cross-Section

The multi-group effective cross-section by the present resonance self-shielding treatment is compared with the continuous-energy Monte-Carlo result in this sub-section.

The effective cross-sections in the fuel region by GALAXY with the present method and those by MVP are shown in **Table 3.4** for UO_2 and MOX cases against the important resonance energy ranges of ^{238}U. As shown in Table 3.4, the present method can accurately predict the effective cross-section, as a result of good agreement for the ultra-fine-group flux between GALAXY and MVP shown in section 3.5.3. The applicability of the present method is confirmed in the next sub-section through the prediction accuracy of *k-infinity* (final results).

Table 3.4 Comparison of multi-group effective cross-sections between GALAXY and MVP.

Fuel type	Energy group in XMAS 172 group structure	Energy [eV]		Macroscopic absorption XS [1/cm]	Relative difference of XS [%]	MVP statistical error [%]
		Upper	Lower	MVP	((GALAXY-MVP)/MVP)	
UO_2	88	7.524	6.160	1.208	1.1	0.1
	80	22.603	19.455	0.699	1.0	0.1
	75	37.266	33.720	0.863	-0.5	0.1
	69	67.904	55.595	0.181	-0.2	0.1
MOX	88	7.524	6.160	1.186	0.8	0.1
	80	22.603	19.455	0.881	0.5	0.1
	75	37.266	33.720	0.610	0.0	0.1
	69	67.904	55.595	0.281	-0.3	0.1

3.5.5 Multi-Group Reaction-Rate and K-infinity

The multi-group reaction-rate and *k-infinity* by the present resonance self-shielding treatment are compared with those obtained by the continuous-energy Monte-Carlo result in this sub-section.

The multi-group reaction-rates in the fuel region by GALAXY with the present method and those by MVP are shown in **Table 3.5** for UO_2 and MOX cases against the important resonance energy ranges of ^{238}U. The *k-infinity* results are also shown in this table. As shown in Table 3.5, the present method can accurately predict the reaction-rate. The reaction-rate preservation scheme efficiently reduces the difference of reaction-rate by GALAXY comparing with MVP result, and as a result, the *k-infinity* well agrees between the two codes.

Table 3.5 Comparison of multi-group reaction-rates and *k-infinity* between GALAXY and MVP.

Fuel type	Energy group in XMAS 172 group structure	Energy [eV]		Relative difference of macroscopic absorption rate [%] ((GALAXY-MVP)/MVP)		MVP statistical error for reaction rate [%]	Relative difference of k-infinity [pcm] ((GALAXY-MVP)/MVP)		MVP statistical error for k-infinity [pcm]
		Upper	Lower	Without RR (1)	With RR (2)		Without RR	With RR	
UO_2	88	7.524	6.160	3.1	-0.9	0.1	-502	-46	4
	80	22.603	19.455	4.3	0.8	0.1			
	75	37.266	33.720	6.2	2.7	0.1			
	69	67.904	55.595	2.0	0.5	0.1			
MOX	88	7.524	6.160	3.2	-0.6	0.1	-360	-49	5
	80	22.603	19.455	4.5	1.2	0.1			
	75	37.266	33.720	6.9	2.6	0.1			
	69	67.904	55.595	2.0	0.4	0.1			
(1) Without RR: Do NOT apply reaction rate preservation scheme									
(2) With RR: Apply reaction rate preservation scheme									

3.5.6 Calculation Time

The breakdown of calculation time for the present method is shown in **Table 3.6**. As shown in Table 3.6, the calculation time for the ultra-fine-group flux is very short. On the basis of its short computation time, the present method can be easily applied for the fuel assembly geometry, i.e., the ultra-fine-group calculation by Equations (3.21)-(3.24) for each fuel cell independently with the cell dependent coefficients α_n, β_n, ε_n and θ.

Here, it should be noted that reading of the ultra-fine-group cross-section library takes only once, thus the time is negligible against the total calculation time of the lattice physics calculations.

Table 3.6 Calculation time.

Process	CPU time [sec]	
	UO_2	MOX
Ultra-fine-group XS library read (only one time)	0.31	0.28
Ultra-fine-group flux calculation	0.22	0.23
Generation of effective XS and correction factor	0.02	0.03

3.5.7 Extension for Multi-Region Problem

Treatment of Gd_2O_3 bearing fuel rod, which requires sub-division of the pellet, is also important theme for the resonance calculation, and it is still open problem to extend the present method for the general multi-region problem. Thus only UO_2 and MOX fuels are covered in this paper.

In order to apply for the general multi-region system such as radially sub-divided Gd_2O_3 bearing fuel rod, the more time consuming methods, i.e., the direct heterogeneous ultra-fine-group calculation or the sub-group method [1, 23], may be required. It is sure that the sub-group method can easily treat the multi-region system. However, the other important factors such as the resonance interference effect, which can be treated in the present method, cannot directly be taken into account in the sub-group method. Some investigations are carried out [24], but the more research is desired in this field.

3.6 Verification for UO_2/MOX Multi-Assembly Problem

3.6.1 Analysis Condition

In this section, verifications of the new method for resonance self-shielding treatment are carried out using UO_2/MOX multi-assembly color-set problem. The fundamental calculation condition is common for the unit pin-cell problem in section 3.5.

Objective of the verification is to show the applicability of the present method for the general multi-cell problem including several types of fuel rods whose compositions are different each other. The multi-assembly problem is designed based on PWR type 17 $\times$17 UO_2 and MOX fuel assemblies. The ratio for the number of loading between UO_2 and MOX assemblies is assumed to be 3:1 in order to yield the local gradient of the flux spatial distribution in the target system. Hot Full Power (HFP) operating conditions are set as the typical LWR neutron spectrum conditions. The specifications of the color-set problem are shown in **Table 3.7**, and the geometrical configuration is shown in **Figure 3.12** (details of cell arrangement are shown in section 3.6.2). As shown in Figure 3.12, calculation geometry consists of four quarter-assemblies with a perfect reflective boundary condition.

Table 3.7 Specifications of the multi-assembly model.

Item		Specification
Material	Fuel	UO_2 assembly: 4.8wt% ^{235}U UO_2
		MOX assembly:
		High: 7.2wt% Pu-f MOX
		Middle: 4.2wt% Pu-f MOX
		Low: 3.1wt% Pu-f MOX
	Cladding	Zr
	Moderator	Borated water
Temperature	Fuel	976K
	Cladding	600K
	Moderator	580K
Boron concentration		1000ppm
Geometry	Cell pitch	1.26cm
	Pellet radius	0.4095cm
	Cladding outer radius	0.475cm
	Cladding thickness (Gap is omitted)	0.0655cm
	Assembly gap	0.08cm

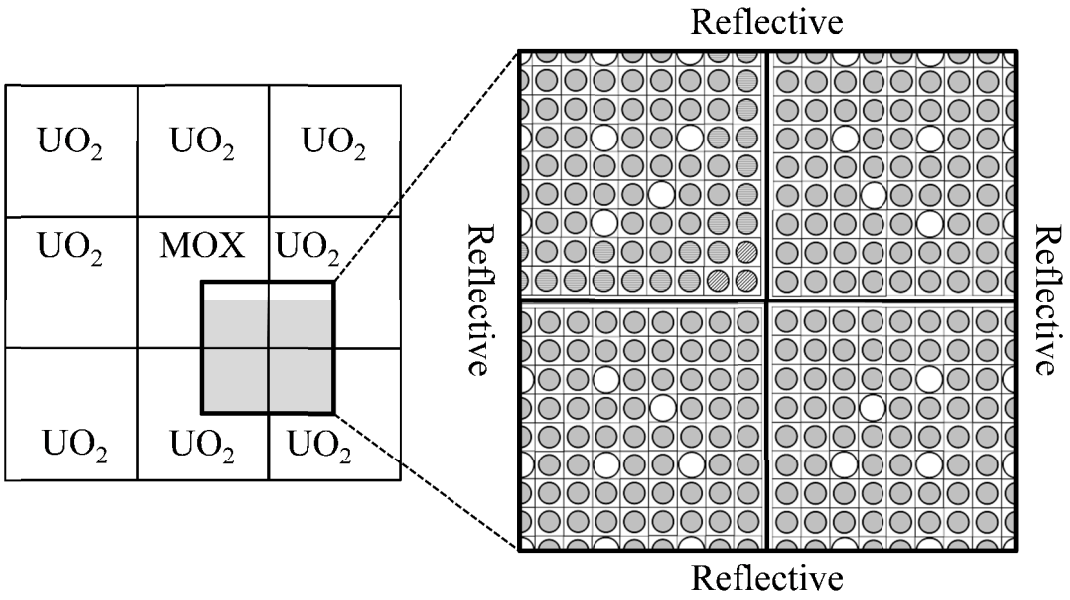

Figure 3.12 Geometry of multi-assembly model.

The calculation results by GALAXY are compared with those by continuous-energy Monte-Carlo code MVP [22]. ENDF/B-VII.0 [19] nuclear data library is used in all the MVP calculations to be consistent with GALAXY calculations. The total number of neutron sampling for MVP calculations is set to 100 million histories.

3.6.2 Pin-by-Pin Effective Dancoff Factor

As described in section 3.2.7, the rational coefficients α_n, β_n are generated for pin-by-pin resolution in a fuel assembly. In order to observe the trend of pin-by-pin rational coefficients, the equivalent 1-term Dancoff factor by the present resonance self-shielding treatment, which is named as the effective Dancoff factor in this paper, is generated by the following equation [1]:

$$D_{eff} = \left\{ \sum_{n=1}^{N} \beta_n \sqrt{\alpha_n} \right\}^2 , \tag{3.66}$$

where the multi-group cross-section or the resonance integral is assumed to be expressed as a function of the square root of heterogeneous term for the background cross-section. By taking into account that the heterogeneous term is proportional to α_n, and β_n corresponds to the weight of n-th term, D_{eff} can be obtained by averaging $\sqrt{\alpha_n}$ with β_n weight.

The pin-by-pin effective Dancoff factor in each fuel region by GALAXY with the present method is shown in **Figure 3.13** for lower half part of the geometry. Figure 3.13 also shows cell arrangement in the multi-assembly geometry. As shown in Figure 3.13, D_{eff} is larger on the fuel rods near the water enriched non-fuel cells than on the other fuel rods. This trend is consistent with the fundamental property of the Dancoff factor. On the other hands, the fuel composition dependence of D_{eff} is extremely small, as can be observed by comparison among the symmetric positions. D_{eff} (or α_n, β_n in the

present method) essentially considers the geometry effect, and is generated to be constant against the change of optical length or macroscopic cross-section for each fuel rod.

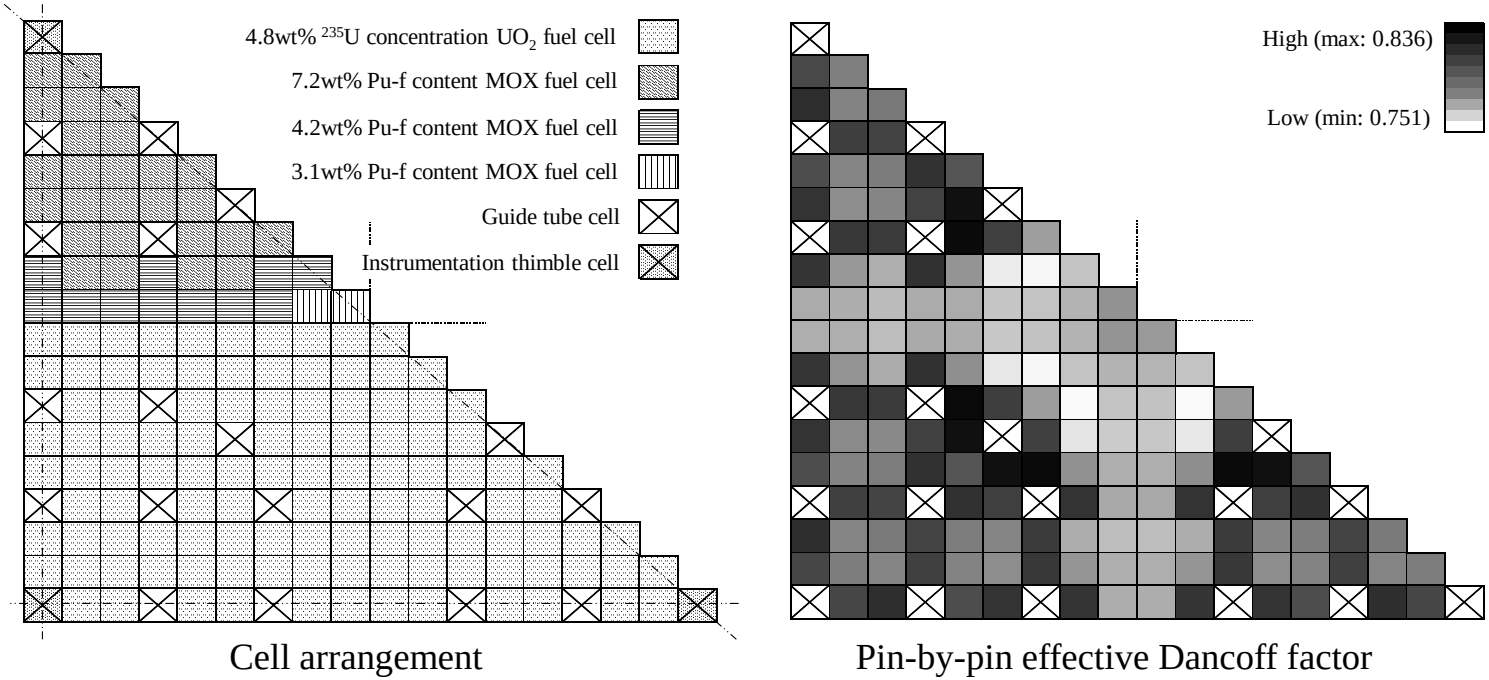

Figure 3.13 Cell arrangement and pin-by-pin effective Dancoff factor.

In the present method, the spatial and energy dependences of the flux are well decomposed by utilizing the rational equation. The spatial dependence is taken into account by the pin-by-pin coefficients α_n, β_n based on the equivalence theory, while the energy dependence is directly considered by the ultra-fine-group cross-sections for each fuel rod based on the slowing-down calculation. In this framework, the ultra-fine-group slowing-down calculations can be performed for each fuel cell individually through the pin-by-pin coefficients α_n, β_n, even if the optical lengths of each fuel rod are different each other in an assembly. As a result, the present method can be applied for the general multi-cell problem in which the fuel compositions are different for each fuel rod in the target system.

The above treatment is appropriate based on the fact that the more detailed spatial dependence of flux is obtained from the multi-group flux calculation step. The decomposition of space and energy is an efficient assumption for the purpose of the ultra-fine-group flux calculations, in which the obtained flux is not used as a final solution of the lattice physics calculation but as a weighting function to generate the appropriate multi-group effective cross-section against each limited energy range.

3.6.3 Pin-by-Pin Reaction-Rate and K-infinity

The pin-by-pin absorption and fission rates and *k-infinity* by the present resonance self-shielding treatment are compared with those obtained by the continuous-energy Monte-Carlo result in this sub-section.

The pin-by-pin absorption and fission rate distributions by GALAXY with the present method and the difference between GALAXY and MVP are shown in **Figures 3.14-3.15** for lower half part of the geometry. Here, 1σ MVP statistical uncertainties of the reaction-rates are smaller than 0.3%. The *k-infinity* results for the multi-assembly system are also shown in **Table 3.8**. As shown in the results, the present method can accurately predict both the *k-infinity* and the pin-by-pin reaction-rate, even for the complicated geometry including both UO_2 and different types of Pu content MOX fuel rods.

Table 3.8 Comparison of *k-infinity* between GALAXY and MVP for multi-assembly problem.

k-infinity		Relative difference of k-infinity [pcm]	MVP statistical error for
GALAXY	MVP	((GALAXY-MVP)/MVP)	k-infinity [pcm]
1.27701	1.27790	-70	4

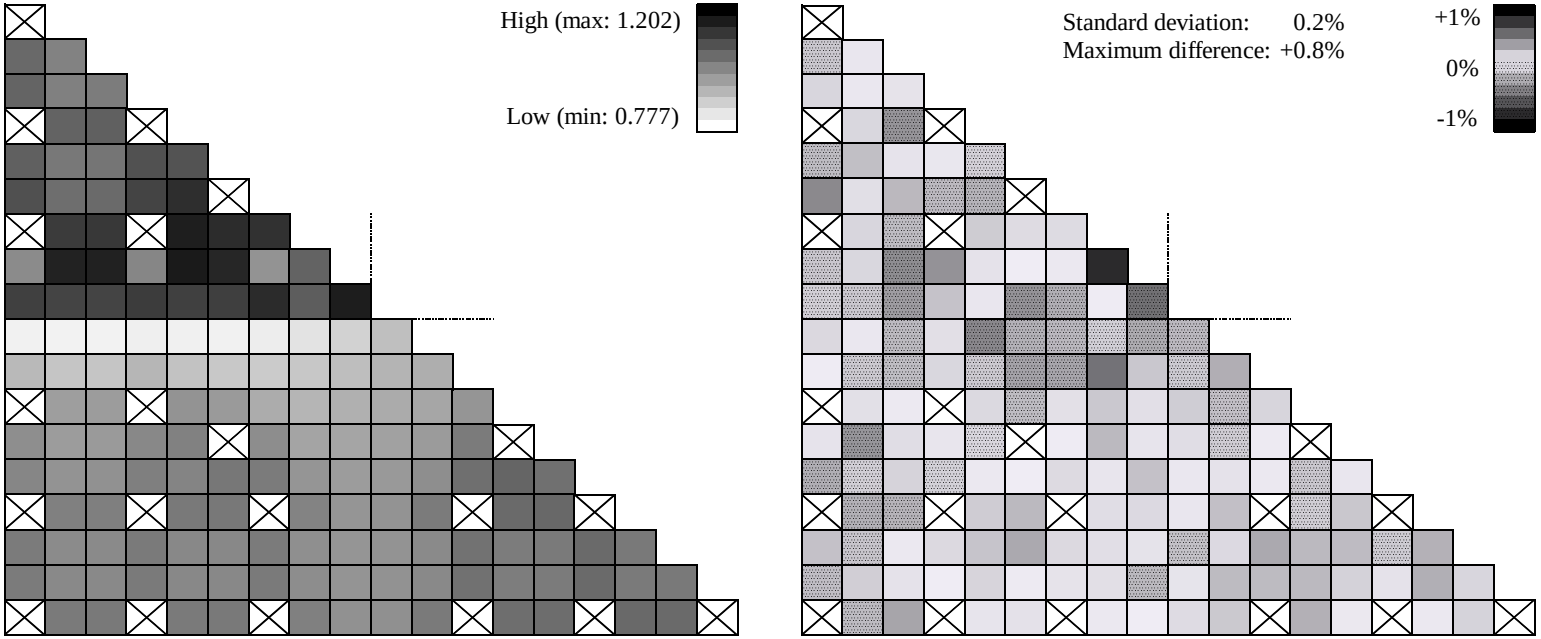

Figure 3.14 Comparison of pin-by-pin absorption rate distribution between GALAXY and MVP.

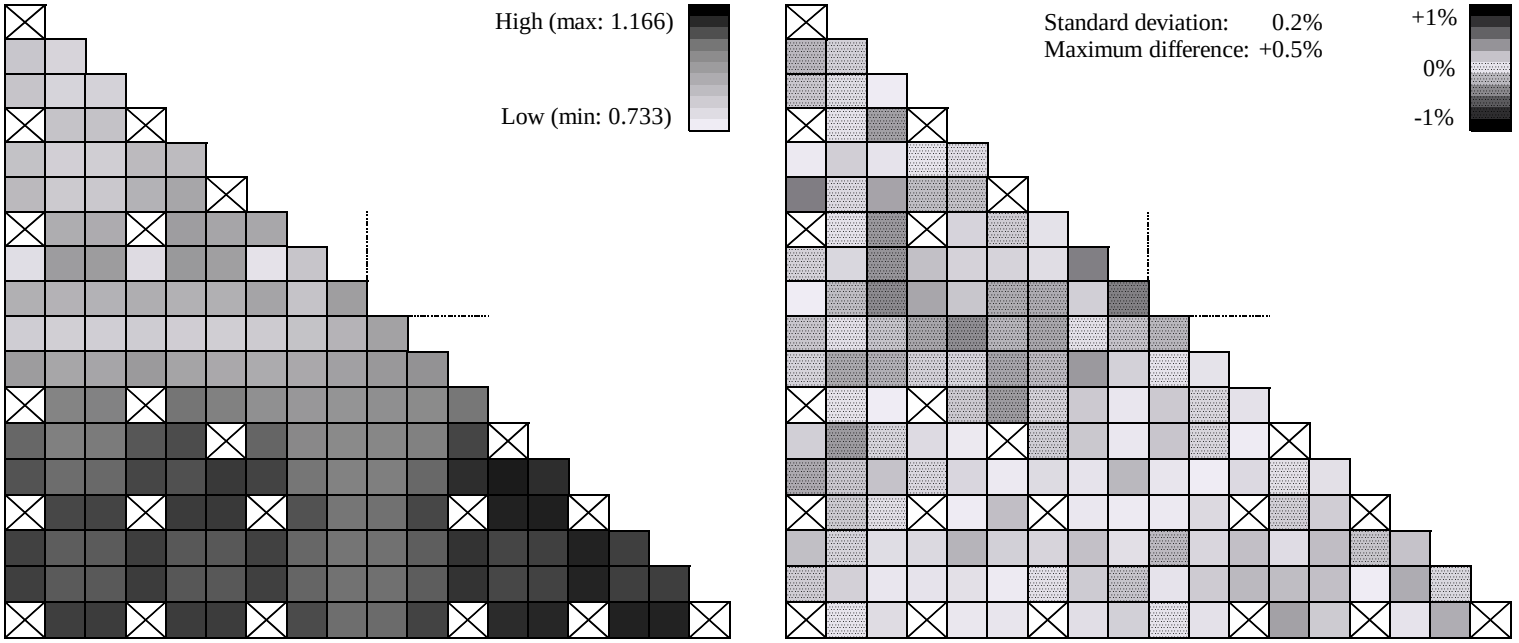

Figure 3.15 Comparison of pin-by-pin fission rate distribution between GALAXY and MVP.

3.7 Extensive Monte-Carlo Benchmark

3.7.1 Analysis Condition

In this section, verifications of the reactivity prediction in lattice physics code GALAXY are carried out with the new resonance self-shielding treatment. The *k-infinity* and some important reactivity coefficients are compared between GALAXY with the present method and continuous-energy Monte-Carlo code MVP.

The main application of GALAXY is generation of assembly nuclear constants used for core design and safety analysis of PWR. In these analyses, the prediction accuracy of Doppler and moderator reactivity is especially important. As a result, the corresponding Doppler temperature coefficient, the moderator density coefficient and the boron worth by GALAXY are verified by comparison with MVP results. The ENDF/B-VII.0 nuclear data library is used in all the MVP calculations to be consistent with GALAXY calculations.

3.7.2 Doppler Reactivity

In this sub-section, the accuracy of Doppler reactivity prediction by GALAXY is evaluated. Fuel temperature change is the main factor for the Doppler reactivity in PWR. The corresponding reactivity coefficient is Doppler temperature coefficient (DTC). In the present Doppler benchmark, DTC generated by GALAXY is compared with that by MVP.

The Doppler reactivity is mainly induced by change of the amount for ^{238}U resonance absorption due to the fuel temperature changes. The contribution of resonance absorption for ^{238}U depends not only on the fuel composition but on the range of fuel temperature and burnup. From this point of view, the Mosteller's original benchmark [25, 26] is extended to the different fuel temperature and burnup ranges in the present study. The verification is essentially the investigation of the prediction accuracy for DTC against the systematic change of the number density and the energy dependent resonance cross-sections for each nuclide in the fuel region. The unit pin-cell benchmark is prepared for the simple and essential verification.

The specification of Doppler reactivity benchmark is shown in **Table 3.9**. Calculation geometry is shown in **Figure 3.16**. The base condition is the same as that in Mosteller's original benchmark. The gap region between pellet and cladding is explicitly treated in MVP calculations. In contrast, for GALAXY calculations, the gap region is smeared to the cladding region and the number density of cladding region is diluted so that the total number of atom is preserved.

Table 3.9 Specification of the Doppler reactivity benchmark.

Item	Specification	
Fuel type	UO_2, MOX (Reactor-recycle)	
Fuel composition [wt%]	UO_2 (^{235}U concentration)	0.711, 1.6, 2.4, 3.1, 3.9, 4.5, 5.0 (600K and 900K, 0GWd/t)
	MOX (PuO_2 content)	1.0, 2.0, 4.0, 6.0, 8.0 (600K and 900K, 0GWd/t)
Fuel temperature [K]	300, 600, 900, 1200, 1500, 1800, 2100	
Burnup [GWd/t]	0, 20, 40, 60, 80	

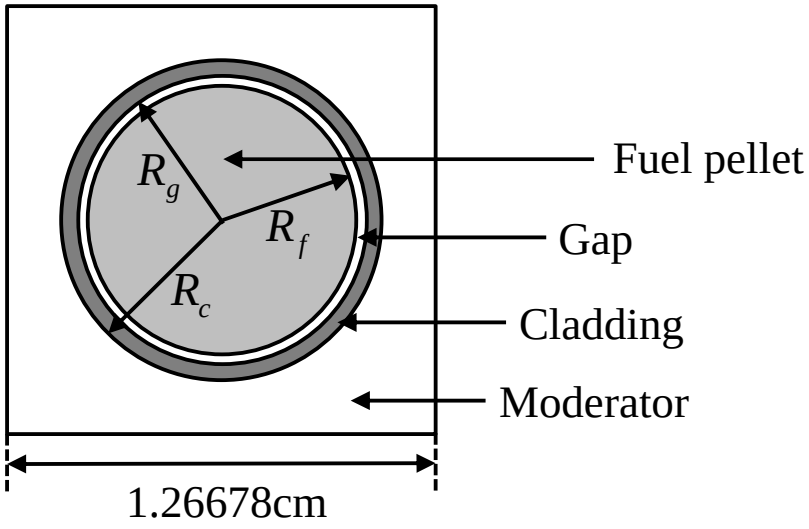

$$R_f = \begin{cases} 0.39398\text{cm (HZP)} \\ 0.39433\text{cm (HFP)} \end{cases} \qquad R_g = 0.40226\text{cm} \qquad R_c = 0.45972\text{cm}$$

Figure 3.16 Geometry of pin-cell model for Doppler reactivity benchmark.

The total number of neutron sampling for MVP calculations is set to 100 million histories, in which the one sided statistical uncertainty of *k-infinity* is about 5pcm ($5\times10^{-5}\,\Delta k/k$).

In the present benchmark, DTC is basically generated as follows:

$$DTC = \left[\left(\frac{k_{HFP}-1}{k_{HFP}}\right)-\left(\frac{k_{HZP}-1}{k_{HZP}}\right)\right] \Big/ (T_{HFP}-T_{HZP}) = \left(\frac{1}{T_{HFP}-T_{HZP}}\right)\cdot\left(\frac{k_{HFP}-k_{HZP}}{k_{HZP}k_{HFP}}\right), \quad (3.67)$$

where T and k denote the fuel temperature and *k-infinity*, respectively. Indices "HZP" and "HFP" denote the hot zero power and hot full power conditions, respectively. Both GALAXY and MVP calculations are based on the asymptotic scattering model, in which the scattering kernel is expressed as Equation (3.3). It should be noted that the recent topic for the more exact scattering modeling, i.e., the thermal motion and the temperature dependent resonance scattering treatment to the heavy nuclides [27, 28], is out of scope in this paper.

In this benchmark, (1) fuel composition dependence (Mosteller's original benchmark), (2) fuel temperature and (3) burnup dependences (extended benchmarks) of DTCs are verified. Topic (1) includes both UO_2 and MOX fuel cells in which the fuel composition range satisfies the commercial PWR fuel specifications. Topics (2) and (3) are set by extending the original 5.0wt% UO_2 and 8.0wt% MOX fuel conditions.

For the fuel temperature dependence (2), only the fuel temperature is systematically changed between room temperature (300K) and very high temperature (2100K) conditions against the original HFP (900K) 5.0wt% UO_2 and 8.0wt% MOX cases. The corresponding DTCs are generated for each temperature range, i.e., DTCs between 300-600K, 600-900K,$\cdots$, 1800K-2100K.

For the burnup dependence (3), the depletion calculation is carried out by GALAXY

in advance against the same original HFP (900K) cases. 80GWd/t is set as the maximum burnup, and the obtained nuclide compositions for each burnup point are used in the verifications. The common number densities to the depleted fuels are used both for GALAXY and MVP, and the burnup calculation by MVP is not carried out at all.

The differences of *k-infinity* between GALAXY and MVP are summarized in **Table 3.10**. Here the difference for each case *n* is evaluated as:

$$(\Delta k / k)_n = \frac{k_{n,\mathrm{GALAXY}} - k_{n,\mathrm{MVP}}}{k_{n,\mathrm{MVP}}}, \tag{3.68}$$

where $k_{n,\mathrm{GALAXY}}$ and $k_{n,\mathrm{MVP}}$ denote the *k-infinity* for case *n* calculated by GALAXY and MVP, respectively.

Table 3.10 Comparison of *k-infinity* between GALAXY and MVP in the Doppler reactivity benchmark.

Fuel type	Changed parameter	Number of samples	Difference [pcm] (GALAXY-MVP)/MVP		MVP statistical error [pcm]
			Average	Maximum	Average
UO_2	Fuel composition	14	-61	-101	4
	Fuel temperature	7	-65	-111	4
	Burnup	10	28	120	5
MOX	Fuel composition	10	-31	-55	5
	Fuel temperature	7	-56	-104	5
	Burnup	10	29	148	6
All (UO_2+MOX)	Fuel composition	24	-49	-101	4
	Fuel temperature	14	-61	-111	5
	Burnup	20	28	148	5

The averaged and maximum differences $(\Delta k/k)_{\text{avg}}$, $(\Delta k/k)_{\max}$ are also evaluated as:

$$(\Delta k/k)_{\text{avg}} = \frac{1}{I}\sum_{i=1}^{I}(\Delta k/k)_i \,, \tag{3.69}$$

$$(\Delta k/k)_{\max} = (\Delta k/k)_j \quad \left\{ j \;\middle|\; \max_i \left|(\Delta k/k)_i\right| = \left|(\Delta k/k)_j\right| \right\}, \tag{3.70}$$

where *I* denotes the number of sample. These equations are also used in section 3.7.3.

As shown in Table 3.10, the differences are very small for fuel composition, fuel temperature and fuel burnup changes.

Figures 3.17-3.19 show the calculation results of *DTC* to each parameter change for UO_2 and MOX fuel cells. The fuel temperatures in Figure 3.18 correspond to the midpoint between the neighboring two temperatures. The differences of *DTC* between GALAXY and MVP are summarized in **Table 3.11**. The average difference of *DTC* is almost within the 2~3σs of statistical uncertainty for MVP propagated by *k-infinity* statistical errors, thus considering the 3σs MVP statistical uncertainty, the differences for *DTC* between GALAXY and MVP are small for each parameter change.

It is concluded that GALAXY with the present resonance self-shielding treatment can accurately predict the Doppler reactivity.

Table 3.11 Comparison of Doppler temperature coefficient between GALAXY and MVP in the Doppler reactivity benchmark.

Fuel type	Changed parameter	Number of samples	Difference [%] (GALAXY-MVP)/MVP		MVP statistical error [%]
			Average	Maximum	Average
UO_2	Fuel composition	7	1.4	2.4	0.6
	Fuel temperature	6	2.3	3.8	0.8
	Burnup	5	1.5	2.6	0.7
MOX	Fuel composition	5	1.9	2.5	0.7
	Fuel temperature	6	1.9	2.4	0.8
	Burnup	5	1.9	3.0	0.8
All (UO_2+MOX)	Fuel composition	12	1.6	2.5	0.7
	Fuel temperature	12	2.1	3.8	0.8
	Burnup	10	1.7	3.0	0.7

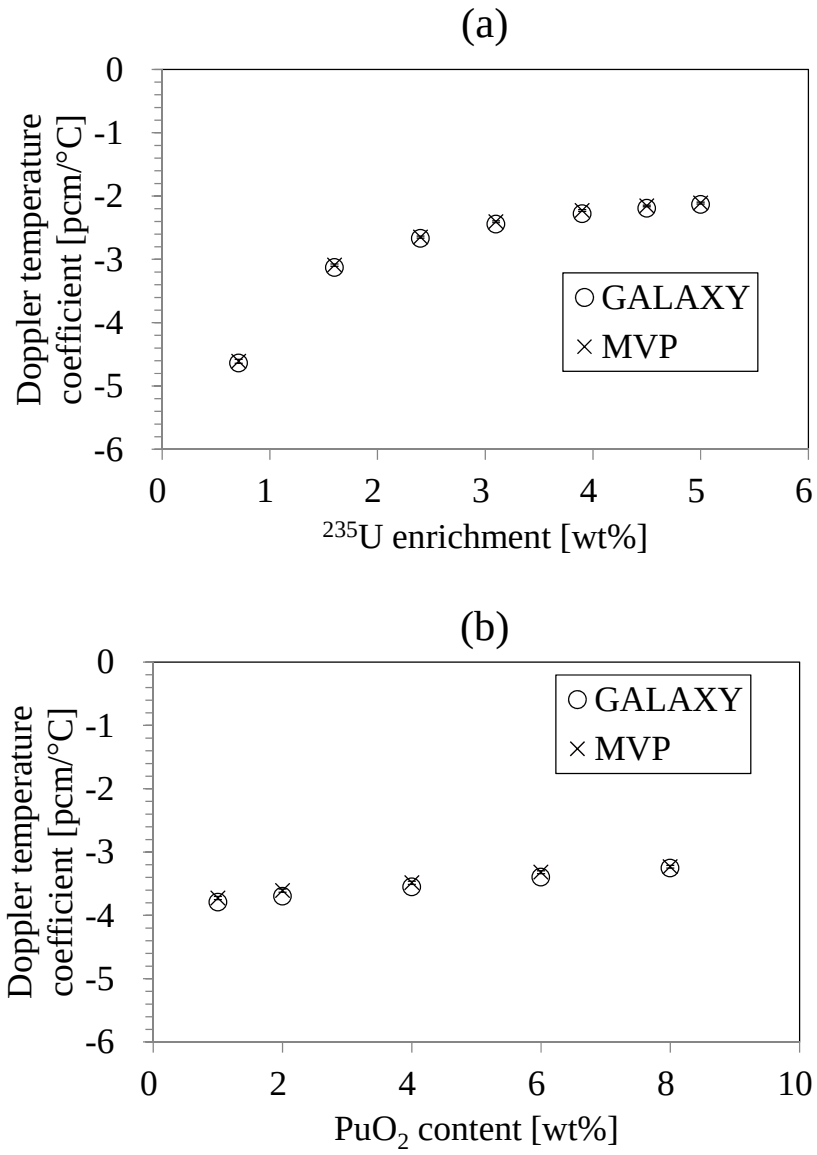

Figure 3.17 Comparison of Doppler temperature coefficient between GALAXY and MVP for fuel composition change ((a) UO_2, (b) MOX).

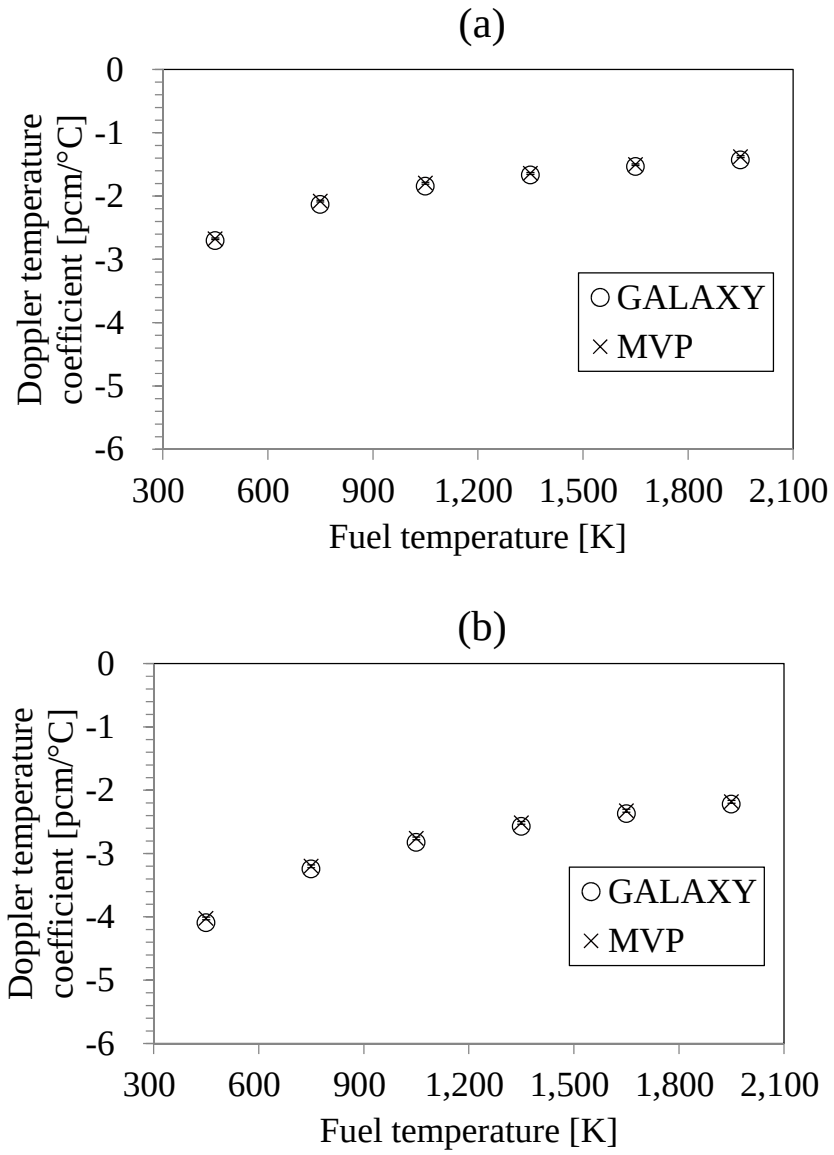

Figure 3.18 Comparison of Doppler temperature coefficient between GALAXY and MVP for fuel temperature change ((a) UO_2, (b) MOX).

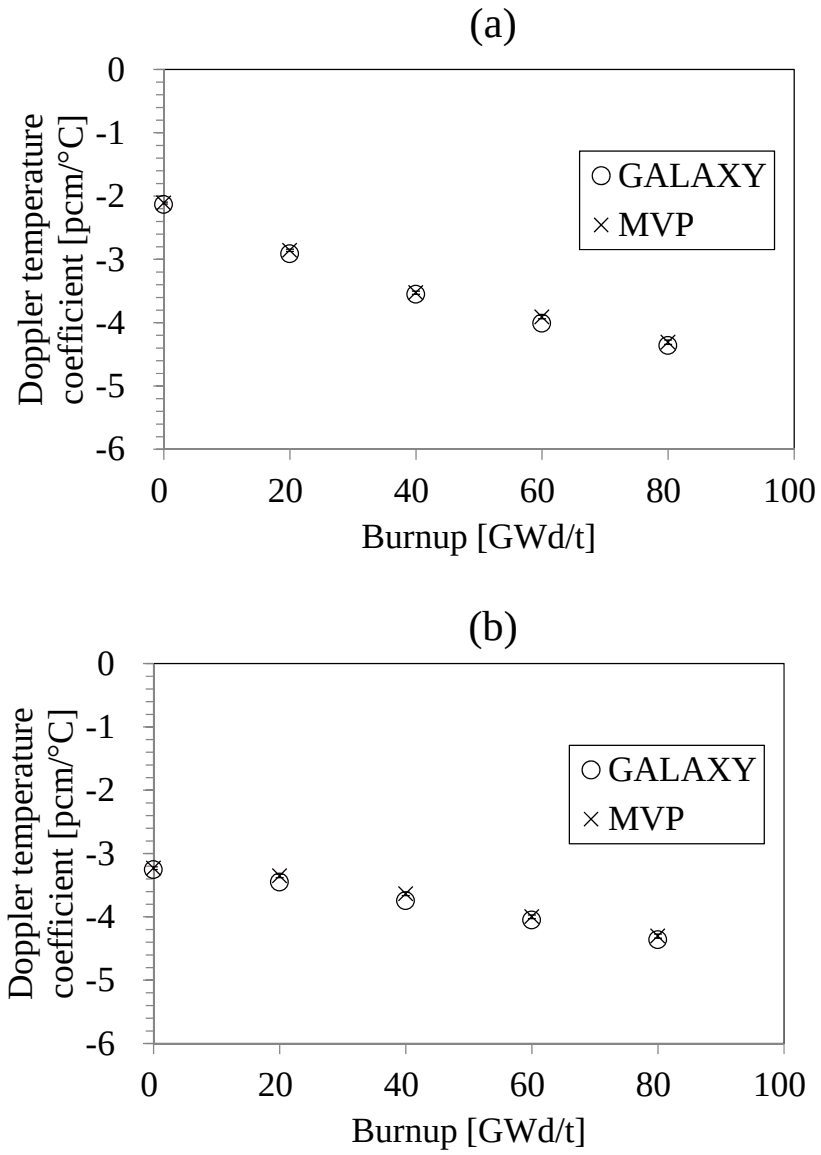

Figure 3.19 Comparison of Doppler temperature coefficient between GALAXY and MVP for burnup change ((a) UO_2, (b) MOX).

3.7.3 Moderator Reactivity

In this sub-section, the accuracy of moderator reactivity prediction by GALAXY is evaluated. Moderator density and boron concentration changes are the main factors for the moderator reactivity in PWR. The corresponding reactivity coefficients are moderator density coefficient (MDC) and boron worth (BW). In the present moderator benchmark, MDC and BW generated by GALAXY are compared with those by MVP.

Moderator reactivity is mainly induced by change of the amount for neutron moderation and absorption due to the moderator density and boron concentration changes. The Mosteller's original benchmark [25, 26] is extended to the different moderator density and boron concentration in the present study. The verification is essentially the investigation of the prediction accuracy for MDC and BW against the systematic change of the number density for each nuclide in the moderator region. The unit pin-cell benchmark is prepared for the simple and essential verification.

The specification of moderator reactivity benchmark is shown in **Table 3.12**. The base condition such as calculation geometry is the same as that in Mosteller's original benchmark. The number densities of the boron nuclides to the boron concentration C_b are generated by using those for the original 1400ppm condition ($ND_B(1400\text{ppm})$) based on the assumption of negligible displacement for the water:

$$ND_B(C_b) = ND_B(1400\,\text{ppm}) \cdot \frac{C_b[\text{ppm}]}{1400[\text{ppm}]}. \tag{3.71}$$

Table 3.12 Specification of the moderator reactivity benchmark.

Item	Specification
Fuel type	UO_2, MOX (Reactor-recycle)
Moderator density [g/cm^3]	1.00, 0.80, 0.66163 (original condition), 0.55, 0.40, 0.25, 0.10
Boron concentration [ppm]	0, 700, 1400 (original condition), 2100, 2800, 3500, 4500

The total number of neutron sampling for MVP calculations is set to 100 million histories, in which the one sided statistical uncertainty of *k-infinity* is about 5pcm ($5\times10^{-5}\,\Delta k/k$).

In the present benchmark, MDC and BW are generated as follows:

$$\begin{aligned} MDC &= \left[\left(\frac{k_2-1}{k_2}\right)-\left(\frac{k_1-1}{k_1}\right)\right]\Big/(\rho_2-\rho_1) \\ &= \left(\frac{1}{\rho_2-\rho_1}\right)\cdot\left(\frac{k_2-k_1}{k_1k_2}\right), \end{aligned} \tag{3.72}$$

$$\begin{aligned} BW &= \left[\left(\frac{k_2-1}{k_2}\right)-\left(\frac{k_1-1}{k_1}\right)\right]\Big/(C_{b,2}-C_{b,1}) \\ &= \left(\frac{1}{C_{b,2}-C_{b,1}}\right)\cdot\left(\frac{k_2-k_1}{k_1k_2}\right), \end{aligned} \tag{3.73}$$

where ρ, C_b and k denote the moderator density, boron concentration and *k-infinity*, respectively. Indices 1 and 2 denote the different ρ or C_b conditions, respectively.

In this benchmark, (1) moderator density and (2) boron concentration dependences

of *MDC*s and *BW* s are verified for each fuel type.

For the moderator density dependence (1), the moderator density is systematically changed between a typical room temperature condition (1.0g/cm^3) and a mist condition (0.1g/cm^3). The range includes the HFP normal operation condition (upper: ~ 0.8g/cm^3), and, the loss of the main feed water supply + ATWS (Anticipated Transient Without Scram) conditions (lower: ~ 0.4g/cm^3). For the boron concentration dependence (2), the boron concentration is systematically changed between 0 to 4500ppm corresponding to the typical boron concentration ranges in commercial PWRs.

The *MDC*s are generated for each moderator density range, i.e., *MDC*s between 1.0-0.8g/cm^3, 0.8-0.66163g/cm^3,$\cdots$, 0.25-0.1g/cm^3. The *BW* s are generated for each boron concentration range, i.e., *BW* s between 0-700ppm, 700-1400ppm, $\cdots$, 3500-4500ppm.

The differences of *k-infinity* between GALAXY and MVP are summarized in **Table 3.13**. As shown in Table 3.13, the differences are very small for moderator density and boron concentration changes.

Table 3.13 Comparison of *k-infinity* between GALAXY and MVP in the moderator reactivity benchmark.

Fuel type	Changed parameter	Number of samples	Difference [pcm] (GALAXY-MVP)/MVP		MVP statistical error [pcm]
			Average	Maximum	Average
UO_2	Moderator density	7	-14	111	4
	Boron concentration	7	-47	-74	4
MOX	Moderator density	7	-37	-67	5
	Boron concentration	7	-33	-58	5
All (UO_2+MOX)	Moderator density	14	-26	111	5
	Boron concentration	14	-40	-74	5

Figures 3.20-3.21 show the calculation results of *MDC* and *BW* to each parameter change for UO_2 and MOX fuel cells. The moderator densities and boron concentrations in the figures correspond to the midpoint between the neighboring two conditions. The differences of *MDC* and *BW* between GALAXY and MVP are summarized in **Tables 3.14-3.15**, respectively. The average difference of *MDC* and *BW* is almost within the 2~3σs of statistical uncertainty for MVP propagated by *k-infinity* statistical errors, thus considering the 3σs MVP statistical uncertainty, the differences for *MDC* and *BW* between GALAXY and MVP are small for each parameter change.

In Figure 3.20, *MDC* based on the equivalence theory are also shown for comparisons. The present method can accurately predict *MDC* including lower moderator density ranges than the concentional equivalence theory.

Table 3.14 Comparison of moderator density coefficient between GALAXY and MVP in the moderator reactivity benchmark.

Fuel type	Number of samples	Difference [%] (GALAXY-MVP)/MVP		MVP statistical error [%]
		Average	Maximum	Average
UO_2	6	-0.9	-2.2	0.5
MOX	6	-0.1	-2.9	0.3
All (UO_2+MOX)	12	-0.5	-2.9	0.4

Table 3.15 Comparison of boron worth between GALAXY and MVP in the moderator reactivity benchmark.

Fuel type	Number of samples	Difference [%] (GALAXY-MVP)/MVP		MVP statistical error [%]
		Average	Maximum	Average
UO_2	6	-0.1	-0.2	0.1
MOX	6	-0.4	-0.8	0.4
All (UO_2+MOX)	12	-0.3	-0.8	0.3

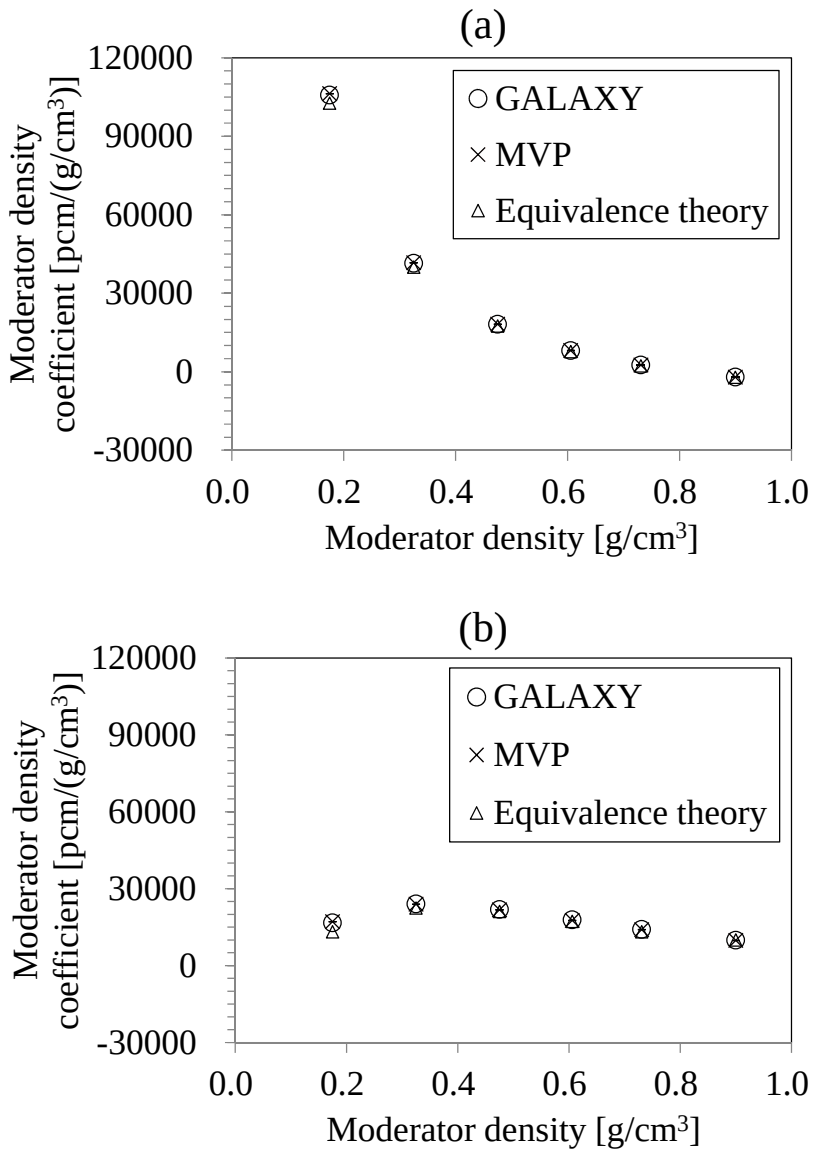

Figure 3.20 Comparison of moderator density coefficient between GALAXY and MVP ((a) UO_2, (b) MOX).

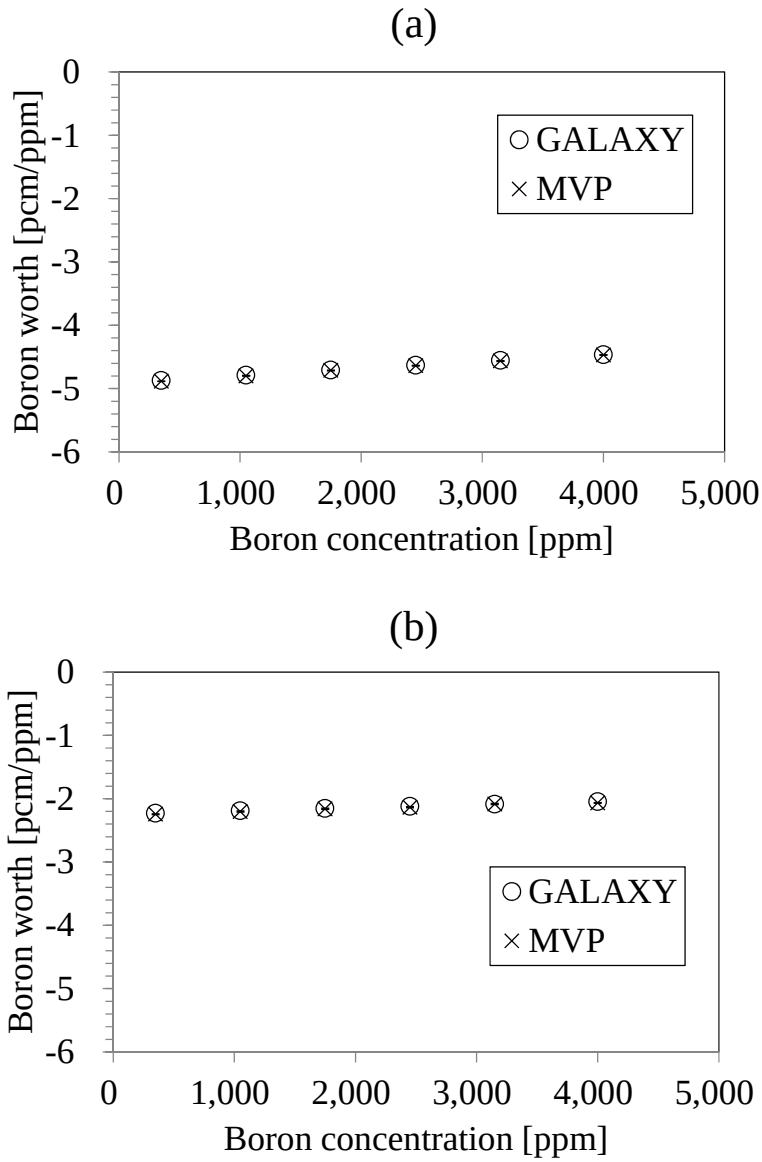

Figure 3.21 Comparison of boron worth between GALAXY and MVP ((a) UO_2, (b) MOX).

Figure 3.22 shows the calculation results of *MDC* by forcing $\theta = 1$ in the slowing-down equation. This situation corresponds to the assumption of $1/E$

asymptotic spectrum for the non-fuel region. The differences of *MDC* between GALAXY and MVP are still small as well as Figure 3.20. In the hard spectrum conditions such as a lower moderator density situation, the influence of epi-thermal energy ranges including the wide resonance of ^{238}U is relatively small. This fact leads to the small effect of non-fuel scattering source treatment using θ.

It is concluded that GALAXY with the present resonance self-shielding treatment can accurately predict the moderator reactivity.

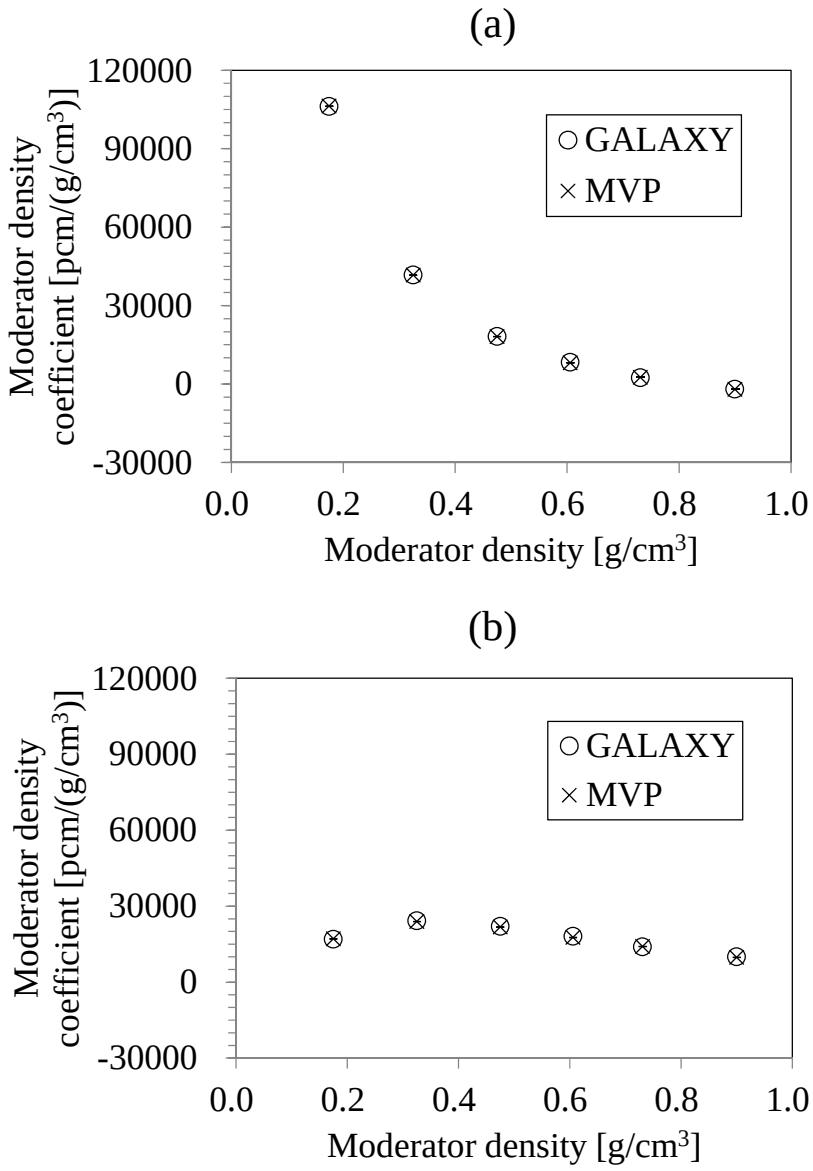

Figure 3.22 Comparison of moderator density coefficient between GALAXY and MVP for $\theta = 1$ ((a) UO_2, (b) MOX).

3.8 Conclusion

A new hybrid resonance self-shielding treatment method in the reactor physics field is developed in the present study. The present method is constructed by integrating the equivalence theory and the ultra-fine-group slowing-down calculation from the theoretical point of view. The main features of the present method are summarized as follows.

The fundamental flux derivation scheme is based on the equivalence theory. The essence of the ultra-fine-group slowing-down equation is effectively incorporated into the scattering source calculation. The accurate non-fuel flux is efficiently treated by utilizing the multi-term rational approximation and its coefficients. A new form of energy dependent neutron flux has two aspects: (1) multi-term rational approximation (equivalence theory), (2) slowing-down calculation (ultra-fine-group treatment). The multi-group condensation error can be eliminated by incorporating a semi-analytical reaction-rate preservation scheme.

The present method is implemented in the MHI lattice physics code GALAXY. By comparing the neutronics characteristics obtained by GALAXY and continuous energy Monte-Carlo code MVP, the good agreements between two codes are confirmed for the wide range of state point parameters from the normal operation to the accident conditions for PWR. From the verification results, applicability of the present method for general lattice physics calculations is confirmed.

GALAXY implemented with the new method achieves high accuracy with short computation time. Therefore it can be efficiently applied to generation of the nuclear constants used in nuclear design and safety analysis of commercial light water reactors.

3.9 References

[1] Stamm'ler RJJ, Abbate MJ. Methods of steady-state reactor physics in nuclear design. London: Academic Press; 1983. IX, Group constants in the resonance region; 286.

[2] Carlvik I. A Method for calculating collision probabilities in general cylindrical geometry and application to flux distributions and Dancoff factors. Proc. Third Int. Conf. Peaceful Uses of Atomic Energy; 1964 August 31- September 9; Geneva, Switzerland.

[3] Sugimura N, Yamamoto A. Resonance treatment based on ultra-fine-group spectrum calculation in the AEGIS code. J. Nucl. Sci. Technol. 2007; **44**, 958.

[4] Okumura K, Kugo T, Kaneko K, and Tsuchihashi K. SRAC2006: A comprehensive neutronics calculation code system. Japanese Atomic Energy Agency (JAEA); 2007. JAEA 2007-004.

[5] Hazama T, Chiba G, and Sugino K. Development of a fine and ultra-fine group cell calculation code SLAROM-UF for fast reactor analyses. J. Nucl. Sci. Technol. 2006; **43**, 908.

[6] Rhodes J, Smith K, and Lee D. CASMO-5 development and applications. advances in nuclear analysis and simulation (PHYSOR2006); 2006 September 10-14; Vancouver, BC, Canada [CD-ROM].

[7] Martinolli E, et. al. APOLLO2-A - AREVA's new generation lattice physics code: methodology and validation. Proceedings of International Conference on Physics of Reactors (PHYSOR2010); 2010 May 9-14; Pittsburgh, PA, USA [CD-ROM].

[8] Koike H, Yamaji K, Kirimura K, Sato D, Matsumoto H, and Yamamoto A.

Advanced resonance self-shielding method for gray resonance treatment in lattice physics code GALAXY. J. Nucl. Sci. Technol. 2012; **49**, 725.

[9] Yamaji K, Matsumoto H, Kirimura K, Takeda T, and Yamamoto A. Development of a new lattice physics code GALAXY for flexible geometry representation in next generation core analysis system. Trans. Am. Nucl. Soc., 2007 November 11-15, Washington, USA **97**, 573 [CD-ROM].

[10] Askew R. A characteristics formulation of the neutron transport equation in complicated geometries. U.K. Atomic Energy Authority 1972; AEEW-M1108,.

[11] Williams ML. Correction of multigroup cross sections for resolved resonance interference in mixed absorbers. Nucl. Sci. Eng. 1983; **83**, 37.

[12] Wehlage E, Knott D, and Mills VW. Modeling resonance interference effects in the lattice physics code LANCER02. Intl. Topl. Mtg. on Math. & Comp. (M&C2005); 2005 September 12-15; Avignon, FR [CD-ROM].

[13] Koike H, Yamaji K, Kirimura K, Kosaka S, and Matsumoto H. Quantification of resonance interference effect for multi-group effective cross-section in lattice physics calculation. Proceedings of International Conference on Physics of Reactors (PHYSOR2014); 2014 September 28-October 3; Kyoto, JPN [CD-ROM].

[14] Goldstein R and Cohen ER. Theory of resonance absorption of neutrons. Nucl. Sci. Eng. 1962; **13**, 132.

[15] Kavenoky A. The SPH homogenization method. Proc.Meeting Homogenization Methods in Reactor Physics; 1978 November 13–15, Lugano, Switzerland.

[16] Yamamoto A, Endo T, and Koike H. Improved derivation of multigroup effective cross section for heterogeneous system by equivalence theory. Nucl. Sci. Eng.

2011; **168**, 75.

[17] Kier PH and Robba AA. A program for computation of resonance absorption in multiregion reactor cells. ANL-7326, 1967.

[18] MacFarlane RE and Miur DW. The NJOY nuclear data processing system version 91. Los Alamos National Laboratory; 1994. LA-17740-M.

[19] Chadwick MB, et al. ENDF/B-VII.0: next generation evaluated nuclear data library for nuclear science and technology. Nuclear Data Sheets 107; 2006.

[20] Sartori E. Standard energy group structures of cross section libraries for reactor shielding, reactor cell and fusion neutronics applications: VITAMIN-J, ECCO-33, ECCO-2000 and XMAS, JEF/DOC-315, Revision 3. 1990; NEA Data Bank.

[21] Yamamoto A. Evaluation of background cross section for heterogeneous and complicated geometry by the enhanced neutron current method. J. Nucl. Sci. Technol., 2008; **45**, 1287.

[22] Nagaya Y, Okumura K, Mori T, and Nakagawa M. MVP/GMVP II: general purpose Monte Carlo codes for neutron and photon transport calculations based on continuous energy and multigroup methods. Japanese Atomic Energy Agency (JAEA); 2005. JAERI 1348.

[23] Nikolaev MN, Ignatov AA, Isaev NV, and Khokhlov VF. The method of subgroups for considering the resonance structure of the cross sections in neutron calculations. Sov. At. Energy, 1970; **29**, 689.

[24] Yamamoto A, Koike H, and Yamane Y. A new framework of resonance calculation method based on the sub-group method (1); Theory. Trans. Am. Nucl. Soc., 2009 June 14-18, Georgia, USA **100**,647 [CD-ROM].

[25] Mosteller RD. The Doppler-defect benchmark: overview and summary of results. Los Alamos National Laboratory; 2007. LA-UR-07-1000.

[26] Mosteller RD. Computational benchmarks for the Doppler reactivity Defect. Los Alamos National Laboratory; 2006. LA-UR-06-2968.

[27] Ouisloumen M and Sanchez R. A model for neutron scattering off heavy isotopes that accounts for thermal agitation effects. Nucl. Sci. Eng., 1990; **107**, 189.

[28] Lee D, Smith K, and Rhodes J. The Impact of ^{238}U resonance elastic scattering approximations on thermal reactor Doppler reactivity. Nucl. Sci. Eng., 2009; **36**, 274.

CHAPTER 4. DEVELOPMENT OF GENERALIZED RESONANCE SELF-SHIELDING METHODOLOGY FOR INTRA-PELLET MULTI-REGION GEOMETRY AND NON-UNIFORM EFFECT BASED ON A UNIFIED THEORY

4.1 Introduction

Resonance self-shielding treatment [1] is an important part for the lattice physics calculations in reactor physics field. Accurate treatment of ^{238}U wide resonance cross-sections and their influences on flux depressions is a key issue to guarantee a sufficient prediction accuracy of criticality and reactivity coefficients for commercial LWRs (light water reactors) core analysis.

In order to establish a practical resonance treatment method, the effective cross-section is required to be generated with short computation time, while keeping its sufficient accuracy. In the past studies conducted by the authors, many of the technical issues have been solved to establish a sophisticated resonance treatment. A brief summary and the development history of the past and present studies are shown in **Figure 4.1** [2-11]. In the present study, a unified resonance treatment method is developed to obtain the sufficient accuracy for effective cross-sections without a direct heterogeneous ultra-fine-group calculation. As shown in Figure 4.1, treatment of the complicated spatial self-shielding effect for radially and azimuthally sub-divided

multi-region geometry within each fuel rod is addressed in the present paper.

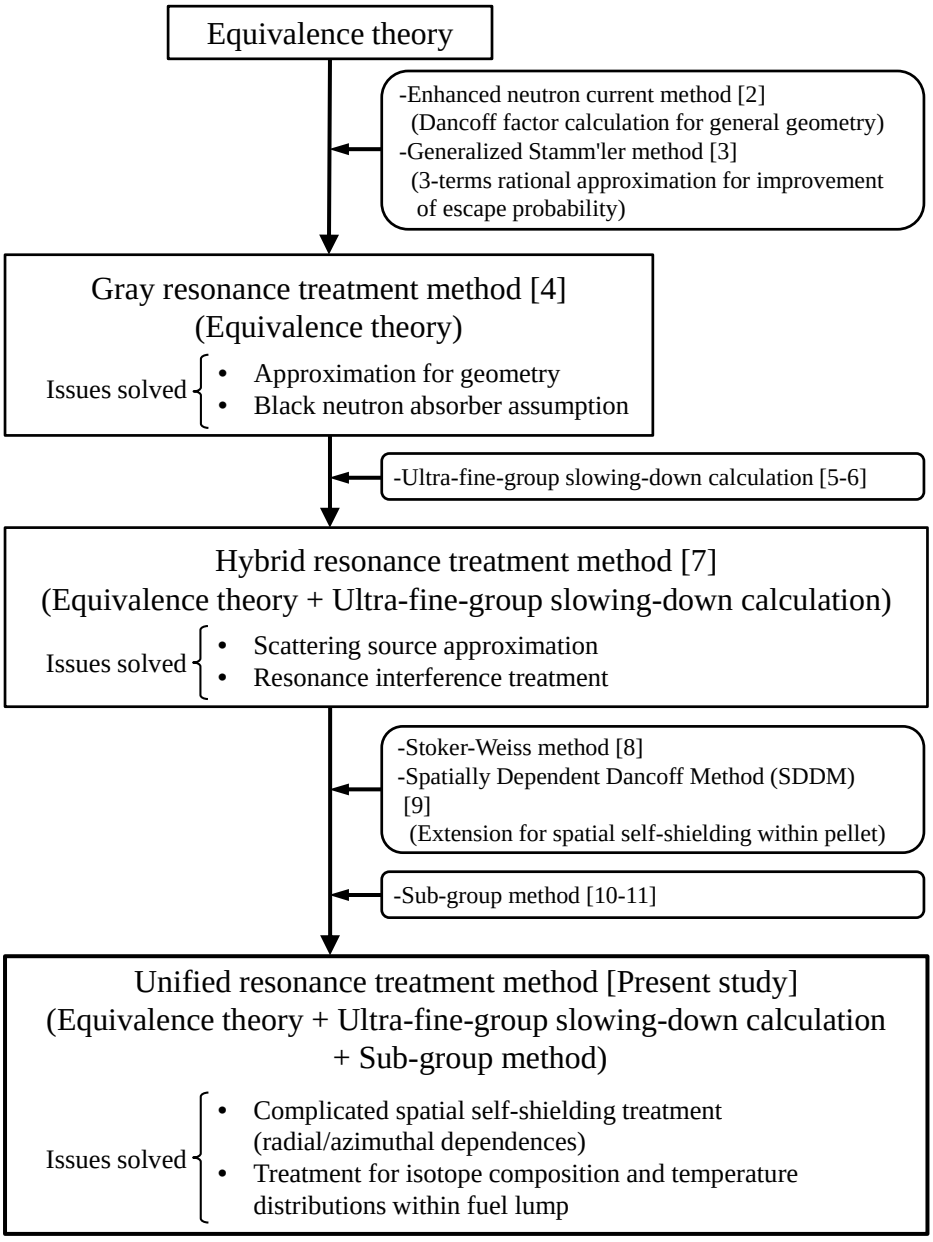

Figure 4.1 Brief summary and development history of the past and present studies.

In the first technical achievement by the authors [4], approximation for geometry and black neutron absorber assumption in the equivalence theory [1] are solved. Several spatial effects in a lattice physics theory (i.e., heterogeneous effect between fuel and non-fuel regions, shadowing effect due to the neighboring fuel rods, and irregular lattice effect by the local water enriched regions) can be incorporated into the pin-by-pin rational coefficients. The flux response as a function of macroscopic total cross-sections obtained from MOC (Method of characteristics) [12] fixed source calculations is directly taken into account for pin-by-pin resolution.

In the second technical achievement by the authors [7], scattering source and resonance interference treatments are improved. The essence of the ultra-fine-group slowing-down calculation [5-6] is incorporated into the equivalence theory, and the hybrid resonance treatment method is established. At this stage, the resonance treatment for both pin-cell and fuel assembly geometries is established to generate accurate effective cross-sections with short computation time. It can be applied to the wide range of neutron spectrum conditions including low moderator density ranges in severe accident states, as long as each fuel region is not sub-divided.

In the current development state, extension of the above hybrid resonance treatment is desired for a complicated spatial self-shielding treatment of each fuel lump. Especially for the cylindrical fuel rod geometry, which is widely adopted for commercial LWR fuel assemblies, generation of radially and azimuthally dependent effective cross-sections is not easy with keeping sufficient accuracy.

From the above background, an objective of the present study is to develop a new

resonance treatment method that can accurately take into account the complicated spatial self-shielding effect with short computation time. In order to solve this issue, the essence of sub-group method [10-11] is incorporated into the hybrid resonance treatment method in the second achievement [7] mentioned above. As a result, the unified resonance treatment is established as a multi-hybrid model of the equivalence theory, the ultra-fine-group calculation and the sub-group method. Although another concept of unified approach for the three methods has already been suggested by the authors [13], the present method is based on a more robust scheme from the theoretical point of view.

In the current methodologies related to the resonance treatment, the simpler approaches have already been proposed, e.g., a pin-cell based direct ultra-fine-group slowing-down calculation with pre-tabulated collision probabilities [6]. The present method in this study adopts rather complicated calculation procedures in actual implementation than the direct slowing-down calculation mentioned above. However, the present method has an advantage on accurate and efficient spatial treatment for radially/azimuthally sub-divided fuel regions defined on the detailed core analysis applications. Especially for the azimuthally sub-divided fuel rods adjacent to a large water region, the pin-cell based slowing-down calculation cannot directly be applied. Therefore, the present method has a potential to become an alternative approach against the direct slowing-down calculation, from the view point of its capability to treat complicated calculation conditions.

In the enhancement activities for core analysis methodology, a general direction of the development is to increase a resolution of space/energy dependences for neutron

flux in the transport calculation. A possible computational performance in the future application phase is considered in the development. Therefore, the suggestion of an extended capability for azimuthal resonance treatment will be useful as a new option for the advanced analysis scheme, even though the current lattice physics codes do not treat the azimuthal dependece of the effective cross-sections.

In this paper, the fundamental theory and the verification results of the new resonance treatment are described in detail. The contents of each section are summarized as follows.

<Section 4.2>

The unified resonance treatment is proposed based on a two-step cross-section collapsing scheme. The equivalence theory, the ultra-fine-group calculation and the sub-group method are integrated.

<Section 4.3>

A two-step reaction-rate preservation scheme for the reduction of energy discretization error is established, which is consistent with the unified resonance treatment.

<Section 4.4>

Verification of the new method is carried out.

<Section 4.5>

Conclusions of this study are summarized.

4.2 Unified Resonance Self-Shielding Treatment

4.2.1 Concept for Two-Step Resonance Calculation

The new method is established by enhancing and integrating the conventional methods, and its concept is based on two-step neutron flux calculations. The 1st step calculation is performed to obtain ultra-fine-group fluxes on a simple geometry based on the hybrid treatment of equivalence theory and ultra-fine-group slowing-down calculation. Then, by using the obtained ultra-fine-group fluxes, sub-group cross-sections and sources are generated for discrete energy ranges explicitly defined by the resonance cross-section level. Next, the 2nd step calculation is performed to obtain sub-group fluxes on an exact geometry based on the sub-group method. Finally, multi-group effective cross-sections are generated by the sub-group cross-sections and the sub-group fluxes.

A concept of the two-step resonance treatment is shown in **Table 4.1**. By utilizing a concept of multi-stage cross-section collapsing strategies [14] widely used in reactor physics field, two-step calculation, i.e., “coarse geometry + fine energy” (1st step) and “fine geometry + coarse energy” (2nd step) calculations, is performed. Here, the main calculations in the present method are summarized in **Table 4.2**. The corresponding section numbers for each main calculation are also shown in the table.

Table 4.1 Concept of two-step resonance treatment.

Item \ Step	1st step	2nd step
Theory	Equivalence theory + Ultra-fine-group calculation	Sub-group method
Spatial resolution	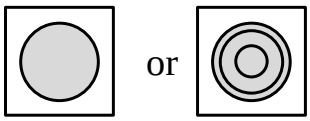	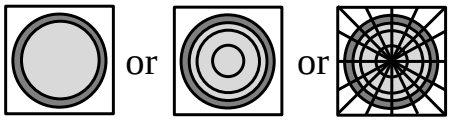
Energy resolution	Ultra-fine-group (~100,000)	Sub-group (3~10 for each multi-group)
Collapsed cross-section	$\sigma_{sg}^{i} = \frac{\int_{sg} dE\sigma(E)\phi_i(E)}{\int_{sg} dE\phi_i(E)}$	$\sigma_{g}^{i} = \frac{\sum_{sg\in g} \sigma_{sg}^{i}\phi_{sg}^{i}}{\sum_{sg\in g} \phi_{sg}^{i}}$

Table 4.2 Summary of the main calculation procedures for the present method.

Main calculation procedures	Corresponding sections or reference documents	Corresponding steps in Section 4.2.6
Generation of pin-by-pin rational coefficients	References 4, 7	(4)
Ultra-fine-group slowing-down calculation for simplified geometry	Reference 7, Section 4.2.2	(1)-(5)
Extension of ultra-fine-group flux for each fuel rod to radial multi-region problem	Section 4.2.3	(6)-(9)
Generation of spatially-dependent sub-group parameter	Sections 4.2.4-4.2.5	(1), (10)-(13)
Sub-group flux calculation	Section 4.2.5	(14)
Generation of effective cross-section	Section 4.2.5	(15)

The main features of the new method are summarized below.

In the 1st step calculation, the hybrid resonance treatment based on the equivalence theory and the ultra-fine-group calculation [7] is applied, and the ultra-fine-group flux for each fuel region is accurately obtained.

In the case of radial multi-region problem with treating the concentric cylinder within a fuel rod, the ultra-fine-group flux for each fuel lump is expanded to each ring region coupled with the basic idea of Stoker-Weiss method [8] and SDDM (Spatially-Dependent Dancoff Method) [9]. The direct heterogeneous ultra-fine-group transport calculation is not required at all.

Because the effective cross-sections generated by direct collapsing with the above ultra-fine-group fluxes for each ring region are not sufficiently accurate for the radial multi-region problem, the ultra-fine-group cross-section is collapsed not for the whole multi-group energy range, but for the partial sub-group energy range defined by the resonance cross-section level. Note that several sub-groups are generally included in each multi-group.

In the 2nd step calculation, the sub-group method is applied to the exact geometry by using the sub-group cross-sections obtained from the 1st step calculation. In the case of azimuthally-dependent self-shielding treatment, MOC is used as a flux calculation method.

The effective cross-section, i.e., the final product of resonance calculation, is generated by collapsing the sub-group cross-section with the sub-group flux as a weighting function.

4.2.2 Integration of Equivalence Theory and Ultra-Fine-Group Slowing-Down Calculation

In the past study, the hybrid resonance self-shielding method has been established by the authors through integrating the equivalence theory and the ultra-fine-group slowing-down calculation [7]. According to Reference [7], a final form of the neutron flux for each fuel region in a fuel assembly is written as:

$$\phi_f(E) = \frac{1}{E}\sum_{n=1}^{N}\beta_n \frac{\Sigma_{sd}^f(E)l_f + \mu(E)\alpha_n}{\Sigma_t^f(E)l_f + \alpha_n}, \tag{4.1}$$

where

$$\Sigma_{sd}^f(E) = E\sum_k \frac{N_k^f}{(1-\alpha_k)}\int_E^{E/\alpha_k}\frac{dE'\sigma_s^k(E')\phi_f(E')}{E'}, \tag{4.2}$$

$$\mu(E) = \theta + (1-\theta)\frac{E}{\Sigma_p^{nf}}\sum_k \frac{N_k^{nf}\sigma_p^k}{(1-\alpha_k)}\int_E^{E/\alpha_k}\frac{dE'\varphi_{nf}(E')}{E'}, \tag{4.3}$$

$$\varphi_{nf}(E) = \frac{1}{E}\sum_{n=1}^{N}\beta_n \frac{\Sigma_{sd}^f(E)l_f + \mu(E)\varepsilon_n\alpha_n}{\Sigma_t^f(E)l_f + \varepsilon_n\alpha_n}. \tag{4.4}$$

4.2.3 Extension of Neutron Flux to the Radial Multi-Region Geometry

Although the hybrid resonance self-shielding method described in Section 4.2.2 can treat any type of fuel lump geometry in an assembly that can be handled by MOC flux calculation, the spatially-dependent resonance self-shielding effect within a specific fuel lump cannot be directly treated. One of the important issues in this research field is consideration of the radially-dependent resonance self-shielding effect within a cylindrical fuel rod. In this section, the neutron flux in a local ring region within a fuel rod is derived as a natural extension of Equations (4.1)-(4.4). Here, the radially sub-divided fuel rod discussed in this section is shown in **Figure 4.2**.

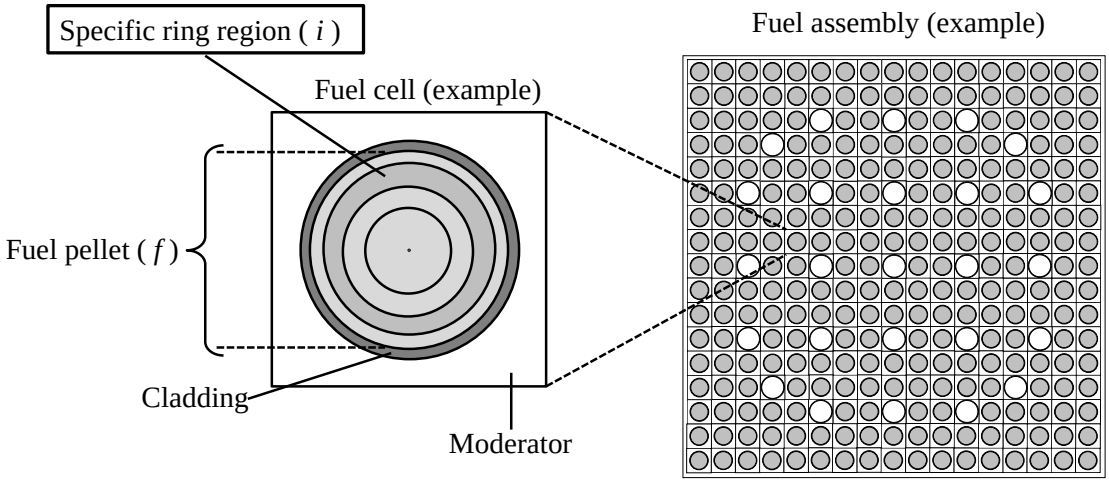

Figure 4.2 Radially sub-divided fuel rod.

The integral form of neutron transport equation for multi-region heterogeneous system consisting of multiple fuel ring regions and a non-fuel region is written as:

$$\Sigma_t^i(E)\phi_i(E)V_i = \sum_{j\in f} S_j(E)V_j P_{j\to i}(E) + S_{nf}(E)V_{nf} P_{nf\to i}(E). \quad (4.5)$$

In the following derivation, the non-fuel region is defined as the multiple regions except for fuel region. For a typical LWR unit cell, non-fuel region is composed of cladding and moderator regions.

The reciprocity theorem between regions i and j is written as:

$$\Sigma_t^i(E)V_i P_{i\to j}(E) = \Sigma_t^j(E)V_j P_{j\to i}(E). \quad (4.6)$$

By applying Equation (4.6) to the neutron source term, the 1st term in the right-hand side of Equation (4.5) is rewritten as:

$$\sum_{j\in f} S_j(E)V_j P_{j\to i}(E) = \Sigma_t^i(E)V_i \sum_{j\in f} \frac{P_{i\to j}(E)}{\Sigma_t^j(E)} S_j(E). \quad (4.7)$$

The 2nd term in the right-hand side of Equation (4.5) is also rewritten as:

$$S_{nf}(E)V_{nf} P_{nf\to i}(E) = \Sigma_t^i(E)V_i \frac{P_{i\to nf}(E)}{\Sigma_p^{nf}} S_{nf}(E), \quad (4.8)$$

where the total cross-section for the non-fuel region is approximated as the potential scattering cross-section, i.e., $\Sigma_t^{nf}(E) \cong \Sigma_s^{nf}(E) \cong \Sigma_p^{nf}$.

By assuming that the macroscopic total cross-section and scattering source are spatially flat within a fuel pellet, Equation (4.7) is approximated as:

$$\begin{aligned}\sum_{j\in f} S_j(E)V_j P_{j\to i}(E) &\cong \Sigma_t^f(E)V_i \sum_{j\in f} \frac{P_{i\to j}(E)}{\Sigma_t^f(E)} S_f(E) = S_f(E)V_i \sum_{j\in f} P_{i\to j}(E) \\ &= S_f(E)V_i \cdot \{1 - P_{i\to nf}(E)\},\end{aligned} \quad (4.9)$$

where $S_f(E)$ denotes the scattering source for the fuel region, and the following

relation for collision probability is used:

$$\sum_{j\in f} P_{i\to j}(E) + P_{i\to nf}(E) = 1.$$

(4.10)

When the scattering source for the non-fuel region is written as $S_{nf}(E) = \mu(E)\frac{\Sigma_p^{nf}}{E}$, which is consistent with the hybrid resonance treatment briefly described in Section 4.2.2, Equation (4.8) is approximated as:

$$\begin{aligned} S_{nf}(E)V_{nf}P_{nf\to i}(E) &\cong \left\{\mu(E)\frac{\Sigma_p^{nf}}{E}\right\}\cdot\Sigma_t^f(E)V_i\frac{P_{i\to nf}(E)}{\Sigma_p^{nf}} \\ &= \frac{1}{E}\Sigma_t^f(E)V_i\mu(E)P_{i\to nf}(E), \end{aligned} \tag{4.11}$$

where $\mu(E)$ is already defined by Equation (4.3) in Section 4.2.2.

Substitution of Equations (4.9) and (4.11) into the right-hand side of Equation (4.5), and some transformations can yield:

$$\phi_i(E) = \{1 - P_{i\to nf}(E)\}\cdot\frac{S_f(E)}{\Sigma_t^f(E)} + \frac{1}{E}\mu(E)P_{i\to nf}(E). \tag{4.12}$$

Since the scattering source for the fuel region is expressed as $S_f(E) = \frac{\Sigma_{sd}^f(E)}{E}$, which is consistent with the hybrid resonance treatment in Section 4.2.2, Equation (4.12) is further modified as:

$$\phi_i(E) = \frac{1}{E}\cdot\left[\{1 - P_{i\to nf}(E)\}\cdot\frac{\Sigma_{sd}^f(E)}{\Sigma_t^f(E)} + \mu(E)P_{i\to nf}(E)\right]. \tag{4.13}$$

In the multi-term rational approximation of the fuel escape probability, $P_{i\to nf}(E)$ is formulated as [4]:

$$P_{i\to nf}(E)=\sum_{m=1}^{4}\gamma_{i,m}\sum_{n=1}^{N}\beta_n\frac{\alpha_n}{\Sigma_t^f(E)l_{i,m}+\alpha_n}. \tag{4.14}$$

Equation (4.14) is identical to the SDGM (Spatially-Dependent Gray resonance self-shielding Method) formulation [4], and its derivation idea is based on the Stoker-Weiss method [8] and SDDM [9]. A geometrical treatment of the escape probability, which is composed of four lump components ($m=1,2,3,4$), is shown in **Figure 4.3**.

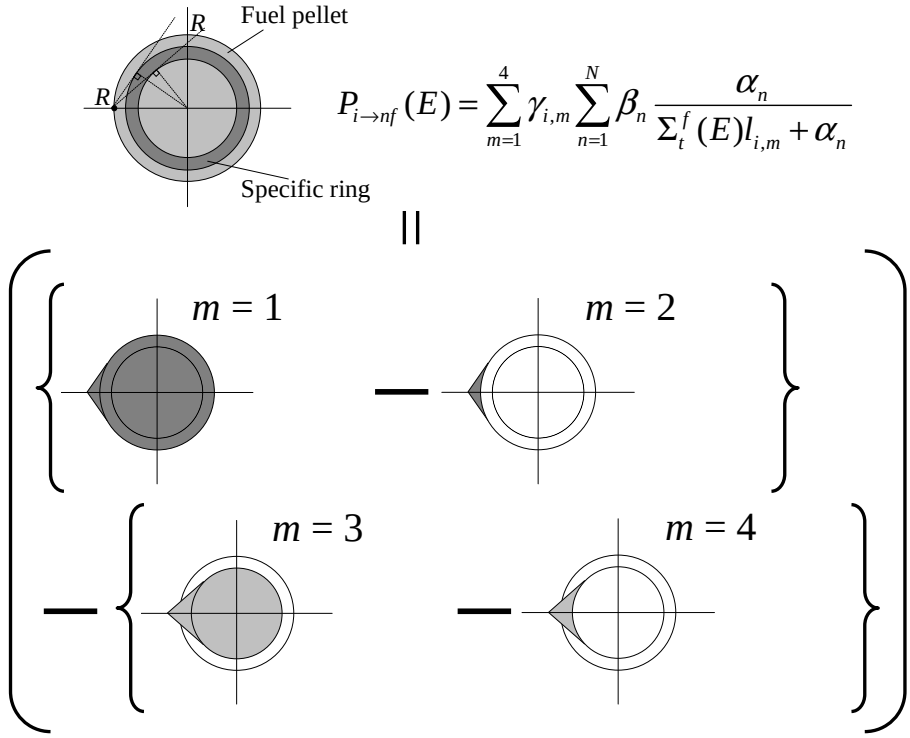

Figure 4.3 Geometrical treatment of spatially-dependent fuel escape probability.

Here, $\gamma_{i,m}$ in Equation (4.14) denotes the coefficient that captures the geometrical information of the ring i and is defined as:

$$(\gamma_{i,1},\gamma_{i,2},\gamma_{i,3},\gamma_{i,4}) \equiv \left(\frac{\rho_i l_{i,1}}{l_i}, -\frac{\rho_i l_{i,2}}{l_i}, -\frac{\rho_{i-1} l_{i,3}}{l_i}, \frac{\rho_{i-1} l_{i,4}}{l_i} \right). \tag{4.15}$$

$l_{i,m}$ denotes the mean chord length of m-th lump derived by the following analytical form:

$$l_{i,m} = \frac{2R}{\pi} \cdot \left(\sqrt{1-\rho^2} + \frac{1}{\rho} \sin^{-1} \rho \pm \frac{\pi}{2} \rho \right), \quad \begin{cases} m=1: +\pi\rho/2, \rho = \rho_i \\ m=2: -\pi\rho/2, \rho = \rho_i \\ m=3: +\pi\rho/2, \rho = \rho_{i-1} \\ m=4: -\pi\rho/2, \rho = \rho_{i-1} \end{cases}. \tag{4.16}$$

By substituting Equation (4.16) into Equation (4.15), $\sum_{m=1}^{4} \gamma_{i,m} = 1$. Considering that $\sum_{n=1}^{N} \beta_n = 1$, the following relation is derived:

$$\sum_{m=1}^{4} \gamma_{i,m} \sum_{n=1}^{N} \beta_n = 1. \tag{4.17}$$

By substituting Equations (4.14) and (4.17) into Equation (4.13), the energy-dependent neutron flux for the ring region i within a fuel pellet is derived as:

$$\begin{aligned} \phi_i(E) &= \frac{1}{E} \cdot \left[\{1 - P_{i\to nf}(E)\} \cdot \frac{\Sigma_{sd}^f(E)}{\Sigma_t^f(E)} + \mu(E) P_{i\to nf}(E) \right] \\ &= \frac{1}{E} \left[\left\{ \sum_{m=1}^{4} \gamma_{i,m} \sum_{n=1}^{N} \beta_n - \sum_{m=1}^{4} \gamma_{i,m} \sum_{n=1}^{N} \beta_n \frac{\alpha_n}{\Sigma_t^f(E) l_{i,m} + \alpha_n} \right\} \cdot \frac{\Sigma_{sd}^f(E)}{\Sigma_t^f(E)} \right. \\ &\quad \left. + \mu(E) \sum_{m=1}^{4} \gamma_{i,m} \sum_{n=1}^{N} \beta_n \frac{\alpha_n}{\Sigma_t^f(E) l_{i,m} + \alpha_n} \right] \\ &= \frac{1}{E} \left[\sum_{m=1}^{4} \gamma_{i,m} \sum_{n=1}^{N} \beta_n \frac{\Sigma_{sd}^f(E) l_{i,m}}{\Sigma_t^f(E) l_{i,m} + \alpha_n} + \sum_{m=1}^{4} \gamma_{i,m} \sum_{n=1}^{N} \beta_n \frac{\mu(E) \alpha_n}{\Sigma_t^f(E) l_{i,m} + \alpha_n} \right] \\ &= \frac{1}{E} \sum_{m=1}^{4} \gamma_{i,m} \sum_{n=1}^{N} \beta_n \frac{\Sigma_{sd}^f(E) l_{i,m} + \mu(E) \alpha_n}{\Sigma_t^f(E) l_{i,m} + \alpha_n}. \end{aligned} \tag{4.18}$$

The scattering source $S_i(E)$ is also calculated as Equation (4.19), which is consistent with the hybrid resonance treatment:

$$S_i(E) = \begin{cases} \sum_k \frac{N_k^i}{(1-\alpha_k)} \int_E^{E/\alpha_k} \frac{dE' \sigma_s^k(E') \phi_i(E')}{E'} & (i \in \text{fuel}) \\ \mu(E) \frac{\Sigma_p^i}{E} & (i \in \text{non fuel}) \end{cases} . \quad (4.19)$$

Here, the isotropic and elastic down-scattering approximations in the center-of-mass system are applied to each ring region within a fuel pellet. The scattering source for the non-fuel region is consistent with the hybrid resonance treatment.

By considering the spatially-dependent scattering source within a fuel pellet, the neutron flux is modified from Equation (4.18) as:

$$\phi_i(E) = \frac{1}{E} \eta(E) \sum_{m=1}^{4} \gamma_{i,m} \sum_{n=1}^{N} \beta_n \frac{\Sigma_{sd}^i(E) l_{i,m} + \mu(E) \alpha_n}{\Sigma_t^f(E) l_{i,m} + \alpha_n}, \quad (4.20)$$

where

$$\Sigma_{sd}^i(E) \equiv E S_i(E), \quad (4.21)$$

and $\eta(E)$ denotes the energy-dependent flux normalization factor in which the fuel-pellet averaged flux obtained from Equation (4.1) can be preserved. $\Sigma_{sd}^i(E)$ and $\eta(E)$ are the only differences between Equations (4.20) and (4.18).

4.2.4 1st Step Resonance Calculation Based on Equivalence Theory and Ultra-Fine-Group Slowing-Down Calculation

As described in Section 4.2.1, the two-step resonance calculations are performed in the present method. The 1st step calculation is based on the equivalence theory and the ultra-fine-group slowing-down calculation, and the space-dependent ultra-fine-group neutron fluxes for each fuel region are appropriately obtained.

As already shown in Section 4.2.2, the ultra-fine-group fluxes for each fuel region within an assembly are calculated from a set of slowing-down equations shown in Equations (4.1)-(4.4). Besides, as derived in Section 4.2.3, spatially-dependent ultra-fine-group fluxes and scattering sources for each ring region within a fuel pellet can be obtained. It should be noted that the fluxes for each ring can be obtained analytically with small computational burdens. $\Sigma_{sd}^{f}(E)$ and $\mu(E)$ in Equation (4.18) are the byproducts of the solution of Equations (4.1)-(4.4), and thus fluxes for each ring region are easily regenerated.

In principle, the radially-dependent effective cross-sections for each ring region can be generated at this single step by using the ultra-fine-group flux solution as a collapsing weight. However, as shown in a derivation scheme of the equation, the following assumptions are applied.

The ultra-fine-group macroscopic total cross-section and scattering source are spatially flat within a fuel pellet (Equation (4.9)). The fuel escape probabilities for each fuel ring are expressed by the multi-term rational approximation based on the SDGM formulation (Equation (4.14)).

As shown in the verification results of Section 4.4, these assumptions cause the prediction error of effective cross-sections for each ring region, as a result of the prediction error of the ultra-fine-group flux.

In order to mitigate the influence of prediction error for the flux, the effective cross-sections are not generated at this step. Instead, the sub-group cross-sections are generated by using the ultra-fine-group fluxes obtained from the 1st step calculation. A more accurate spatial transport of neutrons within a fuel pellet is taken into account in the 2nd step calculation by the additional transport calculations based on the sub-group method. The lack of accurate collision probability information for all the region-to-region combinations in a target system, which is due to the assumptions in Equations (4.9) and (4.14), is compensated by the 2nd step calculation. The details are described in the next section.

4.2.5 2nd Step Resonance Calculation Based on Sub-Group Method

The 2nd step calculation is based on the sub-group method, and the space-dependent sub-group neutron fluxes for each region are obtained.

In the typical resonance energy ranges, the scattering source is isotropic [6] and the fission source can be ignored. Therefore, the integro-differential form of neutron transport equation is written as:

$$\mathbf{\Omega}\cdot\nabla\psi_i(E,\mathbf{\Omega})+\Sigma_t^i(E)\psi_i(E,\mathbf{\Omega})=\frac{S_i(E)}{4\pi}, \tag{4.22}$$

where $\mathbf{\Omega}$ denotes unit vector for direction, and $\psi_i(E,\mathbf{\Omega})$ denotes angular flux for region i.

By integrating Equation (4.22) against an explicit sub-group energy range $sg(\in g)$, in which the discrete energy range is permitted, the sub-group transport equation is derived as:

$$\mathbf{\Omega}\cdot\nabla\psi_{sg}^i(\mathbf{\Omega})+\Sigma_{t,sg}^i\psi_{sg}^i(\mathbf{\Omega})=\frac{S_{sg}^i}{4\pi}, \tag{4.23}$$

where

$\Sigma_{t,sg}^i\equiv\dfrac{\int_{sg}dE\Sigma_t^i(E)\phi_i(E)}{\int_{sg}dE\phi_i(E)}$: macroscopic sub-group total cross-section,

$\psi_{sg}^i(\mathbf{\Omega})\equiv\int_{sg}dE\,\psi_i(E,\mathbf{\Omega})$: sub-group angular flux,

$S_{sg}^i\equiv\int_{sg}dES_i(E)$: sub-group scattering source.

Here, the angular dependence of energy-dependent flux within each sub-group is

ignored.

The typical scheme to solve Equation (4.23) is MOC or S_N (discrete ordinate) method. If MOC is adopted as a flux calculation scheme for Equation (4.23), the spatially-dependent flux for each sub-group can be obtained for any type of complicated geometry, which can be represented by the MOC. Although the integro-differential form of neutron transport equation is shown as a typical example, the integral form of equation based on the collision probability method can also be utilized.

The microscopic sub-group cross-section for resonance nuclide r and reaction type x is also defined in the same manner as:

$$\sigma_{x,sg}^{r,i} \equiv \frac{\int_{sg} dE \sigma_x^r(E)\phi_i(E)}{\int_{sg} dE \phi_i(E)}, \tag{4.24}$$

The sub-group cross-sections are generated by the direct energy collapsing of $\sigma_x^r(E)$ with $\phi_i(E)$ weight obtained from the 1st step calculation.

As described in Section 4.2.4, the sub-group transport calculation is performed in order to mitigate the influence of prediction error of $\phi_i(E)$ for $\sigma_{x,sg}^{r,i}$. From this point of view, sub-group energy structure should be divided not by the neutron energy but by the resonance cross-section level. Based on a reference ultra-fine-group cross-section $\Sigma_{\text{ref}}(E)$, the sub-group energy structure is determined as:

$$sg = \left\{ E \middle| \Sigma_{sg,\min}^{\text{bound}} \le \Sigma_{\text{ref}}(E) < \Sigma_{sg,\max}^{\text{bound}} \right\}, \tag{4.25}$$

where $\Sigma_{sg,\max}^{\text{bound}}$ and $\Sigma_{sg,\min}^{\text{bound}}$ denote the maximum and minimum resonance cross-section

boundaries for sub-group $sg(\in g)$, respectively. Typically, $\Sigma_{\mathrm{ref}}(E)$ is defined by a volume-averaged ultra-fine-group cross-section for all the fuel regions in a target system such as a fuel assembly. According to the preliminary sensitivity studies, the macroscopic absorption cross-section is a better index than the total cross-section. Though the boundaries $\Sigma_{sg,\max}^{\mathrm{bound}}$ and $\Sigma_{sg,\min}^{\mathrm{bound}}$ are determined for each sub-group sg with arbitrary interval division of resonance cross-section within a group g, the equal interval with logarithmic scale is better than that with linear scale. A concept for determination of sub-group structure is shown in **Figure 4.4**.

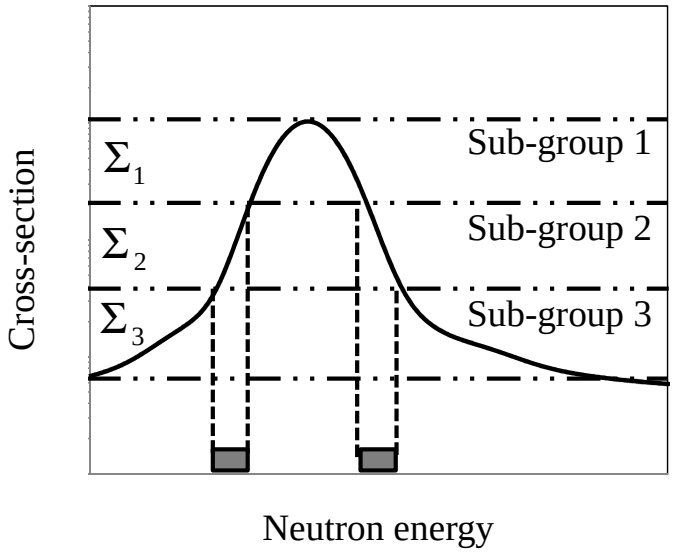

Figure 4.4 Concept for determination of sub-group structure (discrete energy range for sub-group 2 is shown as an example).

Here, it should be noted that the defined sub-group energy structure is commonly

used for all the spatial regions in sub-group cross-section generation. Even if the fuel temperature distribution within a fuel pellet is taken into account, the only one sub-group structure, e.g., a structure defined by $\Sigma_{\mathrm{ref}}(E)$ for effective fuel temperature [15] condition, must be applied. If the different sub-group energy structures are used for each region in sub-group cross-section generation, i.e., the different $\Sigma_{\mathrm{ref}}(E)$ s are applied to each region, the neutron balance among each region and each sub-group is not preserved due to inconsistency of energy group structure for each sub-group, which is an essential issue for the conventional sub-group method. By applying a union sub-group energy structure, the treatment of fuel temperature distribution is improved. Therefore, the sub-group method itself is improved on the unifying process of the conventional three resonance treatments in the present study.

In the conventional sub-group method, the concrete energy ranges are not explicitly specified for each sub-group. In other words, the sub-group is implicitly defined through “band probability” (see section 1.1.4). In contrast, the present method explicitly defines the sub-group energy structure and applys the fixed structure even for the fuel temperature distribution case. This improved treatment resolves the inconsistency of an energy range for each spatial region with different temperatures, and enables to perform the sub-group transport calculation with high accuracy.

The sub-group scattering source $S_{sg}^{i} = \int_{sg} dE S_i(E)$ is also generated from $S_i(E)$ based on Equation (4.19). From the viewpoint of computational efficiency, the sub-group scattering source calculation in the present method has an advantage compared with the conventional sub-group method. The scattering source can be calculated with fine energy resolution by Equation (4.19), and thus the accurate

sub-group scattering source is easily obtained in advance by energy integration of $S_i(E)$. This fact enables to treat the scattering source term as a constant in Equation (4.23), as well as the sub-group cross-section. Therefore, Equation (4.23) can be solved independently for each sub-group, and any considerations of sub-group to sub-group transmission probability are not required at all.

Finally, the sub-group flux ϕ_{sg}^{i} is obtained by integrating the angular flux solutions of Equation (4.23). In addition to the integro-differential form of equation, ϕ_{sg}^{i} can also be obtained from the integral form of transport equation based on the collision probability method.

By using the sub-group cross-sections and fluxes, the microscopic effective cross-section for resonance nuclide r, reaction type x and energy group g is derived as:

$$\begin{aligned}\sigma_{x,g}^{r,i} &= \frac{\int_g dE\,\sigma_x^r(E)\phi_i(E)}{\int_g dE\,\phi_i(E)} = \frac{\sum_{sg\in g}\int_{sg} dE\,\sigma_x^r(E)\phi_i(E)}{\sum_{sg\in g}\int_{sg} dE\,\phi_i(E)} \\ &= \frac{\sum_{sg\in g}\frac{\int_{sg} dE\,\sigma_x^r(E)\phi_i(E)}{\int_{sg} dE\,\phi_i(E)}\int_{sg} dE\,\phi_i(E)}{\sum_{sg\in g}\int_{sg} dE\,\phi_i(E)} = \frac{\sum_{sg\in g}\sigma_{x,sg}^{r,i}\phi_{sg}^{i}}{\sum_{sg\in g}\phi_{sg}^{i}}.\end{aligned} \tag{4.26}$$

As described before, $\sigma_{x,sg}^{r,i}$ is generated by the ultra-fine-group flux solution $\phi_i(E)$ in the 1st step resonance calculation (see Sections 4.2.2-4.2.4). $\sigma_{x,sg}^{r,i}$ has a fuel rod position dependence within a fuel assembly because Equations (4.1)-(4.4) are solved

with position-dependent rational coefficients. In addition, $\sigma_{x,sg}^{r,i}$ has a radial dependence within each fuel pellet because the solution of Equations (4.1)-(4.4) can be extended to the radial multi-region geometry for cylindrical fuel rod based on a derivation in Section 4.2.3.

On the other hand, ϕ_{sg}^{i} is calculated by using $\sigma_{x,sg}^{r,i}$ and S_{sg}^{i}. ϕ_{sg}^{i} is obtained with a fine spatial resolution which can be treated by the adopted flux solver. Therefore, at least, fuel rod position and intra-pellet radial dependences of effective cross-sections can be taken into account in the present method. Besides, intra-pellet azimuthal dependence of effective cross-sections can also be considered through ϕ_{sg}^{i} if the flux calculation scheme such as the MOC and the collision probability method is adopted for a sub-group flux calculation.

4.2.6 Calculation Flow

A calculation flow of the two-step resonance treatment is shown in **Figures 4.5-4.6**. The calculation procedure is described below. Steps (1)-(9) and (10)-(15) correspond to the 1st and 2nd step resonance calculations, respectively. Note that the details for Step (4) are described in Reference [7].

(1) Read the microscopic ultra-fine-group cross-section data σ_{fg} (fg : ultra-fine-group number) from the library. (Note: In the following description, continuous energy-dependent parameters are converted to ultra-fine-group form, e.g., $\sigma(E) \rightarrow \sigma_{fg}$, for numerical treatment.)

(2) Read the relative atomic weight to the neutron, A, and the microscopic potential scattering cross-section σ_p.

(3) Read the heterogeneous region volume V and the number density N.

(4) Perform the hybrid resonance self-shielding calculation [7] based on integration of the equivalence theory and the ultra-fine-group calculation.

(5) Generate the ultra-fine-group source terms ($\Sigma^f_{sd,fg}$ and μ_{fg}) for $1 \leq fg \leq FG$ (FG: the number of ultra-fine-group).

(6) Generate $l_{i,m}$ and $\gamma_{i,m}$ based on Equations (4.16) and (4.15), respectively.

(7) Calculate the ring-region-dependent ultra-fine-group flux $\phi_{i,fg}$ for

$1 \le fg \le FG$ based on Equation (4.18), by using $\phi_{i,fg}$ and μ_{fg}.

(8) Calculate the ring-region-dependent ultra-fine-group scattering source $S_{i,fg}$ for $1 \le fg \le FG$ based on Equation (4.19), by using $\phi_{i,fg}$ and μ_{fg}.

(9) Update $\phi_{i,fg}$ based on Equations (4.20)-(4.21).

(10) Set the reference cross-section Σ_{ref} and the cross-section boundaries (maximum: $\Sigma_{sg,\max}^{\text{bound}}$, minimum: $\Sigma_{sg,\min}^{\text{bound}}$) for each sub-group used in Equation (4.25).

(11) Define the discrete energy structure for each sub-group based on Equation (4.25).

(12) Generate the sub-group cross-section $\sigma_{x,sg}^{r,i}$ for $1 \le sg \le SG$ (SG: the number of sub-group) based on Equation (4.24), by using $\phi_{i,fg}$.

(13) Generate the sub-group scattering source S_{sg}^{i} for $1 \le sg \le SG$ based on $S_{sg}^{i} = \int_{sg} dE S_i(E)$, by using $S_{i,fg}$.

(14) Perform the one-group fixed source calculations for each sub-group, and obtain the fluxes ϕ_{sg}^{i} for each region.

(15) Generate the effective cross-section $\sigma_{x,g}^{r,i}$ based on Equation (4.26), by using $\sigma_{x,sg}^{r,i}$ and ϕ_{sg}^{i}.

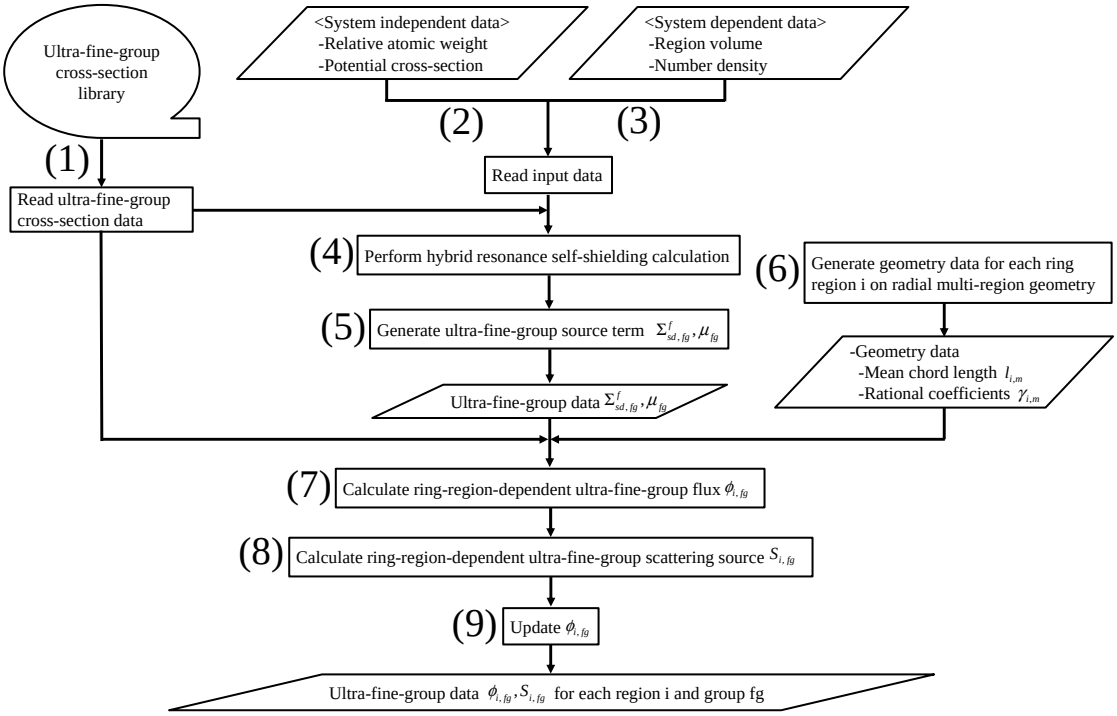

Figure 4.5 Calculation flow of unified resonance treatment (1st step).

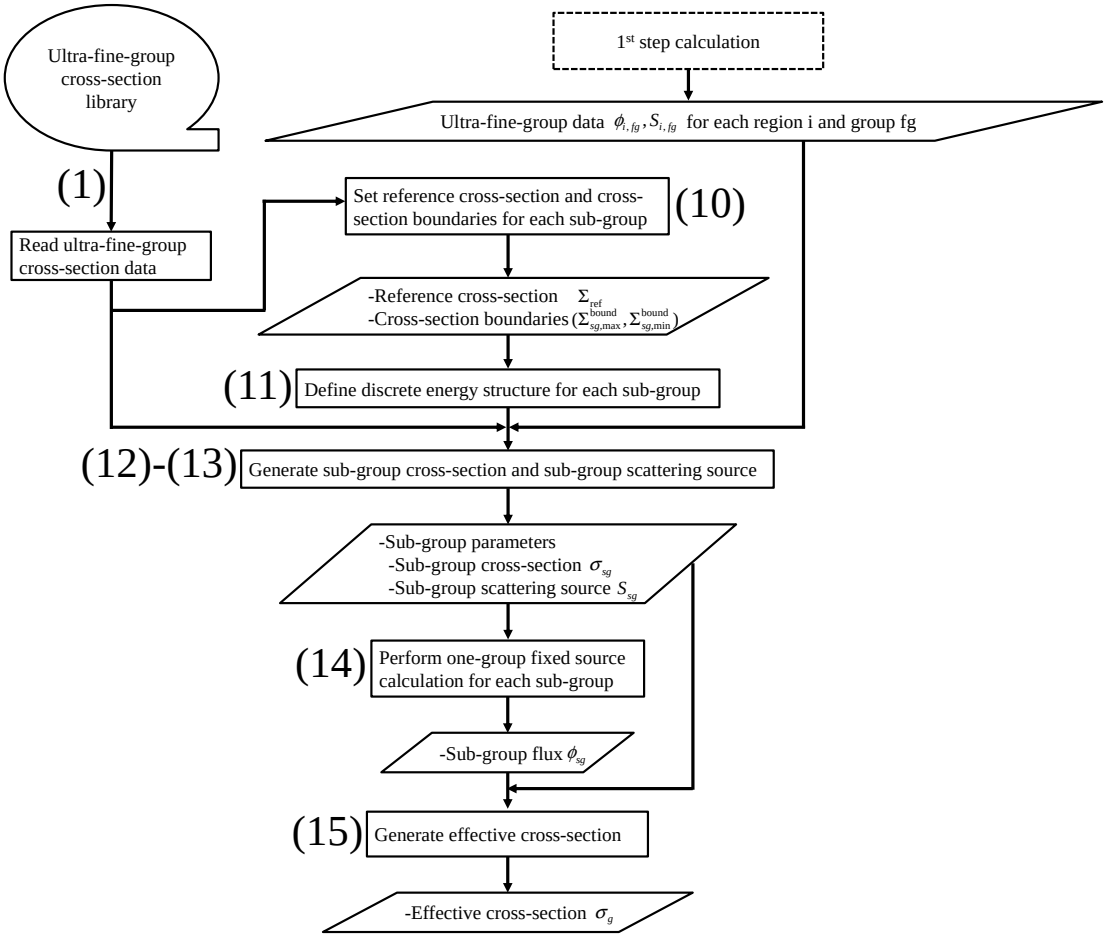

Figure 4.6 Calculation flow of unified resonance treatment (2nd step).

4.2.7 Relation to the Conventional Methods

As described in Section 4.1, the present resonance treatment is a unified approach of the conventional three methods, i.e., equivalence theory, ultra-fine-group slowing-down calculation and sub-group method.

The present method is equivalent to the equivalence theory, if (i) NR approximation of the scattering source, i.e., $\Sigma_{sd}^{f}(E) \approx \Sigma_{p}^{f}$ and $\mu(E) \approx 1$ (see Equations (4.2)-(4.3)), is applied to the 1st step calculation, (ii) the resonance absorptions of background isotopes are ignored, and (iii) the number of sub-groups is set as one for the 2nd step calculation. The present method is also equivalent to the ultra-fine-group slowing-down calculation, if the sub-group is the same as the ultra-fine energy group structure for the 2nd step calculation. If the problem-independent sub-group parameters are prepared in advance, the present method is equivalent to the sub-group method. Therefore, the present resonance treatment is a generalized approach of the conventional three resonance self-shielding methods.

4.3 Reaction-Rate Preservation for Reduction of Energy Discretization Error

4.3.1 Concept for Two-Step Reaction-Rate Preservation Scheme

The effective cross-sections obtained from the direct energy collapsing with flux weight cannot be directly applied to the subsequent multi-group flux calculation due to the energy collapsing error. In order to reduce the error, a reaction-rate preservation scheme is necessary for heterogeneous geometry. In the conventional scheme [6-7] based on the SPH method [16], the group-dependent correction factor f_g^i is derived as:

$$f_g^i = \frac{\int_g dE \sigma_x^r(E)\phi_i(E)}{\sigma_{x,g}^{r,i}\tilde{\phi}_g^i} = \left[\frac{\int_g dE \sigma_x^r(E)\phi_i(E)}{\tilde{\phi}_g^i}\right] \Bigg/ \left[\frac{\int_g dE \sigma_x^r(E)\phi_i(E)}{\int_g dE \phi_i(E)}\right] = \frac{\int_g dE \phi_i(E)}{\tilde{\phi}_g^i}, \quad (4.27)$$

where $\tilde{\phi}_g^i$ denotes the flux obtained with $f_g^i \sigma_{x,g}^{r,i}$.

The present resonance self-shielding treatment, especially for the 1st step calculation, is based on the ultra-fine-group calculation, and thus the conventional scheme can be applied in principle.

Besides, the present method includes the essence of the equivalence theory. The energy-dependent neutron flux can be regenerated by the analytical form of the multi-term rational equation. Considering the fundamental concept of the reaction-rate preservation scheme in the equivalence theory [17], the following equation to solve f_g^i is formulated as a natural extension of the hybrid resonance treatment in Reference [7]:

$$f_g^i \sum_{m=1}^{4} \gamma_{i,m} \sum_{n=1}^{N} \beta_n \frac{\Sigma_{sd,g}^i l_{i,m} + \mu_g \alpha_n}{f_g^i \Sigma_{t,g}^i l_{i,m} + \alpha_n} = \int_g dE \phi_i(E), \quad (4.28)$$

where

$$\Sigma^i_{sd,g} \equiv \int_g dE\eta(E)\frac{1}{E}\Sigma^i_{sd}(E) = \int_g dE\eta(E)S_i(E), \tag{4.29}$$

$$\mu_g \equiv \int_g dE\frac{1}{E}\eta(E)\mu(E). \tag{4.30}$$

Equations (4.20)-(4.21) are used in the above derivation. Here, it should be noted that Equations (4.27) or (4.28) is valid only if $\phi_i(E)$ is obtained with high accuracy. As described in Section 4.2.3, some approximations are applied to the derivation process of $\phi_i(E)$, and thus $\phi_i(E)$ is not necessarily so accurate for direct application to Equations (4.27) or (4.28). Therefore, a new reaction-rate preservation scheme is developed in the present study so that the influence of prediction error of $\phi_i(E)$ is mitigated.

The fundamental form of reaction-rate preservation equation is written as:

$$\int_g dE\sigma^r_x(E)\phi_i(E) = f^i_g\sigma^{r,i}_{x,g}\tilde{\phi}^i_g. \tag{4.31}$$

From the viewpoint of consistency with the present two-step resonance treatment described in Section 4.2, Equation (4.31) is divided into the following two equations:

$$\int_g dE\sigma^r_x(E)\phi_i(E) = \sum_{sg\in g} f^i_{sg}\sigma^{r,i}_{x,sg}\tilde{\phi}^i_{sg}, \tag{4.32}$$

$$\sum_{sg\in g} f^i_{sg}\sigma^{r,i}_{x,sg}\tilde{\phi}^i_{sg} = f^i_g\sigma^{r,i}_{x,g}\tilde{\phi}^i_g, \tag{4.33}$$

where $\tilde{\phi}^i_{sg}$ denotes the flux obtained with $f^i_{sg}\sigma^{r,i}_{x,sg}$. Equation (4.32) is the reaction-rate preservation equation between ultra-fine-group and sub-group treatments, and Equation (4.33) is the reaction-rate preservation equation between sub-group and multi-group treatments. Equation (4.32) is decomposed for each sub-group as:

$$\int_{sg} dE \sigma_x^r(E)\phi_i(E) = f_{sg}^i \sigma_{x,sg}^{r,i} \tilde{\phi}_{sg}^i . \quad (4.34)$$

Note that Equation (4.32) is satisfied if Equation (4.34) is valid.

In the present resonance treatment, the sub-group-wise correction factor f_{sg}^i and the corrected flux $\tilde{\phi}_{sg}^i$ are generated as the 1st step calculation by Equation (4.34). Then, the multi-group-wise correction factor f_g^i is obtained as the 2nd step calculation by Equation (4.33). If Equations (4.28)-(4.30) are directly used, a significant error for f_g^i is induced, as shown in Section 4.4.3.4. By utilizing the sub-group based information, direct propagation of $\phi_i(E)$ prediction error to f_g^i is mitigated. This treatment is called the two-step reaction-rate preservation scheme in the present study, and its detail is described in the following sections.

4.3.2 1st Step Correction Factor Calculation for Sub-Group Level

The correction factor calculation for the 1st step is carried out based on Equation (4.34). By the same derivation scheme for the reaction-rate preservation in the hybrid resonance treatment, Equation (4.34) is rewritten as:

$$f_{sg}^{i}\sum_{m=1}^{4}\gamma_{i,m}\sum_{n=1}^{N}\beta_{n}\frac{\Sigma_{sd,sg}^{i}l_{i,m}+\mu_{sg}\alpha_{n}}{f_{sg}^{i}\Sigma_{t,sg}^{i}l_{i,m}+\alpha_{n}}=\int_{sg}dE\phi_{i}(E), \tag{4.35}$$

where

$$\Sigma_{sd,sg}^{i}\equiv\int_{sg}dE\eta(E)S_{i}(E), \tag{4.36}$$

$$\mu_{sg}\equiv\int_{sg}dE\frac{1}{E}\eta(E)\mu(E). \tag{4.37}$$

Equations (4.20)-(4.21) are used in the above derivation.

Equation (4.35) is used to calculate a correction factor for reaction-rate preservation, which is consistent with the resonance treatment in Sections 4.2.2-4.2.3. All the terms except for f_{sg}^{i} are byproducts of the solution of the methods described in Sections 4.2.2-4.2.3. f_{sg}^{i} is easily obtained from iterative calculation until f_{sg}^{i} is converged. From Equation (4.35), f_{sg}^{i} for (s+1)-th iteration is generated by using s-th result as follows:

$$f_{sg}^{i}(\mathrm{s}+1)=\frac{\int_{sg}dE\phi_{i}(E)}{\sum_{m=1}^{4}\gamma_{i,m}\sum_{n=1}^{N}\beta_{n}\frac{\Sigma_{sd,sg}^{i}l_{i,m}+\mu_{sg}\alpha_{n}}{f_{sg}^{i}(\mathrm{s})\Sigma_{t,sg}^{i}l_{i,m}+\alpha_{n}}}. \tag{4.38}$$

The method includes the iteration scheme, but any additional iterative flux calculations

are no longer required. The calculation time of f_{sg}^{i} is negligible compared with the conventional scheme.

4.3.3 2nd Step Correction Factor Calculation for Multi-Group Level

The correction factor calculation for the 2nd step is carried out based on Equation (4.33). By substituting Equation (4.26) into Equation (4.33), the correction factor is derived as:

$$f_g^i = \frac{\sum_{sg\in g} f_{sg}^i \sigma_{x,sg}^{r,i} \tilde{\phi}_{sg}^i}{\sigma_{x,g}^{r,i} \tilde{\phi}_g^i} = \frac{\sum_{sg\in g} f_{sg}^i \sigma_{x,sg}^{r,i} \tilde{\phi}_{sg}^i}{\frac{\sum_{sg\in g} \sigma_{x,sg}^{r,i} \phi_{sg}^i}{\sum_{sg\in g} \phi_{sg}^i} \tilde{\phi}_g^i} = \frac{\sum_{sg\in g} f_{sg}^i \sigma_{x,sg}^{r,i} \tilde{\phi}_{sg}^i}{\sum_{sg\in g} \sigma_{x,sg}^{r,i} \phi_{sg}^i} \frac{\sum_{sg\in g} \phi_{sg}^i}{\tilde{\phi}_g^i}. \quad (4.39)$$

In the above equation, the microscopic cross-section is included in f_g^i, and thus it depends on resonance nuclide and reaction type. This definition of correction factor leads to the large computational burdens.

In order to avoid the nuclide and reaction type dependent correction factor calculations, the modified correction factor $\tilde{f}_g^i$ and the effective cross-section $\tilde{\sigma}_{x,g}^{r,i}$ are defined so as to satisfy the following relation:

$$\tilde{f}_g^i \tilde{\sigma}_{x,g}^{r,i} = f_g^i \sigma_{x,g}^{r,i}. \quad (4.40)$$

By substituting Equation (4.40) into the right-hand side of Equation (4.33), the following equation is obtained:

$$\sum_{sg\in g} f_{sg}^i \sigma_{x,sg}^{r,i} \tilde{\phi}_{sg}^i = \tilde{f}_g^i \tilde{\sigma}_{x,g}^{r,i} \tilde{\phi}_g^i. \quad (4.41)$$

Here, $\tilde{\sigma}_{x,g}^{r,i}$ is defined as an effective cross-section in which the energy discretization error associated with the collapsing only from the ultra-fine-group to the sub-group is removed, that is:

$$\tilde{\sigma}_{x,g}^{r,i} \equiv \frac{\sum_{sg\in g} f_{sg}^{i} \sigma_{x,sg}^{r,i} \tilde{\phi}_{sg}^{i}}{\sum_{sg\in g} \tilde{\phi}_{sg}^{i}}. \quad (4.42)$$

By substituting Equation (4.42) into Equation (4.41), the modified multi-group correction factor $\tilde{f}_{g}^{i}$ is derived as:

$$\tilde{f}_{g}^{i} = \frac{\sum_{sg\in g} f_{sg}^{i} \sigma_{x,sg}^{r,i} \tilde{\phi}_{sg}^{i}}{\tilde{\sigma}_{x,g}^{r,i} \tilde{\phi}_{g}^{i}} = \frac{\sum_{sg\in g} f_{sg}^{i} \sigma_{x,sg}^{r,i} \tilde{\phi}_{sg}^{i}}{\frac{\sum_{sg\in g} f_{sg}^{i} \sigma_{x,sg}^{r,i} \tilde{\phi}_{sg}^{i}}{\sum_{sg\in g} \tilde{\phi}_{sg}^{i}} \tilde{\phi}_{g}^{i}} = \frac{\sum_{sg\in g} \tilde{\phi}_{sg}^{i}}{\tilde{\phi}_{g}^{i}}. \quad (4.43)$$

As shown in Equation (4.43), $\tilde{f}_{g}^{i}$ does not depend on resonance nuclide and reaction type like an SPH factor. In other words, $\tilde{\sigma}_{x,g}^{r,i}$ is defined in Equation (4.42) so that the resonance nuclide and reaction type dependence of the correction factor can be removed.

Finally, the corrected effective cross-section, which is provided for the subsequent multi-group flux and depletion calculations in a lattice physics code, is $\tilde{f}_{g}^{i} \tilde{\sigma}_{x,g}^{r,i}$. It should be noted that the effective cross-section, which is comparable to the continuous energy Monte-Carlo results tallied by a simple flux weight scheme, is $\sigma_{x,g}^{r,i}$.

4.3.4 Calculation Flow

Calculation flow of the two-step reaction-rate preservation scheme established in Sections 4.3.1-4.3.3 is shown in **Figure 4.7**. The calculation procedure is described as follows:

(1) Generate the sub-group-wise correction factor f_{sg}^{i} based on Equation (4.35) with iteration scheme of Equation (4.38).

(2) Perform one-group fixed source calculations for each sub-group by using the corrected sub-group cross-section $f_{sg}^{i}\sigma_{x,sg}^{r,i}$ as an input, and obtain the sub-group flux $\tilde{\phi}_{sg}^{i}$. This calculation can be carried out independently.

(3) Generate the partially-corrected effective cross-section $\tilde{\sigma}_{x,g}^{r,i}$, in which the energy discretization error from the ultra-fine-group to the sub-group collapsing is removed, based on Equation (4.42).

(4) Set the initial value of $\tilde{f}_{g}^{i}$ as $\tilde{f}_{g}^{i}=1$.

(5) Perform one-group fixed source calculation for each multi-group by using the corrected effective cross-section $\tilde{f}_{g}^{i}\tilde{\sigma}_{x,g}^{r,i}$ as an input, and obtain the multi-group flux $\tilde{\phi}_{g}^{i}$. This calculation can be carried out independently.

(6) Generate the multi-group-wise modified correction factor $\tilde{f}_{g}^{i}$ based on Equation (4.43).

(7) Iterate (5)-(6) until $\tilde{f}_g^{\,i}$ is converged.

Steps (1)-(3) and (4)-(7) correspond to the 1st and 2nd step correction factor calculations, respectively.

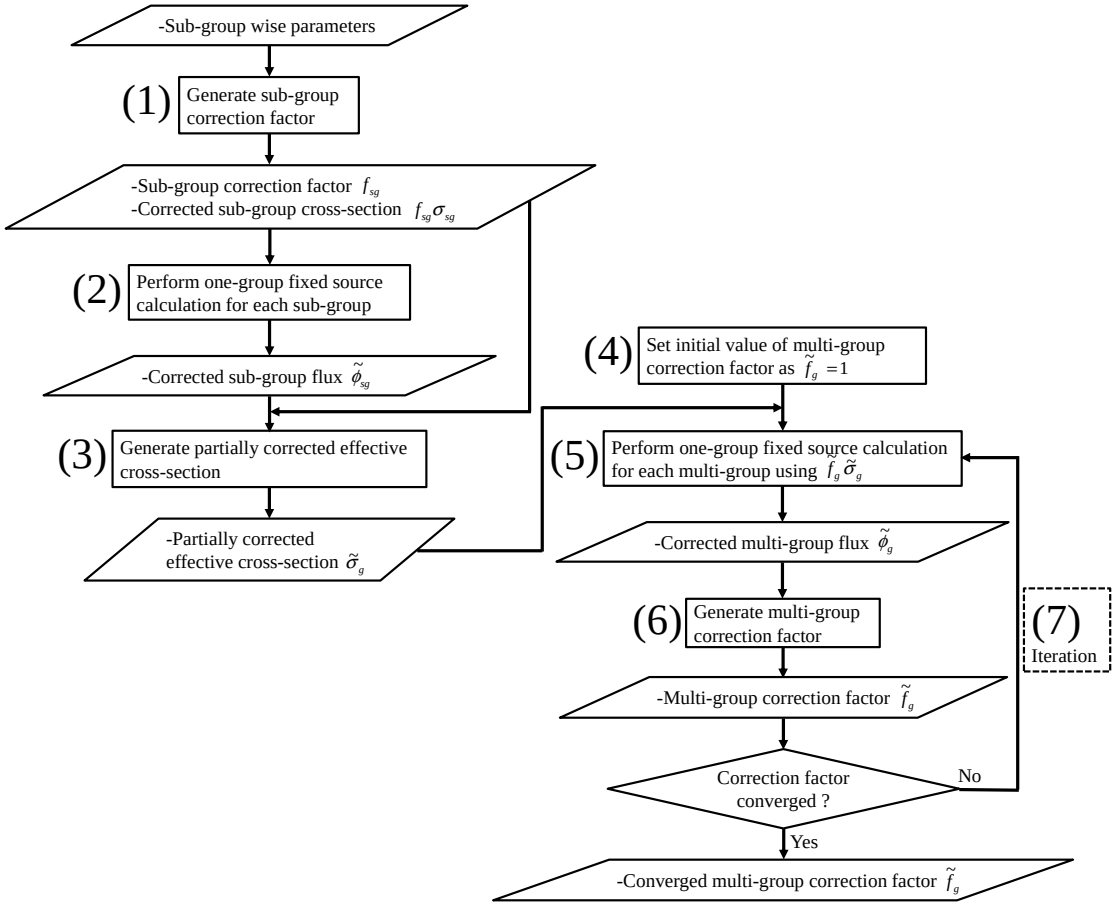

Figure 4.7 Calculation flow of two-step reaction-rate preservation scheme.

4.4 Verification

4.4.1 Concept

In this section, the present resonance treatment is verified by the numerical calculations. The present method is composed of multiple components based on a unified theory, and thus each component is verified first (Section 4.4.3). Then, the effective cross-sections, i.e., final products of the resonance calculation, are analyzed for various cases as a total verification (Section 4.4.4). The reference solutions are obtained from the continuous energy Monte-Carlo calculations based on the exact geometry modeling and fine cross-section representation with continuous energy resolution. A part of the references is obtained from the heterogeneous ultra-fine-group slowing-down calculation based on a deterministic method.

The analysis condition is shown in Section 4.4.2. The verification results for fundamental parameters of the present method are shown in Section 4.4.3. The application results for various pin-cell and multi-cell problems are shown in Section 4.4.4. The verification list is shown in **Table 4.3**.

Table 4.3 Verification list.

Section	Objective	Geometry	Verified model	Verified parameter	Sub-section
4.4.3	Confirm prediction accuracy of main products in the present method	Pin-cell	Slowing-down calculation with multi-term rational equation	Ultra-fine-group neutron flux	4.4.3.1
			Sub-group definition according to resonance cross-section level	Sub-group cross-section	4.4.3.2
			Final product of resonance calculation	Effective cross-section	4.4.3.3
			Reaction-rate preservation scheme	Cross-section correction factor	4.4.3.4
			Final product of lattice physics calculation	Reaction-rate	4.4.3.5
4.4.4	Confirm applicability of the present method for various pin-cell and multi-cell problems	Pin-cell	Spatial self-shielding treatment with spatial variation of ultra-fine-group macroscopic cross-section	Radially-dependent effective cross-sections with isotope composition distribution	4.4.4.1
				Radially-dependent effective cross-sections with temperature distribution	4.4.4.2
			Spatial self-shielding treatment	Radially and azimuthally dependent effective cross-sections	4.4.4.3
		3x3 multi-cell	Spatial self-shielding treatment for irregular lattice	Azimuthally-dependent effective cross-sections with large water region	4.4.4.4

4.4.2 Analysis Condition

Analysis condition of the new resonance treatment is described in this section.

In order to perform each process in the calculation scheme of the present method (see Sections 4.2.6 and 4.3.4), a standalone program is developed. The MHI (Mitsubishi Heavy Industries, Ltd.) lattice physics code GALAXY (Geometrically Arbitrary, Lattice physics and Assembly calculation code in X-Y coordinate system) [18, 4, 7, 21] is used for several steps in the process. In concrete, '(1)-(5) and (14)' in Figures 4.5-4.6 and '(2) and (5)' in Figure 4.7 are performed by GALAXY. The GALAXY ultra-fine-group cross-section library (120,000 groups) [7] based on ENDF/B-VII.0 [19] is also utilized.

The number of rational equation terms used for one-region fuel is set to $N = 2$. Note that the total number of terms used for multi-region fuel is $4N = 8$ (see Equation (4.18)). The microscopic effective capture cross-sections of ^{238}U are generated for 88th energy group (6.16-7.52eV) of the XMAS 172 energy group structure [20], in which the wide resonance cross-section of ^{238}U is included. The number of sub-groups is 5, and the sub-group energy structure is determined by Equation (4.25) based on the ultra-fine-group macroscopic absorption cross-section of the fuel region as $\Sigma_{\mathrm{ref}}(E)$. The sub-group boundary for the absorption cross-section is determined by a division with equal interval in logarithmic scale. The sub-group transport calculation is performed by the collision probability method based on the equivalent Dancoff method [21]. These conditions are applied to almost all the analyses in this paper. The sensitivities for the above calculation conditions against effective cross-sections are investigated in advance, and it is confirmed that the calculation conditions are sufficient

from the view point of prediction accuracy for effective cross-sections.

UO_2 (4.8wt% ^{235}U) pin-cells with HFP (hot full power) operating conditions are set as the typical LWR neutron spectrum condition. The specifications of the pin-cell problem are shown in **Table 4.4**, and the geometrical configuration is shown in **Figure 4.8**. The pellet region is sub-divided into 10 equal volume rings for radial direction. The fuel composition and temperature are assumed to be flat within a pellet. Calculation for the one-region pellet model is also performed for comparisons.

Table 4.4 Specifications of the pin-cell model.

Item		Specification
Material	Fuel	UO_2 (4.8wt% ^{235}U)
	Cladding	Zr
	Moderator	Borated water
Temperature	Fuel	976K
	Cladding	600K
	Moderator	580K
Boron concentration		1000ppm
Geometry	Cell pitch	1.26cm
	Pellet radius	0.4095cm
	Cladding outer radius	0.475cm
	Cladding thickness (Gap is omitted)	0.0655cm

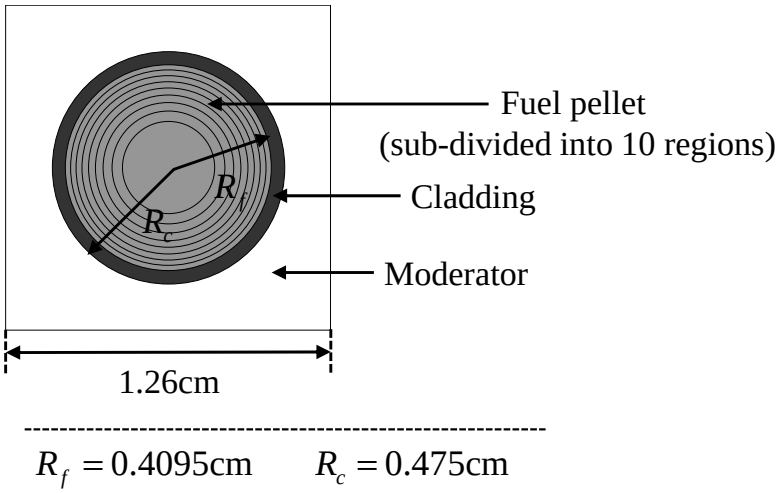

Figure 4.8 Geometry of pin-cell model.

In Sections 4.4.3.1, 4.4.3.3 and 4.4.3.5, the calculation results by the present method are compared with those by the continuous energy Monte-Carlo code MVP (Monte Carlo code for vector processors) [22]. The ENDF/B-VII.0 nuclear data library is used in all the MVP calculations to be consistent with the calculations by the present method. The total number of neutron sampling for MVP calculations is set to 100 million histories, in which the 1σ statistical error of the effective cross-sections is about 0.1%.

For the scattering kernel treatment, all the analyses including the reference calculations by the continuous energy Monte-Carlo are performed with the conventional asymptotic scattering model, as shown in Equation (4.2). In this paper, discussion for the selection of scattering model, i.e., the asymptotic model or the exact resonance scattering model [23, 24], is out of scope. The present resonance treatment is verified with reference calculations based on the same scattering model.

In Sections 4.4.3.2 and 4.4.3.4, the calculation results by the present method are

compared with those by the direct ultra-fine-group slowing-down calculation with heterogeneous geometry. The heterogeneous slowing-down calculation is performed by the equivalent Dancoff method [21] implemented in GALAXY, which is a different resonance treatment from the hybrid resonance treatment [7] and the present method.

The equivalent Dancoff method is applied to a part of the reference calculations, in which the continuous energy Monte-Carlo calculations cannot be used to obtain reference results since specific conditions dedicated for the deterministic method are used and cannot be reproduced by the Monte-Carlo method. The reliability of the equivalent Dancoff method itself is also shown in Section 4.4.3.3 through comparisons of effective cross-sections against the MVP results.

4.4.3 Verification for Fundamental Parameters of the Present Method

4.4.3.1 Ultra-Fine-Group Neutron Flux

The ultra-fine-group neutron flux by the 1st step calculation of the present method is compared with the continuous energy Monte-Carlo result in this section.

As described in Section 4.4.2.2, a set of the slowing-down equations (Equations (4.1)-(4.4)) are solved for one-region pellet system, based on the hybrid resonance treatment [7] of the equivalence theory and the ultra-fine-group slowing-down calculation. $\Sigma_{sd}^{f}(E)$ and $\mu(E)$ are numerically obtained as byproducts of the solution for Equations (4.1)-(4.4). Then by Equations (4.20)-(4.21), which are derived in Section 4.2.3, the ultra-fine-group flux for each sub-region of a pellet is analytically obtained.

The ultra-fine-group fluxes for each sub-region of a pellet by the present method and those by the continuous energy Monte-Carlo calculation (MVP) are shown in **Figure 4.9** including 88th energy group (6.16-7.52eV) of XMAS 172 energy group structure. The results for Regions 1, 8, 9 and 10 (sequentially numbered from the center to the surface of a pellet) are plotted for convenience. As shown in Figure 4.9, the present method (1st step calculation) can roughly predict the ultra-fine-group neutron flux comparable to the continuous energy Monte-Carlo results. However, a slight difference is observed. The flux differences are induced by the approximation of spatially-dependent fuel escape probability and scattering source within a pellet, which are applied to the flux derivation scheme in Section 4.2.3. As shown in Section 4.4.3.3, the differences of the ultra-fine-group flux directly cause the differences of effective cross-section between the present method “without 2nd step calculation” and the MVP. The differences of effective cross-section owing to ultra-fine-group flux estimation are

mitigated by the 2nd step calculation based on the sub-group flux, as shown in Section 4.4.3.3.

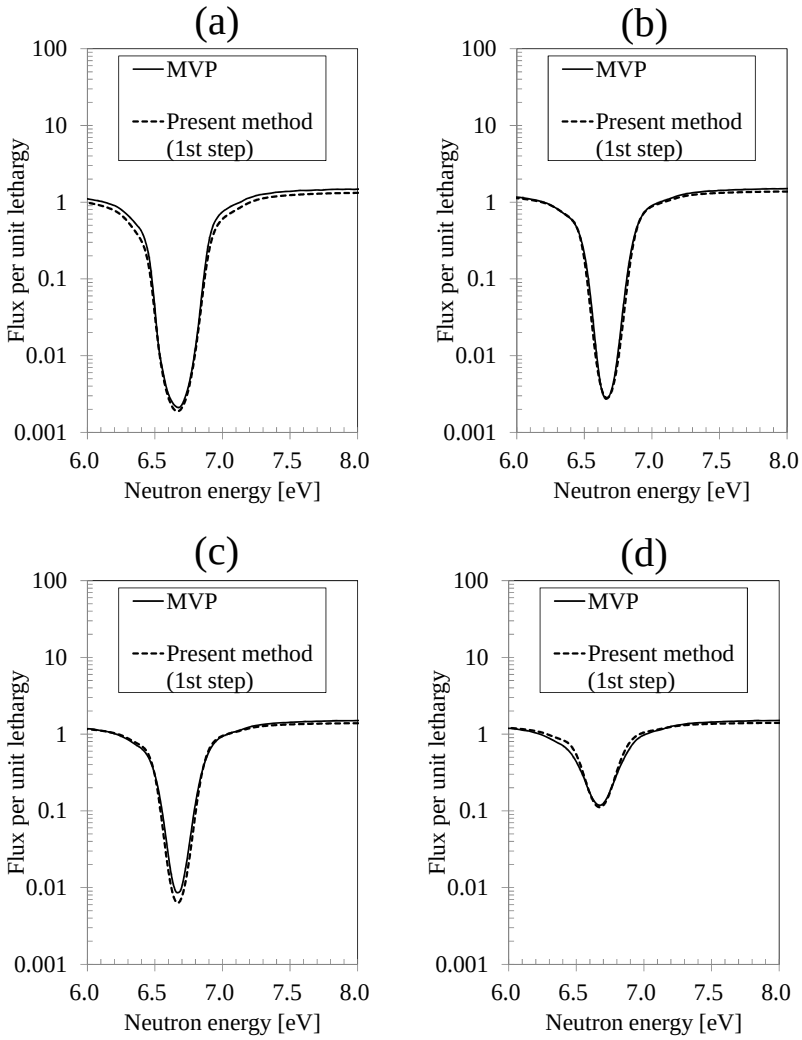

Figure 4.9 Comparison of ultra-fine-group fluxes between the present method (1st step calculation) and the continuous energy Monte-Carlo calculation (MVP) ((a) region 1, (b) region 8, (c) region 9, (d) region 10).

A breakdown of the calculation time for ultra-fine-group flux calculation in all the ring regions within a pellet is shown in **Table 4.5**. As shown in Table 4.5, the calculation time is very short, and thus the time is negligible against the total computation time of the lattice physics calculations. On the basis of its short computation time, the present method can be easily applied to the large and heterogeneous geometry such as a fuel assembly. In the present method, at first, the fuel-rod-wise ultra-fine-group flux is independently obtained for each fuel cell by Equations (4.1)-(4.4) and the cell-dependent coefficients α_n, β_n, ε_n and θ. Then, the obtained ultra-fine-group data in each fuel rod is expanded for each ring region by using the ring-dependent coefficients γ_m. Utilization of a set of coefficients for the rational equation improves the computational efficiency of the ultra-fine-group calculation, compared with the direct heterogeneous ultra-fine-group transport calculation.

Table 4.5 Calculation time for the ultra-fine-group flux.

Process	CPU time [sec]
Ultra-fine-group cross-section library read (only one time) (*)	0.31
Ultra-fine-group flux calculation for two region problem (*)	0.22
Spatially-dependent flux calculation	0.07
Spatially-dependent scattering source calculation	0.04
Flux update	0.08
(*) Reference [7]	

4.4.3.2 Sub-Group Cross-Section

The sub-group cross-sections in fuel regions are generated by the present method. The results are compared with the reference solutions obtained from the direct heterogeneous ultra-fine-group calculation by the equivalent Dancoff method.

The sub-group cross-sections and the corresponding differences from the direct heterogeneous ultra-fine-group calculation results are shown in **Figure 4.10**. The differences of the effective cross-section between the present method "without 2nd step calculation" and the reference solution are also shown in the figure. As shown in Figure 4.10, the present method can accurately predict the sub-group cross-sections, while the effective cross-section generated by the present method "without 2nd step calculation" includes some differences.

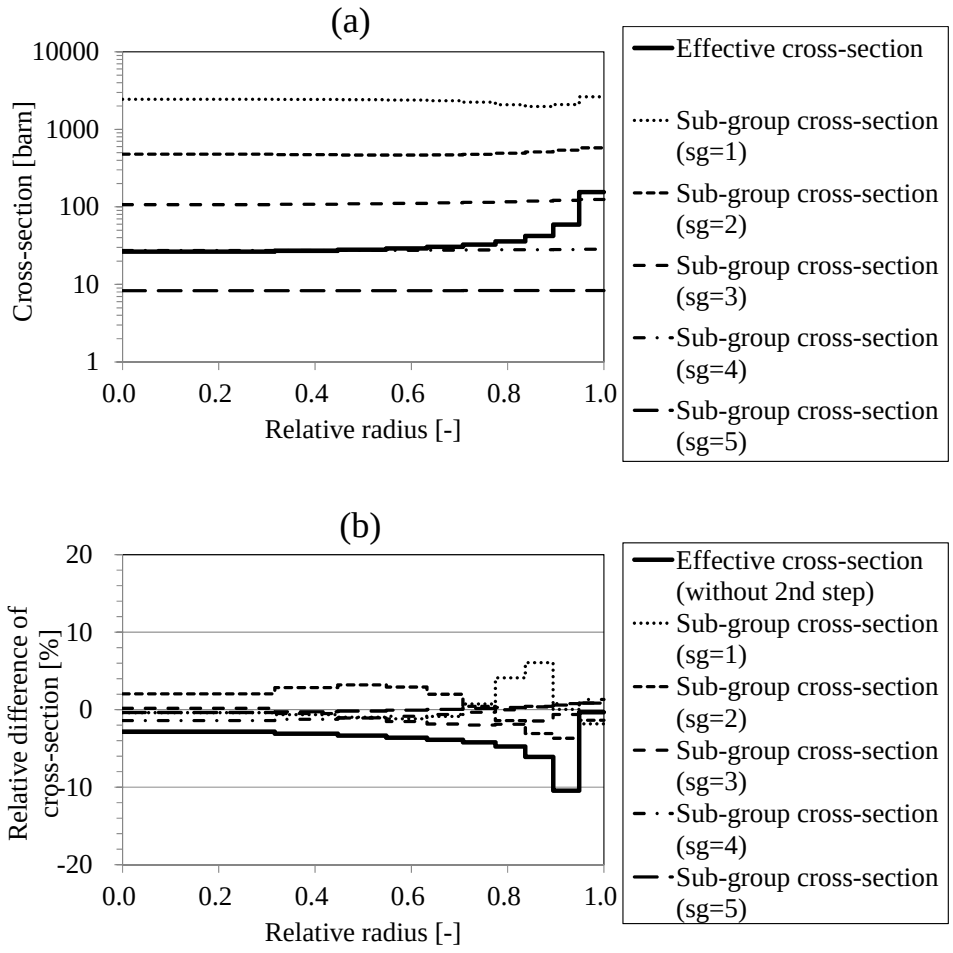

Figure 4.10 Sub-group cross-sections and their differences from the direct heterogeneous ultra-fine-group calculation results ((a) Reference solution of microscopic capture cross-section of ^{238}U, (b) Difference from reference solution).

The influence of ultra-fine-group flux error (see Section 4.3.1) on sub-group cross-section is mitigated by defining the sub-group energy structure, not for energy but for macroscopic absorption cross-section level.

4.4.3.3 Effective Cross-Section

The effective cross-sections in fuel regions are generated by the present method. The results are compared with the reference solutions obtained from the continuous energy Monte-Carlo code MVP. The results based on the equivalence theory (SDGM [4] with the NR approximation), the direct heterogeneous ultra-fine-group calculation (the equivalent Dancoff method [21]) and the present method "without 2^{nd} step calculation" are also obtained for comparison.

The effective cross-sections and the corresponding differences from the MVP results are shown in **Figure 4.11**. As shown in Figure 4.11, the present method (1^{st} + 2^{nd} step calculation) can accurately predict the effective cross-sections.

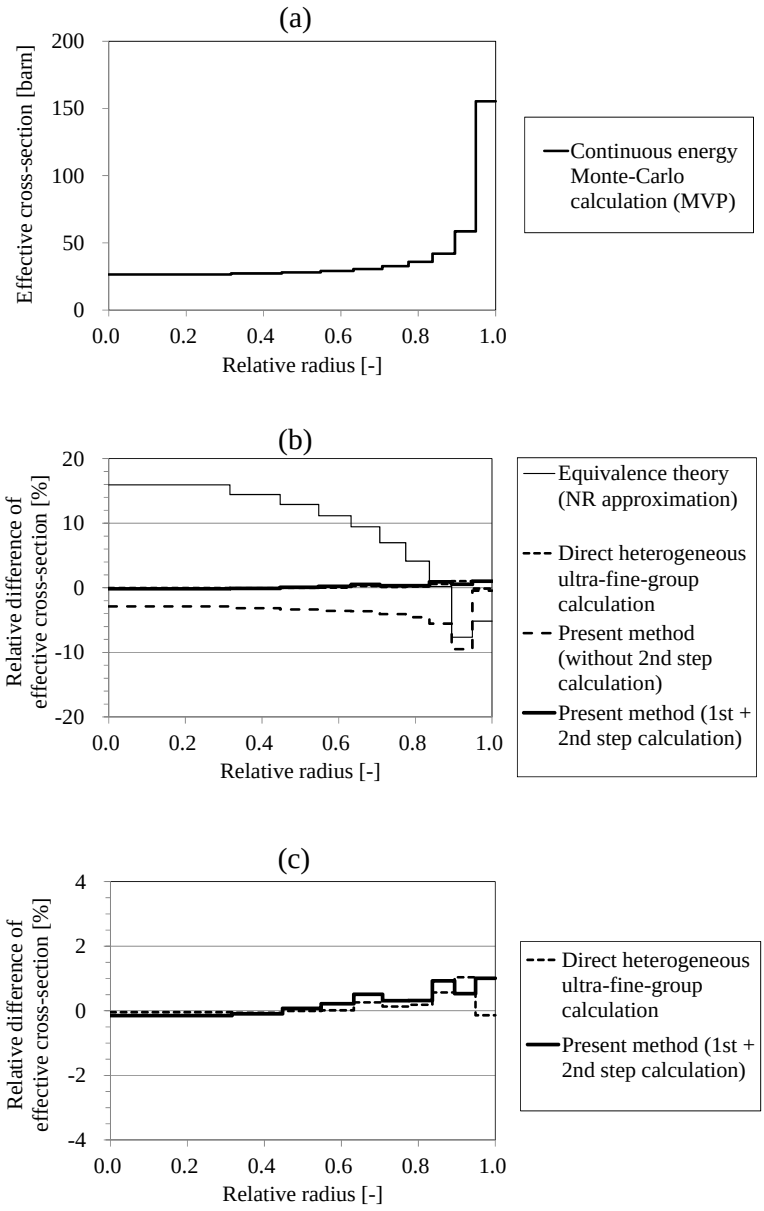

Figure 4.11 Effective cross-sections and their differences from the continuous energy Monte-Carlo calculation (MVP) ((a) Reference solution of microscopic effective capture cross-section of ^{238}U, (b) Difference from reference solution, (c) Difference from reference solution (high accuracy results only)).

In contrast, the results obtained by the equivalence theory with NR approximation and by the present method "without 2nd step calculation" show the large difference from the reference solutions. For the latter method, the difference is due to the prediction error of ultra-fine-group fluxes in the case of treating radially sub-divided fuel region (see Section 4.4.3.1).

From the result, the effectiveness of incorporating the sub-group method as the 2nd step calculation is confirmed. The influence of ultra-fine-group flux error on the final effective cross-section is efficiently reduced by the two-step flux calculation scheme of the present method, i.e., the flux calculation for "coarse geometry + fine energy" (1st step) and that for "fine geometry + coarse energy" (2nd step). The prediction accuracy of effective cross-section is appropriately improved by reflecting the more detailed information of spatial neutron transport within a pellet based on the 2nd step sub-group calculation.

The differences of the effective cross-sections from those of the MVP results are summarized in **Table 4.6**. The results obtained by one-region pellet model are also shown in the table. From Table 4.6, the present two-step method provides an excellent result for multi-region case, which is almost comparable to the direct heterogeneous ultra-fine-group calculation.

Table 4.6 Differences of effective cross-section from the continuous energy Monte-Carlo calculation (MVP).

Method	Relative difference of effective cross-section from MVP[%]		
	Pellet one-region problem	Pellet multi-region problem	
		Average	Maximum
Continuous energy Monte-Carlo calculation (MVP) (*)	0.06	0.11	0.15
Equivalence theory (NR approximation)	1.53	6.23	15.92
Direct heterogeneous ultra-fine-group calculation	0.41	0.20	1.04
Present method (without 2^{nd} step calculation)	1.08	-4.08	-9.52
Present method (1^{st} + 2^{nd} step calculation)	1.17	0.37	1.01
(*) Statistical error			

The calculation efficiency is also an important viewpoint for the total performance of a target method. The required number of one-group fixed source transport calculations is estimated in **Table 4.7**. In the conventional equivalence theory based on the Dancoff method, the one-group calculation is required only one time in the black neutron absorber condition. If the equivalence theory based on the gray resonance treatment [4] is adopted, the one-group calculation is required several times for a wide range of macroscopic total cross-section conditions. After all, the conventional equivalence theory requires only 1-20 times of one-group transport calculations. In contrast to the equivalence theory, the direct heterogeneous ultra-fine-group method generally requires 10,000-200,000 times of one-group transport calculations, which is large computational burden.

Table 4.7 Estimation for the number of one-group fixed source transport calculations.

Method	The number of one-group flux calculations [-]
Equivalence theory	1-20
Direct heterogeneous ultra-fine-group calculation	10,000-200,000
Present method	500-1,000

The present method has an intermediate feature between the above two methods. If the number of multi-groups, in which the resonance self-shielding treatment is required, is 100, and the number of sub-groups is set to 5 for each group, the required number of one-group transport calculations is 100×5=500. As a result, the required number of one-group transport calculations in the present method is less than 1/10 of that in the direct heterogeneous ultra-fine-group method, as shown in Table 4.7.

The calculation time for a fuel assembly geometry is an important point for practical lattice physics calculations. The calculation time for a fuel assembly is estimated in **Table 4.8**. In the estimation, the steady-state calculations for a typical PWR type 17×17 4.8wt% UO_2 assembly are carried out by the lattice physics code GALAXY.

As for the treatment of fuel pellet, the two cases (“no-division” and “sub-division for radial direction with 10 equal volume rings”) are analyzed. For each case, the resonance treatment methods based on the equivalence theory [4] and the direct ultra-fine-group calculation [21] are applied for comparison with the present method, and their calculation times are directly measured. Since the present method is not implemented

into the GALAXY code at the current development state, the result for the present method is inferred by the results for the other methods and the quantitative information in Tables 4.5 and 4.7. The multi-group flux calculation is performed by “172 group CCCP (current-coupling collision probability) method + 22 group MOC” [21] for all cases.

As shown in **Table 4.8**, the estimated calculation times by the present method are less than one-third of those by the direct ultra-fine-group calculation for resonance calculation part. The ratios of resonance calculation part against the “resonance + flux” calculations are less than 1/2 in the present method. From the results, the present method can efficiently generate effective cross-sections for large and complicated geometry such as a fuel assembly, comparing with the direct ultra-fine-group calculation.

Table 4.8 Brief estimation for the calculation time on fuel assembly geometry.

Pellet division	Method	CPU time ratio[-]	
		Comparison with direct het. ufg. calc.(*)	Contribution of resonance calc.(**)
No	Equivalence theory	0.17	0.15
	Direct heterogeneous ultra-fine-group calculation	1.00	0.49
	Present method	0.30	0.23
Yes	Equivalence theory	0.08	0.39
	Direct heterogeneous ultra-fine-group calculation	1.00	0.88
	Present method(***)	0.12	0.46
(*) CPU time ratio between "specific method" and "direct ultra-fine-group calculation" for resonance calculation part			
(**) CPU time ratio between "resonance calculation" and "resonance + multi-group flux calculation" for each method			
(***) Estimated values from other results			

Finally, the total performance is benchmarked for major resonance treatments, taking into account of the quantitative information in Tables 4.6-4.8. The result of qualitative comparison is summarized in **Table 4.9**. As shown in Table 4.9, the present method is better than all the three conventional methods, from the viewpoint of both calculation accuracy and time.

Table 4.9 Qualitative comparison of overall performance for resonance self-shielding treatments.

Method		Calculation accuracy	Calculation time
Conventional	Equivalence theory	Acceptable (normal design condition)	Excellent
	Ultra-fine-group calculation	Excellent	Acceptable (pin-cell)
	Sub-group method	good	good
Present		Excellent	good

4.4.3.4 Cross-Section Correction Factor

The correction factors for effective cross-section in fuel regions to reduce energy discretization error are generated by the present method. The results are compared with the reference solutions obtained from the direct heterogeneous ultra-fine-group calculation by the equivalent Dancoff method (see Equation (4.27) in Section 4.3.1). The results based on the present method "without 2^{nd} step sub-group calculation" (see Equation (4.28) in Section 4.3.1) are also obtained for comparison.

In the two-step reaction-rate preservation scheme, the relative convergence criterion of the correction factors is set as 0.1%. Only 10 iterations are necessary for the 2^{nd} step calculation in this verification with this convergence criterion.

The correction factors and the corresponding differences from the direct heterogeneous ultra-fine-group calculation results are shown in **Figure 4.12**. As shown in Figure 4.12, the present method (1^{st} + 2^{nd} step calculation) can accurately predict the correction factor.

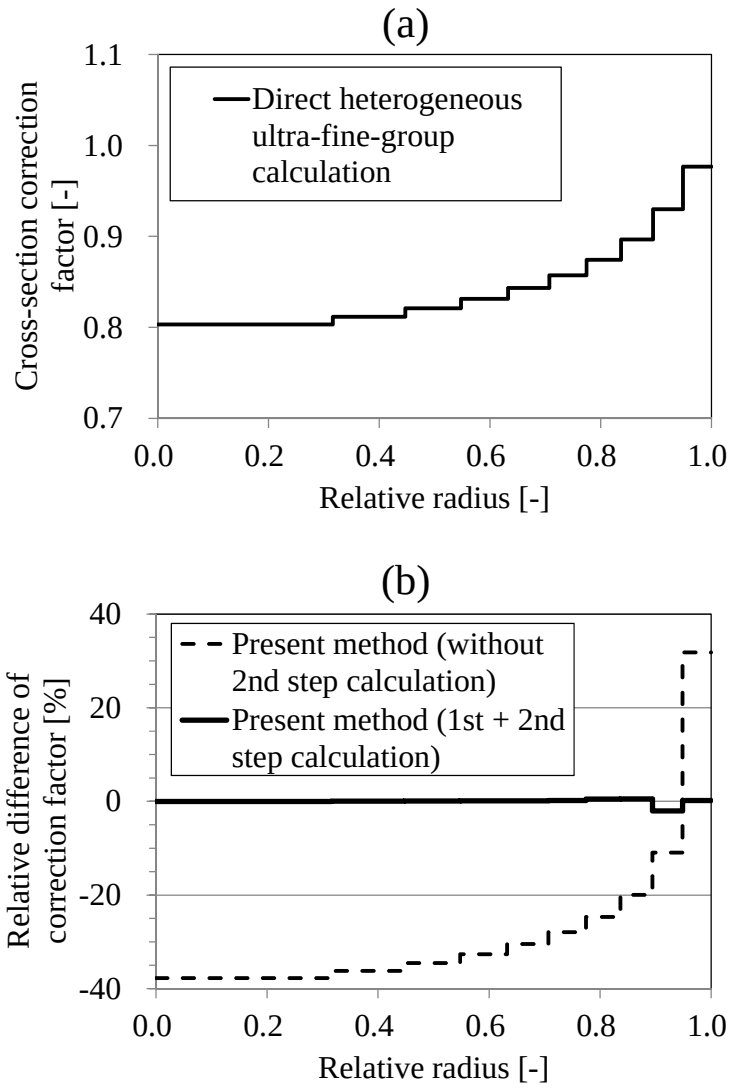

Figure 4.12 Correction factors and their differences from the direct heterogeneous ultra-fine-group calculation results ((a) Reference solution of cross-section correction factor, (b) Difference from reference solution).

In contrast, the results obtained by the present method "without 2nd step calculation" show the large difference from the reference solutions. The prediction error of

ultra-fine-group fluxes in the case of treating radially sub-divided fuel region is the cause of the difference (see Section 4.3.1).

From the result, the effectiveness of incorporating the sub-group method as the 2nd step calculation is confirmed. The influence of ultra-fine-group flux error on the final correction factor is efficiently reduced by the two-step reaction-rate preservation scheme, i.e., the ultra-fine-group to the sub-group collapsing, and the sub-group to the multi-group collapsing.

4.4.3.5 Reaction-Rate

One of the final product of lattice physics calculation is reaction-rate. In order to confirm the influence of effective cross-section differences on reaction-rate, the energy-integrated macroscopic absorption rates in fuel regions are generated from the multi-group transport calculation by the lattice physics code GALAXY. The radially-dependent microscopic effective cross-section set, which is generated from a standalone program based on the present method, is directly supplied to the GALAXY.

The results are compared with the reference solutions obtained from the continuous energy Monte-Carlo code MVP. The results based on the direct heterogeneous ultra-fine-group calculation by GALAXY are also obtained for comparison. In the reaction-rate calculation for each method, the neutron fluxes are normalized so that the volume and energy integrated neutron generation rate is unity.

The absorption rates and the corresponding differences from the MVP results are shown in **Figure 4.13**. In this analysis, the 1σ statistical error of absorption rates by MVP is about 0.02%. The maximum relative differences from the MVP results are -0.4% for the present method, and -0.2% for the direct ultra-fine-group calculation, respectively. The difference is less than $\pm 0.1\%$ for most ring regions in both methods, thus the present method can accurately predict the reaction-rates, which is comparable to the direct ultra-fine-group calculation.

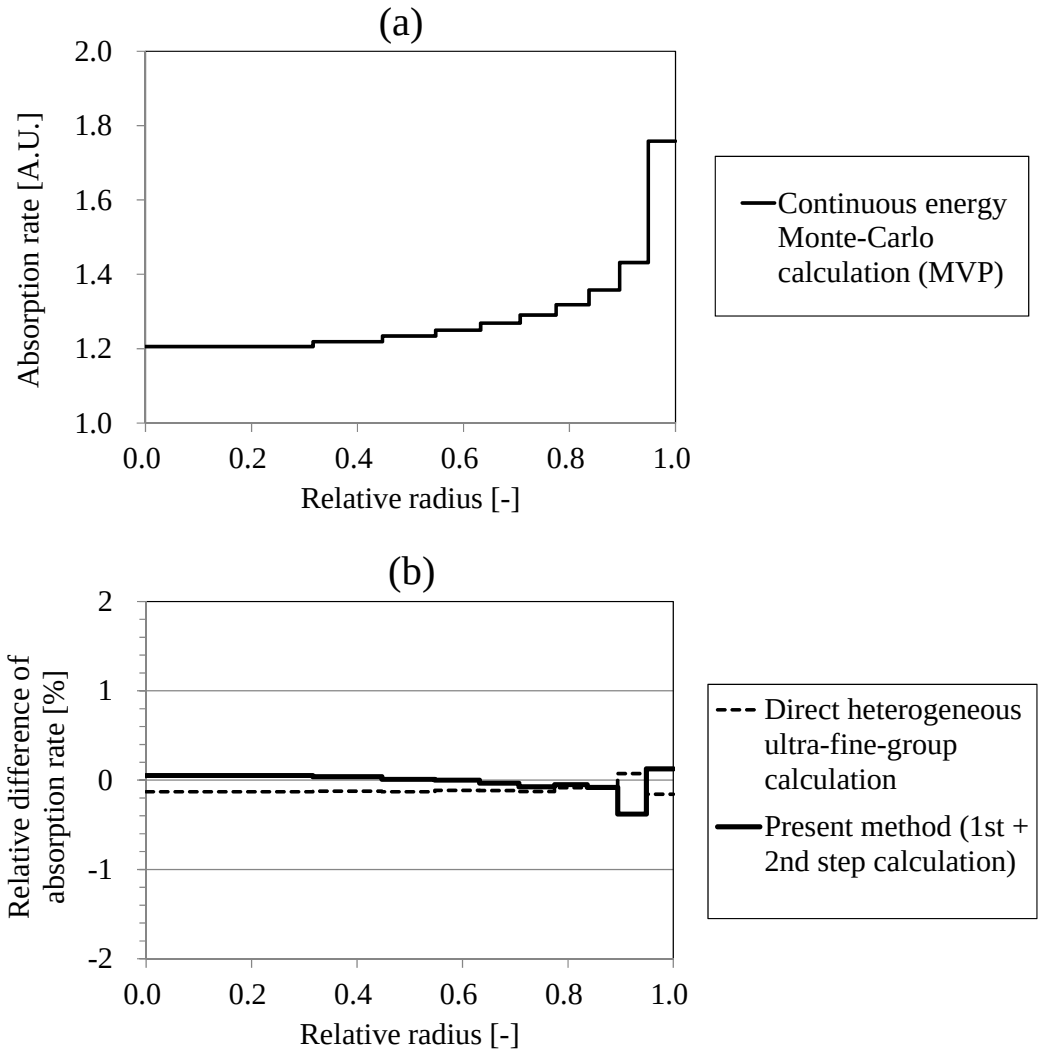

Figure 4.13 Reaction-rates and their differences from the continuous energy Monte-Carlo calculation (MVP) ((a) Reference solution of macroscopic absorption rate, (b) Difference from reference solution).

4.4.4 Application for Various Pin-Cell and Multi-Cell Problems

4.4.4.1 Radially-Dependent Effective Cross-Sections with Non-Uniform Isotope Composition for Unit Pin-Cell

In this section, the pin-cell with non-uniform isotope composition is treated, in which the fuel composition is radially distributed. As a typical application for the LWR lattice calculations, the depleted fuel and the annular fuel are taken into account. For both fuels, the calculation conditions except for the number densities in fuel regions are the same as those given in Section 4.4.2.

For the depleted fuel case, the GALAXY depletion calculation is performed in advance, and the number densities for each nuclide and each ring region within a pellet are obtained. In this verification, the number densities only for main actinide nuclides, i.e., ^{235}U, ^{238}U, ^{239}Pu, ^{240}Pu and ^{241}Pu, are extracted for simplicity on the burnup condition of 60GWd/t, as shown in **Figure 4.14**. The typical Pu build-up effect on a peripheral region of the pellet can be observed from the figure.

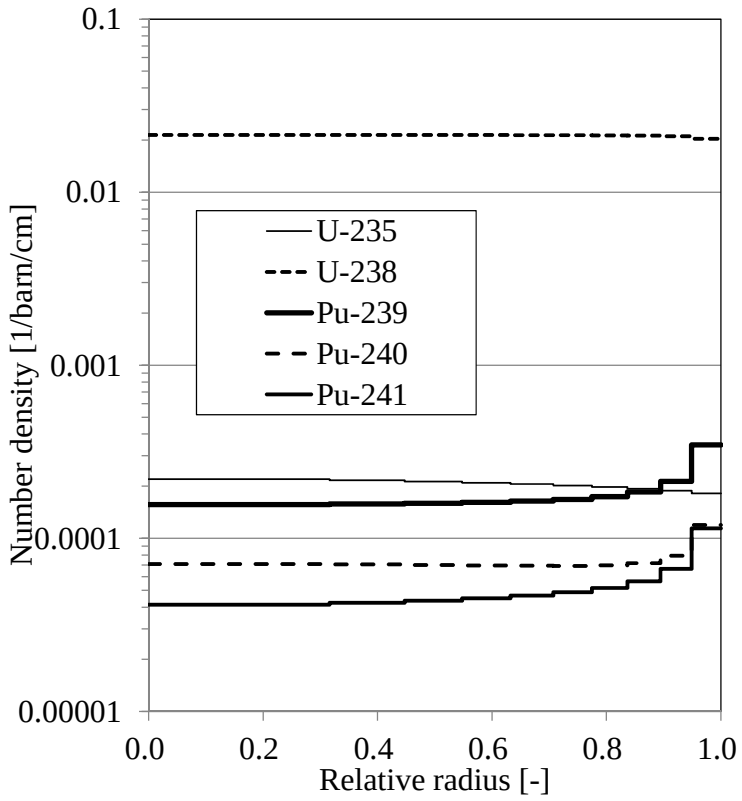

Figure 4.14 Distribution of fuel isotope composition within a pellet.

In this verification, the microscopic effective capture cross-sections of ^{238}U are generated with the given region-dependent number densities. The effective cross-sections generated by the present method are compared with the reference solutions obtained from the continuous energy Monte-Carlo code MVP. The results are shown in **Figure 4.15**. As shown in the figure, the present method can accurately predict the effective cross-sections with radially-distributed isotope composition. The spatially-dependent biases against fresh fuel condition also agree well with the Monte-Carlo results, and therefore the consistency between uniform and non-uniform fuel composition treatments is confirmed for the present method.

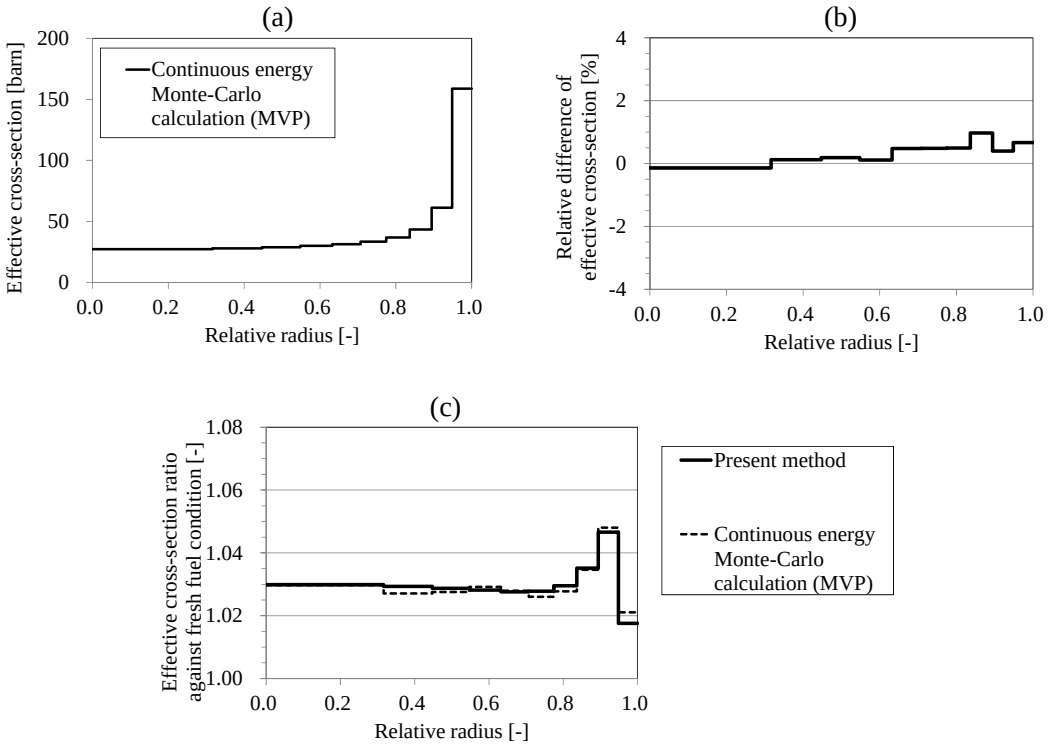

Figure 4.15 Effective cross-sections and their differences from the continuous energy Monte-Carlo calculation (MVP) with non-uniform isotope composition ((a) Reference solution, (b) Difference from reference solution, (c) Ratio against fresh fuel condition).

For the annular fuel case, material for the inner-most region of the pellet, which is sub-divided into 10 equal volume rings for radial direction, is assumed as air. Similar with the above depleted fuel case, the comparison of the effective cross-sections is shown in **Figure 4.16**. As shown in the figure, the present method can accurately predict the effective cross-sections of annular fuel. The consistency between solid and annular

fuel treatments is confirmed for the present method.

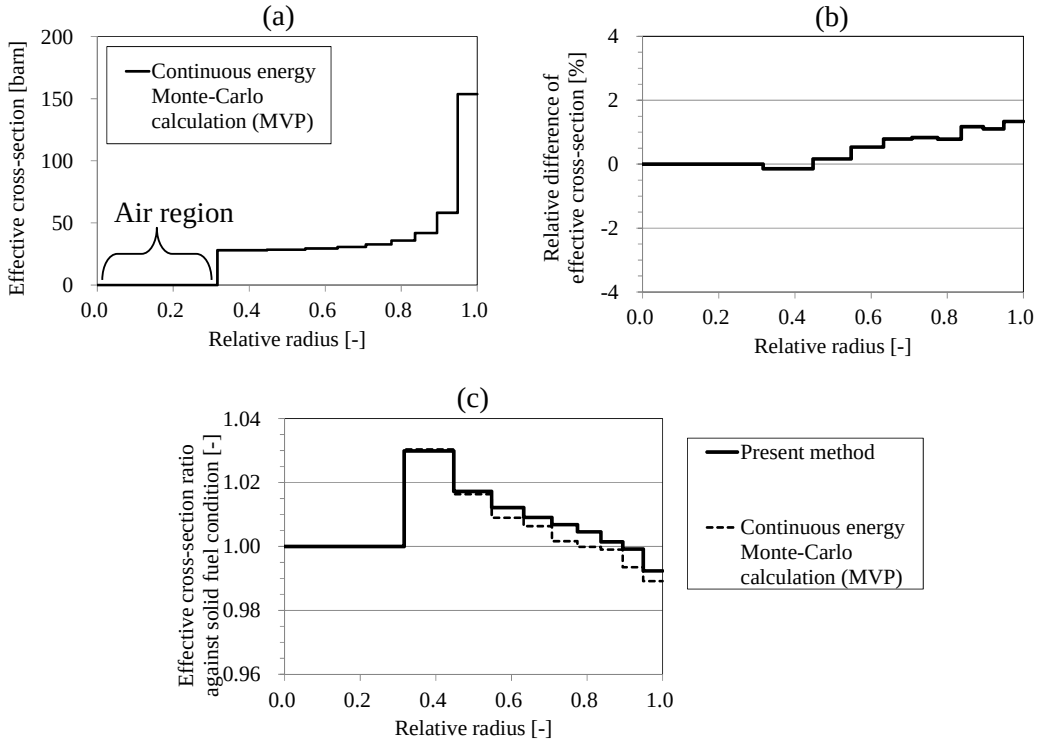

Figure 4.16 Effective cross-sections and their differences from the continuous energy Monte-Carlo calculation (MVP) for annular fuel ((a) Reference solution, (b) Difference from reference solution, (c) Ratio against solid fuel condition).

4.4.4.2 Radially-Dependent Effective Cross-Sections with Non-Uniform Temperature for Unit Pin-Cell

In this section, the pin-cell with non-uniform temperature is treated, in which the fuel temperature is radially distributed. The calculation conditions except for the fuel temperatures are the same as those given in Section 4.4.2.

The fuel temperature distribution used for the verification is shown in **Figure 4.17**. The corresponding effective fuel temperature which is averaged with a chord weight [15] is the same as that in Table 4.4.

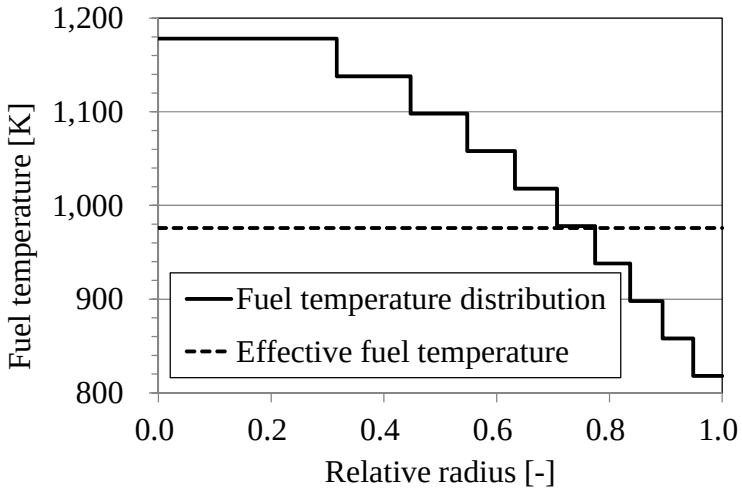

Figure 4.17 Distribution of fuel temperature within a pellet.

In this verification, the microscopic effective capture cross-sections of ^{238}U are generated with the given region-dependent temperatures. The effective cross-sections generated by the present method are compared with the reference solutions obtained from the continuous energy Monte-Carlo code MVP. The results are shown in **Figure**

4.18. As shown in the figure, the spatially-dependent biases against flat temperature condition agree well with the Monte-Carlo results, and therefore the consistency between uniform and non-uniform fuel temperature treatments is confirmed for the present method.

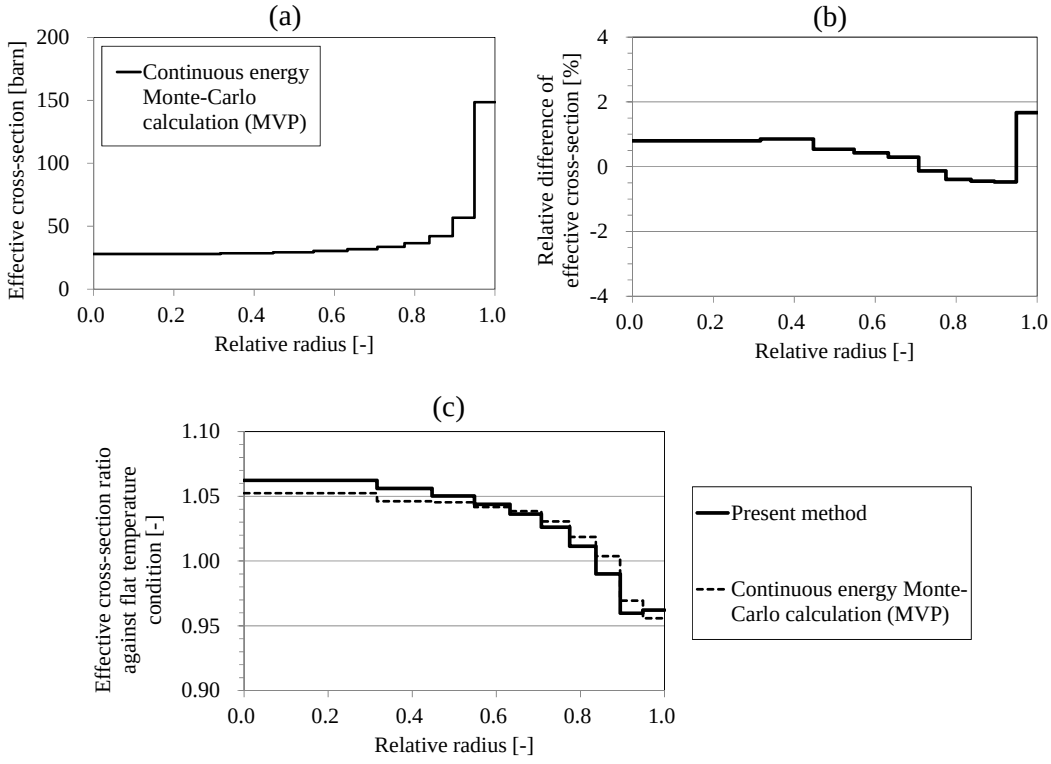

Figure 4.18 Effective cross-sections and their differences from the continuous energy Monte-Carlo calculation (MVP) with non-uniform fuel temperature ((a) Reference solution, (b) Difference from reference solution, (c) Ratio against flat fuel temperature condition).

4.4.4.3 Radially and Azimuthally Dependent Effective Cross-Sections for Unit Pin-Cell

In this section, the radially and azimuthally divided pin-cell is treated. The calculation conditions except for the sub-division of fuel region in azimuthal direction are the same as those given in Section 4.4.2. The fuel pellet is sub-divided into 32 sector regions for 2π with equal azimuthal angle interval.

In this verification, the azimuthally-dependent microscopic effective capture cross-sections of ^{238}U are generated. The sub-group cross-sections are generated as the azimuthally-independent values in the 1st step of the present method. The azimuthal dependence against the final effective cross-sections is taken into account by the 2nd step sub-group flux calculation with direct two-dimensional geometry modeling based on MOC.

It should be noted that the azimuthal dependence denotes the sector region dependence of effective cross-sections. The azimuthal dependence is not equal to the angular dependence of effective cross-sections due to the angular dependence of neutron flux for polar and azimuthal directions.

The effective cross-sections generated by the present method are compared with the reference solutions obtained from the continuous energy Monte-Carlo code MVP. The total number of neutron sampling for MVP calculations is set to 500 million histories, in which the 1σ statistical error of the effective cross-sections is about 0.1-0.2%.

The results are shown in **Figure 4.19**. As shown in the figure, the present method can accurately predict the azimuthally-dependent effective cross-sections, in which the cross-sections tend to be larger for the diagonal directions than that for the horizontal

and vertical directions due to the difference of adjacent moderator region volume. The spatially-dependent biases against one-region fuel condition also agree well with the Monte-Carlo results, and therefore the consistency between one-region and azimuthal multi-region treatments is confirmed for the present method.

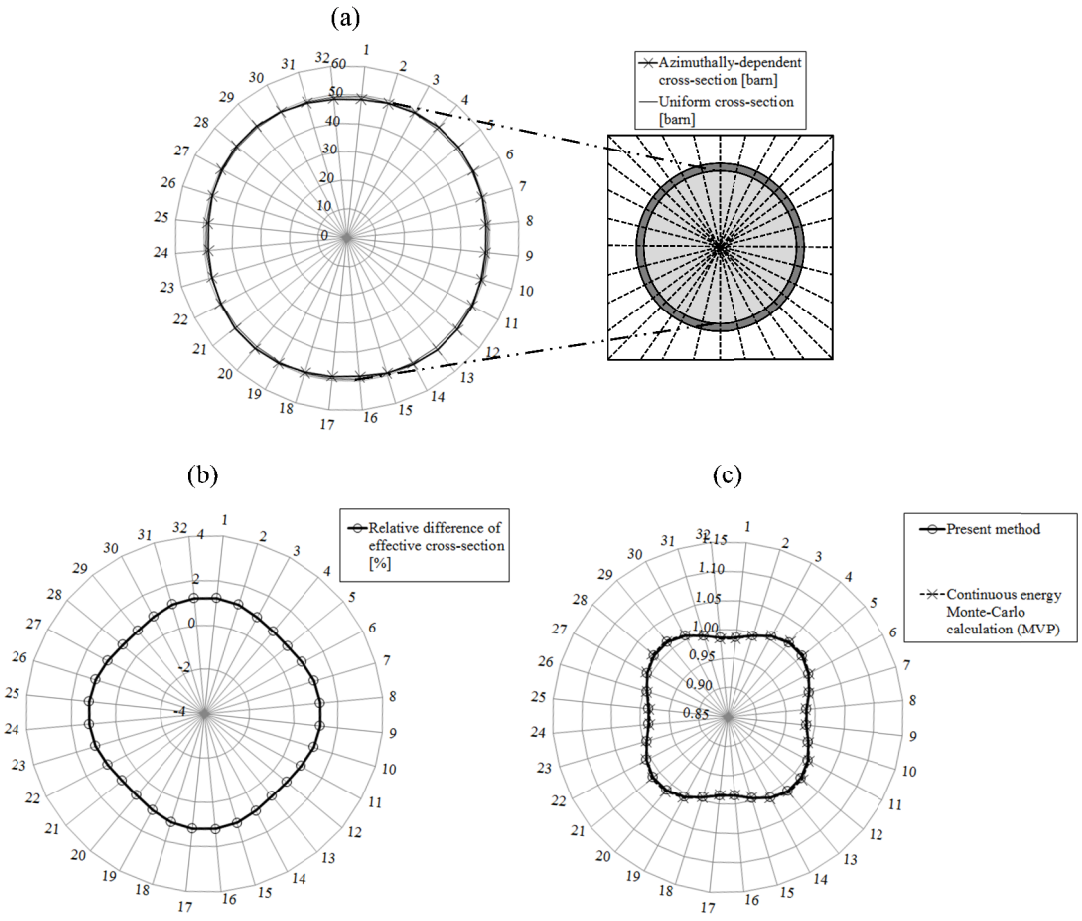

Figure 4.19 Azimuthally-dependent effective cross-sections and their differences from the continuous energy Monte-Carlo calculation (MVP) for unit pin-cell ((a) Reference solution of microscopic effective capture cross-section of ^{238}U, (b) Difference from reference solution (c) Ratio against one-region fuel condition).

Both the radially and azimuthally dependent effective cross-sections are also compared with the reference solutions from MVP. The results for azimuthally-dependent effective cross-section ratios for each ring region are shown in **Figure 4.20**. The results for radially-divided regions 1, 7, 8, 9, and 10 (sequentially numbered from the center to the surface of a pellet) are plotted for convenience. As shown in the figure, the present method can accurately predict both the radial and azimuthal dependences of effective cross-sections.

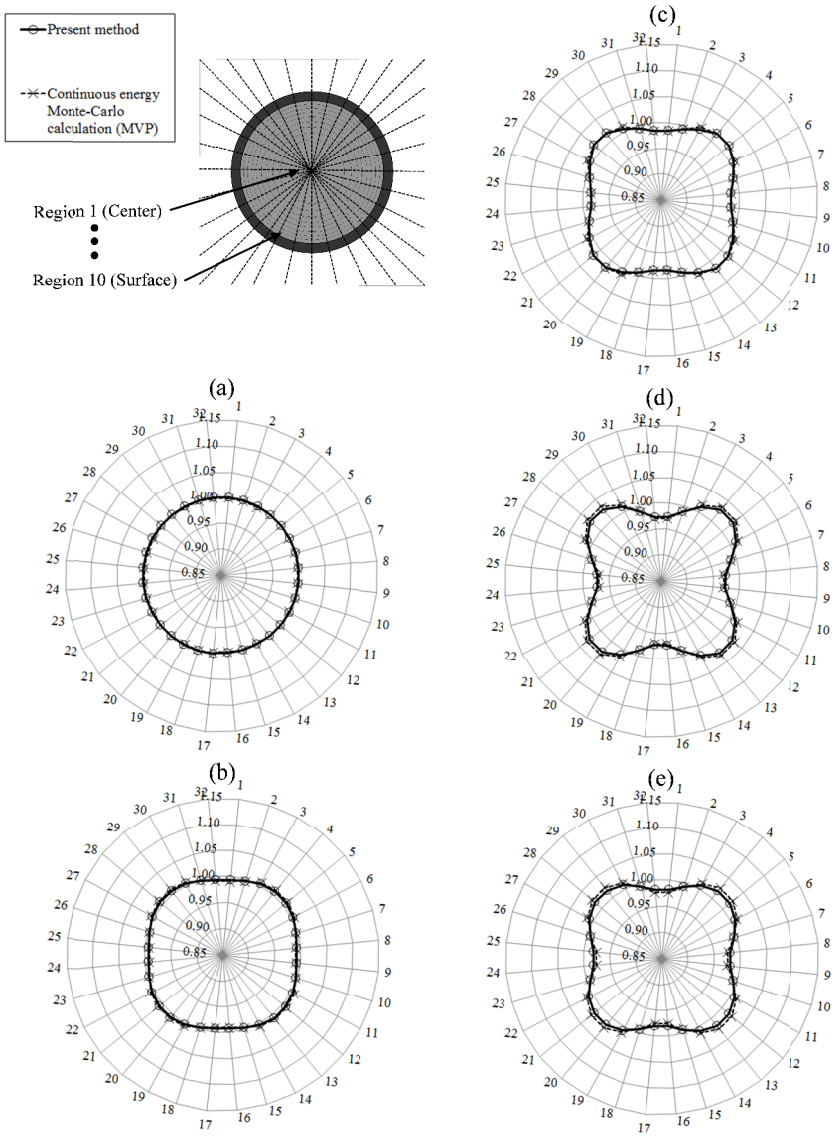

Figure 4.20 Azimuthally-dependent effective cross-section ratios in each ring region for unit pin-cell ((a) Region 1, (b) Region 7, (c) Region 8, (d) Region 9, (e) Region 10).

As can be observed from Figure 4.20, the azimuthal dependence of effective cross-sections tends to be larger for the pellet surface (region 10) than that for the pellet

center (region 1) due to the difference of distance from moderator region. The heterogeneous effect, which is a main contributor for yielding azimuthal dependence, is small for the pellet center. Thus the effective cross-sections are azimuthally flat for pellet center region.

Though the difference of effective cross-sections between the present method and MVP is not shown in Figure 4.20, the difference is confirmed to be less than $\pm 2\%$ for all the 320 regions, which is a consistent result with Figure 4.11 in Section 4.4.3. Therefore, the present method can accurately predict spatially-dependent effective cross-sections for both radially and azimuthally sub-divided fuel condition.

4.4.4.4 Azimuthally-Dependent Effective Cross-Sections for 3×3 Multi-Cell Including Large Water Region

Finally, the 3×3 multi-cell divided in azimuthal direction is treated. A large water cell is set in the center region, simply simulating a guide thimble or an instrumentation tube in a typical PWR (Pressurized Water Reactor) fuel assembly. The calculation conditions of fuel regions except for the sub-division of fuel region in azimuthal direction are the same as those given in Section 4.4.2. The fuel pellet is sub-divided into 32 sector regions for 2π with equal azimuthal angle interval.

The effective cross-sections generated by the present method are compared with the reference solutions obtained from the continuous energy Monte-Carlo code MVP. The total number of neutron sampling for MVP calculations is set to 1 billion histories, in which the 1σ statistical error of the effective cross-sections is about 0.3%.

The results are shown in **Figure 4.21** and **Figure 4.22**. As shown in the figures, the present method can accurately predict the azimuthally-dependent effective cross-sections. The spatially-dependent biases against one-region fuel also agree well with the Monte-Carlo results, and therefore the consistency between one-region fuel and azimuthal multi-region treatments is confirmed for the present method.

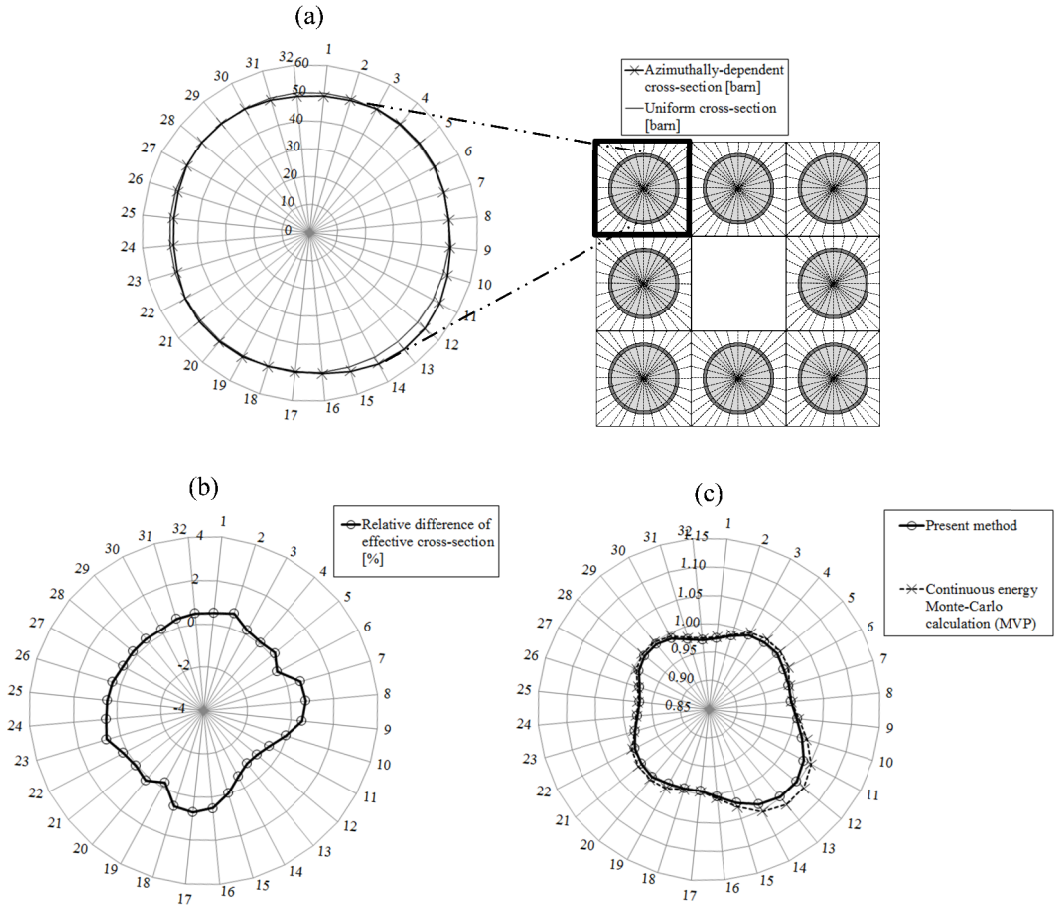

Figure 4.21 Azimuthally-dependent effective cross-sections and their differences from the continuous energy Monte-Carlo calculation (MVP) for 3×3 multi-cell with large water region (corner fuel) ((a) Reference solution of microscopic effective capture cross-section of ^{238}U, (b) Difference from reference solution (c) Ratio against one-region fuel condition).

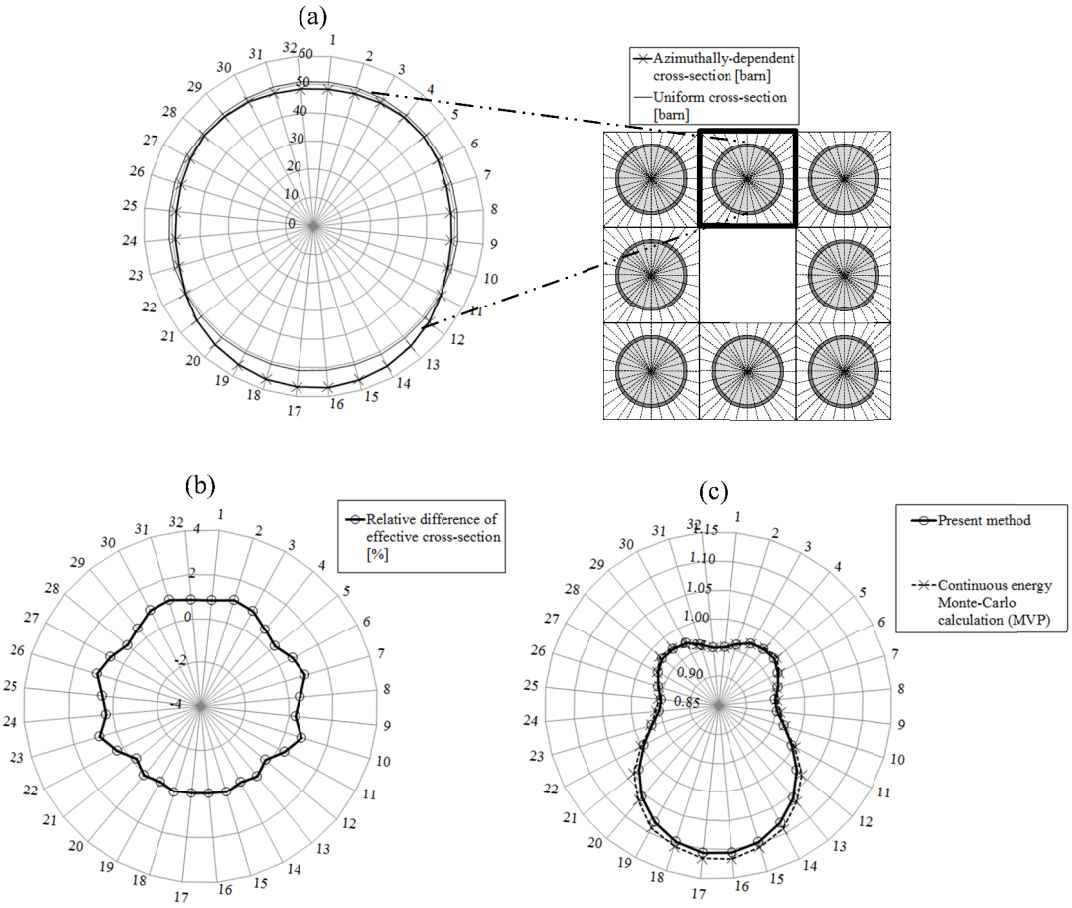

Figure 4.22 Azimuthally-dependent effective cross-sections and their differences from the continuous energy Monte-Carlo calculation (MVP) for 3×3 multi-cell with large water region (vertical fuel) ((a) Reference solution of microscopic effective capture cross-section of ^{238}U, (b) Difference from reference solution (c) Ratio against one-region fuel condition).

In the conventional methods, only the direct heterogeneous ultra-fine-group slowing-down calculation and the sub-group method with two-dimensional exact geometry can generate the azimuthally-dependent effective cross-sections. Therefore,

the present method is an efficient alternative to treat azimuthally-dependent resonance self-shielding effect, while keeping sufficient accuracy.

4.5 Conclusion

The unified resonance self-shielding method is developed for general application of lattice physics calculations. The present method can accurately treat the radially and azimuthally dependent resonance self-shielding effect without the direct heterogeneous ultra-fine-group calculation.

A calculation scheme of the present method is based on the concept of multi-stage cross-section collapsing strategies, and is composed of two-step calculation, i.e., “coarse geometry + fine energy” (1^{st} step) and “fine geometry + coarse energy” (2^{nd} step) calculations. The 1^{st} step calculation corresponds to the hybrid model of the equivalence theory and the ultra-fine-group calculation, and the 2^{nd} step corresponds to the sub-group method. The two-step reaction-rate preservation scheme is also established to reduce energy discretization error.

From the various verification results, radially and azimuthally dependent effective cross-sections generated by the new method show good agreement with the continuous energy Monte-Carlo results for pin-cell and multi-cell geometries including non-uniform fuel compositions and temperature distributions within a pellet.

The present method can accurately generate effective cross-sections with short computation time in lattice physics calculations, and has a potential for the general application toward the next generation core analysis codes that require high fidelity and sophisticated modeling of reactors.

4.6 References

[1] Stamm'ler RJJ, Abbate MJ. Methods of steady-state reactor physics in nuclear design. London: Academic Press; 1983.

[2] Yamamoto A. Evaluation of background cross section for heterogeneous and complicated geometry by the enhanced neutron current method. J. Nucl. Sci. Technol., 2008; **45**, 1287.

[3] Hébert A and Marleau G. Generalization of the Stamm'ler method for the self-shielding of resonant isotopes in arbitrary geometries. Nucl. Sci. Eng., 1991; **108**, 230.

[4] Koike H, Yamaji K, Kirimura K, Sato D, Matsumoto H and Yamamoto A. Advanced resonance self-shielding method for gray resonance treatment in lattice physics code GALAXY. J. Nucl. Sci. Technol. 2012; **49**, 725.

[5] Kier PH and Robba AA. A program for computation of resonance absorption in multiregion reactor cells. 1967. (ANL-7326).

[6] Sugimura N and Yamamoto A. Resonance treatment based on ultra-fine-group spectrum calculation in the AEGIS code. J. Nucl. Sci. Technol. 2007; **44**, 958.

[7] Koike H, Yamaji K, Kirimura K, Kosaka S, Matsumoto H and Yamamoto A. Integration of equivalence theory and ultra-fine-group slowing-down calculation for resonance self-shielding treatment in lattice physics code GALAXY. J. Nucl. Sci. Technol. 2016; **53**, 842.

[8] Stoker CC and Weiss ZJ. Spatially dependent resonance cross sections in a fuel rod. Ann. Nucl. Energy, 1996; **23**, 765.

[9] Matsumoto H, Ouisloumen M and Takeda T. Development of spatially dependent

resonance shielding method. J. Nucl. Sci. Technol. 2005; **42**, 688.

[10] Nikolaev MN, Ignatov AA, Isaev NV and Khokhlov VF. The method of subgroups for considering the resonance structure of the cross sections in neutron calculations. Sov. At. Energy, 1970; **29**, 689.

[11] Ribon P and Maillard J.M. Probability tables and gauss quadrature; Application to neutron cross-sections in the unresolved energy range. Topical meeting on advances in reactor physics and safety, 1986; Saratoga Springs.

[12] Askew R. A characteristics formulation of the neutron transport equation in complicated geometries. Winfrith: Atomic Energy Authority; 1972 (AEEW-M1108).

[13] Yamamoto A, Koike H and Yamane Y. A new framework of resonance calculation method based on the sub-group method (1); Theory. Trans. Am. Nucl. Soc. 2009 **100**: 647 [CD-ROM].

[14] Cacuci DG. Handbook of nuclear engineering, Springer, Berlin, 2010.

[15] Kruijf WJM De and Janssen AJ. The effective temperature to be used for calculating resonance absorption in a $^{238}UO_2$ lump with a nonuniform temperature profile. Nucl. Sci. Eng. 1996; **123**, 121.

[16] Kavenoky A. The SPH homogenization method. Proc.Meeting Homogenization Methods in Reactor Physics; 1978 Nov 13–15; Lugano, IAEA-TECDOC-231, International Atomic Energy Agency; 1978.

[17] Yamamoto A, Endo T and Koike H. Improved derivation of multigroup effective cross section for heterogeneous system by equivalence theory. Nucl. Sci. Eng. 2011; **168**, 75.

[18] Yamaji K, Matsumoto H, Kirimura K, Takeda T and Yamamoto A. Development of a new lattice physics code GALAXY for flexible geometry representation in next generation core analysis system. Trans. Am. Nucl. Soc. 2007; **97**: 573 [CD-ROM].

[19] Chadwick MB, Oblozinsky P, Herman M, et al. ENDF/B-VII.0: next generation evaluated nuclear data library for nuclear science and technology. Nuclear Data Sheets. 2006; 107: 2931-3060.

[20] Sartori E. Standard energy group structures of cross section libraries for reactor shielding, reactor cell and fusion neutronics applications: VITAMIN-J, ECCO-33, ECCO-2000 and XMAS, JEF/DOC-315, Revision 3. Gif-sur-Yvette: NEA Data Bank; 1990.

[21] Yamaji K, Koike H, Kamiyama Y, Kirimura K, Kosaka S and Matsumoto H. Validation of lattice physics code GALAXY with new resonance and fast transport method, Proc. of ICAPP 2015, 2015; Nice, France.

[22] Nagaya Y, Okumura K, Mori T and Nakagawa M. MVP/GMVP II: general purpose Monte Carlo codes for neutron and photon transport calculations based on continuous energy and multigroup methods. Ibaraki: Japanese Atomic Energy Research Institute (JAERI); 2005. (JAERI 1348).

[23] Ouisloumen M and Sanchez R. A model for neutron scattering off heavy isotopes that accounts for thermal agitation effects. Nucl. Sci. Eng., 1990; **107**: 189.

[24] Lee D, Smith K, and Rhodes J. The Impact of ^{238}U resonance elastic scattering approximations on thermal reactor Doppler reactivity. Ann. Nucl. Energ., 2009; **36**(3):274.

CHAPTER 5. CONCLUSIONS

5.1 Summary of This Dissertation

This dissertation is devoted to development of a new resonance self-shielding methodology for generation of effective cross-sections, which are the input of neutron flux calculation in lattice physics calculation of fuel assembly geometry for light water reactors (LWRs) core analysis.

In general, core design calculation for commercial LWRs is composed of two-step calculations, i.e., lattice physics calculation followed by core calculation. In the lattice physics calculation, the detailed neutronics characteristics of fuel assembly are solved and the assembly-averaged cross-sections (nuclear constants) are generated. Then the core calculation is performed by using the nuclear constants as input data.

The lattice physics calculation scheme is composed of resonance calculation and neutron flux calculation, and the nuclear constants are generated based on the results of resonance and flux calculations.

In the resonance calculation, the averaged cross-sections for resonance energy ranges, i.e., effective cross-sections, are generated by taking into account of resonance self-shielding effect. The resonance self-shielding effect is driven by resonance absorptions of neutrons and their influences on flux depressions, which are mainly induced by heavy nuclides such as ^{238}U. ^{238}U is a main nuclide for LWR nuclear fuel. The various fuel assembly specifications, e.g., geometry, fuel composition and temperature conditions, are considered in the resonance calculation. Then in the flux

calculation, the spatial and energy distribution of neutron flux within a fuel assembly is calculated by solving neutron transport equation for the fuel assembly geometry. The multi-group effective cross-sections obtained from the resonance calculation are used as input data in the flux calculation.

As for the flux calculation, the detailed neutron transport method based on the method of characteristics (MOC) is widely applied in the current high performance computers. For the resonance calculation, in contrast, several technical issues exist from the view point of calculation accuracy within practical computation time which is suitable to the combination of flux calculation method.

In the present study, a new resonance self-shielding methodology is developed for the treatment of generalized geometry and extensive neutron spectrum conditions. The treatment of generalized geometry contributes to the improvement of prediction accuracy for core nuclear design. It is also suitable for next generation core analysis methodology which can be applied to the uncertainty quantification and/or reduction of neutronics parameters. The treatment of extensive neutron spectrum conditions contributes to the application of transient and severe accident conditions (lower moderator density ranges) appeared in safety analysis.

From these backgrounds, the objective of this dissertation is to enhance the reactor analysis methodology through developing a new resonance self-shielding treatment by solving the above issues.

Through the enhancement of the methodology, the prediction accuracy of neutronics characteristics is improved, not only for the normal operation but also for the severe accident conditions of the reactors. These enhancements associated with the core

analysis methodology contribute to the activities for improvement of nuclear power safety, which is an overall objective of this study.

The current resonance self-shielding treatment is mainly classified into three categories, i.e., the equivalence theory, the ultra-fine-group calculation and the sub-group method.

The equivalence theory has rich experiences to the applications for the conventional lattice physics calculations, and its calculation efficiency is in practical level. However, it is difficult to guarantee accuracy for the wide application range. Especially for the calculation accuracy, the fundamental improvement of its theory has not been conducted in the past 30 years.

In contrast, the ultra-fine-group calculation enables to obtain high accurate results, while it requires long computation time. Therefore, it has rarely been applied to a large and complicated geometry such as a fuel assembly for LWRs.

The sub-group method has intermediate nature between the equivalence theory and the ultra-fine-group calculation from the view point of calculation accuracy and efficiency. Since the sub-group method has an issue for prediction of Doppler reactivity considering non-uniform fuel temperature distribution, it has rarely been applied to the practical core designs.

In order to solve the above issues for calculation accuracy and efficiency on the conventional resonance treatments, a new resonance self-shielding methodology has been established in the present study, by theoretically enhancing and integrating the

conventional three methods. The present resonance self-shielding methodology is developed for the treatment of generalized geometry and extensive neutron spectrum conditions. The summary of technical achievements is described as follows.

(1) DEVELOPMENT OF ADVANCED RESONANCE SELF-SHIELDING METHODOLOGY FOR GENERALIZED LATTICE GEOMETRY AND GRAY NEUTRON ABSORBER BASED ON EQUIVALENCE THEORY (Chapter 2)

In the 1st stage of the development, the equivalence theory is focused and its fundamental theory is improved.

In the conventional equivalence theory, the energy-dependent neutron flux is approximated as a rational equation. In the approximation, the fuel material is assumed as a black body (perfect neutron absorber) for treating an effect for lattice arrangement of each fuel rod within an assembly. The approximation is a cause of error for resonance calculation.

In order to remove the cause of error, a new resonance treatment has been developed. In the new treatment, gray neutron absorption effect, which means that the fuel material is not necessarily a perfect neutron absorber, is theoretically incorporated based on a multi-term rational equation of the neutron flux.

The gray effect is taken into account by performing neutron flux calculations for the wide range of fuel material conditions between black and white body (non neutron absorber) including gray neutron absorber.

In the present method, the neutron fluxes are calculated based on the MOC, which

can treat generalized geometry. Therefore, the present method enables to remove both the geometrical modeling approximation and the black body approximation, and to precisely treat the complicated lattice geometry within a fuel assembly.

(2) DEVELOPMENT OF HYBRID RESONANCE SELF-SHIELDING METHODOLOGY FOR ENERGY DEPENDENT SCATTERING SOURCE AND RESONANCE INTERFERENCE EFFECT BASED ON INTEGRATION OF EQUIVALENCE THEORY AND ULTRA-FINE-GROUP SLOWING-DOWN CALCULATION (Chapter 3)

Though the conventional equivalence theory can generate effective cross-sections with short computation time, it has several issues due to its theoretical approximations. The issues to be solved in this chapter are scattering source approximation which is important for consideration of extensive neutron spectrum conditions, and ignoring the effect of multiple resonance nuclides on flux depression (resonance interference effect).

As the 2nd stage of the development, a derivation scheme of the energy-dependent neutron flux in the equivalence theory is reviewed based on the 1st technical achievement in Chapter 2. In concrete, the accurate scattering source treatment in the ultra-fine-group slowing-down calculation is incorporated into the conventional equivalence theory.

As a result, a new form of energy-dependent neutron flux in the fuel region is derived. The new hybrid equation leads to a theoretical integration of the conventional equivalence theory and the ultra-fine-group calculation.

By applying the new hybrid resonance treatment, various neutronics parameters such as reactivity, which is important for safety analysis, can accurately be predicted with short computation time. The predicted values obtained from the present method agree well with those from the continuous energy Monte-Carlo method, and the computation time of the present method is confirmed to be the practical level in LWR assembly calculations.

(3) DEVELOPMENT OF GENERALIZED RESONANCE SELF-SHIELDING METHODOLOGY FOR INTRA-PELLET MULTI-REGION GEOMETRY AND NON-UNIFORM EFFECT BASED ON A UNIFIED THEORY (Chapter 4)

The hybrid resonance treatment based on integration of the equivalence theory and the ultra-fine-group calculation can accurately generate effective cross-sections with short computation time for the extensive range of neutron spectrum conditions, as long as each fuel region within a fuel assembly is not sub-divided. This hybrid method cannot be applied to the fuel regions which are each sub-divided into the multiple regions.

In this chapter, a new resonance treatment, which can be applied to the sub-divided regions, has successfully been developed by further incorporating the efficient treatment in the sub-group method into the hybrid resonance treatment developed in Chapter 3.

In the new method, a concept of multi-stage neutron transport method generally adopted in the field of core nuclear design calculation is incorporated into the resonance calculation. From its concept, a two-step resonance calculation scheme is constructed by

combining the “simplified geometry + ultra-fine energy group” and “exact geometry + few energy group” calculation.

In the 1st step calculation, the ultra-fine-group neutron fluxes are calculated for the simplified geometry, and the sub-group cross-sections are generated by using the flux as a collapsing weight. The sub-group structure is defined as a discrete energy range by considering the magnitude of resonance cross-section.

Then in the 2nd step calculation, the sub-group neutron flux is calculated by using the sub-group cross-section in a fine geometry. Finally, the spatially-dependent effective cross-sections are generated by collapsing the sub-group cross-sections with the sub-group fluxes as a weight.

The 1st step calculation corresponds to the hybrid method of “equivalence theory + ultra-fine-group calculation”, and the 2nd step calculation corresponds to the sub-group method, respectively. Therefore, a generalized resonance treatment is now established based on the unified theory of the conventional three methods.

By comparison of the results by the present method with those by the continuous energy Monte-Carlo method, it is confirmed that the present method can accurately generate spatially-dependent effective cross-sections for radially sub-divided multi-region geometry within a fuel pellet. The accurate results are obtained, not only for the spatially flat fuel composition and temperature conditions, but also for the spatially dependent fuel composition and temperature conditions.

Furthermore, it is also confirmed that the present method can accurately generate both radially and azimuthally dependent effective cross-sections, which has been

difficult for efficient treatment in the conventional methods.

The present method can be applied, not only to the conventional lattice physics calculations for pin-cell or single fuel assembly geometry, but also to the multi-group heterogeneous transport calculations for multi-assembly or full core geometry with large and detailed spatial/energy resolutions. The present method has a potential to provide the accurate effective cross-section sets with practical computation time for such applications.

As a result of the above technical achievements in the present study, several issues associated with the calculation accuracy and calculation efficiency is solved in the field of resonance calculation. Applicability of the new resonance self-shielding treatment to the LWR core analysis is confirmed. The verified performance of the new methodology for the calculation accuracy and efficiency is illustrated in **Figure 5.1**. The figure is made from Figure 1.15 with the typical verification results of Tables 4.6 and 4.8.

For the development of the new resonance self-shielding methodology, treatment of generalized geometry is achieved through (1) and (3), and treatment of extensive neutron spectrum conditions is achieved through (2) and (3), respectively. From the achievements, the core analysis methodology is enhanced, and the advanced technology will contribute to the activities for improvement of nuclear power safety.

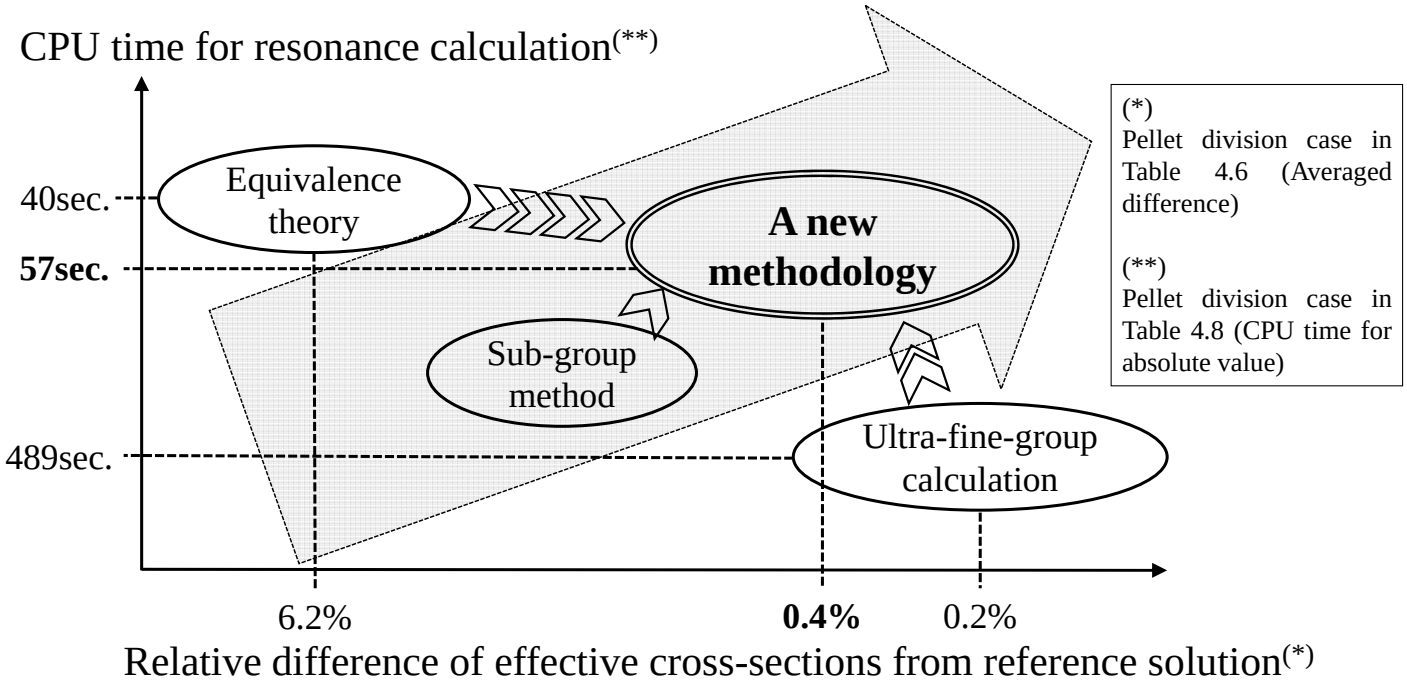

Figure 5.1 Verified performance of the new methodology for the calculation accuracy and efficiency.

5.2 Recommendations for Future Works

In the present study, the fundamental applicability of the proposed resonance treatment is confirmed. In order to apply the present resonance treatment as the more practical one to the nuclear reactor core analysis, several technical issues should be addressed. The issues are summarized as five items, and are described as follows.

(1) Improvement of macroscopic total cross-section points for one-group fixed source MOC calculation (related to Chapter 2)

As described in Chapter 2, the present resonance treatment requires one-group fixed source MOC calculation for several macroscopic total cross-section points. As different from the conventional Dancoff method which requires the only one flux calculation against black limit condition, the present method executes multiple flux calculations.

The number of flux calculations directly influences on the total computation time of the resonance calculation, thus the optimum selection of macroscopic cross-section conditions is desirable. The macroscopic cross-section values and their number of points should be selected from the view point of both calculation accuracy and efficiency.

(2) Optimization of sub-group definition based on discrete energy structure (related to Chapter 4)

Related to Chapter 4, the definition of sub-group energy structure directly influences on the prediction accuracy of effective cross-sections in the case of small number of sub-groups. Though the best definition of the structure in the present study is an equal

interval division for the logarithm of macroscopic absorption cross-section, the result is qualitatively obtained, and its theoretical background is not sufficient.

From this view point, the theoretical foundation to define the best sub-group energy structure is desirable to reduce the number of sub-groups while keeping the sufficient accuracy of effective cross-sections.

One of the ideas is to define the explicit sub-group energy structure so that the energy range within the target multi-group reproduces the band probability obtained from the fitting or moment method.

(3) Simplification of calculation scheme for unified resonance treatment (related to Chapter 4)

If a more simplified implementation of the unified resonance self-shielding treatment is desired for existing lattice physics code, several calculation steps can be replaced by the alternative approach.

For example, generation scheme for rational coefficients can be replaced by the scheme based on the Carlvik's two-term rational coefficients with correction of lattice effect proposed by Stamm'ler. In this case, only one transport calculation is required with the black limit condition, and non-linear least square fitting process can be removed.

For another example, the calculation of non-fuel slowing-down term $\mu(E)$ can be removed if $\mu(E)$ is assumed to be unity, which is almost valid for normal operation condition of LWRs. On the basis of the above simplifications, prediction accuracy of the

ultra-fine-group flux may be worse than that by the original scheme. In such a situation, increasing the number of sub-groups is recommended to keep sufficient accuracy of effective cross-sections.

(4) Application of faster calculation scheme on MOC transport calculation specified for one-group fixed source problem (related to Chapters 2, 3 and 4)

The one-group fixed source calculation based on the MOC is utilized both for generation of rational coefficients in the energy-dependent flux (Chapters 2 and 3) and sub-group flux calculation (Chapter 4). Since the computational burden of these flux calculations is relatively high in the resonance calculation, the fast calculation scheme dedicated for a one-group fixed source problem is desirable.

Since the neutron sources are not updated at all for the application to the resonance calculation, the dedicated programing of MOC flux solver specified for one-group fixed source calculation is an efficient approach to improve calculation efficiency.

(5) Application of unified resonance treatment for eigenvalue problem on fuel assembly or full core geometries (related to Chapter 4)

Though some of the present resonance treatments, i.e., equivalence theory based method (Chapter 2) and “equivalence theory + ultra-fine-group calculation” based hybrid method (Chapter 3), have been implemented to a lattice physics code, the final product of this study, i.e., the unified resonance treatment (Chapter 4), has not been implemented yet.

The application of the unified resonance treatment for eigenvalue problem on fuel assembly or full core geometries is desirable to demonstrate the influence on prediction accuracy for neutronics parameters. Therefore, the implementation of the unified resonance treatment for a core analysis code is an important issue.

By applying the present resonance treatment, the heterogeneous region-wise effective cross-sections can be generated on detailed spatial resolution, both for single fuel assembly or full core level in principle.

In these sophisticated modeling of nuclear reactors, the analysis of detailed phenomenon for neutronics (including the complicated depletion property), and some feedback effects, e.g., thermal-hydraulic and mechanical properties of fuel rods, will be possible.

APPENDIX

A1 Sensitivity Analysis for Calculation Condition of a Unified Method

In order to confirm the appropriateness of calculation conditions for the unified resonance treatment shown in Section 4.4.2, several sensitivity analyses are performed to confirm the variation of microscopic effective capture cross-sections of ^{238}U:

(i) Update for flux

The effect of flux update described in Section 4.2.3 is shown in **Figure A1**. As shown in Figure A1, the differences of effective cross-sections without 2^{nd} step calculation from the continuous energy Monte-Carlo results (MVP results) are efficiently reduced by the update scheme. This effect leads to the slight reduction of difference for final effective cross-section (1^{st} + 2^{nd} step calculation).

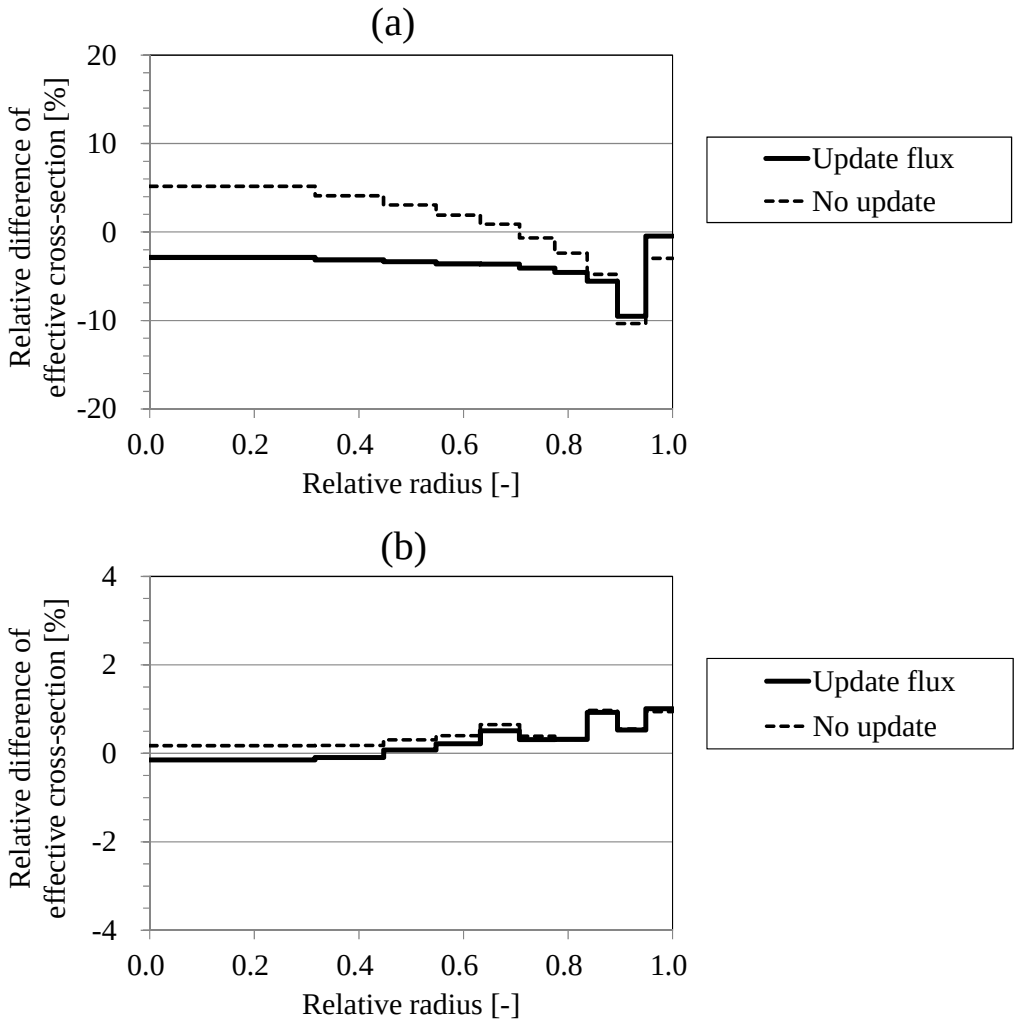

Figure A1 Effect of flux update on the difference of effective cross-sections ((a) Difference of effective cross-section (without 2nd step calculation) (b) Difference of effective cross-section (1st + 2nd step calculation)).

(ii) Sub-group energy structure

The sensitivities of the sub-group energy structure are investigated. The sub-group energy structure is determined by the following three candidates:

(a) Equal division for continuous lethargy,
(b) Equal division for macroscopic absorption cross-section,
(c) Equal division for logarithm of macroscopic absorption cross-section.

Definition (a) is a conventional multi-group approach and the sub-group energy structure is generated based on a continuous energy range. In contrast, Definitions (b) and (c) yield discrete energy group structure based on Equation (4.25).

The differences of effective cross-sections from the MVP results are shown in **Figure A2**. As shown in Figure A2, Definition (c) shows the most accurate result. Definition (b) is better than (a), owing to the accuracy of sub-group cross-sections because the influence of ultra-fine-group flux error is mitigated (see Section 4.4.3.2). In this analysis, the numbers of ultra-fine-groups in each sub-group are (30, 15, 16, 20, 319) for Definition (b), and (75, 36, 52, 132, 105) for Definition (c), in which the sub-group is numbered from the resonance peak range to the foot range. The number of ultra-fine-group groups is equally distributed in each sub-group in Definition (c) rather than (b). Therefore, (c) can utilize all the sub-group transport results more evenly and efficiently, and thus can improve the final accuracy of effective cross-sections.

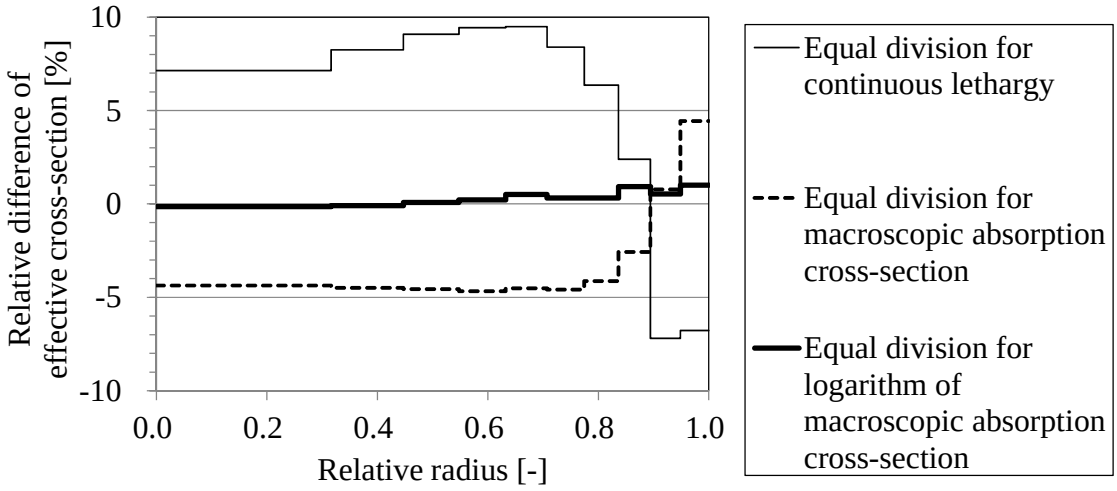

Figure A2 Sensitivity of sub-group energy structure on the difference of effective cross-sections.

(iii) Reference cross-section selection for sub-group definition

The sensitivities of the reference macroscopic cross-section selection for sub-group definition in Equation (4.25) are investigated. The differences of effective cross-sections from the MVP results are shown in **Figure A3**. As shown in Figure A3, the difference is smaller for absorption cross-section than that for total cross-section, owing to the more direct reflection of resonance absorption information. As a result of the improvement for microscopic effective capture cross-sections of ^{238}U, the accuracy of macroscopic total cross-section is also improved.

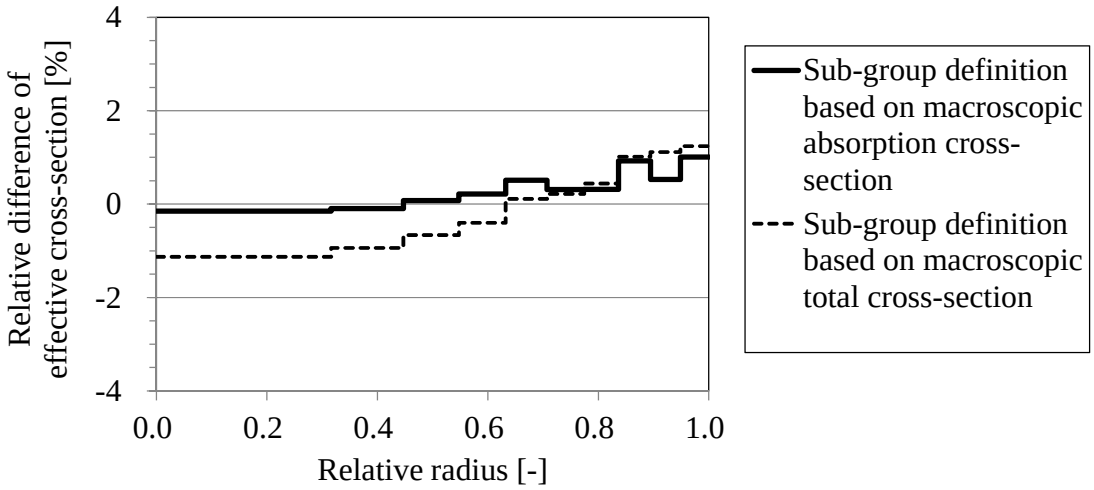

Figure A3 Sensitivity of reference cross-section selection for sub-group definition on the difference of effective cross-sections.

(iv) Number of sub-group

The sensitivities of the number of sub-groups are investigated. The differences of effective cross-sections from the MVP results are shown in **Figure A4**. As shown in Figure A4, the difference becomes smaller as the number of sub-groups increases. When the number of sub-groups is 5, the effective cross-sections are mostly converged to the finer results.

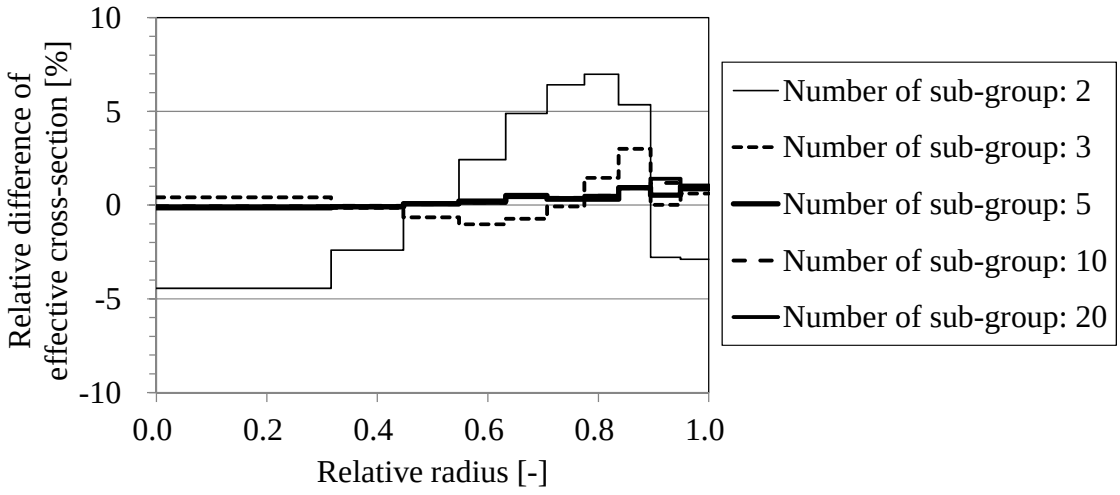

Figure A4 Sensitivity of the number of sub-group on the difference of effective cross-sections.

(v) Scattering source treatment for ultra-fine-group flux calculation

As shown in Section 4.4.3.3, the present method can obtain the accurate effective cross-sections. One of the important elements for its prediction accuracy is the energy-dependent scattering source treatment, which is carefully handled in Section 4.2 from the viewpoint of both calculation accuracy and efficiency. In order to confirm the effect of an efficient scattering source treatment in the present method, the direct heterogeneous ultra-fine-group calculation with the scattering source based on the NR approximation is performed for comparison.

The effect of energy-dependent scattering source treatment in Section 4.2 is shown in **Figure A5**. As shown in Figure A5, the differences of effective cross-sections from the MVP results are smaller for the present method than that for the direct heterogeneous ultra-fine-group calculation with the NR approximation. Therefore, the energy-dependent scattering source treatment is important for sufficient prediction accuracy.

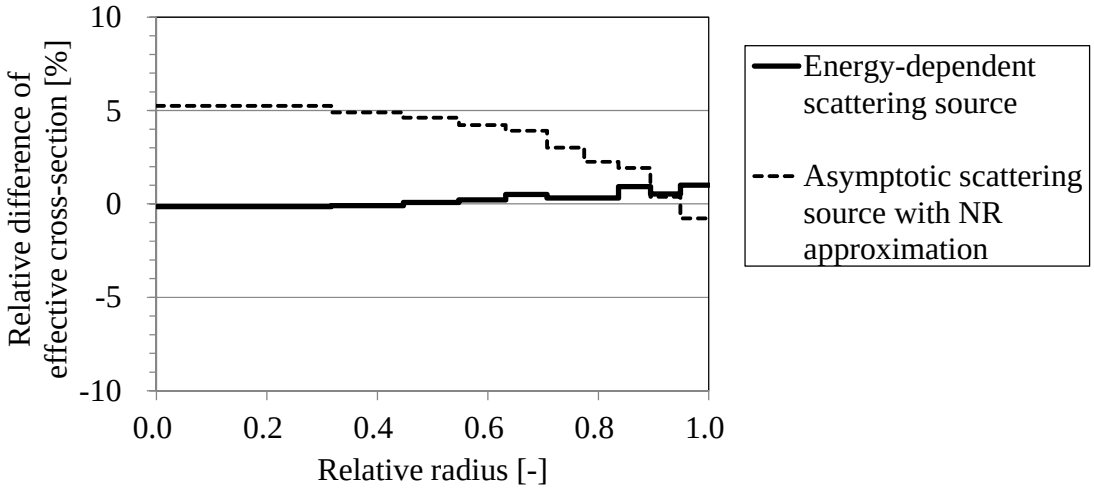

Figure A5 Effect of energy-dependent scattering source treatment on the difference of effective cross-sections.

(vi) Selection of transport method for sub-group flux calculation

The sensitivities of the transport method on the calculation result of sub-group flux are investigated. The differences of effective cross-sections from the MVP results are shown in **Figure A6**. As shown in Figure A6, both the collision probability method (one-dimensional cylindrical geometry with white boundary) and the MOC (exact two-dimensional geometry with reflective boundary) provide comparable results, at least for the radial multi-region system.

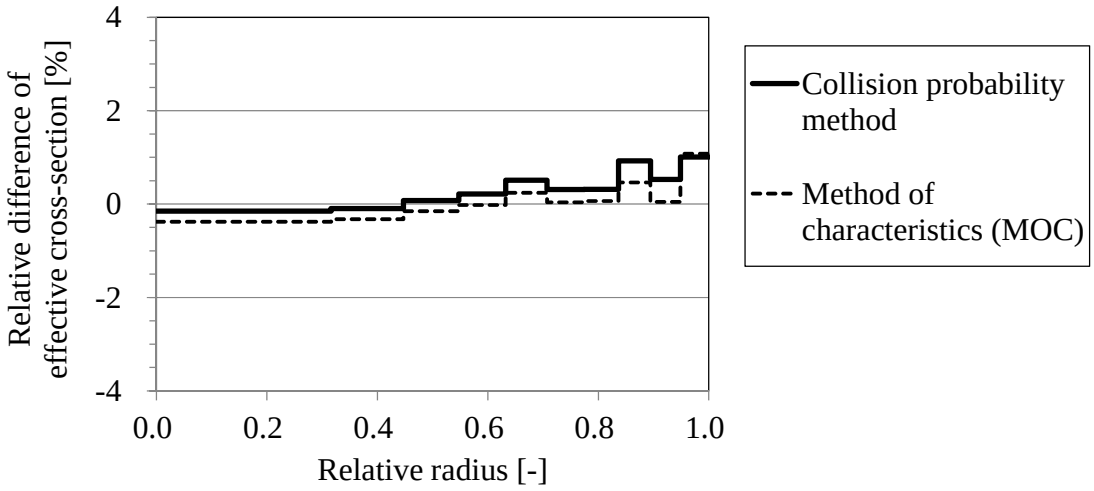

Figure A6 Sensitivity of transport method for sub-group flux calculation on the difference of effective cross-sections.

A2 Azimuthally-Dependent Resonance Treatment Based on Equivalence Theory

Another new resonance treatment for azimuthally-dependent self-shielding effect is derived as an extension of the conventional equivalence theory. In the conventional equivalence theory based on a multi-term rational equation with NR approximation, the flux for fuel region is written as:

$$\phi_f(E) = \frac{1}{E}\sum_{n=1}^{N}\beta_n \frac{\Sigma_p^f l_f + \alpha_n}{\Sigma_t^f(E) l_f + \alpha_n}. \tag{A1}$$

In the present concept, the azimuthal dependence of flux is effectively incorporated by the chord length as follows:

$$\phi_i(E) = \frac{1}{E}\sum_{n=1}^{N}\beta_n \frac{\Sigma_p^f l_{i,eff} + \alpha_n}{\Sigma_t^f(E) l_{i,eff} + \alpha_n}, \tag{A2}$$

where $l_{i,eff}$ is defined as "effective chord length" of sector region i within a pellet. $l_{i,eff}$ incorporates the effect of difference for adjacent moderator region volume in each sector.

In the black limit, i.e., a perfect neutron absorber assumption for fuel region consistent with Dancoff factor calculation, the total reaction-rate is converged as:

$$\begin{aligned}\lim_{\Sigma_t^f\to\infty}\Sigma_t^f\phi_i(\Sigma_t^f) &= \lim_{\Sigma_t^f\to\infty}\Sigma_t^f\sum_{n=1}^{N}\beta_n\frac{\Sigma_p^f l_{i,eff}+\alpha_n}{\Sigma_t^f l_{i,eff}+\alpha_n} = \lim_{\Sigma_t^f\to\infty}\Sigma_t^f\sum_{n=1}^{N}\beta_n\frac{\Sigma_p^f+\frac{\alpha_n}{l_{i,eff}}}{\Sigma_t^f+\frac{\alpha_n}{l_{i,eff}}} \\ &= \sum_{n=1}^{N}\beta_n\left(\Sigma_p^f+\frac{\alpha_n}{l_{i,eff}}\right) = \Sigma_p^f + \frac{\sum_{n=1}^{N}\beta_n\alpha_n}{l_{i,eff}},\end{aligned} \tag{A3}$$

where $\phi_i(\Sigma_t^f)$ denotes lethargy-averaged neutron flux obtained from Equation A2. From Equation A3, $l_{i,eff}$ is derived as:

$$l_{i,eff} = \frac{\sum_{n=1}^{N} \beta_n \alpha_n}{\lim_{\Sigma_t^f \to \infty} \Sigma_t^f \phi_i(\Sigma_t^f) - \Sigma_p^f}. \tag{A4}$$

$l_{i,eff}$ can be generated by using $\lim_{\Sigma_t^f \to \infty} \Sigma_t^f \phi_i(\Sigma_t^f)$ data obtained from one-group MOC fixed source calculation.

As a natural extension of the conventional equivalence theory, the n-th background cross-section for resonance nuclide r in sector region i is written as:

$$\sigma_b^{in} = \frac{\sum_{k \neq r} N_k^f \sigma_p^k + \frac{\alpha_n}{l_{i,eff}}}{N_r^f}. \tag{A5}$$

By using Equation A5, the microscopic effective cross-section is generated based on multi-term rational equation.

In a special case of one-term rational equation, i.e., $N = 1$, Equation A5 is simplified as:

$$\begin{aligned} \sigma_b^i &= \frac{\sum_{k \neq r} N_k^f \sigma_p^k + \frac{\alpha_1}{l_{i,eff}}}{N_r^f} = \frac{\sum_{k \neq r} N_k^f \sigma_p^k + \alpha_1 \frac{\lim_{\Sigma_t^f \to \infty} \Sigma_t^f \phi_i(\Sigma_t^f) - \Sigma_p^f}{\alpha_1}}{N_r^f} \\ &= \frac{\lim_{\Sigma_t^f \to \infty} \Sigma_t^f \phi_i(\Sigma_t^f)}{N_r^f} - \sigma_p^r, \end{aligned} \tag{A6}$$

where Equation A4 is used. The form of Equation A6 is consistent with the enhanced neutron current method, and therefore this treatment is an extended version of the

equivalence theory.

This resonance treatment is applied to the 3×3 multi-cell geometry in Section 4.4.4.4 ($N = 2$). The results of effective cross-sections divided by that for one-region pellet condition are shown in **Figure A7**. As shown in the figure, this method can roughly predict the azimuthal dependence of effective cross-sections. Although the prediction accuracy by the present unified method (Figures 4.21-22) is better than that by the equivalence theory based method (Figure A7), the latter method is an only scheme which can directly generate azimuthally-dependent effective cross-sections based on the equivalence theory.

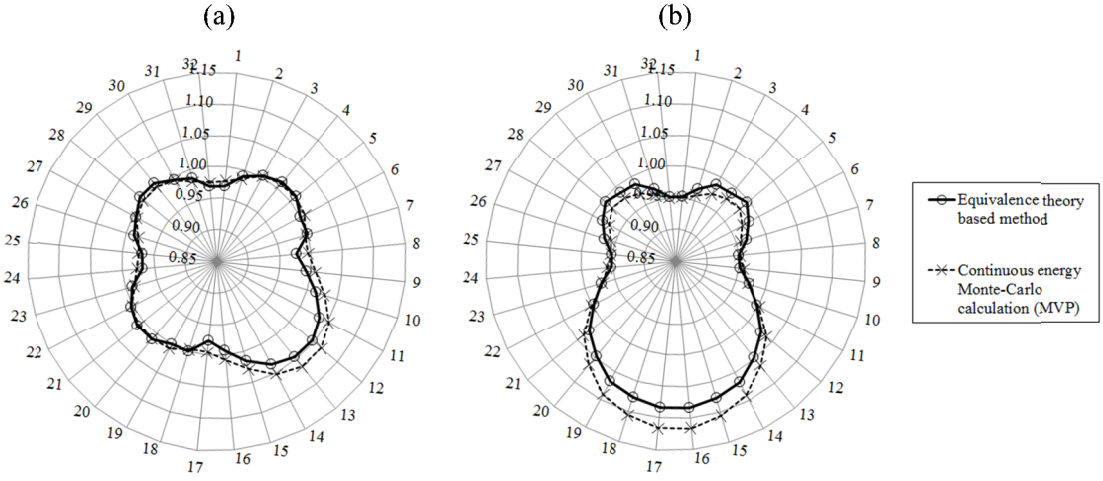

Figure A7. Azimuthally-dependent effective cross-section ratio from equivalence theory based method for 3×3 multi-cell with large water region ((a) Corner fuel, (b) Vertical fuel).

ACKNOWLEDGEMENT

The author would like to express the deepest appreciation to his advisor, Professor Akio Yamamoto of Nagoya University. Professor Yamamoto taught him a fundamental attitude as a professional, as well as many invaluable advices and suggestions through the course of this study.

The author owes an important debt to Professor Akira Uritani, Professor Yoshiyuki Tsuji, Associate professor Atsushi Okamoto and Associate professor Kenichi Watanabe of Nagoya University, and Professor Takanori Kitada of Osaka University for their helpful comments to complete this dissertation.

The author would like to thank staffs in core & safety engineering department of Mitsubishi Heavy Industries, Ltd. (MHI), and core engineering department of MHI nuclear systems & solution engineering, co, Ltd. (MHI NS ENG) for their supports to study in the doctoral course of Nagoya University.

The author got many precious ideas for this dissertation from the GalaxyCosmo-S development. Therefore, the author wishes to thank the development members, especially, Dr. Hideki Matsumoto, Dr. Shinya Kosaka, Mr. Daisuke Sato, Dr. Kazuya Yamaji, Mr. Kazuki Kirimura and Mr. Yohei Kamiyama of MHI, and Mr. Masaru Ido for fruitful discussions in the development.

At last, the author saves a concluding paragraph to thank his family. The author would like to express his gratitude to his wife Takako and his parents for their continuous support and encouragement, and to his daughter Yui with her lovely smile.

LIST OF PUBLICATIONS

Publication in Journals

< Journal of Nuclear Science and Technology (JNST) >

[1] Koike H, Yamaji K, Kirimura K, Sato D, Matsumoto H and Yamamoto A. Advanced resonance self-shielding method for gray resonance treatment in lattice physics code GALAXY. J. Nucl. Sci. Technol. 2012; **49**, 725. (*)

[2] Koike H, Yamaji K, Kirimura K, Kosaka S, Matsumoto H and Yamamoto A. Integration of equivalence theory and ultra-fine-group slowing-down calculation for resonance self-shielding treatment in lattice physics code GALAXY. J. Nucl. Sci. Technol. 2016; **53**, 842. (**)

[3] Koike H, Kirimura K, Yamaji K, Kosaka S and Yamamoto A. Radially and azimuthally dependent resonance self-shielding treatment for general multi-region geometry based on a unified theory. J. Nucl. Sci. Technol. 2018; **55**, 41.

(*) The corresponding paper received 45th encouragement award of Atomic Energy Society of Japan (AESJ).

(**) The corresponding paper received 48th best paper award of Atomic Energy Society of Japan (AESJ).

Publication in Conference Proceedings

< American Nuclear Society (ANS) >

[1] Koike H, Yamamoto A and Yamane Y. Development of a resonance calculation method based on discrete treatment of energy ranges. Trans. Am. Nucl. Soc. (ANS2008 Winter Meeting); 2008 November 9-13; Reno, USA [CD-ROM].

[2] Yamamoto A, Koike H and Yamane Y. A new framework of resonance calculation method based on the sub-group method (1); theory & (2); calculation. Trans. Am. Nucl. Soc. (ANS2009 Annual Meeting); 2009 June 15-18; Atlanta, USA [CD-ROM]. (***)

(***) The corresponding paper received Best Paper Award from the Reactor Physics Division (RPD) of the American Nuclear Society.

< Proceeding of International Conference on Physics of Reactors (PHYSOR) >

[3] Koike H, Yamaji K, Sato D, Tsubota S, Matsumoto H and Yamamoto A. A resonance calculation method based on the multi-terms rational approximation for general geometry with gray resonance absorbers. Proc. Int. Conf. on Physics of Reactors (PHYSOR2010); 2010 May 9-14; Pittsburgh, USA [CD-ROM].

[4] Koike H, Yamaji K, Kirimura K, Kosaka S, and Matsumoto H. Quantification of resonance interference effect for multi-group effective cross-section in lattice physics calculation. Proc. Int. Conf. on Physics of Reactors (PHYSOR2014); 2014 September 28-October 3; Kyoto, JPN [CD-ROM].

< International Conference on Nuclear Engineering (ICONE) >

[5] Koike H, Matsumoto H, Yamaji K and Sato D. Spatially dependent gray resonance shielding method for generating radial power profiles within pellet. Proc. 19th Int. Conf. on Nucl. Eng. (ICONE19); 2011 October 24-25; Suita, JPN [CD-ROM].

< International Congress on Advances in Nuclear Power Plants (ICAPP) >

[6] Koike H, Yamaji K, Kirimura K and Kosaka S. Application of hybrid resonance self-shielding treatment based on integration of equivalence theory and ultra-fine-group calculation. Proc. of ICAPP2017 (ICAPP2017); 2017 April 24-28; Fukui and Kyoto, JPN [CD-ROM]. (****)

(****) The corresponding paper received Outstanding Young Generations Presentation Award of ICAPP2017.

< Atomic Energy Society of Japan (AESJ) >

[7] Koike H, Matsumoto H, Yamaji K, Sato D and Tsubota S. Development of Mitsubishi PWR nuclear design code system GALAXY/COSMO-S -(3) Calculation methodology of power distribution within fuel pellet for GALAXY-. Atomic energy society of Japan (2010 fall meeting of the AESJ); 2010 September 15-17; Sapporo, JPN [CD-ROM] (in Japanese).

[8] Koike H, Yamaji K, Sato D and Matsumoto H. Development of Mitsubishi PWR nuclear design code system GALAXY/COSMO-S -(4) Cross section library based on multi-term hyperbolic tangent formulation for GALAXY-. Atomic energy society of Japan (2011 annual meeting of the AESJ); 2011 March 28-30; Fukui, JPN [CD-ROM] (in Japanese).

[9] Koike H, Kirimura K, Matsumoto H and Yamamoto A. Development of Mitsubishi PWR nuclear design code system GALAXY/COSMO-S -(5) Integrated reaction rate preservation method of heterogeneous system for resonance calculation based on multi-term rational equation-. Atomic energy society of Japan (2011 fall meeting of the AESJ); 2011 September 19-22; Kita-kyushu, JPN [CD-ROM] (in Japanese).